CHEMICAL RECYCLING OF PLASTIC PACKAGING WASTE: THE GERMAN APPROACH

Dr. Gerhard Fahrbach
Duales System Deutschland GmbH
Frankfurter Str. 720-726, 51145 Köln
Germany

INTRODUCTION

The Packaging Ordinance, introduced in Germany in 1991, for the first time prescribes the principle of „prevention, reduction and recycling", and holds manufacturers and retailers directly responsible for the disposal of the packaging they have put into circulation. Packaging from households and small businesses is no longer classified as „ the household waste" as such; it has to be collected separately. In 1991, Duales System Deutschland GmbH (DSD) was founded as a private dual waste management system responsible for the nationwide collection, sorting, and recycling of post-consumer sales packaging, and thus releasing companies from their individual take-back obligation. Initially founded by 95 companies from the retail trade and the consumer goods and packaging industries, DSD, as of today, has about 600 shareholders.

THE SYSTEM

The services offered by DSD are available to consumers all over Germany. Yellow bags and bins are distributed to households for the collection of light-weight packaging made of plastics, metals and composites. Glass is collected in color-coded bottle-banks set up close to residential areas. The packaging is then collected either at the curbside or from the containers by waste management companies contracted by DSD. These contractors are also responsible for the sorting of the contents of the yellow bag/bin. In over 360 sorting plants, the packaging waste is sorted into four fractions: Plastics, metals, composite cardboard, and other composites. The economically more efficient automated sorting is increasingly replacing manual sorting processes. The waste management companies then forward the sorted packaging to the guarantors. These guarantors have signed contracts with DSD in which they guarantee to accept and recycle the material fractions delivered to them. While the task of recycling aluminum, tinplate and composite sales packaging is handed over to industry, DSD is responsible for the collected plastics. DKR, a subsidiary, was founded to coordinate and organize the recycling of plastics packaging.

The principle of recovery and recycling and the Dual System have proved to be a success. In 1996, over 5.4 Million tons of post-consumer sales packaging were collected by the Dual System. This corresponds to 86% of the sales packaging from households and small businesses. Nine out of ten German households participate in the sorting. On average, each citizen collected 71.2 kg of used sales packaging in 1996. Out of the total quantity collected, 84% was sorted and forwarded to recycling. The individual figures for the different material fractions in 1996 are given in Table 1.

DSD's services are financed over the Green Dot trade mark. Fillers, manufacturers and retailers pay DSD a license fee for the right to mark their packaging with the Green Dot trade mark. This fee pays for the collection and sorting of sales packaging, and in the case of plastics also the recycling, as shown in Figure 1. The Dual System is thus financed exclusively by German industry. The costs for the „green dot" costs are largely passed on to consumers via the product price. The license fees are calculated based on the material, the weight of the packaging, and the number of items being circulated in the German market. The fees for the different kinds of packaging thus take into account the actual waste management costs caused by these different kinds of packaging. The licensing fee for plastic packaging is by far the highest because, unlike with other materials, the costs of preparation and recycling are included in the „Green Dot" fee for plastic packaging.

The Dual System not only meets the recycling quotas set forth in the Packaging Ordinance, but also effectively realizes the principles of prevention and reduction. To reduce license fees, manufacturers and fillers optimize packaging and packaging materials. The German environmental ministry estimates that the amount of sales packaging has dropped by 900.000 tons between 1991 and 1995. The recyling achievements in the packaging sector have become a model for an ecologically oriented economy in Germany. „Closing the loop" is the basic concept in this economy and in the „Kreislaufwirtschaftgesetz" (Product Recycling and Waste Management Act), which came into force in October 1996 as an extension of the „Verpackungsverordnung". Taking things one step further, this act, for the first time, makes all branches of industry fully responsible for their products, right throiugh from manufacture to disposal.

PLASTIC RECYCLING

In 1996, approximately 800,000 tons of plastic packaging were used in Germany. Out of this total, 535,000 t were forwarded to recycling. The collected material is sorted into five fractions: EPS, bottles, cups, film, and mixed plastics. The composition of plastic packaging waste in Germany in 1995 is given in Table 2. The Packaging Ordinance requires that the collected plastic packaging be

materially recycled. Initially, material recycling was thought of in terms of mechanical recycling only. However, the extensive sorting necessary to separate the packaging waste in order to isolate relatively pure plastics was found to be too difficult and too expensive. With the introduction of the so-called „mixed fraction" to reduce the sorting efforts, chemical recycling has come into play as a viable alternative to mechanical recycling. Today, most of the containers and films - mainly oversized items which consist of polypropylene and polyethylene - undergo mechanical recycling. The mixed plastics are prepared for feedstock recycling. Although contamination and heterogeneity are not a problem in the mixed plastics fraction, the material still has to be sorted to an agreed-upon specification (Figure 2) in order to be suited for feedstock preparation.

In the preparation process, which is crucially important for successful feedstock recycling, the pre-sorted material is converted into a homogeneous, pourable bulk material. This bulk material must be easy to transport, store and handle. DSD, together with the preparators and the feedstock recyclers, has developed a specification (Figure 3) to define a bulk material which is suitable for all the different feedstock recycling techniques available: The preparation process involves several shredding and separating steps and an agglomeration step to compact the material. Initially, preparation was based on a wet technique. Here, the material fractions were separated in a sink-float process. Although the output quality of the material was very high, this wet process involved intensive washing and therefore was expensive and questionable from an ecological point of view. DSD, together with the preparation plants, has developed an alternative dry technique, where the sink-float step is replaced by air separation and vibrating conveyors. Additionally, magnetic separators and eddy-current separators, as well as sieves, are used.

In a final preparation step, the material, which is now largely free of non-plastic components, is compacted. Depending on the type of machinery used for compacting, the final product takes the form of agglomerate or pellets. Compacting to an agglomerated or pelletized form is a very important step in the preparation. Before the material is compacted, it has a very low density (< 60 kg/m^3) and would be very difficult to handle in subsequent feedstock recycling processes. The new dry technique has considerably reduced the costs of feedstock preparation, while the quality and consistency of the output material still perfectly meets the specification.

Preparation plants with a capacity of more than 10.000 t/y per line can operate economically. Currently, about 10 plants with a total available capacity of approximately 310,000 tons (output) prepare the mixed plastics for the feedstock recycling. This material is all produced according to the same specification regardless of the recycling process it subsequently undergoes.There are three main usages for mixed plastics as a feedstock: Liquefaction/ pyrolysis, gasification, and the blast furnace. Currently, about nine German plants are involved in the feedstock recycling of post-consumer plastics, with an available capacity that by January 1998 will be sufficient to recycle the prepared material, as presented in Figure 4.

CONCLUSION

With environmental issues becoming more and more serious, the demand for economically efficient and ecologically effective recycling technologies is rapidly increasing all over the world. Over the past five years, Duales System Deutschland has collected significant know-how in waste management, in the collection and sorting of household waste, and particularly in the crucial preparation of plastics for feedstock recycling processes. DSD is now actively exploring cooperation agreements with researchers and companies from other countries to develop economically competitive and ecologically superior alternatives to existing disposal methods.

Table 1. Recycling of post-consumer packaging in 1996

	Packaging consumption	*Quantity recycled*
Glass	3,148,740 t	2,686,639 t
Paper/cardboard	1,402,286 t	1,318,641 t
Plastics	791,816 t	534,953 t
Tinplate	374,598 t	301,789 t
Composites	560,860 t	444,753 t
Aluminum	44,415 t	35,926 t
Total	**6,322,715 t**	**5,322,701 t**

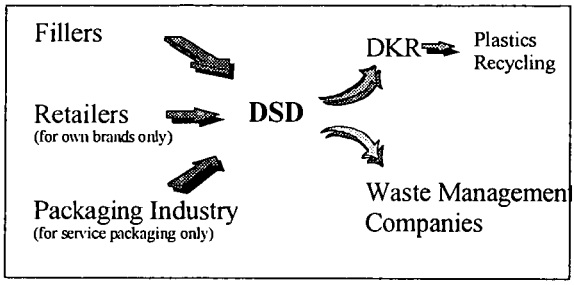

Figure 1. DSD-financing: Flow of payments

Table 2: Waste plastic collection: Quantities supplied for preparation in 1995

Fraction	Quantity (t)	% of Total
EPS	3,500	0.6%
Cups	10,000	1.9%
Bottles	53,000	9.8%
Film	143,500	26.6%
Mixed Plastics	330,000	61.1%
Total	**540,000**	**100%**

A Composition/ Description
Mixed Plastics from Plastic Packaging and Plastic Containing Articles

B Purity
Plastic Content > 90 (wt.) %

C Impurities
Total < 10 (wt.) % Metal < 3 (wt.) %

D Typical Impurities (from other containers and packaging)
Metal, Glass, Paper, Aluminium Coated Plastics, Cardboard Composites

E Typical Impurities (from other sources)
Rubber, Stones, Wood, Textiles, etc.

F Packaging Bales (80 cm x 80 cm x 120 cm)

Figure 2. Product specification: Mixed plastics fraction

Granular Size	≤ 1,0 cm
Granular Fines (< 250μ)	≤ 1,0 (wt.) %
Appearance	Pourable
Moisture Content	< 1,0 (wt.) %
Density	≥ 0,3 kg/l
Chlorine	≤ 2,0 (wt.) %
Ash (@ 650 C) Total	≤ 4,5 (wt.) %
Ash (@ 650 C) Metal	≤ 1,0 (wt.) %
Plastics Content - Total	≥ 90,0 (wt.) %
Plastics Content - Polyolefin	≥ 70,0 (wt.) %
Plastics Content -Engineering Resins	≤ 4,0 (wt.) %

Figure 3. Product specification: Mixed plastics agglomerate

Contractor	Consumption (t/y) 1997	Consumption (t/y) January 1, 1998
KAB	80,000	80,000
BASF	20,000	20,000
Stahlwerke Bremen	80,000	80,000
Eko-Stahl	13,000	15,000
Thyssen	18,000	18,000
KHS	12,000	40,000
HKM	0	50,000
(Additional Capacity for Gasification)	(70,000)	(70,000)
Total	***293,000***	***373,000***

Figure 4. Feedstock recycling: Available capacities in German plants

EFFECT OF FERRIC OXIDE CATALYST ON THE CRACKING OF POLYSTYRENE AND POLYETHYLENE

Jyi-Pemg A. Wann*, Tohru Kamo, Hiroshi Yamaguchi**, and Yoshiki Sato

National Institute for Resources and Environment, 16-3 Onogawa, Tsukuba, 305 Japan
*Dept. of Chemical & Fuels Engineering, University of Utah, Salt Lake City, UT 84112
**Combustion System Lab, NKK Corp., 1-1 Minamiwatarida-cho, Kawasaki, 210 Japan

Keywords: Catalytic Cracking, PS, PE

INTRODUCTION

Investigations on waste plastic recycling are receiving public attentions mainly because of the increasing pressure of disposal problems from the ascending consumption of plastics. Our previous study [1] demonstrated that, at 440 °C and 60 min reaction time, liquid-phase cracking using tetralin and n-decane solvents increased oil yields from polystyrene (PS) but decreased oil yields from high-density polyethylene (HDPE), when compared to the crackings in solvent-free environment. Significant oil yield synergism was further observed for the cracking of PS and HDPE mixtures when sufficient hydrogen stabilization from the solvent was absent.

Our research continued to study the type of catalyst that may be applied to the liquid-phase cracking of plastics. This communication reports the effects of an Fe_2O_3/S catalyst, which is known for hydrogenolysis activities, on the liquid-phase cracking of PS and HDPE and their 50/50 mixtures.

EXPERIMENTAL

Figure 1 illustrates the experimental scheme of the liquid-phase cracking using a batch-mode 300-mL autoclave reactor. The plastics used were commercial-grade pellets of PS and HDPE. Reagent-grade tetralin, n-decane (n-C10) and decalin (cis- and trans- mixture) were used as the solvent for liquid-phase cracking without further purification. For catalytic runs, powders of 3 wt% iron(III) oxide and 2.4 wt% sulfur, both based on the total weight of feed plastics, were added.

A total weight of 80 g of feed reactants including the plastics and the liquid solvent, if used, was charged for each autoclave reaction experiment. The concentration of the plastics in each experiment with solvent feed was generally 25 wt% except for the cases investigating the effect of decalin dilution on PS and HDPE crackings. Experiments were also performed under solvent-free environment for comparison purposes. For mixtures of PS and HDPE, the ratio of PS to HDPE was 1/1 on a w/w basis. After being charged with feed reactants, the reactor was purged and then filled with nitrogen gas for non-catalytic runs, or with hydrogen gas for catalytic runs. The initial pressure was 4.0 MPa (570 psig) at ambient temperatures. The reaction was conducted at 440 °C for 60 min with constant stirring at 1000 rpm.

The volume of produced gases was measured using a wet gas meter and the composition analyzed using a GC equipped with a TCD. The yield and the average molecular weight of gaseous products were determined based on the gas volume measured and the gas composition analyzed. The product liquid slurry was distilled under a vacuum pressure as low as 1 torr at 330 °C. The recovered liquid distillate was further analyzed using another GC equipped with a 50-m long glass capillary column (Hewlett Packard Ultra-1) and an FID. The oven temperature of the GC unit was controlled starting from 60 °C at a 3.0 °C/min rate to 300 °C, at which it was kept isothermally for a period of 30 min. A GC-MS was used to assist the identification of the components of interest.

The total conversion was determined according to the following equation:

$$\text{total conversion, wt\%} = 100\% - \frac{\text{wt. of vacuum residue - wt. of catalyst as FeS}}{\text{net wt. of feed plastics}}$$

The oil yield was calculated by subtracting gas yield from the total conversion. For catalytic runs, the catalyst was assumed to have transformed to FeS after the reactions. The hydrogen consumption was calculated by determining the loss of hydrogen in the charged hydrogen gas less the amount consumed for the formation of hydrogen sulfide.

RESULTS AND DISSCUSSION

Cracking of PS

As illustrated in Table 1, the total conversion at 440 °C of the non-catalytic thermal runs was found to follow the order that tetralin > decalin > n-decane > solvent-free. The hydrogen donation capabilities of decalin and n-decane are essentially negligible, as compared to that of tetralin. Figure 2 shows the effect of decalin dilution, in terms of PS feed concentration, on the conversion and product selectivity. At a high temperature of 440 °C, secondary reactions quickly transform styrene, which is considered the primary product of PS cracking [2, 3], to products such as ethylbenzene, toluene, and cumene. With the increased interactions among reactive species, condensation reactions could prevail during the PS cracking. For the solvent-free case, the interactions among product species were the most intensive and the conversion could not be improved in the absence of sufficient hydrogenation. Results from GC-MS analysis of the oil fractions show that components such as terphenyls, quarterphenyls, and polyphenyls of higher order might have formed in the heavy fractions.

At 440 °C, tetralin not only buffered but also quickly stabilized reactive species by hydrogenation. For the case of catalytic cracking using Fe_2O_3/S catalyst and decalin solvent, the total conversion increased to completion with a low gas yield of 0.6 wt%. The high conversions obtained for the cracking in tetralin and catalytic hydrogenation environments suggest that hydrogen stabilization could promote PS conversion to produce light oil.

The gas yields from PS cracking were generally low except when using n-decane as the solvent. Substantial amounts of C1-C4 n-alkanes were produced in gaseous products when n-decane was used as the solvent at 440 °C. This suggests that n-decane could be susceptible to decomposition during PS cracking.

Cracking of HDPE

Typical product yields of HDPE cracking in the different reaction environments are presented in Table 2. At 440 °C, HDPE cracking shows the trend opposite to PS cracking by giving decreased total conversions in the presence of the solvents. This is mainly due to the different cracking mechanisms of HDPE and PS. At 440 °C, HDPE decomposition slowly produces a series of successive n-alkanes and α-alkenes. For the solvent-free environment, intensive interactions led to a moderately high conversion of 55.6 wt%. However, for the cracking in tetralin solvent environment, the total conversion was sharply reduced to a negligible level. At 440 °C, tetralin appeared to stabilize decomposition radical fragments at quite fast rates, slowing down the production of distillate oil from HDPE. The use of n-decane and decalin non-donor solvents under nitrogen atmosphere also significantly suppressed HDPE decomposition by dispersing the interactions among reactive species. The order of average molecular weight (MW) of gaseous products follows the same trend for the cracking in both PS and HDPE under the non-catalytic environments, showing that n-decane > solvent-free > decalin > tetralin. It is evident that tetralin effectively reduced the chances of further interactions. When n-decane was used as the solvent for HDPE cracking, small amounts of n-alkanes and α-alkenes with the carbon chain lengths less than 7 were produced, suggesting that n-decane could also be susceptible to decomposition during the HDPE cracking.

The cracking of HDPE using Fe_2O_3/S catalyst under hydrogen atmosphere in decalin solvent gave a total conversion substantially higher than that of the corresponding non-catalytic run. This indicates that the catalyst may have a cracking activity to increase the rate of HDPE decomposition to produce distillate oil in heavy fraction. The hydrogen consumption was low, and the catalyst showed quite different behaviors from tetralin in that the catalyst was able to hydrogenate α-olefins and showed cracking activity with HDPE. Only small concentrations of α-olefins and branched alkanes were found in the oil fraction obtained from the catalytic run.

The effect of decalin dilution on product selectivity of HDPE cracking is illustrated in Figure 3. As the HDPE feed concentration increased, both the oil and gas yields also increased. However, a decrease in total conversion did not occur for high HDPE feed loadings. Although black soot-like material was observed on the reactor wall and around stirrer shaft surfaces, occurrence of condensation reactions in HDPE cracking at 440 °C appeared not as severe as in PS cracking. Unlike PS, HDPE does not readily convert to its monomer precursor. When a normal alkane molecule is decomposed, it

probably first converts to a pair of n-alkane and α-alkene, which may or may not have the same chain lengths. Figure 3 indicates that, as the conversion becomes greater, the selectivity increases for lighter n-alkanes whereas it remains relatively constant or slightly decreases for lighter α-alkenes under the non-catalytic environment. The carbon distribution pattern further indicates that HDPE cracking may start with random cleavage on the carbon-carbon main chains and then followed by β-scission to the free radical positions, producing n-alkanes and α-alkenes of various chain lengths.

Cracking of PS and PE Mixtures

Table 3 presents the results of non-catalytic and catalytic liquefaction runs for 50/50 PS and PE mixtures at 440 °C for 60 min. For the non-catalytic thermal runs, strong interactions among the cracking products from PS and HDPE mixtures result in oil yield synergism [1]. The results further show that the combination of Fe_2O_3 and sulfur provides an effective way for hydrogenation, simply by judging from the hydrogen consumed from the gas phase. The order of hydrogen consumption based on the charged H_2 agrees well with the hydrogen need during the plastics cracking. The solvent-free run required the most hydrogen because of its high concentration (i.e., 100 wt%) of the mixed plastics, when compared with other runs that used 25 wt% loading with a solvent medium. The catalytic run using tetralin as the solvent consumed the least amount of hydrogen from the gas phase, due to the affluent hydrogen supply from the solvent. For those runs using decalin and n-decane as the solvent media, their hydrogen consumption requirements were intermediate.

In Table 3 except the case using n-decane solvent, the total conversions and C5-C9 n-alkanes yields decreased by the application of Fe_2O_3/S catalyst. This is attributed to the effective catalytic hydrogenation that is able to stabilize reactive species and suppress the oil yield synergism. The catalyst clearly exhibited its activities increasing the selectivity for light aromatic components produced from the PS cracking, stabilizing the reactive species, and suppressing HDPE from induced cracking.

When n-decane was used as the solvent, the production of C5-C9 n-alkanes was exceedingly high from both the non-catalytic and catalytic runs, when compared to other reaction environments. The total conversion of the catalytic run was not decreased but slightly increased. This may be explained as a combined result of induced and accelerated cracking of HDPE by PS decomposition products, n-decane cracking, and the cracking and hydrogenation activities of the catalyst.

PS decomposes to styrene at a temperature as low as 400 °C. As indicated in Table 1, the cracking of PS could significantly induce the cracking of n-decane below a temperature at which the hydrogenation could take place to stabilize reactive species. Other solvents such as tetralin and decalin are more stable than n-decane and were not susceptible to PS-induced cracking into reactive species. Moreover, it is also noted that the slow cracking of HDPE at 440 °C might also slightly induce the cracking of n-decane, or vice versa, under the non-catalytic condition. Under the combined effect, the decomposition of HDPE could be induced and accelerated by the presence of reactive species from both n-decane and PS cracking, giving the high yields of C5-C9 n-alkanes and n-alkylbenzenes with C6-C9 side chains.

When using the Fe_2O_3/S catalyst, although slightly more cracking could occur for HDPE to produce oils in heavy fraction, there also exists a hydrogen stabilization effect from the gas phase counteracting the induced cracking of HDPE. This leads to an overall result of slightly increases in total conversion and oil yield. The GC chromatogram indicates that less concentrations of α-olefins and branched alkanes were contained in the oil produced from the catalytic runs. Interaction products such as n-alkylbenzenes with C6-C9 side chains were also present in the oil fractions but generally in smaller yields.

PS cracking at 440 °C could proceed much faster than the effective hydrogenation. For the major products from PS, ethylbenzene selectivity was sharply increased and became the most dominant component probably due to direct hydrogenation to the styrene during both liquid- and gas-phase hydrogenations. The trend for other components also follows in similar fashions for their variations, namely, the selectivity for cumene increased while for toluene decreased.

The rate of HDPE cracking may be slowed down to an extent depending on the reaction environment either by using tetralin solvent or Fe_2O_3/S catalyst in hydrogen atmosphere. Tetralin was able to stabilize decomposition free radicals but was not as

effective as the catalyst in the hydrogenation of unsaturated bonds. There would need significantly additional hydrogen supply if HDPE could have been cracked effectively. The existence of oil yield synergism produces more varieties of components by increased interactions. The catalytic cracking of PS and HDPE mixtures in n-decane solvent showed a high conversion with a low gas yield.

CONCLUSIONS

Fe_2O_3/S catalyst showed a hydrogenation activity for the cracking of PS in a non-hydrogen donor solvent at 440 °C to yield a total conversion of 100 wt%. It demonstrated an effective way of converting PS using liquid-phase cracking and a hydrogenation catalyst. The catalyst slightly increased the conversion of HDPE under a similar condition by exhibiting cracking and hydrogenation activities. When used in the cracking of PS and HDPE mixtures, the catalyst decreased total conversions by suppressing interactions among reactive products under solvent-free, tetralin, and decalin environments. When n-decane was used as the solvent for the cracking of PS and HDPE mixtures, the catalyst was able to maintain effective decomposition of PS and HDPE, and give a decreased gas yield in hydrogen atmosphere.

ACKNOWLEDGEMENTS

This work was performed under STA Research Fellowship arranged by the National Science Foundation, USA, and the Science and Technology Agency, Japan. The author J.-P. Anthony Wann likes to express his sincere thanks to Professors David M. Bodily and Larry L. Anderson, of University of Utah, and Dady B. Dadyburjor, of West Virginia University, for their supports of this research.

REFERENCES

1. Wann, J.-P. A., Kamo, Y., Yamaguchi, H., and Sato, Y., "Reaction Behaviors of Mixed Plastics in Liquid-Phase Cracking," ACS Preprint, Div. Fuel Chem., 41(4), 1161-1164, (1996).
2. Stevens M. P., Polymer Chemistry: An Introduction, Addition-Wesley Publishing, Reading, Massachusetts, 1975, p. 206.
3. Lin, R and White, R. L., "Catalytic Cracking of Polystyrene," ACS Preprint, Div. Fuel Chem., 41(4), 1165-1169, (1996).

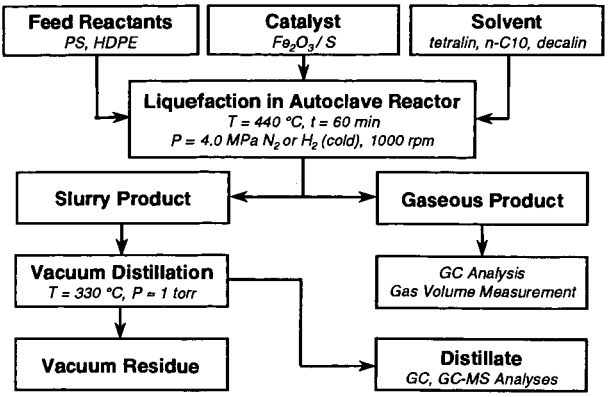

Figure 1. Schematic Illustration of Plastics Liquefaction Experiment

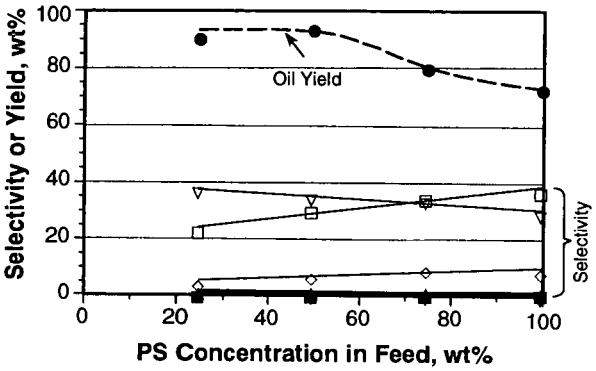

Figure 2. Effect of Decalin Solvent Dilution on PS Cracking at 440 °C and 60 min (Legend: □ ethylbenzene ◇ cumene ▽ toluene △ propylbenzene ■ benzene ▼ styrene ● oil)

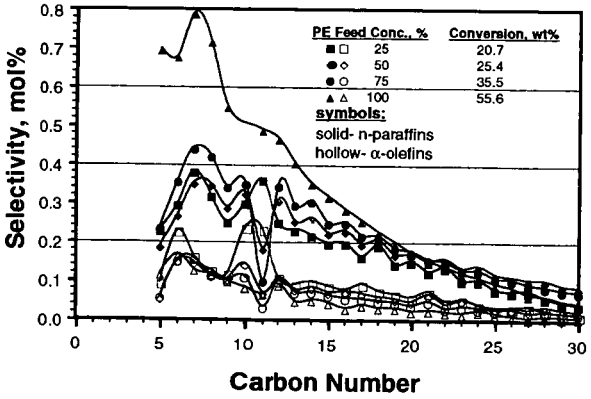

Figure 3. Effect of Decalin Dilution on PE Cracking at 440 °C and 60 min

Table 1. Product Yields of PS Cracking in Different Reaction Environments at 440 °C

Reaction Environment	Non-Catalytic, N_2				Catalytic, H_2
	Solvent-Free	Tetralin	Decalin	n-Decane	Decalin
Total Conversion, wt%	**73.2**	**96.5**	**91.8**	**89.0**	**100.0**
Oil Yield, wt%	**72.9**	**95.8**	**90.8**	**83.8**	**99.4**
benzene, wt%	0.9	0.2	0.4	0.7	0.7
toluene, wt%	21.6	40.8	33.8	33.3	24.4
ethylbenzene, wt%	27.4	27.7	21.2	13.4	41.4
styrene, wt%	0.0	0.5	0.4	0.5	0.0
cumene, wt%	6.6	5.5	4.1	3.7	8.3
propylbenzene, wt%	1.3	1.5	1.4	1.6	1.6
Gas Yield, wt%	**0.3**	**0.7**	**1.0**	**5.1**	**0.6**
Gas MW (average)	18.1	5.6	10.2	30.2	28.7
Hydrogen Consumption‡					
wt% of plastics					0.8
wt% of H_2 charged					18.4

Table 2. Product Yields of HDPE Cracking in Different Reaction Environments at 440 °C

Reaction Environment	Non-Catalytic, N_2				Catalytic, H_2
	Solvent-Free	Tetralin	Decalin	n-Decane	Decalin
Total Conversion, wt%	**55.6**	**1.1**	**20.7**	**24.8**	**38.5**
Oil Yield, wt%	**53.9**	**1.0**	**20.1**	**22.6**	**37.8**
C5-C9 n-alkanes, wt%	6.8	0.1	1.1	8.7	0.9
Gas Yield, wt%	**1.7**	**0.1**	**0.6**	**2.2**	**0.7**
Gas MW (average)	27.5	5.5	22.6	31.3	45.1
H_2 Consumption‡					
wt% of plastics					0.1
wt% of H_2 charged					1.8

Table 3. Results of Non-Catalytic Thermal and Catalytic Liquefaction Runs for 50/50 PS and PE Mixtures at 440 °C for 60 min

Reaction Environment	Solvent-Free		Tetralin		Decalin		n-Decane	
	Thermal	Catalytic	Thermal	Catalytic	Thermal	Catalytic	Thermal	Catalytic
Total Conversion, wt%	**81.5**	**70.2**	**55.6**	**51.6**	**78.4**	**66.6**	**76.0**	**79.4**
Oil, wt%	**80.3**	**69.1**	**55.1**	**51.2**	**76.8**	**65.9**	**72.7**	**77.2**
C5-C9 n-alkanes	5.9	1.4	0.4	0.2	2.1	1.0	17.6	17.8
n-alkylbenzenes with C6-C9 side chains	1.1	0.2	0.3	0.2	1.1	1.0	3.9	1.0
Toluene, wt%	19.9	14.2	19.4	5.7	19.1	13.2	20.4	12.5
Ethylbenzene, wt%	16.4	21.6	12.7	29.4	8.1	21.5	5.1	23.3
Cumene, wt%	3.3	4.8	2.7	5.2	1.1	4.2	0.8	2.0
Gas, wt%	**1.2**	**1.1**	**0.5**	**0.4**	**1.6**	**0.7**	**3.2**	**2.1**
Gas MW (average)	23.2	36.0	4.4	41.7	15.9	33.7	28.1	33.0
H_2 Consumption‡								
wt% of plastics		0.6		0.4		0.7		0.9
wt% of H_2 charged		**50.S**		**9.1**		**17.0**		**20.9**

Note: ‡ Not including contribution from feed solvent

Effect of Solid Acid Catalysts on Waste Plastic Liquefaction

J. Rockwell, N. Shah and G.P. Huffman
CFFLS, 533 S. Limestone St.
University of Kentucky
Lexington, KY 40506

Keywords: plastic, solid acid catalyst, liquefaction.

Introduction

The use of solid acid catalysts for liquefaction of plastic and coprocessing of coal with plastic has proven effective. [1-8] However, very good results have been obtained under thermal liquefaction conditions and there is some question as to whether the use of a catalyst is justified. In the current study, seven different catalysts were tested with two waste plastics: a relatively clean waste plastic provided by the American Plastics Council and a somewhat dirtier plastic provided by the Duales System Deustchland (DSD). Liquefaction experiments were carried out at 435 and 445 °C on the APC plastic and at 445 °C on the DSD plastic.

The results at 435 °C show significant differences in the total conversions and oil yields. However, at 445 °C, the liquefaction yields with different catalysts showed relatively small differences. For the APC plastic, simulated distillation measurements on the oil fraction obtained at 445 °C did show significant differences. The oils from most of the catalytic runs exhibited higher fractions of gasoline (IBP - 200°C) and kerosene (200 – 275 °C) and lower fractions of heavy oils 275 – 550 °C). The HZSM-5 zeolite catalyst was found to be the most effective. The catalysts were less effective for the DSD plastic, possibly because of poisoning.

Experimental Procedure

All liquefaction experiments were performed using 50 ml tubing bomb microreactors. The feedstocks were a commingled waste plastic obtained from the APC and a post consumer waste plastic provided by the DSD. The APC plastic has been used in a number of previous experiments. [2,3] It is a relatively clean waste plastic that has been subjected to a wet washing process to remove labels and inerts. The DSD sample is the same plastic feedstock used in the German feedstock recycling industry. As discussed elsewhere, [9] this material is subjected to sorting, automated cleaning by magnetic, eddy current, air and screen separation techniques, shredding, and agglomeration. The proximate and ultimate analyses of these materials are given in Table 1.

Table 1. Proximate and ultimate analyses of the APC and DSD waste plastics (wt. %).

Proximate	APC	DSD	Ultimate	APC	DSD
Volatile matter	98.8	93.8	C	84.7	79.0
Fixed carbon	0.74	1.08	H	13.7	13.5
Ash	0.45	4.44	N	0.65	0.67
Moisture	0.01	0.16	S	0.01	0.08
			Cl	0.03	1.26
			0 (difference)	0.91	5.49

Approximately 10 g of feedstock was weighed and placed in a tubing bomb. Catalyst was added at a 1 wt. % concentration (0.1g). The bomb was then purged with H_2 gas and charged to a final cold pressure of 200 psig. The apparatus was immersed into a fluidized sand bath at the desired temperature and agitated at 400 rpm. All of the data reported here were obtained from experiments run at 435 °C for 30 minutes or 445 °C for 60 minutes. After liquefaction, the sandbath is lowered and the tubing bomb is air-cooled to room temperature. The gas is collected in a 40 ml gas bomb and weighed. The remaining sample is analyzed by conventional solvent extraction methods. The total liquid conversion is the THF extractable material, while the oil yield is defined as the pentane soluble liquid. Asphaltenes + preashpaltenes (A + PA) are defined as the product that is soluble in THF but not in pentane.

For each reaction condition, two samples were run. A sample of the liquid product was taken directly from the second tubing bomb and subjected to simulated distillation (SIMDIS) analysis using a Perkin-Elmer gas chromatograph with the following operating parameters: column – Petrocol B, 20' X 1/8" packed column; temperature - -10 to 360 °C with 10 °C/min ramp;

detector – FID at 380°C; flow rate – 35 ml/min He. SIMDIS software provided by Perkin-Elmer was used to analyze the data. The results are reported as boiling point (BP) ranges as follows: gasoline - IBP-200 °C; kerosene - 200-275 °C; and heavy oil - 275-550 °C.

Seven different catalysts were used in the liquefaction experiments. These included a commercial HZSM-5 zeolite, [10] a ZrO_2/WO_3 catalyst, [11] and a number of catalysts synthesized in our laboratories. The latter included ferrihydrite treated with citric acid (FHYD/CA), [12] a ferrihydrite containing with 5 % Mo (FHYD/Mo), [13] a SiO_2-Al_2O_3 binary oxide, [2] and two TiO_2-SiO_2 binary oxides with different atomic ratios ([Ti]/[Ti+Si]) = 0.85 and 0.85(+)) prepared using the method of Doolin *et al.* [14]

Liquefaction Results

The liquefaction results are shown in Figures 1-3 for the APC plastics. At 435 °C, the HZSM-5 catalyst gives the best oil yield and total liquid yield. However, it is not much more effective than the other catalysts tested. Furthermore, the yield results obtained with no catalyst (thermal) are as good as or better than those obtained with all of the catalysts tested except HZSM-5. At 445 °C, there is little or no difference in the yields obtained from the thermal run and the various catalytic runs. The simulated distillation results, however, show that the catalysts do have an effect on the quality of the oil product. It is seen that the thermal run gives a gasoline fraction of about 27%, while the HZSD-5 oil product exhibited a gasoline fraction of 42%. The other catalysts gave intermediate gasoline fractions, ranging from 28% for the SiO_2-Al_2O_3 to 38% for the TiO_2-SiO_2 ([Ti]/[Ti+Si]=0.95).

Some results for the DSD waste plastic are shown in Figures 4 and 5. At 445 °C, it is again seen that the addition of a catalyst has very little effect. A high oil yield is obtained thermally, and no significant change occurs as a result of adding 1 wt. % of any of the catalysts. Additionally, the preliminary SIMDIST results on these samples indicate that the catalysts also have very little effect on oil quality. The experiments on the DSD plastics will be completed with all catalysts at both temperatures. Chemical analyses on the oil products will be performed to determine the effect of the catalysts on heteroatom content, particularly Cl.

Conclusions

The current results indicate that, at high liquefaction temperatures (445 °C), low concentrations (~1 wt. %) of solid acid catalysts have relatively small effects on either the yield or the quality of products derived from liquefaction of waste plastic. Although further testing is needed, this suggests that thermal hydroprocessing of waste plastics at 440-450 °C is adequate to produce a good oil product. This would decrease the operating costs of any commercial developments of this technology. [9]

Acknowledgement: The authors would like to acknowledge the U.S. Department of Energy for supporting this research under DOE contract No. DE-FC22-93-PC93053 as part of the research program of the Consortium for Fossil Fuel Liquefaction Science.

References:

1. M.M. Taghiei, Z. Feng, F.E. Huggins, and G.P. Huffman, **1994**, *Energy & Fuels*, 1228-1232.
2. Z. Feng, J. Zhao, J. Rockwell, D. Bailey and G.P. Huffman, **1996**, *Fuel Proc. Tech.*, **49**,17-30.
3. W.B. Ding, W. Tuntawiroon, J. Liang, L.L. Anderson, **1996**, *Fuel Proc. Tech.*, **49**, 49-63.
4. M. Luo and C.W. Curtis, **1996a**, *Fuel Proc. Tech.*, **49**, 91-117.
5. W. Zmierczak, Xin Xiao, Joseph Shabtai, **1996**, *Fuel Proc. Tech.*, **49**, 31-48.
6. J. Shabtai, X. Xiao, and W. Zmierczak, **1997**, *Energy & Fuels*, **11**, 76-87.
7. X. Xiao, W. Zmierczak and J. Shabtai, **1995**, *Amer. Chem. Soc., Div. Fuel Chem. Preprints*, **40(1)**, 4-8.
8. K.R. Venkatesh, J. Hu, W. Wang, G.D. Holder, J.W. Tierney and I. Wender, **1996**, *Energy & Fuels*, **10**, 1163-1170.
9. G.P. Huffman, "Feasibility Study for a Demonstration Plant for the Liquefaction and Coprocessing of Waste Polymers and Coal," paper in this volume and DOE report (in preparation).
10. HZSM-5 provided by Dr. Fred Tungate, United Catalysts Corporation.
11. ZrO_2/WO_3 prepared by Dr. Francis Acholla, Rohm & Haas Corporation.
12. J. Zhao, Z. Feng, F.E. Huggins and G.P. Huffman, **1994**, *Energy & Fuels*, **8**, 1152-3.
13. J. Zhao, Z. Feng, F.E. Huggins and G.P. Huffman, **1994**, *Energy & Fuels*, **8**, J. Zhao, Z. Feng, F.E. Huggins and G.P. Huffman, **1994**, *Energy & Fuels*, **8**, 38-43.
14. P.K. Doolin et al., **1994**, *Catalysis Letters*, **38**, 457.

Figure 1. Liquefaction yields at 435 C, 200 psig H2 (cold), 60 minutes.

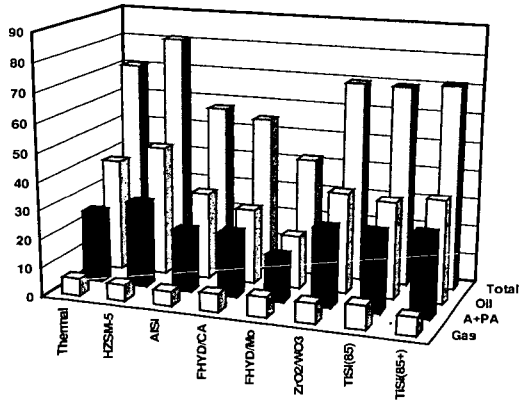

Figure 2. Liquefaction yields at 445 C, 200 psig H2(cold), 60 minutes.

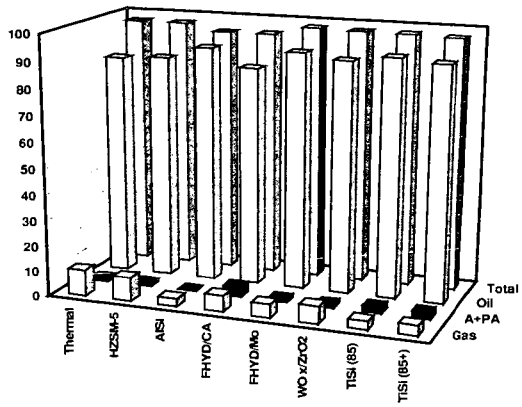

Figure 3. Comparison of simdist results for thermal and catalytic runs.

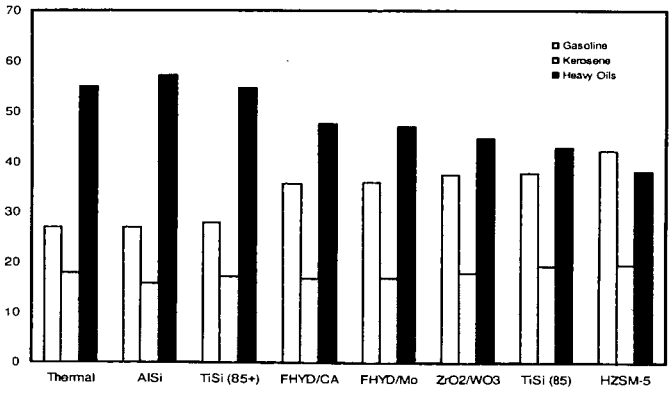

Figure 4. Liquefaction yields for DSD plastic at 445 C.

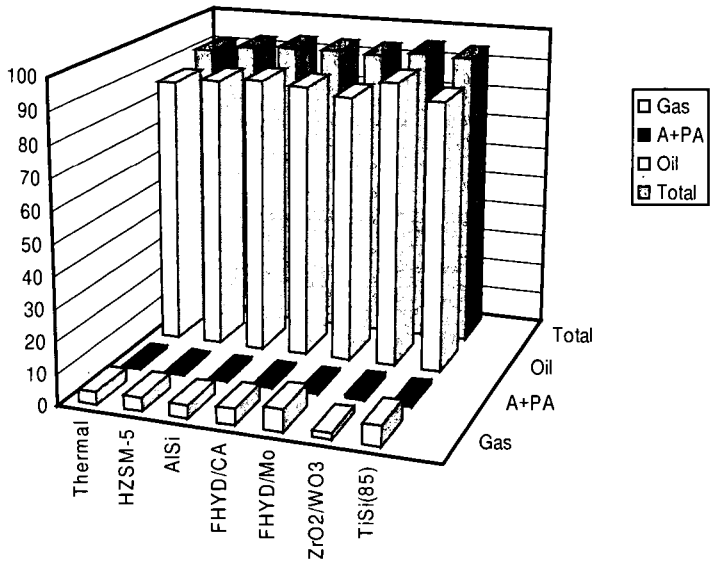

Figure 5. Simdist results for oil from DSD plastic.

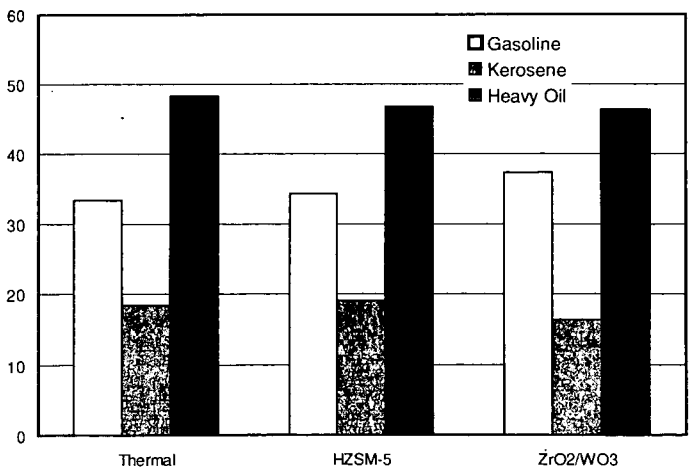

EFFECTS OF CATALYST ACIDITY AND STRUCTURE ON POLYMER CRACKING MECHANISMS

Rong Lin, Darrel L. Negelein, and Robert L. White
Department of Chemistry and Biochemistry
University of Oklahoma, Norman, OK 73019

Keywords: catalytic cracking, polymer cracking, polymer recycling

INTRODUCTION

Communities in the United States need alternatives to municipal solid waste landfilling. Of the solid waste components currently placed into landfills, plastics are particularly undesirable because of their limited biodegradability. A variety of plastic waste recycling methods have been established and new recycling approaches are being developed to avoid placing polymers into landfills. One approach to waste plastic recycling, known as tertiary recycling, consists of converting plastics into useful chemicals. The development of efficient processes for waste plastic tertiary recycling will require detailed fundamental data on the direct catalytic cracking of polymers without complications due to reactions of primary cracking products with polymer residue. Secondary reactions can be minimized by maintaining high catalyst to polymer ratios and providing efficient and rapid removal of volatile products. This work was carried out to investigate the potential use of catalytic cracking to convert plastics wastes into mixtures of useful chemicals. The effects of silica-alumina, HZSM-5 zeolite and sulfated zirconia catalysts on the thermal degradations of poly(ethylene), poly(propylene) and poly(styrene) are described.

EXPERIMENTAL

Samples examined in this study were: poly(ethylene) (PE) (MW=80,300), poly(propylene) (PP) (MW= 250,000), poly(styrene) (PS) (MW=850,000), and these polymers coated on silica-alumina, HZSM-5, and sulfated zirconia cracking catalysts (10-20% (wt/wt)). All polymer samples were purchased from Aldrich Chemical Company (Milwaukee, WI). The silica-alumina catalyst was provided by Condea Chemie GmbH (Hambug, Germany) and contained 11.8% by weight alumina and had a surface area of 282 m^2/g. The HZSM-5 zeolite was obtained from Mobil Oil (Paulsboro, NJ) and was characterized by a 1.5% alumina content and a 355 m^2/g surface area. The sulfated zirconia catalyst was synthesized by following procedures described previously[1]. The sulfated zirconia catalyst had a surface area of 157 m^2/g and contained 9% by weight sulfate. Polymer/catalyst samples were prepared by dissolving polymers in proper solvents, adding catalyst, and then rotoevaporating the mixture to remove solvents. The resulting PE and PP coated catalyst samples were dried at 120°C, and the PS coated catalyst samples were dried at 90°C for several hours.

The apparatus used for pyrolysis-GC/MS, TG-MS and TG-GC/MS measurements have been described previously[2,3]. Pyrolysis separations were achieved by using a HP 5890 capillary GC with a DB-5 column (0.25 μm film thickness). The gas chromatograph oven temperature program consisted of a 2 min isothermal period at -50°C followed by a 5°C/min ramp to 40°C followed by a 10°C/min ramp to 280°C, and then isothermal at 280°C for 5 minutes for PE and PP samples. For PS samples, the GC oven temperature programs consisted of a 2 minute isothermal period at -50°C followed by a 10°C/min ramp to 280°C, and then another isothermal period at 280°C for 5 minutes. For TG-MS studies, samples were heated from 50°C to 600°C at nominal heating rates of 1, 10, 25, and 50°C/min, with a He purge gas flow rate of 50 mL/min. For TG-GC/MS studies, a Valco Instruments, Inc. (Houston, TX) eight port heated sample injector was employed to divert small volumes (ca. 100 μL) of TG effluent into a 30 m DB-5 capillary column (0.25 μm film thickness). TG-GC/MS signal averaged mass spectra were acquired at rates ranging from one to two per second, depending on the mass range that was scanned. A 5 mL/min He carrier gas flow rate through the TG-GC/MS chromatographic column was employed for all separations. TG-GC/MS column effluent was split prior to entering the mass spectrometer to maintain an ion source pressure of 5 x 10^{-5} torr.

RESULTS AND DISCUSSION

Figure 1 shows pyrolysis GC/MS results for neat PE and PE/catalyst samples obtained at 500 °C and demonstrates the dramatic effects of catalysts on PE thermal degradation[4]. All four chromatograms shown in Figure 1 were obtained by using the same separation conditions and they are plotted on the same time scale. The bottom chromatogram represents the volatile products from pyrolysis of neat PE at 500°C and contains numerous high molecular weight species. However, in the presence of cracking catalysts, more than 85% of volatile products were hydrocarbons in the C_2 to C_{10} range. Therefore, the effect of the catalyst was to restrict the molecular weight range of volatile products, leading to the formation of low molecular weight species. With increasing catalyst acidity, more saturated hydrocarbons were produced relative to unsaturated hydrocarbons. Large amounts of aromatics were detected for the sample containing HZSM-5 zeolite. The most abundant volatile products generated by PE cracking were isoalkenes, which differs from previous reports that isoalkanes were the primary products. However, the mechanisms proposed for isoalkane formation require protonation of initially formed alkenes followed by hydride abstraction from the polymer residue. The rapid removal of volatile products during cracking minimized secondary reactions and therefore was an effective means to study the effects of catalysts on the initial polymer cracking reactions. TG-MS results indicated that poly(ethylene) cracking on all three catalysts occurred in three steps. Saturated and unsaturated hydrocarbons evolved in the first two steps and aromatics evolved in the third step.

Pyrolysis GC/MS results for neat PP and PP/catalyst samples obtained at 500 °C are shown in Figure 2. The presence of catalysts led to the preferred formation of low molecular weight species. Volatile product distributions depended on the choice of catalyst[5]. It was found that the most abundant neat PP thermal degradation volatile products were C_3 to C_{15} olefin homologues separated by three carbon atom intervals. The most abundant saturated volatile products were C_5 alkanes. Catalytic cracking of PP/SA samples produced a significantly different volatile product distribution than neat PP thermal degradation. The most abundant volatile products were C_4, C_5 and C_6 alkenes. The amount of char remaining on catalyst surfaces was found to be approximately 1% of the initial polymer mass. In the presence of ZrO_2/SO_4 catalyst, the most abundant volatile products were saturated hydrocarbons. All of the volatile products detected were C_{10} or smaller. However, an increase in unsaturated volatile product yields was found at higher temperature. The significant difference between PP/Si-Al and PP/ZrO_2/SO_4 cracking products indicates that catalyst acidity plays a vital role in determining volatile product slates. Sulfated zirconia, a very strong acid catalyst, significantly lowered the temperature at which catalytic cracking occurred and facilitated hydride abstractions, resulting in large yields of saturated hydrocarbons and the formation of large amounts of residue (ca. 15%). Like the PP/Si-Al sample, the PP/HZSM-5 sample yielded primarily unsaturated volatile products. The organic residue left on catalysts was estimated to be approximately 1%. In contrast to the PP/Si-Al and PP/ZrO_2/SO_4 samples, HZSM-5 channels restricted reaction volume, which resulted in relatively large yields of alkyl aromatics.

Catalytic cracking mechanisms of PS also differ considerably from the thermal degradation mechanisms[6]. Pyrolysis GC/MS results (Figure 3) indicate that styrene was the most abundant volatile product resulting from neat PS thermal degradation. The relative yield of styrene was 68% when PS was pyrolyzed at 400 °C. However, benzene was the most abundant product when PS was catalytically cracked. The relative yield of benzene was found to be as high as 60% for the PS/HZSM-5 sample and over 30% for samples containing Si-Al and sulfated zirconia catalysts. Very little styrene was detected for all three PS/catalyst samples. TG-GC/MS results for the PS/ZrO_2/SO_4 sample are shown in Figure 4. The broken line in this figure denotes the TG weight loss curve for the sample. Polymer decomposition occurred primarily between 150 and 350 °C. The second weight loss step results from the decomposition of the catalyst. The solid line in Figure 4 denotes the TG-GC/MS total ion current, which is plotted as a function of the TG temperature at which GC injections were made. This plot contains 31 separate chromatograms obtained during one TG weight loss analysis. It can be seen that at low temperature there is only one peak, corresponding to benzene. With the increasing of temperature, more peaks appear in chromatograms, indicating the formation of more cracking products. Peaks at high temperature (i.e > 400 °C) correspond to the formation of SO_2 and suggest that the sulfated zirconia catalyst decomposed. Figure 5 shows a TG-GC/MS chromatogram obtained from TG effluent that was injected when the TG sample

temperature was 240 °C. More than 25 peaks were detected in this chromatogram. The broken line in Figure 5 denotes the GC oven temperature ramp employed for separations. It was found that benzene was by far the most abundant volatile product and was produced at temperatures well below those at which the other volatile products were detected. All of the PS/catalyst samples produced alkyl benzenes and indanes, but styrene and indenes were only detected for samples containing HZSM-5 zeolite.

TG analyses were carried out to investigate the effects of catalysts on volatilization activation energies. TG weight loss data obtained by using different heating rates (1, 10, 25 and 50 °C/min) were used to calculate volatilization activation energies by using the method described by Friedman[7]. Volatilization activation energies calculated from TG weight loss information are given in Table 1. The highest volatilization activation energies were obtained for the neat polymer samples. All three catalysts lowered the activation energy for PE thermal degradation significantly. The order of catalyst activities was found to be in the order of increasing catalyst acidity: ZrO_2/SO_4 > HZSM-5 > Si-Al.

CONCLUSIONS

The effects of different catalysts on catalytic cracking product distributions derived from polymer/catalyst samples were studied. It was found that volatile product distributions were affected by the choice of catalyst as well as the cracking conditions. In general, catalysts caused volatile hydrocarbon products to be smaller than neat polymer thermal decomposition products. Overall volatilization activation energies for PE, PP, and PS thermal decompositions were considerably reduced by the presence of cracking catalysts and the magnitude of the reduction depended directly on the catalyst acidity. A lowering of the overall volatilization activation energies by cracking catalysts is desired for polymer recycling applications because it greatly reduces the cracking temperature required to decompose plastic wastes, which, reduces operational costs of the process.

ACKNOWLEDGEMENT

Financial support for this work from the National Science Foundation (CTS-9509240) is gratefully acknowledged.

REFERENCES

1. A. Jatia, C. Chang, J.D. MacLeod, T. Okubo, M.E. Davis, *Catal. Lett.*, 5, 21(1994).
2. R.L. White, J. Anal. Appl. Pyr., 18, 269(1991).
3. E.C. Sikabwe, D.L. Negelein, R. Lin, R.L. White, *Anal. Chem.*, in press.
4. R. Lin, R.L. White, *J. Appl. Polym. Sci.*, 58, 1151(1995).
5. D.L. Negelein, R. Lin, R.L. White, *J. Appl. Polym. Sci.*, submitted
6. R. Lin, R.L. White, *J. Appl. Polym. Sci.*, 63, 1287(1997).
7. H.L. Freidman, *J. Polym. Sci.*, 6C, 183(1963).

Table 1. Volatilization Activation Energies (kcal/mol)

Catalyst	PE	PP	PS
none	59 ± 1	48 ± 1	49 ± 1
Si-Al	37 ± 3	33 ± 1	39 ± 1
HZSM-5	31 ± 1	29 ± 1	36 ± 1
ZrO_2/SO_4	28 ± 2	27 ± 1	29 ± 2

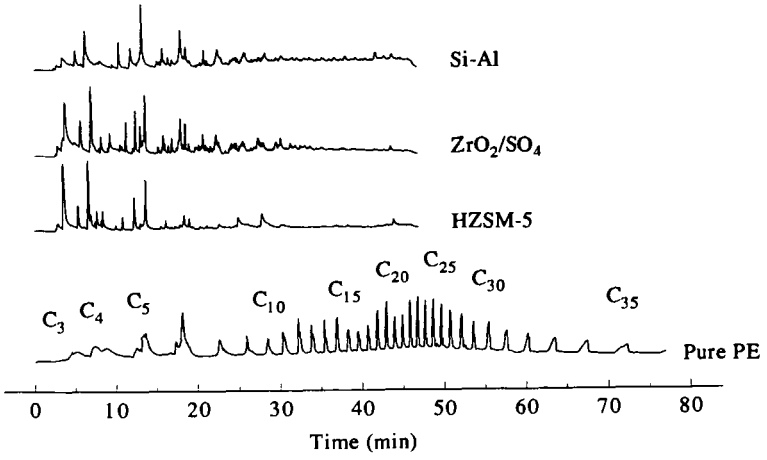

Figure 1 - 500 °C pyrolysis GC/MS chromatograms for poly(ethylene) samples.

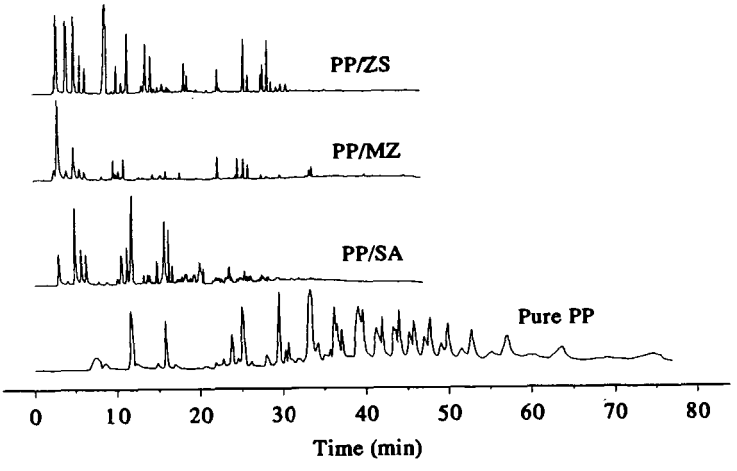

Figure 2 - 500 °C pyrolysis GC/MS chromatograms for poly(propylene) samples.

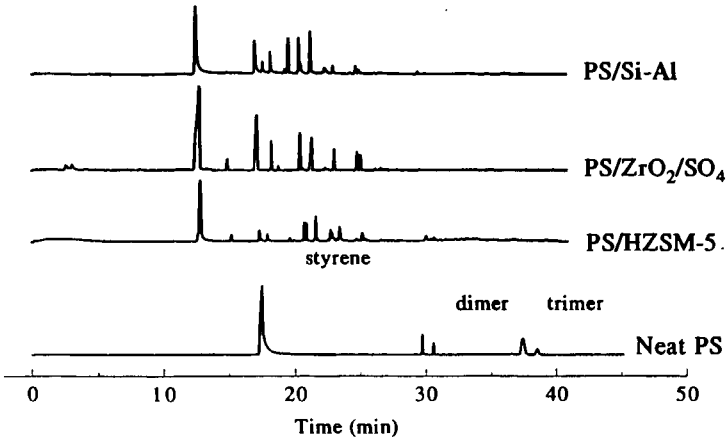

Figure 3 - 400 °C pyrolysis GC/MS chromatograms for poly(styrene) samples.

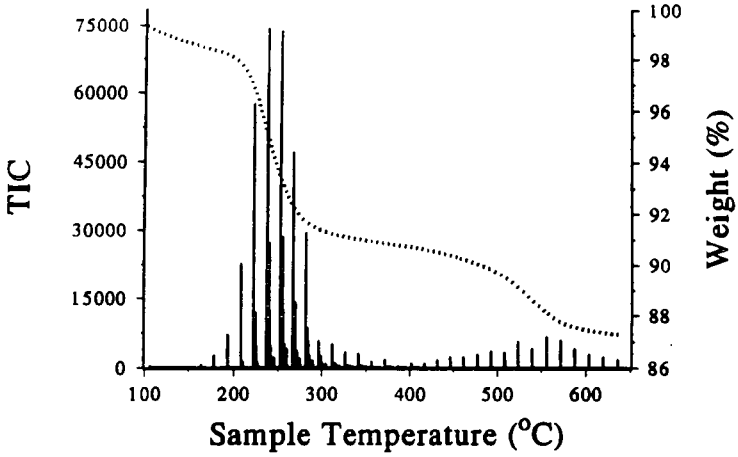

Figure 4 - TG-GC/MS weight loss curve (dotted line) and chromatograms (solid line) for the $PS/ZrO_2/SO_4$ sample.

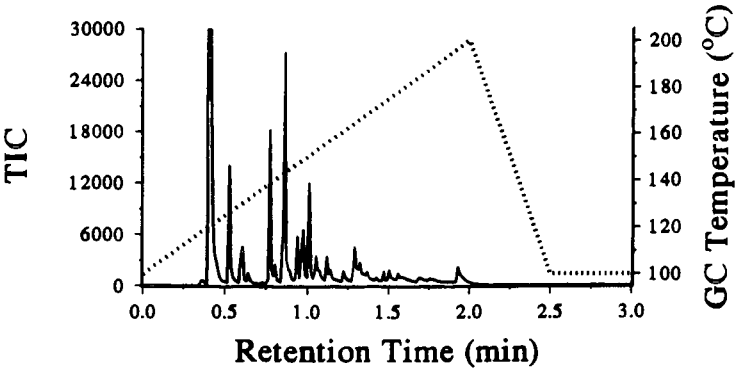

Figure 5 - TG-GC/MS chromatogram measured at 240 °C.

CATALYTIC DEGRADATION OF HIGH DENSITY POLYETHYLENE AND WASTE PLASTIC BELOW 200 °C

G.S. Deng, W.H. McClennen, H.L.C. Meuzelaar, Center for
Micro Analysis and Reaction Chemistry, University of Utah, S.L.C, UT84112

Introduction

High density polyethylene (HDPE) is the dominant component of several major waste plastic streams. Furthermore, under thermally as well as catalytically controlled degradation conditions, HDPE is clearly an excellent potential source of hydrocarbon products. Unfortunately, HDPE is notoriously resistent against thermal degradation, requiring pyrolysis temperatures well above 400°C in order to exhibit sufficiently high degradation rates[1]. These high temperatures lead to loss of selectivity, increased secondary reactions, coke formation and reduced catalyst life. Although Wender et al. reported catalytic scission of polymethylenic bonds at temperatures as low as 160°C in short chain paraffinic compounds such as hexadecane[2], few authors have reported successful catalytic conversion of HDPE below 300 °C. The two main obstacles encountered appear to be the limited mobility of long chain molecules even in the molten stage and poor hydrogen (H_2) diffusion, thus leading to transport-limited interactions between catalytic sites and potential bond scission sites. Also the frequent presence of organic and inorganic moieties other than HDPE that negatively affect catalyst performance, e.g. through catalyst deactivation ("fouling") poses a formidable obstacle against successful catalytic convertions of waste plastic. Attempts to reduce transport limitations for long chain HDPE molecules have included use of very high catalyst loadings[3], or improved mixing and blending techniques for catalyst and polymer e.g. by means of cryogenic milling[4] or through solvent blending[3].

The present research was concerned with a systematic investigation of the catalytic degradation of HDPE polymers at low temperature under H_2 pressure, using finely dispersed superacid catalysts, i.e. $Pt/ZrO_2/SO_4$. A Cahn model 151 high pressure thermogravimetry (HPTG) system with specially constructed on-line gas chromatography/mass spectrometry (GC/MS module) capable of recording temperature programmmed GC/MS profiles at 90 second intervals provides detailed kinetic (rates, yields) and mechanistic (product identity) information from a single HPTG run.

Experimental

Materials. Four different HDPE samples were studied: (1) a pure HDPE (den., 0.96g/cm^3; average MW, 250,000; Tm, 135 °C) provided by HTI and originally manufactured by Solvay polymers; (2) a pure HDPE (den., 0.959 g/cm^3; average MW, 125,000; Tm, 130°C) obtained from Aldrich Chemical Co.; (3) a HDPE-rich commingled waste plastic sample (primarily HDPE with 5-10% polypropylene, 3-5% polystyrene and 1-2% inorganic fillers plus organic colorizing agents) provided by the American Plastics Council (APC) and included in the University of Utah Waste Materials Sample Bank; (4) a cleaned milk bottle without its cap and label.

Catalysts. The solid superacid catalysts ZrO_2/SO_4 and Pt-stabilized ZrO_2/SO_4 (0.5%Pt), were prepared by Wender and Shabtai as described in previous papers[2,5]. The zeolite-based HZSM-5 catalyst was supplied by Aldrich Chemical Co.

Experimental Procedure. Experiments with high density polyethylene (HDPE) and HDPE-rich waste plastic in the presence of various catalysts were performed in a high pressure TG/GC/MS system under different hydrogen pressures (or helium). Details of the high pressure TG/GC/MS system have been described previously[6]. Different temperature programs were employed to better distinguish the effect of different conditions on reaction kinetics.

Dry blending of catalyst and polymer was performed by hand mixing the powdered material inside a quartz TG crucible with a thin metal rod. To achieve better blending of catalyst and polymer, 30 mg polymer samples were dissolved in 10 ml of toluene at about 100 °C. After the addition of catalyst, the mixture was shaken while the solvent was removed and then dried for 3 hours at 130°C. Sample quantities of 30-40 mg were used in each TG/GC/MS experiment.

Results and Discussion

Catalyst loading and solvent blending

Figure 1a demonstrates that both a catalyst (here at 16% loading) and hydrogen atmosphere are

needed to achieve sustained high degradation rates at 375 °C. However increased hydrogen pressure above 600 psig does not produce markedly higher rates at this temperature. Figure 1b indicates that improved blending of polymer and catalyst using a solution slurry method in toluene can be as effective as increasing catalyst loadings. Interestingly, the first weight loss appears to occur just above 200 °C. As shown in Figure 1c, increasing the catalyst loading to 25% leads to complete decomposition of HDPE below 300 °C during the heat-up phase. Even a (much less reactive) waste plastic sample shows more than 40% weight loss before reaching the isothermal heating stage at 375 °C under these conditions. Therefore, it appears that physical (transport related) process are rate limiting in the case of HDPE polymer. If so, higher conversion rates and lower reaction temperatures should be achievable by measures that increase catalyst loadings and facilitate contact between the catalyst surface and the polymer matrix.

These observations encouraged us to go to much lower temperatures as well as higher catalyst loadings. Figure 2a shows that very fast degradation rates can be achieved at 200 °C and 600 psig H_2 when using pure HDPE and Pt stabilized ZrO_2/SO_4 at 50 % loading whereas only minimal weight loss is observed when using solvent blending of 50% non Pt stabilized ZrO_2/SO_4 or 50% HZSM-5. Clearly, HZSM-5 induced rates are not enhanced by the same factor as the superacid catalyst rates. Apparently, the rate limiting step is not affected by just increasing the amount of catalyst surface available. Possibly other factors such as diffusion into the HZSM-5 zeolite cavity may be rate limiting here, as also evident in figure 1a. Reduction of the H_2 pressure to 25 psig causes marked rate reduction. However, further increase of catalyst loading to 70% can largely enhance the reaction rate and yield as shown in figure 2b.

The reaction conditions illustrated in figure 2b are worth contemplating a little further, as they suggest that HDPE in more or less pure form can nearly be degraded in a household style pressure cooker (200 °C and 25 psig), thus potentially reducing the high cost of high temperature, (high) pressure reaction vessels, and auxilary systems.

Temperature

Figure 3a and b illustrate the effect of temperature on the reaction rates of two different HDPE model compounds, obtained from HTI (MW: 250,000) and Aldrich (MW: 125,000) respectively. Note that the HDPE from HTI appears to be more reactive (in spite of its higher MW) both with regard to maximum rate achieved as well as highest conversion yield. The cause of the nearly 10% residue in the Aldrich sample at 200 °C is unknown. This is not simply char formation, since all of the residue is converted at 400 °C. Further studies are underway to explain this phenomenon.

Pressure of H_2

Figure 4 a,b,c illustrate the effect of changes in H_2 pressure on the two different pure HDPEs and on a HDPE-rich waste plastic sample. The HTI sample degraded faster and more completely at 200 °C than the Aldrich sample. Furthermore, figure 4c illustrates that nearly 80% of the waste polymer sample can be converted at 200 °C.

Sorted waste plastic

The effects of contaminants, additives or residues on the conversion behavior of waste polymers are also well recognized. A variety of organic (e.g. sulfur or nitrogen containing) and inorganic (e.g. heavy metal containing) compounds are known to be capable of deactivating catalysts. Among the catalysts known to be effective in degradating polymethylenic bonds, the superacids are known to be highly susceptible to activity loss through coke deposit formation. Figure 5 shows the behaviour of a variety of waste plastic samples indicating wide differences in the reactivity of the specific waste plastic components which were hand-picked from the APC sample, e.g. clear (HDPE rich) materials, white (filled) cap components and labels (or label like) material. Individual component profiles and mixture profiles are shown in figure 5. Note how the clean milk bottle sample degraded as fast as pure HDPE model compound. "Cap material" behaves much like a moderately char forming polymer. Note that the initial 30% residue formed at 200 °C nearly completely degrades at approx. 450 °C, thus reducing the likelihood that a inorganic filler is responsible for the observed residue. Finally, the paper/label like fraction (handpicked) does not show any detectable weight loss below 300 °C. The mixture samples of "paper" + "plastic" and "paper" + "cap" + "plastic" show marked residue formation. The fact that the measured conversion rates and yields fall well behind the predicted rates of summed weight loss curves of the components suggest the effects of catalytic deactivation.

By examing the evolution profiles of volatile products by means of GC/MS, the distribution of

different types of product distributions as a function of reaction gas and catalysts can be measured. Figure 6 shows that effective catalysts increase the degree of saturation and markedly decrease the degree of aromaticity (nearly zero) in addition to increasing reaction rates and decreasing reaction temperature as shown in Figure 1. HZSM-5 also showed a tendency to promote the formation of aromatic products (not shown here) as noted in previous experiments[7]. In addition, the product distributions of thermal reaction in H_2 or He are different, although their reaction rates are nearly the same as shown in Figure 1a. Typical analytical results corresponding to curve 3 in Figure 2a are demonstrated in Figure 7. The repetitive chromatogram for the whole run (Figure 7a) indicates that the catalytic decomposition of HDPE occurs in the about 16~35 minutes run time (200 °C isothermal) Furthermore, by selecting a particular ion chromatogram, the evolution ratio of the corresponding products during the reaction can be visualized. The expanded total ion chromatogram for one sampling interval (Figure 7b) shows the range of GC separated paraffin products which are similar to the products for non Pt promoted ZrO_2/SO_4^{2-}[7]. The predominance of saturated aliphatic products is shown in the 15 to 37 minute average mass spectrum (7c).

Conclusions

Platinum stabilized ZrO_2/SO_4^{2-} ($Pt/ZrO_2/SO_4^{2-}$) is much more effective than non promoted ZrO_2/SO_4^{2-} in maintaining high conversion rates for HDPE polymers and HDPE-rich waste plastic at 200°C. Also, it readily outperforms HZSM-5. Even under low pressure (25 psig H_2) conditions, $Pt/ZrO_2/SO_4^{2-}$ shows high activity by means of high catalyst loading and solvent blending. In addition, there are wide differences in the reactivity of the various waste plastic components over $Pt/ZrO_2/SO_4^{2-}$. Furthermore, the on-line GC/MS monitoring technique offers an effective tool in studying catalytic conversion processes.

References

(1) Siauw H. Ng, H. Seoud, M. Stanciulescu, Y. Sugimoto, Energy&Fuels ,1995, 9, 735-742.
(2) M.Y. Wen, I. Wender and J.W. Tierney, Energy&Fuels,1990, 4, 372-379.
(3) R.L. White and R. Lin, in Proceedings at Frontiers of Pyrolysis, Colorado, in press.
(4) M. Seehra, E. Hopkins, V. Suresh Babu.M. Ibrahim, the 10th Annual Technical Meeting : The Consortium for Fossil Fuel Liquefaction Science, August 6-9, 1996, PA, p. 36.
(5) J. Shabtai, X. Xiao, W. Zmierczak, Energy&Fuels,1997, 11(1), 76-87.
(6) K. Liu, E, Jakab, W.H. McClennen and H.L.C. Meuzelaar, Am. Chem. Soc., Div. Fuel Chem., Prepr.,1993, 38(3), 823-830.
(7) K. Liu, H.L.C. Meuzelaar, Fuel Processing Technology, 1996, 49, 1-15.

Acknowledgements

The authors are grateful to Dr L.L.Anderson for helpful advice, discussions as well as Drs Wender, Shabtai, and XinXiao for preparing the superacid catalysts. This work was supported by the U.S. Department of Energy through the Consortium for Fossil Fuel Liquefaction Science (Grant No. UKRF-4-43576-90-10).

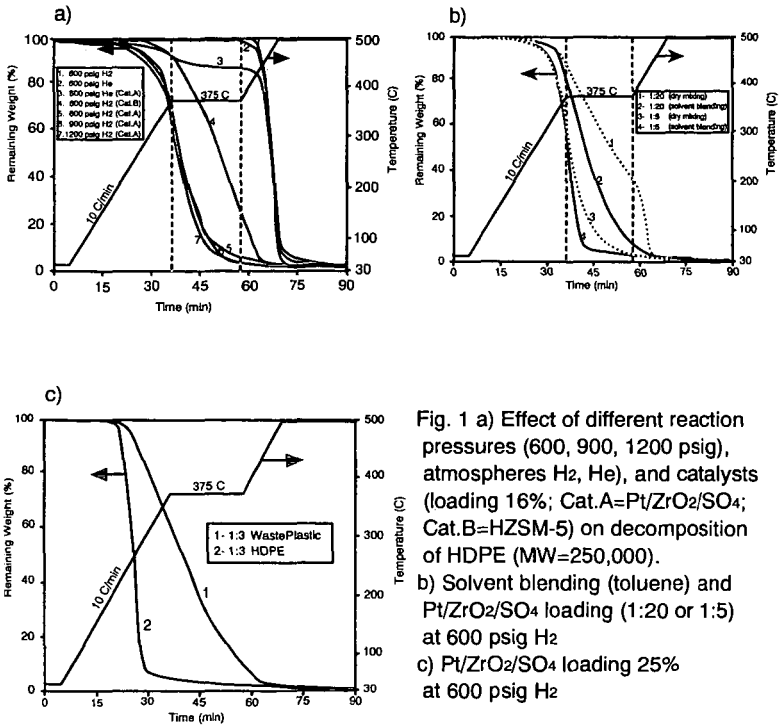

Fig. 1 a) Effect of different reaction pressures (600, 900, 1200 psig), atmospheres H_2, He), and catalysts (loading 16%; Cat.A=Pt/ZrO_2/SO_4; Cat.B=HZSM-5) on decomposition of HDPE (MW=250,000).
b) Solvent blending (toluene) and Pt/ZrO_2/SO_4 loading (1:20 or 1:5) at 600 psig H_2
c) Pt/ZrO_2/SO_4 loading 25% at 600 psig H_2

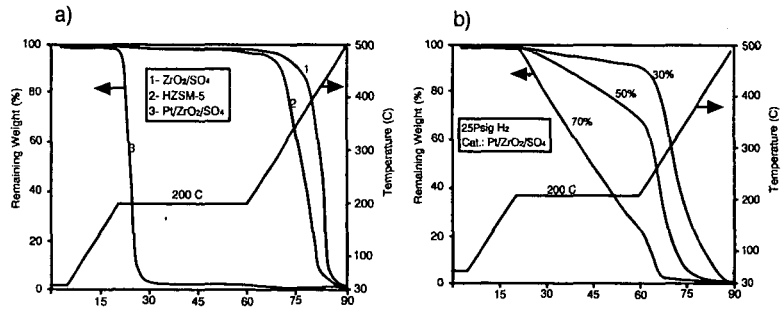

Fig. 2 a) Effect of different catalysts at 50% loading at 600 psig H_2.
b) Effect of different catalyst loadings at 25 psig H_2.

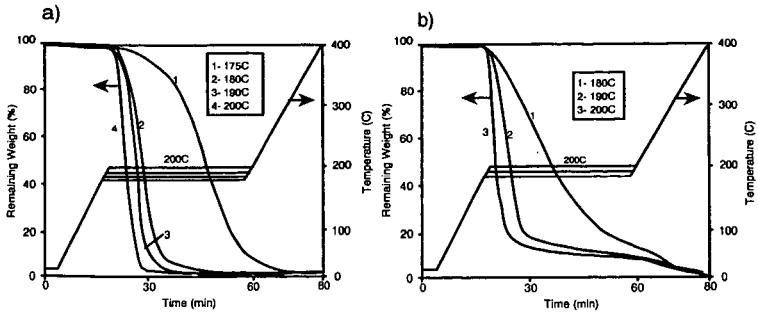

Fig. 3 Effect of temperature on degradation of different HDPEs at 600 psig H_2 with $Pt/ZrO_2/SO_4$ loading 50%
a) HTI HDPE(MW=250,000), b) Aldrich HDPE(MW=125,000)

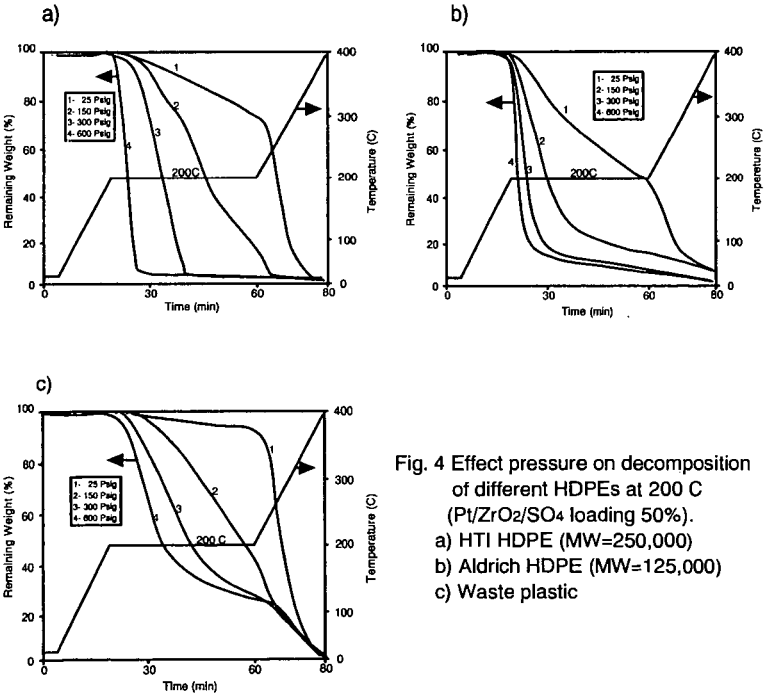

Fig. 4 Effect pressure on decomposition of different HDPEs at 200 C ($Pt/ZrO_2/SO_4$ loading 50%).
a) HTI HDPE (MW=250,000)
b) Aldrich HDPE (MW=125,000)
c) Waste plastic

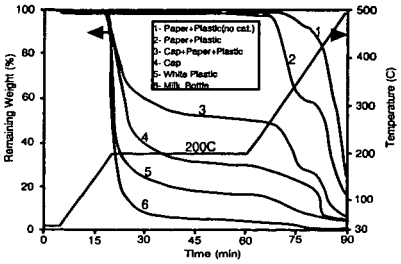

Fig. 5 TG profiles for decomposition of components of waste plastic at $Pt/ZrO_2/SO_4$ loading 50% (except 1)

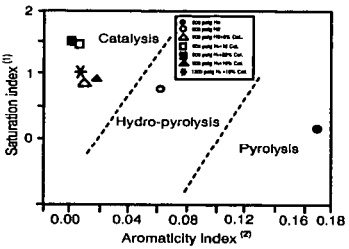

Fig. 6 Comparison of evolution product's saturation and aromaticity with different $Pt/ZrO_2/SO_4$ catalyst loadings and pressures

(1) (m/z77+m/z91)/(m/z43+m/z57)

(2) (m/z43+m/z57)/(m/z41+m/z55)

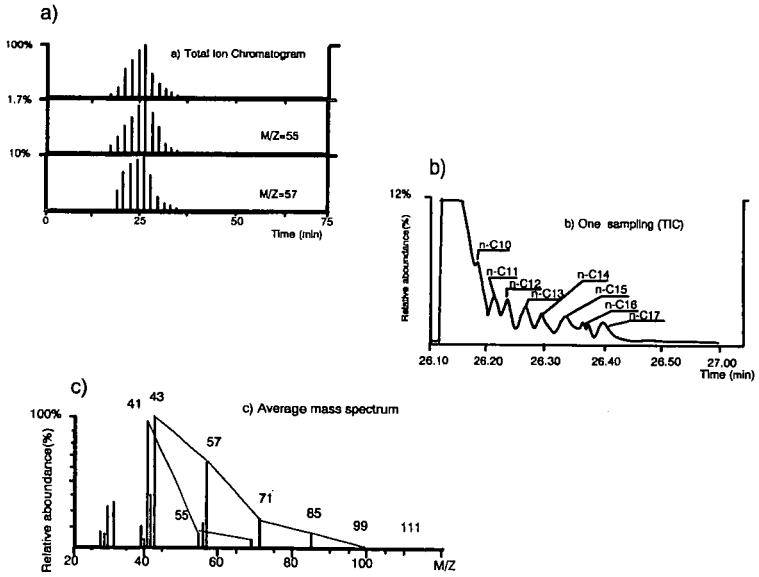

Fig. 7 GC/MS analysis corresponding to Curve 3 in Fig. 2a.

a) Total ion chromatogram.

b) Total ion chromatogram for one sampling interval.

c) Average mass spectrum from 15 to 37 minute from 7a.

AN INTEGRATED APPROACH TO THE RECOVERY OF FUELS AND CHEMICALS FROM MIXED WASTE CARPETS THROUGH THERMOCATALYTIC PROCESSING

Carolyn C. Elam, Robert J. Evans, and Stefan Czernik
National Renewable Energy Laboratory
1617 Cole Boulevard, Golden, Colorado 80401

Keywords: Waste Carpet Recycling, Plastic Recycling, Pyrolysis

INTRODUCTION

The recovery of value from the growing volume of mixed polymers in post-consumer waste presents technical and economic challenges when compared to the typical methods of disposal by landfilling and mass burning, which have raised some environmental concerns. Included with typical polymer waste, which currently ends up in landfills, is nearly 3 billion pounds of carpet per year. The high value of the nylon-6, nylon-6/6, and polyester face fiber material is an incentive for their recovery. However, the nature of the carpet construction (face fiber woven into a mixed polymer and inorganic backing material) makes typical recycling methods, such as regrind and remelt, impractical and uneconomical. Integrated, thermocatalytic processing, starting with selective catalytic pyrolysis to recover the high value monomers and followed by gasification of the residual material to generate process energy, is an approach which has shown great promise for recovering the maximum value from this current waste stream.

Selective pyrolysis is a catalytic, thermal technique which optimize the differences in pyrolysis reaction rates. The pre-sorting requirements for feedstock preparation and the isolation and purification of pyrolysis products are minimized by controlling reaction conditions so that target products can be collected directly in high yields from the waste stream.[1] Figure 1 shows the approach used in this work, which has three major components: (1) identifying target waste streams, (2) developing techniques for the control of conversion processes, and (3) targeting the recovery of high-value chemicals, which are recovered in economically attractive yields. Technoeconomic assessments are used throughout the development process to characterize potential waste streams, identify areas in which improvements can be made, evaluate the overall economic attractiveness of the technology, and compare the technology to competing technologies.

Target wastes include both high-value and high-volume systems. Examples of high-value wastes include the recovery of caprolactam from nylon-6 and bisphenol-A from polycarbonate, both of which currently sell for greater that $0.70 per pound. High-volume wastes include mixed bottles and residential waste. The high-volume wastes are of great importance, but the economics are not favorable due to the low value, generally less than $0.15 per pound, of the monomers and chemicals which can be recovered.

In the initial stages of the work, numerous small scale screening experiments are necessary to identify the appropriate catalyst(s) and conditions to optimize the separation and recovery for each of the waste streams. Milligram scale experiments can be studied using pyrolysis molecular beam mass spectrometer (MBMS). The effective quenching of species in their sampled state through free-jet expansion makes MBMS a valuable tool for identifying pyrolysis products.[2,3] Figure 2 shows a schematic of the MBMS used for these experiments. Milligram samples of the plastics are thoroughly mixed with catalyst in a small metal boat. The boat is subsequently inserted into a furnace where hot helium gas is used to sweep the pyrolysis vapors through the reactor. A portion of the vapors are expanded across the stage one orifice on the apex of a cone. The orifice is the entrance to a low-pressure chamber and the pressure difference is sufficient for free-jet expansion, which preserves both light and heavy compounds produced upon pyrolysis. A second expansion collimates a molecular beam, which is introduced into the ion source of the mass spectrometer.

Unlike other pyrolysis-mass spectrometric techniques, large samples can be employed in MBMS studies. The product evolution curves for four of the major packaging plastics are shown in Figure 3. The mixture of pure plastics was pyrolyzed by heating at a rate

of 40°C/min in flowing helium. The rates of product evolution are shown by the key ion current curves that represent major products from each polymer. The times of maximum product evolution for each polymer are different. This suggests that by use of a controlled heating rate, resolution of the individual polymer pyrolysis products may be possible, even for a complex, mixed, plastic waste stream. The PET-derived terephthalic acid (TPA) curve shows two maxima: the first at ~350°C and the second at ~450°C. The first maximum is the result of acid-catalyzed product formation. This demonstrates how a catalyst can be used to selectively influence the rate of product formation and allow the separation of product formation from other components of a mixture.

Once the range of conditions has been sufficiently narrowed, bench-scale experiments can be performed using a stirred-batch or two inch fluidized bed reactor to enable product collection and analysis via conventional analytical techniques. A two inch glass fluidized bed reactor with a heated vacuum shroud enables observation of the melting characteristics of the material as it moves through the fluidizing medium, quickly identifying and heat or mass transfer limitations. After the conditions have been optimized in the two inch reactor, the process is transferred to a continuously fed, engineering scale, four inch fluidized bed reactor. This reactor allows for careful monitoring of temperature and pressure drops. Bed withdrawal enables the reactor to be run in a continuous mode. Validation of the process at this level enables the scale-up to a process development unit (25 kg/hour).

TECHNOLOGY STATUS

The selective pyrolysis technique has been demonstrated on recovering caprolactam, the monomer of nylon-6, from nylon-6 face fiber carpet, which currently accounts for around 30% of the carpet produced in the United States. A catalyst system allows caprolactam to be recovered at a lower temperature, leaving the polypropylene backing material and the styrene butadiene latex unreacted. Figure 4 shows a ramp and hold experiment, monitored by the MBMS, where nylon-6 and polypropylene are mixed in a steel boat with the catalyst. While the temperature is held around 400°C, caprolactam from the depolymerization of nylon-6 is cleanly recovered. Subsequent heating of the sample pyrolyzes the polypropylene and demonstrates that all of the nylon-6 was depolymerized at the lower temperature. Additional catalyst screening identified a catalyst system which improved the depolymerization further, allowing the reaction temperature to be lowered while maintaining a rapid, clean separation of the components.

Continuous tests were performed in a four inch fluidized bed reactor, using shredded whole carpet, and resulted in reproducible caprolactam yields of 85%. Economic analyses performed independently by industry representatives have shown that high purity caprolactam can be recovered from waste nylon-6 carpet for around $0.50 per pound for a plant which produces 100 million pounds of caprolactam per year. This estimate encompasses the complete process from collection to product purification and assumes that the polypropylene and styrene butadiene used in the carpet backing will be burned for process heat. The major contributor to the production cost is the price for collection and sorting which accounts for around half of the production cost (~$0.25 per pound of caprolactam produced).

Other applications of the selective pyrolysis technology which have been or are being studied include: recovering dimethyl terephthalate (DMT) from PET containing waste streams, such as polyester carpets, mixed bottles and polyester/cotton fabric blends; bisphenol-A from polycarbonate containing wastes, principally electronics; diisocyanates or diamines from polyurethanes, both methylene and toluene based, from both automotive and appliance applications; phenol, cresol, and xylenol from phenolic resins; and styrene from polystyrene containing residential waste. The PET application is the furthest advanced (after the nylon-6 application). Two inch fluidized reactor results have shown that DMT is recovered from pure PET and mixed PET and polypropylene in yields of greater that 85% when methanol is used as a coreactant in conjunction with the catalytic selective pyrolysis. DMT can also be recovered from waste polyester fabric at comparable yields.

FUTURE WORK

Current efforts have turned to addressing the problem of the other face fiber materials, nylon-6/6 and PET. The ultimate goal will be to eliminate the need to sort the carpet by face fiber material. It is envisioned that by combining selective pyrolysis with novel purification and separation techniques, all carpets can be pyrolyzed simultaneously while maintaining the ability to separate and recover the valuable. The remaining material, both the backing material and the polyethylene and polypropylene face fiber carpet, will be combusted to fuel the process. An alternative to simply burning the low value material for process energy is to gasify it to produce a clean synthesis gas. This synthesis gas can be used as a feedstock for the production of a wide range of chemicals.

Successful demonstration of the selective pyrolysis approach to handling mixed carpets will be expanded to a complete "Flexible Chemical Processing" technique, wherein any type of plastic waste will be handled at a single processing plant. Minimal on-sight sorting will be used to group high-value wastes which can undergo selective pyrolysis to recover the monomers or other high-value chemicals. The remaining waste can be gasified to recover synthesis gas. A portion of the synthesis gas will be used to supply energy for the plant, while the remaining will be converted to chemicals, such as methanol, further lessening the demand for petroleum feedstocks. It is estimated that approximately 10 billion pounds of textile, automotive, and home furnishings waste is available for collection per year. Currently, there are at least 25 major cities in the United States which could support a 200 million pound per year processing plant, resulting not only in an economic way to significantly reduced waste, but also in an energy savings of approximately 7 trillion Btu per year per plant.

CONCLUSIONS

Selective pyrolysis is a diverse technology which has shown promise for being able to recover high-value products from complex mixed plastic waste streams. The ability to recover caprolactam from waste nylon-6 carpet has been demonstrated to be both feasible and economical at the engineering scale. This technology combined with novel purification technology has the potential to significantly reduce the nearly 3 billion pounds of annual carpet waste. More importantly, high-value products like caprolactam, which sells for around $0.70 per pounds, are obtained and can be purified to the same grade as virgin material, lessening the demand for petroleum feedstock. Further expansion of this technology will yield the ability to handle even larger plastic waste streams including other textiles, home furnishings, automotive dismantling residue, and residential wastes.

REFERENCES

1. Evans, R.J.; Tatsumoto, K.; Czernik, S.; and Chum, H.L., "Innovative Pyrolytic Approaches to the Recycling of Plastics to Monomers", Proceedings of the RecyclingPlas VII Conference: Plastics Recycling as a Business Opportunity, 175 (1992).

2. Atomic and Molecular Beams, Vol. 1, G. Scoles, ed., Oxford University Press, New York, 14-53 (1988).

3. Evans, R.J. and Milne, T.A., Energy & Fuels, 1(2), 123 (1987); 1(4), 311 (1987).

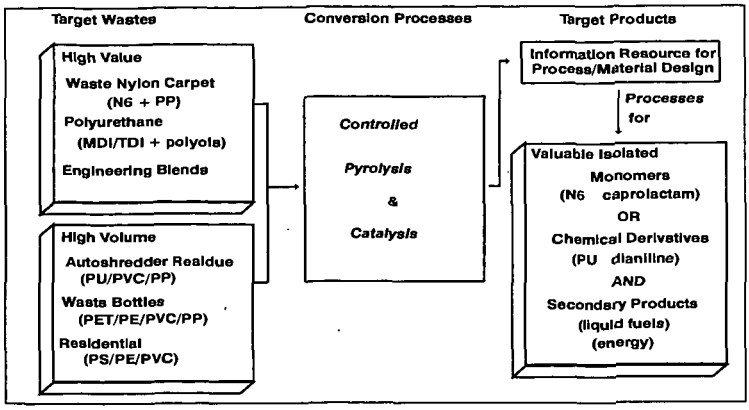

Figure 1. Overview of the NREL approach to the chemical recycling of mixed plastics.

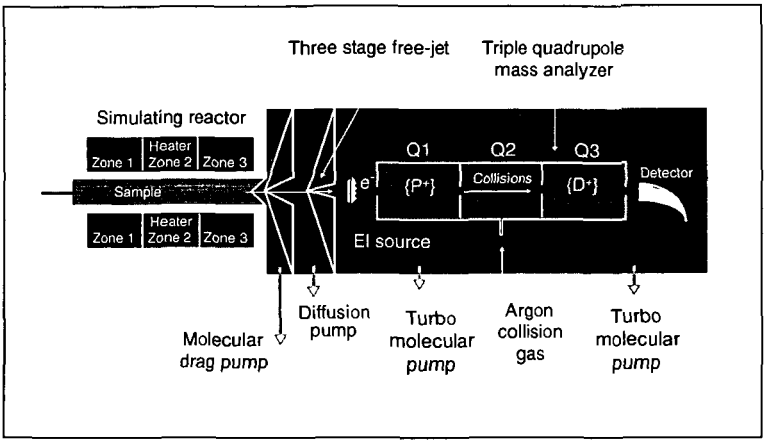

Figure 2. Schematic of Molecular Beam Mass Spectrometric (MBMS) sampling system.

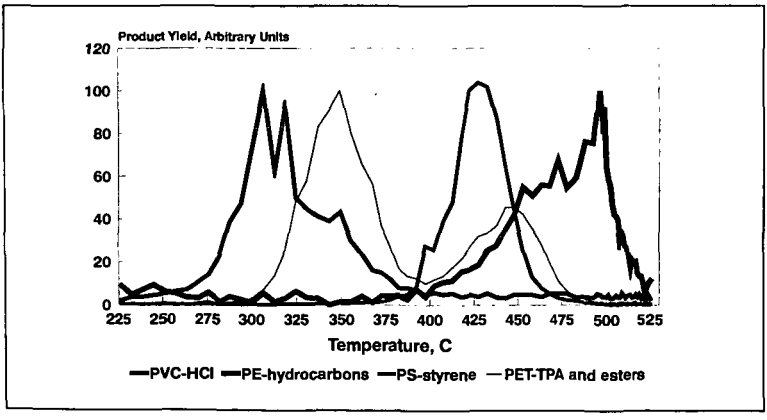

Figure 3. Relative rates of pyrolysis for the four components of a mixture are shown in the time-resolved profile plots of key ion for each polymer: PET - m/z 166, terephthalic acid; polystyrene (PS) - m/z 104, styrene; polyethylene (PE) - m/z 69, $C_5H_9^+$, a typical fragment ion of alkenes; and polyvinylchloride (PVC) - m/z 36, HCl.

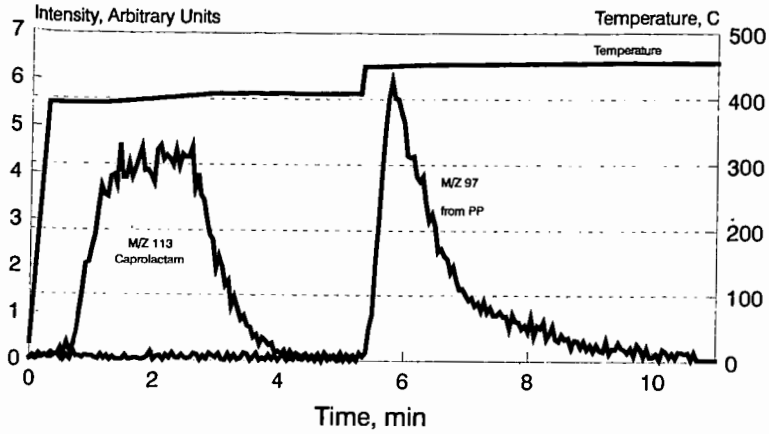

Figure 4. The application of catalytic techniques allows the separation of nylon-6 derived caprolactam from polypropylene derived hydrocarbons.

DISTRIBUTION KINETICS OF DEGRADING POLYMER MIXTURES

Giridhar Madras and Ben J. McCoy
Department of Chemical Engineering and Materials Science
University of California, Davis, CA 95616
email: bjmccoy@ucdavis.edu

ABSTRACT

Disposal of plastic waste is a worldwide problem that has prompted investigation of plastics recycling, including thermolysis methods. Most basic research on degradation, however, is for single polymers. Waste streams usually contain mixtures of polymers and it may be costly to separate them prior to degradation. Degradation rates depend on the mixture type, and adding another polymer can increase, decrease, or leave unchanged the degradation rate of the first polymer. Determining the decomposition mechanisms for polymer mixtures is of great interest for polymer recycling. In this study, we present techniques to determine the degradation kinetics of solubilized binary polymer mixtures by examining the time evolution of molecular-weight distributions (MWDs). Because the reaction mechanism for polymer degradation involves radicals, we have developed an approach that accounts for the elementary reactions of initiation, termination, hydrogen abstraction, and chain scission. We determined the concentration effect of poly(α-methyl styrene) (PAMS) on the random-chain degradation of polystyrene dissolved in mineral oil at 275 °C in a batch reactor by evaluating the time evolution of the MWDs. Molecular-weight moments yielded expressions for the number- and weight-average MW and degradation rate coefficients. The experimental data indicated that the interaction of mixed radicals with polymer by hydrogen abstraction caused the random-chain scission degradation rate of polystyrene to decrease with increasing PAMS concentration.

INTRODUCTION

The rate of polymer degradation can be modified by the addition of conventional free-radical initiators, oxidizers or hydrogen donors but it might be easier to alter the degradation rate by blending two polymers (Gardner et al., 1993). Degradation studies by pyrolysis of polymer mixtures have reported varied results. For example, some reports indicated a significant interaction between polystyrene and polyethylene (Koo and Kim, 1993; Koo et al., 1991; McCaffrey et al., 1996), while others observed no interaction between these polymers (Roy et al., 1978; Wu et al., 1993). The pyrolytic polystyrene degradation rate was significantly enhanced in the presence of poly(methyl acrylate) and poly(butyl acrylate) at 430 °C (Gardner et al., 1993). Richards and Salter (1964), on the other hand, observed that the rate of polystyrene degradation decreased with increasing molecular weight (MW) of added PAMS. These reports suggest the need for an analysis of the underlying reaction mechanisms.

Degradation of polymers in solution has been proposed to ameliorate problems encountered in commercial applications (Sato et al., 1990). The degradation of polystyrene (Murakata et al., 1993; Madras et al., 1996c), poly(styrene-allyl alcohol) (Wang et al., 1995), poly(methyl methacrylate) (Madras et al., 1996a), PAMS (Madras et al., 1996b) in solution have been investigated. No studies on the degradation of polymer mixtures in solution, however, have been reported.

EXPERIMENTS

The HPLC (Hewlett-Packard 1050) system consists of a 100 μL sample loop, a gradient pump, and an on-line variable wavelength ultraviolet (UV) detector. Three PLgel columns (Polymer Lab Inc.) (300 mm x 7.5 mm) packed with cross-linked poly(styrene-divinyl benzene) with pore sizes of 100, 500, and 10,000 Å are used in series. Tetrahydrofuran (HPLC grade, Fisher Chemicals) was pumped at a constant flow rate of 1.00 mL/min. Narrow MW polystyrene standards of MW 162 to 0.93 million (Polymer Lab and Aldrich Chemicals) were used to obtain the calibration curve of retention time versus MW, which was stable during the period of the experiments. The calibration curve, modeled as a second-order polynomial, indicates a higher accuracy in the measurement of lower MW polymers.

The thermal decomposition of polystyrene in mineral oil was conducted in a 100 mL flask equipped with a reflux condenser to ensure the condensation and retention of volatiles. To observe a significant effect of PAMS on the conversion, polystyrene of high MW was chosen. 60 mL of mineral oil (Fisher Chemicals) was heated to 275 °C, and various amounts (0 - 0.60 g) of monodisperse PAMS (MW = 11,000, Scientific Polymer Products), and 0.12 g of monodisperse polystyrene (MW = 330,000, Aldrich Chemicals) were added. The temperature of the solution was measured with a Type K thermocouple (Fisher Chemicals) and controlled within ± 1 °C by a Omega CN-2042 temperature controller. Samples of 1.0 mL were taken at 15 minute intervals and dissolved in 1.0 mL of tetrahydrofuran (HPLC grade, Fisher Chemicals). The chromatograph obtained by injecting 100 μL of this solution into the HPLC-GPC system was converted to MWD. The peaks of the reacted polystyrene, PAMS, and the oligomers were distinct, so that moments could be calculated by numerical integration. Because the solvent mineral oil is UV invisible, its MWD was determined with a refractive index (RI)

detector. No change in the MWD of mineral oil was observed when the oil was heated for 3 hours at 275 °C without polystyrene.

THEORETICAL MODEL

According to the Rice-Herzfeld mechanism, polymers can transform without change in MW by hydrogen abstraction. Their radicals can also undergo chain scission to form lower MW products, or undergo addition reactions yielding higher MW products. Chain scission can occur either at the chain end yielding a specific product, or at a random position along the chain yielding a range of lower MW products.

In the present treatment, two common assumptions simplify the governing equations. The long-chain approximation (LCA) (Nigam et al., 1994; Gavalas, 1966) postulates that the initiation and termination rates are negligible because such events are infrequent compared to hydrogen abstraction and propagation-depropagation chain reactions. The quasi-stationary state approximation (QSSA) applies when radical concentrations are extremely small and their rates of change are negligible. The proposed scheme, based on the Rice-Herzfeld concept (Nigam et al., 1994) of chain reactions, includes the important elementary steps involving radicals.

The degradation rate of polymer A undergoing random-chain scission is influenced by polymer B undergoing chain-end scission. We represent the reacting polymer A and its radicals as $P_A(x)$ and $R^{\bullet}(x)$ and their MWDs as $p_A(x,t)$ and $r(x,t)$, respectively, where x represents the continuous variable, MW. As the polymer reactants and random scission products are not distinguished in the distribution kinetics model, a single MWD, $p_A(x,t)$, represents the polymer in the mixture at any time, t. The initiation-termination reactions are represented as

$$P_A(x) \underset{k_t}{\overset{k_f}{\Leftrightarrow}} R^{\bullet}(x') + R^{\bullet}(x-x') \tag{1}$$

where $\Leftrightarrow$ represents a reversible reaction. The reversible hydrogen abstraction process is

$$P_A(x) \underset{k_H}{\overset{k_h}{\Leftrightarrow}} R^{\bullet}(x) \tag{2}$$

The depropagation chain reaction is

$$R^{\bullet}(x) \overset{k_b}{\rightarrow} P_A(x') + R^{\bullet}(x-x') \tag{3}$$

The polymer B, the chain-end radical, the specific radical, and the specific product are represented as $P_B(x)$, $R_e^{\bullet}(x)$, $R_s^{\bullet}(x)$, $Q_s(x_s)$, respectively, and their corresponding MWDs as $p_B(x,t)$, $r_e(x,t)$, $r_s(x,t)$ and $q_s(x_s,t)$. The formation of chain-end radicals by a reversible random-scission initiation-termination reaction is

$$P_B(x) \underset{k_{ts}}{\overset{k_{fs}}{\Leftrightarrow}} R_e^{\bullet}(x) + R_e^{\bullet}(x - x') \tag{4}$$

Hydrogen abstraction by the chain-end radical is considered reversible,

$$P_B(x) \underset{k_{He}}{\overset{k_{he}}{\Leftrightarrow}} R_e^{\bullet}(x) \tag{5}$$

The chain-end radical can undergo radical isomerization via a cyclic transition state to form a specific radical,

$$R_e^{\bullet}(x) \underset{k_{iH}}{\overset{k_{ih}}{\Leftrightarrow}} R_s^{\bullet}(x) \tag{6}$$

The depropagation reaction yields the specific product and a chain-end radical from a specific radical,

$$R_s^{\bullet}(x) \overset{k_{bs}}{\rightarrow} Q_s(x_s) + R_e^{\bullet}(x-x_s) \tag{7}$$

where x_s is the MW of the specific product.

The interaction of the two degrading polymers is through hydrogen abstraction (McCaffrey et al., 1996) represented as a reversible disproportionation reaction. The end radical of polymer B combines with polymer A to form an intermediate radical complex that undergoes transformation to polymer B and a radical of polymer A,

$$R_e^{\bullet}(x) + P_A(x') \underset{k_D}{\overset{k_d}{\Leftrightarrow}} R_i^{\bullet}(x + x') \underset{k_d}{\overset{k_D}{\Leftrightarrow}} P_B(x) + R^{\bullet}(x') \tag{8}$$

Including the intermediate complex, R_i^*, facilitates the formulation of the population balance equations for the reversible disproportionation. If R_i^* is ignored in equation 1.8, the forward and reverse rate coefficients would be k_d and k_D, respectively.

With the aid of Table 1, the rate expressions and moments can be formulated. Based on LCA, k_f, k_{fs}, k_t and k_{ts} are set to zero. The zeroth moments for the polymer, radicals and the monomer, $p^{(0)}$, $r^{(0)}$, $q^{(0)}$ are defined as

$$p^{(0)}(t) = \int_0^\infty p(x,t)\,dx \tag{9}$$

$$r^{(0)}(t) = \int_0^\infty r(x,t)\,dx \tag{10}$$

$$q^{(0)}(t) = \int_0^\infty q(x,t)\,dx \tag{11}$$

The initial conditions for moments are

$$p_B^{(0)}(t=0) = p_{B0}^{(0)},\ p_A^{(0)}(t=0) = p_{A0}^{(0)} \text{ and } r^{(0)}(t=0) = 0 \tag{12}$$

When QSSA holds,

$$dr^{(0)}/dt = dr_s^{(0)}/dt = dr_e^{(0)}/dt = dr_i^{(0)}/dt = 0 \tag{13}$$

Algebraic manipulations yield

$$p_A^{(0)}(t) = p_{A0}^{(0)} \exp(k_r t) \tag{14}$$

and a plot of $\ln(p^{(0)}/p_0^{(0)})$ is linear in time with slope k_r,

$$k_r = (2\,k_b\,k_h / (k_d\,p_{B0}^{(0)})) + k_b\,(k_{be}+k_h)/k_H \tag{15}$$

The molar concentration is related to the mass concentration, $p^{(1)} = M_n p^{(0)}$, by the average MW, M_n.

The proposed mechanism represents the interaction of radicals of two reacting polymers and shows how the polymer undergoing chain-end scission affects the degradation rate of the polymer undergoing random-chain scission. The degradation rate coefficient is a function of the added polymer concentration, and also depends on the temperature and pressure. This can explain the varied results found in experiments for degradation rates in polymer mixtures.

RESULTS

We have measured the influence of PAMS mass concentration on polystyrene degradation at 275 °C. Because polystyrene degrades by random-chain scission and PAMS degrades by chain-end scission, the polystyrene degradation rate is given by Eqs 14 and 15. The random-scission degradation rate coefficient, k_r, was determined from the experimental data by analyzing the time dependence of the polymer-mixture MWDs. Because the mass of specific products formed by polystyrene chain-end scission at 275 °C for 10 hours is less than 2% (Madras et al., 1996c), we consider that polystyrene degrades solely by random-chain scission.

Polystyrene degrades rapidly at low reaction times due to weak links in the polymer chain caused by side-group asymmetry or chain-branching (Chiantore et al., 1981; Madras et al., 1996c). The weak and strong links in polystyrene can be represented by additive distributions, so that the total molar concentration, $p_{Atot}^{(0)}$, of the polymer is the sum of the molar concentrations of the weak, $p_{Aw}^{(0)}$, and strong links, $p_A^{(0)}$ (Madras et al., 1996c). As the weak link concentration is approximately two orders of magnitude smaller than the strong link concentration, only the random rate coefficients of strong links are examined in this study. The initial molar concentration of the strong links in polystyrene, $p_{A0}^{(0)}$, is determined from the intercept of the regressed line of the $p_{Atot}^{(0)}/p_{Atot0}^{(0)}$ data for $t \geq 45$ minutes (Figure 1). The slopes, corresponding to the rate coefficient for random scission, k_r, are determined from the plot of $\ln(p_A^{(0)}/p_{A0}^{(0)})$ versus time, as given by Eq 14. Madras et al. (1997) show how data are analyzed when the polystyrene degradation rate coefficient is a function of MW, i.e., $k_r(x)$. Equation 15 explains how the polystyrene degradation rate coefficient depends on PAMS concentration. The polystyrene degradation rate coefficient, k_r, decreases with increasing PAMS mass (or molar) concentration. This is consistent with the experimental data (Figure 2 and inset).

The hypothesized interaction of the degrading polymers is through the free radicals and their rates of hydrogen abstraction. When $k_d = k_D = 0$, the two polymers react independently and the moment equations are identical to those derived for a single polymer undergoing chain-end scission or random-chain scission (Madras and McCoy, 1997). The rate coefficient for random-chain scission of polystyrene is a function of the PAMS mixture concentration through the fundamental radical rate parameters, k_b, k_h, k_{be}, k_d, k_H, and the initial number-average molecular weight of PAMS (Eq 15). The addition of PAMS inhibits the random-chain scission of polystyrene, similar to the effect on hydrogen-donors on the degradation of polystyrene (Madras and McCoy, 1997).

ACKNOWLEDGEMENTS

The financial support of Pittsburgh Energy Technology Center Grant No. DOE DE-FG22-94PC94204 and EPA Grant No. CR 822990-01-0 is gratefully acknowledged.

REFERENCES

Chiantore, O.; Camino, G.; Costa, L.; Grassie, N., "Weak Links in Polystyrene," *Poly. Deg. and Stab.*, **3**, 209 (1981).

Gardner, P.; R. Lehrle; D. Turner, Polymer Degradation Modified by Blending with Polymers Chosen on the Basis of Their Φ-Factors," *J. Anal. Appl. Pyr.*, **25**, 11 (1993).

Gavalas, G. R., "The Long Chain Approximation in Free Radical Reaction Systems, " *Chem. Eng. Sci.*, **21**, 133 (1966).

Koo, J.K. , S.W. Kim, Y. H.. Seo, "Characterization of Aromatic Hydrocarbon Formation From Pyrolysis of Polyethylene-Polystyrene Mixtures," *Resources, Conservation and Recycling*, **5**, 365 (1991).

Koo, J.K. , S.W. Kim, "Reaction Kinetic Model for Optimal Pyrolysis of Plastic Waste Mixtures," *Waste Management and Research*, **11**, 515 (1993).

Madras, G., J.M. Smith, B.J. McCoy, "Effect of Tetralin on the Degradation of Polymer in Solution," *I&EC Research*, **34**, 4222 (1995).

Madras, G., J.M. Smith, B.J. McCoy, "Degradation of Poly(Methyl Methacrylate) in Solution," *I&EC Research*, **35**, 1795 (1996a).

Madras, G., J.M. Smith, B.J. McCoy, "Thermal Degradation of Poly(α-Methylstyrene) in Solution," *Poly. Deg. and Stab.*, **52**, 349 (1996b).

Madras, G., J.M. Smith, B.J. McCoy, "Thermal Degradation Kinetics of Polystyrene in Solution," *Poly. Deg. and Stab.*, (1996c); In press.

Madras, G., G.Y. Chung, J.M. Smith, B.J. McCoy, "Molecular Weight Effect on the Dynamics Of Polystyrene Degradation," *I&EC Research*, (1997); In press.

McCaffrey, W.C., Brues, M.J.; Cooper, D.G.; Kamal, M.R., "Thermolysis of Polyethylene Polystyrene Mixtures," *J. App. Poly. Sci.*, **60**, 2133 (1996).

Murakata, T.; Saito, Y.; Yosikawa, T.; Suzuki, T.; Sato, S. "Solvent Effect on Thermal Degradation of Polystrene and Poly-α -methylstyrene," *Polymer*, **34**, 1436 (1993).

Nigam, A; Fake, D. M; Klein M.T. "Simple Approximate Rate Law for Both Short-Chain and Long Chain Rice Herzfeld Kinetics," *AIChE J.*, **40**, 908 (1994).

Richards, D. H., and Salter, D.A., "Thermal Degradation of Vinyl Polymers I--Thermal Degradation of Polystyrene-Poly(a-methylstyrene) Mixtures," Polymer 8, 127 (1967).

Roy, M.; Rollin, A.L.; Schreiber, H.P. "Value Recovery from Polymer Wastes by Pyrolysis," *Poly. Eng. Sci.*, **18**, 721 (1978).

Sato, S.; Murakata, T.; Baba, S.; Saito, Y.; Watanabe, S. "Solvent Effect on Thermal Degradation of Polystyrene," *J. Appl. Poly. Sci.*, **40**, 2065 (1990).

Wang, M., J.M. Smith, B.J. McCoy, "Continuous Kinetics for Thermal Degradation of Polymer in Solution," *AIChE J.*, **41**, 1521 (1995).

Wu, C.H.; Chang, C. Y.; Hor, J.L.; Shih, S.M.; Chen, L.W.; Chang, F.W., "On the Thermal Treatment of Plastic Mixture: Pyrolysis Kinetics," *Waste Management*, **13**, 221 (1993).

Table 1. Distribution Kinetics of Primary Reactions.

Stoichiometric kernels: $\Omega(x,x') = 1/x'$, $\Omega(x_S, x') = \delta(x-x_S)$, $\Omega(x-x_S, x') = \delta[x-(x'-x_S)]$

Reaction Type	Primary Reaction	Rate Expressions	Moment Expressions (k is independent of MW)
Trans-formation	$R(x) \rightarrow P(x)$	$\partial p/\partial t = -\partial r/\partial t = k\, r(x,t)$	$dp^{(n)}/dt = -dr^{(n)}/dt = k\, r^{(n)}(t)$
Random-chain scission	$P(x') \rightarrow Q(x) + R(x' - x)$	$\partial p/\partial t = -k\, p(x,t)$ $\partial q/\partial t = k \int_x^\infty p(x',t)\, \Omega(x,x')\, dx'$ $= \partial r/\partial t$	$dp^{(n)}/dt = -k\, p^{(n)}(t)$ $dq^{(n)}/dt = k\, p^{(n)}(t)/(n+1)$ $= dr^{(n)}/dt$
Chain-end scission	$P(x') \rightarrow Q(x_S) + R(x' - x_S)$ x_S is the MW of the specific product	$\partial p/\partial t = -k\, p(x',t)$ $\partial q/\partial t = k \int_x^\infty p(x',t)\, \Omega(x_S, x')\, dx'$ $\partial r/\partial t = k \int_x^\infty p(x',t)\, \Omega(x-x_S, x')\, dx'$	$dp^{(n)}/dt = -k\, p^{(n)}(t)$ $dq^{(n)}/dt = -k\, x_S^n\, q^{(0)}(t)$ $dr^{(n)}/dt = k \sum_{j=0}^{n} \binom{n}{j} x_s^j (-1)^j p^{(n-j)}$
Addition reaction	$P(x') + Q(x - x') \rightarrow R(x)$	$\partial p/\partial t = -k\, p(x,t) \int_0^\infty q(x',t)\, dx'$ $\partial q/\partial t = -k\, q(x,t) \int_0^\infty p(x',t)\, dx'$ $\partial r/\partial t = k \int_0^x p(x',t)\, q(x - x',t)\, dx'$	$dp^{(n)}/dt = -k\, p^{(n)}(t)\, q^{(0)}(t)$ $dq^{(n)}/dt = -k\, q^{(n)}(t)\, p^{(0)}(t)$ $dr^{(n)}/dt = k \sum_{j=0}^{n} \binom{n}{j} p^{(j)}(t)\, q^{(n-j)}$

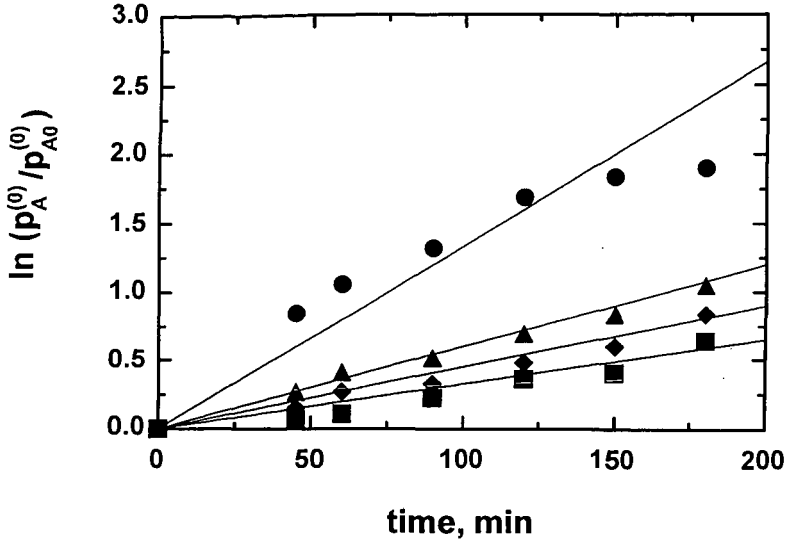

Figure 1. Plot of ln ($p_A^{(0)}/p_{A0}^{(0)}$) versus time for polystyrene degradation at 275 °C for four PAMS concentrations.
● Polystyrene (2/L) only; ▲ Polystyrene (2 g/L) + PAMS (2 g/L); ◆ Polystyrene (2 g/L) + PAMS (5 g/L); ■ Polystyrene (2 g/L) + PAMS (10 g/L).

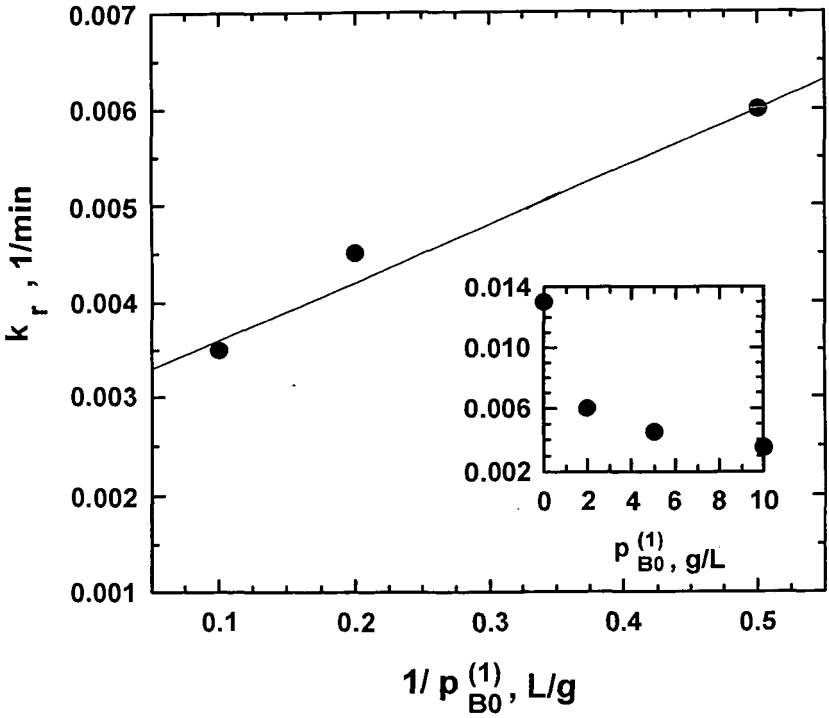

Figure 2. Effect of PAMS mass concentration, $p_{B0}^{(1)}$, on the rate coefficient of random chain scission, k_r, of polystyrene at 275 °C plotted as k_r versus 1/ $p_{B0}^{(1)}$, as given by equation 1.45. The inset shows k_r versus $p_{B0}^{(1)}$.

CONTINUOUS-DISTRIBUTION ANALYSIS FOR POLYETHYLENE DEGRADATION

Yoichi Kodera, W. S. Cha*, and B. J. McCoy*
National Institute for Resources & Environment, AIST,
16-3 Onogawa, Tsukuba, Ibaraki 305, Japan;
*Dept. of Chem. Eng. & Materials Sci., University of California, Davis, CA 95616

INTRODUCTION

A potential method for plastics recycling is to decompose the polymer to lower molecular weight products that can serve as fuel or feedstock. A free-radical mechanism has been proposed to evaluate rate coefficients based upon continuous-distribution kinetics, which provides a simple and reliable method for examining the time-dependence of molecular-weight distributions (MWDs) of reaction products [1]. Population balance equations govern the MWD dynamics for the products. The balance equations are solved by a moment method, which allows the integro-differential equations to be transformed into ordinary differential equations that are readily solved to give the rate coefficient of polymer degradation.

The present objective is to apply these ideas to polyethylene pyrolysis, which gives both random and specific products due to random-chain scission and chain-end scission, respectively. The experimental results of polyethylene pyrolysis are interpreted by the mathematical model to obtain the overall *rate* of degradation and the activation energy. Distribution balance equations for MWDs of random and specific products are proposed to account for initiation-termination and propagation-depropagation reactions, such as hydrogen abstraction, chain cleavage, recombination, disproportionation, and coupling of polymer and the corresponding radical. We will develop the present theory by assuming the rate coefficient k is independent of MW x, which is valid if the change in average MW of the polymer mixture is not too great [2]. The integro-differential governing equations are solved in terms of molecular-weight moments. The moments form a hierarchy of ordinary differential equations, which can be solved numerically up to the desired moment order, usually up to second moments. In the present treatment we invoke two common approximations and solve analytically for algebraic moment expressions. The long-chain approximation (LCA) [3,4] maintains that initiation and termination reaction events are infrequent and therefore their rates are negligible relative to hydrogen abstraction and propagation-depropagation chain reaction rates. The quasi-stationary-state approximation (QSSA) is valid when the concentration of free radicals is extremely small, so that their rate of change with time is negligible compared to other rates. For either chain-end or random-chain scission, the reversible processes reduce to irreversible decomposition reactions when the addition (repolymerization) rate coefficients are relatively very small. Previously derived and experimentally verified expressions for polymer degradation are thus recovered from the general theory.

EXPERIMENTAL

Polyethylene (2 g, Polysciences, density 0.94 g/cm^3, MW 700) was heated with a molten-salt bath in a reactor (an open glass tube placed in a stainless steel vessel) equipped with a gas outlet. Pyrolysis conditions were 390-450 °C for 1-3 h under one atmosphere pressure of nitrogen. Solid and waxy products were recovered from the reactor and the gas outlet. A stainless steel tube at the reactor outlet allowed gaseous products to be collected by water displacement in an inverted graduated cylinder. Solid and waxy products dissolved in 1,2,4-trichlorobenzene were analyzed with a HPLC-GPC (Hewlett-Packard 1050 pump, HP RI detector 1047A) equipped with a 7.5 mm x 50 mm guard column and two 7.5 mm x 300 mm columns packed with PLgel 10 mm Mixed B (Polymer Laboratories). Peak-position calibration for the MWs of polyethylene degradation products was performed with *n*-hexane, triacontane (Aldrich), and narrow MW range polyethylene standards (MW = 170 and 540; Polymer Laboratories) dissolved in 1,2,4-trichlorobenzene. Gaseous products were analyzed by GC (50-m capillary alumina column using He as a carrier gas). The MWD of the initial polyethylene has the mean MWs, M_n = 536 and M_w = 609. The degradation results of MWDs on GPC chromatograms were interpreted as the changes in zero and first moments of the products in the reactor and the gas outlet as a function of time. The mass of volatile fractions was determined as the difference between the mass of the original polyethylene and total mass of reactor residue and gaseous products. The mass of gas was calculated based on the gas volume evolved in the pyrolysis and GC analysis of gaseous products. GPC data of the volatile fraction together with the weights gave the corresponding zeroth moment (molar concentration). The random product concentration was calculated as the sum of the reactor residue and volatile fraction concentrations.

MODELING OF POLYETHYLENE DEGRADATION

The following simplified reaction scheme describes the important elementary reactions and incorporates them in a mathematical model based on continuous-distribution kinetics. We consider that polymer can react in three ways: by transforming without change in molecular-weight, by undergoing chain scission, and by combining to form higher molecular-weight compounds, where P(x) represents *n*- and *iso*-alkane and alkene, R•(x) is the

corresponding radical in the forms of both end and random radicals, and $R_s^{\bullet}(x)$ represents a precursor for a specific product $Q_s(x_s)$ of alkane and alkene. For mathematical simplicity, a single specific product is assumed. We assume that initiation and termination rates are nil because of the negligible contribution of initiation and termination to overall rate of the degradation (changes in moments in the function of time), although they are important steps in the complete Rice-Herzfeld mechanism [5]. Four reactions constitute the model:

(i) intermolecular hydrogen abstraction,

$$P(x) \underset{k_H}{\overset{k_h}{\rightleftharpoons}} R^{\bullet}(x) \qquad (A)$$

This bimolecular process is expressed as pseudo-first-order [1]. The reverse reactions represent pseudo-first-order transformations of radicals into the corresponding polymer in the presence of excess polymer as a source of hydrogen.

(ii) propagation-depropagation for random-chain scission,

$$R^{\bullet}(x) \underset{k_a}{\overset{k_b}{\rightleftharpoons}} P(x') + R^{\bullet}(x-x') \qquad (B)$$

This random-chain scission is an essential step in random degradation. The resulting 1-alkene has a random distribution in MW. The reverse reaction (recombination) is an important step for some conditions, such as polymer-melt pyrolysis for a long period or high pressure thermolysis [6].

(iii) intramolecular hydrogen abstraction in chain-end scission,

$$R^{\bullet}(x) \underset{k_{iH}}{\overset{k_{ih}}{\rightleftharpoons}} R_s^{\bullet}(x) \qquad (C)$$

The Rice-Kossiakoff mechanism [7] suggests the formation of specific products, Q_s, from the bond scission of the main chain of polymer via specific radical $R_s^{\bullet}$, where an end radical (unpaired electron at the chain-end) is converted into the corresponding specific radical. Depending on the chemical structure of polymer, 1,4-radical shift, or 1,5-radical shift via cyclic transition state, or other shifts would be possible. The driving force for the reaction C is the gain of stability of primary end-radical relative to secondary radical, or secondary end-radical relative to tertiary radical.

(iv) propagation-depropagation for chain-end scission,

$$R_s^{\bullet}(x) \underset{k_{as}}{\overset{k_{bs}}{\rightleftharpoons}} Q_s(x_s) + R^{\bullet}(x-x_s) \qquad (D)$$

One can obtain the distribution balance equations for p(x,t), radical r(x,t), and $r_s(x,t)$, and for a specific product $q_s(x_s,t)$ followed by the moment operation to yield [1]:

$$dp^{(n)}/dt = -k_h p^{(n)} + k_H r^{(n)} + k_b Z_{n0} r^{(n)} - k_a p^{(n)} r^{(0)} \qquad (1)$$

$$dq_s^{(n)}/dt = k_{bs} x_s^n r_s^{(0)} - k_{as} q_s^{(n)} r^{(0)} \qquad (2)$$

$$dr^{(n)}/dt = k_h p^{(n)} - k_H r^{(n)} - k_b r^{(n)} + k_a \sum_{j=0}^{n} \binom{n}{j} r^{(j)} p^{(n-j)} + k_b Z_{n0} r^{(n)} - k_a r^{(n)} p^{(0)}$$
$$- k_{ih} r^{(n)} + k_{iH} r_s^{(n)} + k_{bs} \sum_{j=0}^{n} \binom{n}{j} (x_s)^j (-1)^j r_s^{(n-j)} + k_{as} r^{(n)} q_s^{(0)} \qquad (3)$$

$$dr_s^{(n)}/dt = k_{ih} r^{(n)} - k_{iH} r_s^{(n)} - k_{bs} r_s^{(n)} + k_{as} \sum_{j=0}^{n} \binom{n}{j} q_s^{(j)} r^{(n-j)} \qquad (4)$$

where Z_{n0} = 1, 1/2, or 1/3 for n = 0, 1, or 2. The specific product has the unique MW x_s, so that $q_s(x,t) = q_s^{(0)}(t)\,\delta(x - x_s)$, and therefore $q_s^{(n)} = x_s^n q_s^{(0)}$. For the specific product we need to solve for the zeroth moment only. When several specific compounds are present, they are summed over s in the balance equations and the complete MWD is semi-continuous [8]. Zeroth moments (n=0; the time-dependent total molar concentration (mol/volume) of the macromolecule) are given as follows, where QSSA for radical species has been applied:

$$p^{(0)}(t) = \exp(k_d t)/[(\exp(k_d t) - 1)\, k_a/k_b + 1/p_o^{(0)}] \qquad (5)$$

$$dq_s^{(0)}/dt = k_{bs} r_s^{(0)} - k_{as} q_s^{(0)} r^{(0)}$$

$$= [k_{bs}(k_{ih} + k_{as} q_s^{(0)}) / (k_{bs} + k_{iH}) - k_{as} q_s^{(0)}] (k_h/k_H) p^{(0)} \quad (6)$$

$$q_s^{(0)}(t) = (k_{bs} k_{ih} / k_{as} k_{iH}) \{1 - [k_b / [k_b + k_a p_o^{(0)} (\exp(k_d t) - 1)]]^{(k_{as}k_{iH}/k_a(k_{bs}+k_{iH}))}\} \quad (7)$$

The equilibrium relations are found from the long time limit for the zeroth moments of the products due to random-chain scission and chain-end scission: $p^{(0)}(t \to \infty) = p_\infty^{(0)} = k_b/k_a$ and $q_s^{(0)}(t \to \infty) = q_{s\infty}^{(0)} = k_{bs} k_{ih} / k_{as} k_{iH}$. With QSSA, the summation of first moments (n = 1; the mass concentration (mass/volume)) for polymer and radicals (total mass concentration) gives $d[p^{(1)} + q_s^{(1)}]/dt = 0$ confirming the conservation of polymer mass. And $q_s^{(n)} = x_s^n q_s^{(0)}$ gives $dp^{(1)}/dt = - x_s dq_s^{(0)}/dt$. Then,

$$p^{(1)}(t) = p_o^{(0)} - x_s (k_{bs}k_{ih}/k_{as}k_{iH})\{1 - [k_b/[k_b + k_a p_o^{(0)}(\exp(k_d t) - 1)]]^{(k_{as}k_{iH}/k_a(k_{bs}+k_{iH}))}\} \quad (8)$$

$$q_s^{(1)}(t) = x_s (k_{bs}k_{ih}/k_{as}k_{iH})\{1 - [k_b/[k_b + k_a p_o^{(0)}(\exp(k_d t) - 1)]]^{(k_{as}k_{iH}/k_a(k_{bs}+k_{iH}))}\} \quad (9)$$

RESULTS AND DISCUSSION

Polyethylene pyrolysis gave both random products and specific products due to random-chain scission and chain-end scission, respectively. The reaction products were recovered in three portions as a reactor residue, a volatile component from the tubing section of the reactor, and a gas product in the gas collector. The reactor residue and the volatile fraction are interpreted as random-chain scission products based on GPC analysis because they have the MWD of smooth curves on GPC chromatograms. No specific compounds with distinct peaks were observed in the reaction mixture. To interpret the data of polyethylene pyrolysis under our experimental conditions, the reactions A through D were further simplified to the *irreversible* reactions,

$$P(x) \xrightarrow{k_d} P(x') + P(x-x') \quad (E)$$

$$P(x) \xrightarrow{k_{ds}} Q_s(x_s) + P(x-x_s) \quad (F)$$

Recombination of olefinic polymer with radical can be ignored due to the low conversion and the low possibility of the bimolecular reaction. Also, recombination of alkene as specific products with radical (Reaction D) can be ignored due to the high volatility of the specific compounds and the normal pressure of the present experiment. Applying $k_a = k_{as} = 0$ to Eqs 5 and 7 gives the zeroth moments for random product P(x) and specific product $Q_s(x_s)$:

$$p^{(0)}(t) = p_o^{(0)} \exp(k_d t) \quad (10)$$

$$q_s^{(0)}(t) = (k_{ds}/k_d) p_o^{(0)} [\exp(k_d t) - 1] \quad (11)$$

where $k_{ds} = k_{bs}k_h k_{ih} / k_H (k_{bs}+k_{iH})$.

When $k_d t \ll 1$,

$$q_s^{(0)}(t) = k_{ds} p_o^{(0)} t \quad (12)$$

Typical MWD changes of random-chain scission products at 450 °C are shown in Figure 1. Figure 2 shows $\ln[p^{(0)}/p_o^{(0)}]$ versus reaction time, in which the slopes give the rate coefficients k_d for random-chain scission at each reaction temperature. During the earliest period of the pyrolysis, the values of $\ln[p^{(0)}/p_o^{(0)}]$ increase rapidly especially at 410-450 °C. The enhanced rates for chain scission are explained as reactive C-C bonds (weak links) due to branching on the polyethylene main-chain. The calculated rate coefficients for random scission, k_d, are 0.507, 1.78, 3.14, and 5.11 ($\times 10^{-3}$ min^{-1}) at 390, 410, 430, and 450 °C, respectively, based on the reaction time 60-180 min. The activation energy, determined to be 36 kcal/mol by the Arrhenius plot, is reasonable compared with the expected value, from $k_d = k_b k_h / k_H$ in Eq 31, $E_d = E_b + E_h - E_H \approx 37$ kcal/mol ($E_b \approx 29$, $E_h \approx 8$, $E_H \approx 0$ kcal/mol). Figure 3 shows the volumetric amounts of gas evolution with reaction time. The rapid increases of the gas evolution during the first 60 min, consistent with the initial rates in Figure 2, are due to weak-link bond scission at short branches on the main chain. Volumetric amounts of the gas evolution were converted into total molar (ideal gas) concentrations of specific compounds. Eq 12 is applied to the molar concentrations of specific products of the gas evolution at the reaction time 120-180 min. The rate coefficients for chain-end scission, k_{ds}, are 4.83, 4.52, 9.12 and 11.2 ($\times 10^{-4}$ min^{-1}) at 390, 410, 430, and 450 °C, respectively, affording the activation energy for the chain-end scission as 15 kcal/mol. This activation energy is comparable to the expected value, $E_{ds} = E_h + E_{ih} - E_H \approx 8 + 8 - 0 = 16$ kcal/mol ($E_h \approx E_{ih} \approx 8$ kcal/mol; $E_H \approx 0$ kcal/mol), when $k_{bs} \gg k_{iH}$ in Eq 11, which gives $k_{ds} = k_{bs}k_h k_{ih}/k_H(k_{bs}+k_{iH}) \approx k_h k_{ih}/k_H$. The value is lower than for random-chain scission because of the dominant influence of hydrogen abstraction.

CONCLUSIONS

The results of the continuous-distribution kinetics indicate that the degradation rate is expressed as the combination of the rate coefficients for radical fragmentation, hydrogen abstraction, and recombination of radical with alkene. These results provide an effective method to evaluate degradation processes and to obtain the properties of polymers and specific products during degradation. The proposed simplified model for polyethylene random-chain scission and chain-end scission describes the observations. The major features of the polyethylene pyrolysis are (1) the zeroth moment (molar concentration) of random products increases exponentially with time, affording rate coefficients with the activation energy 36 kcal/mol for random-chain scission, and (2) gas evolution provides molar concentration of specific products of chain-end scission, which allows the calculation of rate coefficients with the activation energy 15 kcal/mol.

ACKNOWLEDGMENTS

We thank Dr. Naime Segzi for helpful discussions. The financial support of Pittsburgh Energy Technology Center Grant No. DOE DE-FG22-94PC94204 and EPA Grant No. CR 822990-01-0 is also acknowledged.

REFERENCES

[1] Kodera, Y., McCoy, B. J. **1997**, In review.
[2] Madras, G., Chung, G.-Y., Smith, J. M., McCoy, B. J. *Ind. Eng. Chem. Research*, **1997**, In press.
[3] Gavalas, G. R. *Chem. Eng. Sci.*, **1966**, *21*, 133.
[4] Nigam, A., Fake, D. M., Klein, M.T. *AIChE J.*, **1994**, *40*, 908.
[5] Rice, F. O., Herzfeld, K. F. *J. Am. Chem. Soc.*, **1934**, *56*, 284.
[6] Wu, G., Katsumura, Y., Matsuura, C., Ishigure, K., Kubo, J. *Ind. Eng. Chem. Res.*, **1996**, *35*, 4747.
[7] Kossiakoff, A., Rice, F. O. *J. Am. Chem. Soc.*, **1943**, *65*, 590.
[8] Cotterman, R.L., Bender, R., Prausnitz, J. M. *I&EC Process Des. Dev.*, **1985**, *24*, 194.

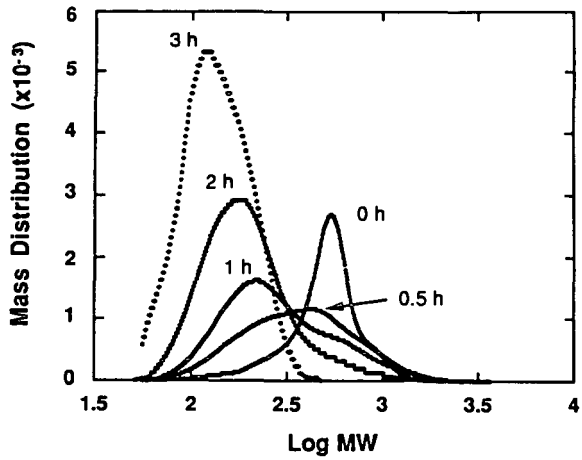

Figure 1. Normalized mass MWDs of original polyethylene (0 h) and the random-chain scission products at 450 °C for 0.5 - 3 h.

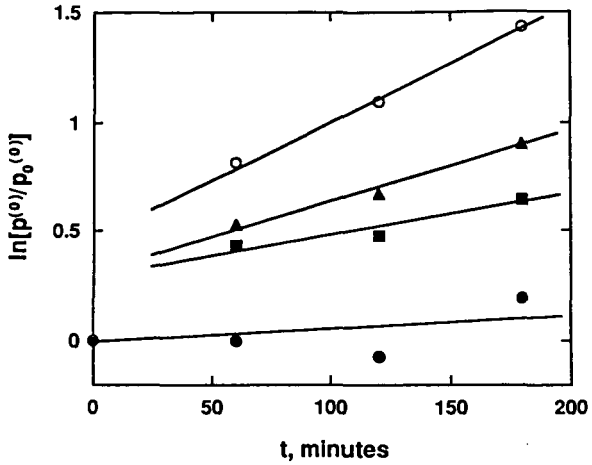

Figure 2. Plot of $\ln[p_o^{(0)}/ p^{(0)}]$ versus reaction time to determine the random-chain scission rate coefficient k_d..
● - 390 °C, ■ - 410 °C, ▲ - 430 °C, ○ - 450 °C

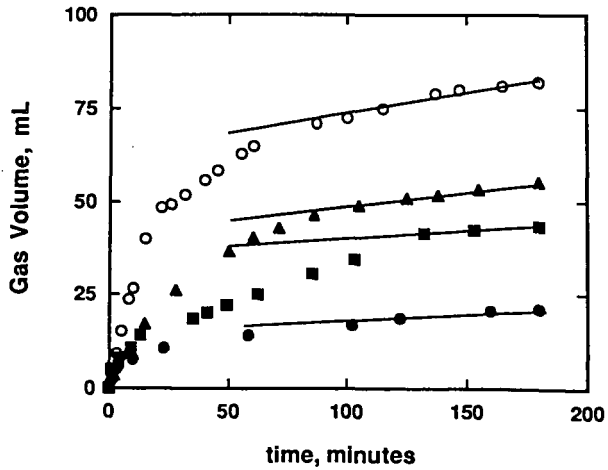

Figure 3. Volumetric amounts of gas evolved by the formation of specific products as a function of reaction time.
● - 390 °C, ■ - 410 °C, ▲ - 430 °C, ○ - 450 °C

HYDROCRACKING OF WASTE PLASTICS TO CLEAN LIQUID FUELS

Weibing Ding, Jing Liang and Larry L. Anderson
3290 MEB
Department of Chemical and Fuels Engineering
University of Utah
Salt Lake City, UT 84112

Keywords: hydrocracking, waste plastics, liquid fuels

ABSTRACT

Recycling of waste plastics and other packaging materials is becoming more necessary since they represent a readily available source of fuels and/or chemicals and a growing disposal problem. One way of accomplishing such recycling is to convert these waste polymers into transportation fuels by thermal and/or catalytic processing. In recent work thermal processing was found to be easily accomplished. However, the products were not of sufficiently high quality to be used as transportation fuels without extensive upgrading. Waste materials from the U.S. (American Plastics Council) and Germany (Duales System Deutchland or DSD) were processed by hydrocracking. Commercial catalysts, KC-2001 and KC-2600 were used in hydrocracking experiments using 27 ml tubing reactors. Effects of reaction temperature, hydrogen pressure, and reaction time on product yields and quality were studied. The liquid products were subjected to detailed analysis by GC, GC/MS, and TG/MS. Possible reaction mechanisms will be proposed based on the analytical data. Other bifunctional catalysts developed in our laboratory were also tested and results will be compared with those obtained using the mentioned commercial catalysts.

INTRODUCTION

Conversion of waste plastic to clean liquid fuels has been widely studied all over the world recently [1,2]. Most bench scale and pilot plant studies employed two-stage processes, i.e., in the first stage, plastic is thermally degraded to crude oil-like liquid products, and the liquids are subjected to further catalytic cracking to produce gasoline-like products in the second stage. This process may be more costly than a single stage processing, i.e., direct conversion of waste plastic to gasoline-like products [3]. The challenge of the latter is to utilize high efficiency catalysts. Pure polymers, such as high density polyethylene, polypropylene, polystyrene, etc., are different than waste plastics which contain some nitrogen, sulfur, and even chorine, as well as impurities. These compounds are believed to be poisonous to some catalysts which were effective in cracking pure polymers. Therefore, a catalyst with not only hydrocracking-hydrogenation ability, but also hydrodenitrogenation-hydrodesulfurization function is needed for directly converting waste plastics to clean liquid fuels.

In this study, two commercial hydrocracking catalysts (KC-2001 and KC-2600), obtained from Akzo Nobel Chemical, Inc., were used for hydrocracking two different kinds of waste plastics; one from the American Plastics Council (APC plastic) and the other from Germany's Duales System Deutschland (DSD plastic). A catalyst (Ni supported on a mixture of zeolite and silica-alumina) made in this lab was also tested and the results are compared.

EXPERIMENTAL

APC plastic, obtained from the American Plastics Council, was ground to -8 mesh. Detailed analyses of this plastic are listed elsewhere [4]. DSD plastic, obtained from Germany's Duales System Deutchland, was used as received except for drying before reaction. The results of ultimate and proximate analyses are listed in Table 1, whereas the results of ash analyses are listed in Table 2 [5]. HZSM-5 and SiO_2-Al_2O_3 (with 13% Al_2O_3 content), were purchased from United Catalysts Inc. and Aldrich Chemical Company, respectively. The average pore size and surface area of the SiO_2-Al_2O_3 were 65 Å and 475 m^2/g respectively; while those of the HZSM-5 were 6.2 Å and ca. 200 m^2/g respectively. The metal salts, nickel (II) nitrate hexahydrate was obtained from Aldrich Chemical Company. KC-2001 and KC-2600 were obtained from Akzo Nobel Chemicals, Inc., whereas as Ni/HSiAl (HSiAl is a mixture of four parts by weight of silica-alumina and one part by weight of HZSM-5) was prepared in this lab. All three catalysts were presulfided before reaction [6].

Hydrocracking reactions of DSD and APC plastics were carried out in a 27 ml tubing reactor at 375 to 480°C for 60 minutes. Typically, 2 g of plastic and a calculated amount of presulfided catalyst, if any, were fed into the reactor, which was then closed, purged with nitrogen,

and then pressurized with hydrogen to the desired initial pressure, usually 1000 psig. The reactor was then immersed into a preheated fluidized sand bath and reached the desired reaction temperature within 3 to 4 minutes. The mixing of reactants and catalyst particles was achieved by horizontal shaking of the reactor at 160 rpm. Detailed reaction procedure and definitions of yields have been reported elsewhere [7].

The gases obtained from the first stage were analyzed by a flame ionization detector by gas chromatography (HP-5890II) using a column packed with HayeSep Q. The liquid products were analyzed by GC/MS using a 30-m long DB-5 capillary column. The boiling point distribution of the liquid products were determined by simulated distillation according to ASTM D 2887-89 and D5307-92. The analysis was performed on a HP-5890 series II gas chromatograph, using a Petrocol B column (6 inches long and 0.125 inches outside diameter).

RESULTS AND DISCUSSION

Hydrocracking of APC Plastic. Some 99% conversion was obtained when APC plastic was noncatalytically degraded at 435°C or at 480°C [7,8]. However, the quality of oil products obtained was far below that of commercial premium gasoline. Hydrocracking catalysts, KC-2600 and Ni/HSiAl, were effective for degradation of APC plastic at 375°C (Figure 1). The conversion was markedly increased in the presence of the mentioned catalysts. Figure 2 shows the GC/MS profile of oil products obtained over KC-2600. The oil contains mostly isoparaffins, some n-paraffins, and small amounts of aromatics as well as cycloparaffins. This indicates that KC-2600 does have hydrocracking and hydroisomerization ability. The oil was also subjected to elemental analysis and no nitrogen and sulfur was detected, suggesting HDN and HDS ability of the catalyst. [6].

Hydrocracking of DSD Plastic. DSD plastic can be hydrocracked thermally to produce gaseous and liquid products. Figure 3 shows the effect of reaction temperature on thermal hydrocracking of this plastic. The conversion was not a function of temperature in the temperature range of 450 to 480°C, although conversion increased markedly with temperature increasing from 370 to 450°C. Different from the APC plastic, this DSD plastic contained about 4.4% ash. Therefore, the maximum conversion should be about 95% and this value was reached at temperatures higher than 450°C. The maximum yield liquid was also obtained at 450°C, indicating further thermal cracking to form smaller size molecules, such as gases, at temperature higher than 450°C. It is reasonable to suggest that 450°C is the optimum temperature for thermally converting DSD plastic to liquid products.

The oil products obtained at 430, 450, and 480°C were subjected to simulated distillation analyses and the results are shown in Figure 4. Not surprisingly, the oil obtained at higher reaction temperatures was lighter than that obtained at lower temperature. The liquids need further treatment for use as transportation fuels, such as gasoline.

The effects of catalysts on hydrocracking of DSD plastic are shown in Table 3. At 375°C, only about 10% conversion was achieved for thermal reaction, however, the conversion reached 66.7% when 40% KC-2001 was added (Figure 3 and Table 3). The effects of the catalysts decreased in the order: KC-2001 > Ni/HSiAl > KC-2600. It is noteworthy that conversion of APC plastic reached over 90% in the presence of KC-2600 or Ni/HSiAl (Figure 1), whereas only 30-50% conversion were obtained for DSD plastic at the same reaction conditions(Table 3). The analyses showed that the main difference between APC plastic and DSD plastic was that the latter contained some chlorine, more ash, and some waste paper (Table 1). These materials may have some negative effects on these catalysts at the conditions used. The conversion of DSD plastic was enhanced when temperature was increased to 400°C and the amount of catalyst was decreased to 20% (Table 3). Some 80% conversion was obtained over 20% KC-2001 at 400C. Additional experiments showed that about 94% DSD plastic was converted to gaseous and liquid products over 40% KC-2001 at 400°C. This indicates that KC-2001 may be a suitable catalyst for hydrocracking of DSD plastic to liquid fuels.

CONCLUSIONS

APC plastic can be converted totally to liquids and gases at 375°C in the presence of a hydrocracking catalyst, Ni/HSiAl or KC-2600. The quality of the liquid products obtained was close to that of a commercial premium gasoline. Catalytic hydrocracking of DSD plastic at the same conditions was found to be more difficult than that of APC plastic. This may be due to the negative effects of some impurities contained in DSD plastic, such as chlorine, ash, and paper. At 400°C, DSD plastic can be nearly totally converted to gaseous and liquid products with 40% KC-2001 catalyst. The products obtained will be analyzed further.

Thermal hydrocracking of DSD plastic is feasible, and the optimum reaction temperature was found to be 450°C. At this condition, DSD plastic can be totally converted and the yield of liquid products can reach as high as some 60%.

ACKNOWLEDGMENT

The authors gratefully acknowledge the funding support from the U.S. Department of Energy through the Consortium for Fossil Fuel Liquefaction Science.

REFERENCES

1. D'Amico, E.; Roberts, M. (1995), Chem. Week, Oct. 04, 32.
2. Frankenhaeuser, M; Inverardi, M.; Mark, F.; Martin, R.; Soderberg, D. (1995), Summary Report of Association of Plastics Manufactures in Europe, EKONO Energy Ltd.
3. Songip, A. R.; Masuda, T.; Kuwahara, H.; Hashimoto, K. (1990), Energy and Fuels, 8, 1238.
4. Ding, W.; Liang, J.; Anderson, L. L. (1996), Fuel Process. Tech., 49, 49-63.
5. Huffman, G. P.; Shah, N. (1996), University of Kentucky.
6. Ding, W.; Liang, J.; Anderson, L. L. (1997), Energy and Fuels, submitted.
7. Ding, W.; Liang, J.; Anderson, L. L. (1997), Fuel Process. Tech., 51, 47-62.
8. Ding, W.; Liang, J.; Anderson, L. L. (1997), Preprints of ACS, Div. Petro. Chem., 42(2), 428-432.

Table 1. Proximate and Ultimate Analyses of DSD Plastic

	wt%
Proximate analysis	
Moisture	0.16
Ash	4.44
Volatile matter	93.77
Fixed carbon	1.08
Ultimate analysis	
Carbon	78.96
Hydrogen	13.5
Nitrogen	0.67
Chlorine	1.26
Sulfur	0.08

Table 2. Ash Analyses of DSD Plastic (by ICP)

	wt%
Al	10.0
As	<40 ppm
Be	<1 ppm
Ca	13.0
Cd	<1 ppm
Co	26 ppm
Cr	0.08
Cu	0.02
Fe	3.5
K	1.85
Mg	2.05
Mn	0.08
Mo	40 ppm
Na	3.9
Ni	0.01
Pb	0.01
Se	<40 ppm
Si	18.0
Ti	12.8
V	21 ppm
Zn	0.43

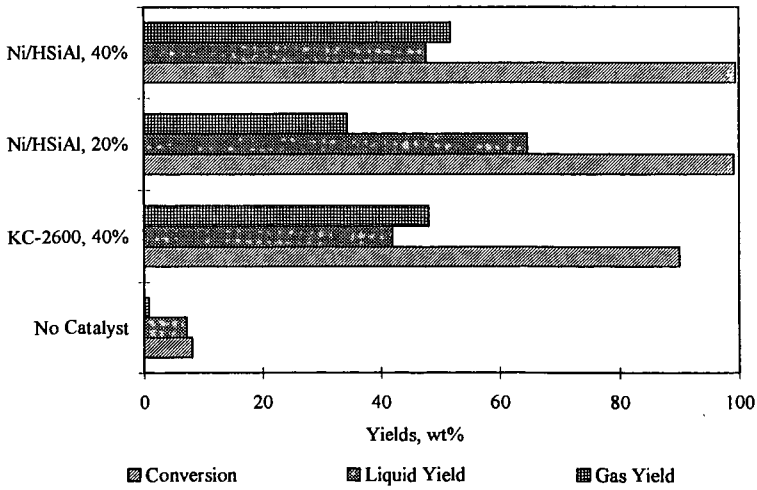

Figure 1. Results of degradation of APC plastic in a 27 ml tubing reactor at 375°C, 1000 psig H_2 (initial), for a reaction time of 1 h with the indicated catalysts.

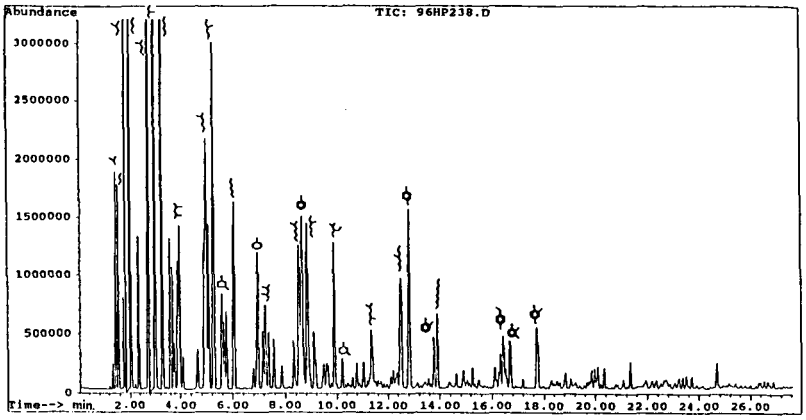

Figure 2. GC/MS analyses of the oil products obtained from hydrocracking of APC plastic in a 27 ml tubing reactor at 375°C, 1000 psig H_2 (initial), for a reaction time of 1 h with 40% KC-2600

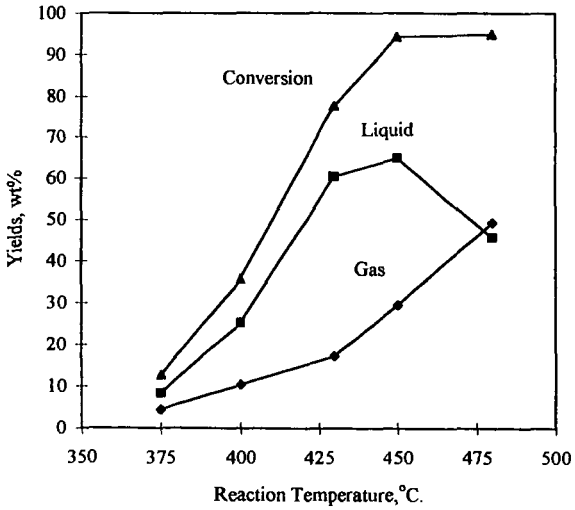

Figure 3. Effect of reaction temperature on thermal hydrocracking of DSD plastic (reaction conditions: 27 ml tubing reactor, 1000 psig H_2 (initial), 60 minutes, 160 rpm)

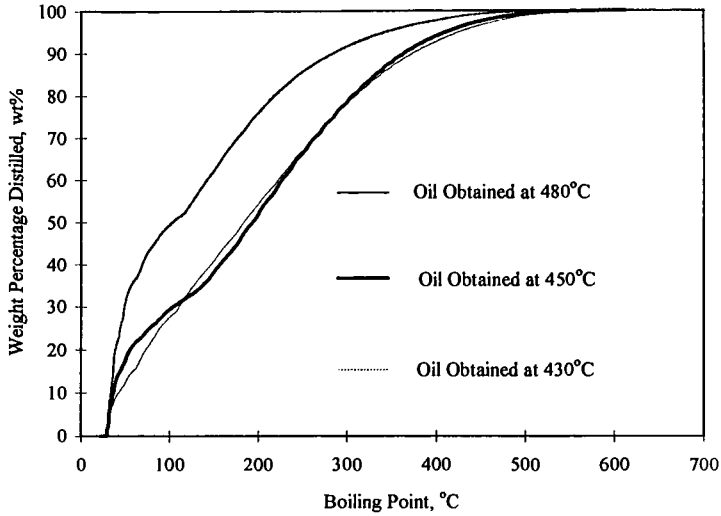

Figure 4. Boiling point distribution of oils obtained from thermal hydrocracking of DSD plastic at 1000 psig H_2 (initial), 60 minutes

Table 3. Results of Catalytic Hydrocracking of DSD Plastic in a 27 ml Tubing Reactor at 1000 psig H_2 (initial), for a Reaction Time of 60 Minutes.

Catalyst	Gas Yield, wt%	Oil Yield[a], wt%	Conversion[b], wt%
375°C			
KC-2001[c], 40%	35.7	31.0	66.7
KC-2600[c], 40%	10.2	20.7	30.9
Ni/HSiAl, 40%	14.8	35.1	49.9
400°C			
KC-2001[c], 20%	39.9	38.8	78.7
KC-2600[c], 20%	15.2	48.2	63.4
Ni/HSiAl, 20%	20.0	45.5	65.5

[a] n-pentane soluble;
[b] Conversion (wt%) = 100(1-weight of pentane insolubles/weight of feed);
[c] Catalysts, obtained from Akzo Nobel Chemicals Inc., may contain $NiMo/Al_2O_3$ and/or NiMo/zeolite.

LIQUID-PHASE CRACKING OF POLYVINYL CHLORIDE (PVC)
ROLE OF SOLVENT ON DECOMPOSITION OF PVC AND REMOVAL OF CHLORINE

Tohru Kamo and Yoshiki Sato

National Institute for Resources and Environment
16-3, Onogawa, Tsukuba-shi, Ibaraki, 305, Japan

Keywords: PVC, Recycling, Dechlorination, Decomposition

INTRODUCTION

Development of feed stock recycling of waste plastics is very important not only for minimization impact for environment but also for saving energy resources. In past two decades, incineration or conventional decomposition of the waste plastic have been studying mainly. However, incineration caused damages in furnace and air pollution problem. Quality of the oil from the conventional decomposition was not enough for fuel or feeds to chemical industry. On the other hand, no hazard byproducts, higher quality oil, lower yields of gas and residue can be expected for liquid-phase cracking of the waste plastic, because products are hydrogenated by solvents and solvents prevent point heating cause coking reaction. We have been studying liquid-phase cracking of used tire (1), polystyrene, and polyethylene in various solvents. Interesting interactions between solvents and plastics were observed (2).

PVC have been used widely as well as other three major plastic, polyethylene, polypropylene, and polystyrene. However, due to high chlorine content and condensation of dechlorinated intermediate product, PVC is one of the most difficult plastics for feed stock recycling. Recently, Y. Maezawa et al. reported PVC was converted into oil at 600 °C with sodium hydroxide (3). However, more than 50 % of hydrocarbon fraction of PVC was converted to residue and gas. In our previous study, we showed advantage of liquid-phase cracking of PVC (4). However, maximum yield oil was only 50 % even at 470 °C under 6.9 MPa of hydrogen, because dechlorinated PVC, heated at 300 °C for three days, was used. In this work, PVC was converted into liquid products directly in tetralin or decalin at 440 °C by using an autoclave specially treated for corrosion by chloride.

EXPERIMENTAL

Reaction procedure: PVC resin (24.0 g) and tetralin or decalin (50.0 g) were charged into a 200 ml magnetic stirred autoclave made of hastelloy C. The most of experiments were carried out at 440 °C for 60 min under an initial pressure of 4.0 MPa of nitrogen gas. In this paper, 0 min of reaction time, shown in figures and table, means that reactor was quenched just after temperature reached 440 °C. In some experiments, copper powder (6 g) or sodium hydroxide (15.6g) was added. In order to study effects of pretreatment of PVC, two kings of dechlorinated PVC, DeCl-1 and DeCl-2, were used. The DeCl-1 was produced from PVC by heating at 300 °C for 12 hours under nitrogen gas. The DeCl-2 was prepared from the products of PVC heated in tetralin at 440 °C for 0 min. In a few experiments, reaction was carried out at 440 °C for 60 min under 10 MPa with nitrogen gas flowing. Reaction products were separated gas, oil, vacuum bottom, and residues by filtration and vacuum distillation. The oil was defined distilled liquid products at 330 °C for 60 min under vacuum. The vacuum bottoms were separated HS (hexane soluble) and HI (hexane insoluble) by soxhlet extraction for more than two days. The HS, HI, and residue were dried for one day at 110 °C under vacuum and weighted.

Analysis of products: Gas products were collected into a Teflon bag through two gas washers filled with water and analyzed by gas chromatography (GASUKURO KOGYO, GC-312, molecular sieve 5A, molecular sieve 13X, Porapak N, gasukuro 54, and VZ-7). Liquid products were analyzed by gas chromatography (CARLO ERBA INSTRUMENTS, HRGC 5300) with capillary column (HP Ultra-1, 0.2 mm, 50m). Each compound in liquid product was identified by GC-MS (Hewlett Packard 5973) with capillary column of HP Ultra-1. Chlorine compounds were identified by GC-MS and GC with atomic emission detector (AED, Hewlett Packard 5921). Chlorohexane and chloronaphthalene were used as an internal standard for quantitative measurement.

RESULTS AND DISCUSSION

Effect of solvent on distribution of products: Distributions of the products from the PVC resin were shown in Fig. 1. Yields of oil, residue in tetralin and decalin for 0 min of reaction time were 39 %, 2.4 % and 73 %, 14% respectively. In our previous experiment, yields of oil and residue from the dechlorinated PVC were 8 %, 13 % for 60 min The significantly higher yield of oil in decalin indicated that direct liquid-phase cracking of PVC was an effective process and PVC was decomposed in a short time while reactor was heated up to 440 °C. On the other hand, lower yields of oil and residue in tetralin implied that decomposition of PVC to oil and condensation to residue was retarded in tetralin. The effect of tetralin might be caused by quick stabilization of radicals by hydrogen from tetralin. The

similar suppressing effect of tetralin was observed in the liquid phase cracking of polyethylene and polystyrene at relatively low temperature. The oil yield in tetralin increased with reaction time. On the other hand, slight increase of oil yield was observed in decalin. These results showed that hydrogen from tetralin enhanced conversion of HS and HI to oil at 440 °C.

Identified compounds in oil from PVC were shown in Table 1. Benzene, toluene, and other alkyl benzene were observed in both solvents. As trace products, anthracene, diphenyl methane, and triphenyl were detected. Characteristic compounds, alkyl tetralin, alkyl naphthalene, tetralin dimmer, and naphthalene dimmer, were produced in tetralin. Almost same yields of benzene, toluene, and alkyl benzene in both solvents implied that these compounds were produced from PVC directly not from tetralin. Particularly, benzene was considered to be produced during heating time, because more than 6 % of benzene was produced for 0 min

Effect of solvent on distribution of chlorine compounds: Lower chlorine contents of products is very important for fuel and feed stock recycling of waste plastics. However, it is difficult to identify each chlorine compound. In this work, we identified main chlorine compounds from PVC by using gas chromatography with atomic emission (AED). Spectrums of chlorine compounds were shown in Fig. 2. Main chlorine compounds from liquid-phase cracking of PVC in tetralin were hydrogen chloride, dichlorobutane, and chlorotetralin. Chlorine contents of the two organic compounds, dichlorobutane and chlorotetralin, were 229 ppm, 171 ppm for 0 min and 14 ppm, 28 ppm for 60 min respectively. When decalin was used as solvent, main chlorine products were hydrogen chloride, dichlorobutane, and chlorodecalin. Chlorine contents of main organic chlorine compounds from liquid phase cracking of PVC were shown in Fig. 3. Total chlorine contents of oil for 0 min and 60 min were 624 ppm, 50 ppm in tetralin and 4040 ppm, 1746 ppm in decalin respectively. These results showed that tetralin was very effective solvent to reduce chlorine contents.

In order to remove chlorine in oil from PVC, sodium oxide have been used in many past experiments. Recently, copper was pointed out to be the catalyst for production of dioxin under incineration (5). Effects of addition of these compounds and pretreatment of PVC on chlorine contents in oil were shown in Fig. 4. In the presence of sodium hydroxide, slight of hydrogen chloride was produced in the gas products, because most of chlorine was converted to sodium chloride. However, total chlorine content of organic chlorine compounds was almost same as that without sodium hydroxide. On the other hand, remarkable increase of dichlorobutane was observed in oil from liquid-phase cracking of PVC with copper powder.

The higher chlorine contents in oil from DeCl-1 and DeCl-2 implied that dechlorination of PVC by heating under nitrogen gas or in tetralin was not effective pretreatment to reduce chlorine in oil. The difficulty of removal of chlorine may be caused by structure of pretreated PVC. The lowest chlorine contents of oil was observed in direct liquid-phase cracking with nitrogen gas flowing.

CONCLUSION

More than 70 % of oil yield was obtained on direct liquid-phase cracking of PVC at 440 °C under nitrogen gas. Particularly, tetralin was effective not only for increase of oil but also for reduction of total chlorine contents in the oil. Benzene was produced from PVC directly. Hydrogen chloride, dichlorobutane, chlorotetralin, and chlorodecalin were main chlorine compounds in oil from PVC. Dichlorobutane increased significantly in the presence of copper. Sodium oxide removed hydrogen chloride perfectly. However, it was not effective to reduce organic chlorine compounds in oil.

PVC was converted to oil contained low chlorine at higher yield by direct liquid-phase cracking. The process was expected to be effective for feed stock recycling of PVC and waste plastics.

ACKNOWLEDGMENTS

The financial support of this project by The Agency of Science and Technology in Japan is gratefully acknowledged. We also greatly thank H. Nii, Mitsubishi Chemical Company, for supply PVC resin.

REFERENCE

1) Y. Sato, J. Kurahashi, J.Jpn.Int.Ene. 74(2), 91(1995).
2) J. P. Wann, T. Kamo, H. Yamaguchi, Y. Sato, Preprint 212th ACS Meeting, Fuel Div. 1161 (1996).
3) Y. Maezawa, F. Tezuka, Y. Inoue, Toshiba Review, 49(1), 39 (1994).
4) T. Kamo, Y. Yamamoto, K. Miki, Y. Sato, Preprint 209th ACS Meeting, Fuel Div. 224 (1995).
5) R. Luijk, D. M. Akkerman, P. Slot, K. Olie and F. Kapteijn, Environ. Sci. Technol., 28(2),312-321(1994).

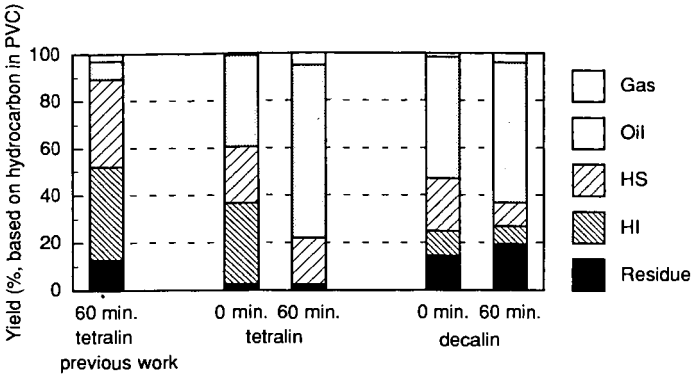

Fig. 1 Distribution of products from PVC at 440 °C

Table 1 Liquid products from PVC at 440C

(%, based on hydrocarbon in PVC)

solvent reaction time	tetralin 0 min	tetralin 60 min	decalin 0 min	decalin 60 min
hydrocarbon in PVC	100.0	100.0	100.0	100.0
solvent	482.2	482.2	482.2	482.2
benzene	6.7	8.9	7.4	9.0
toluene	0.6	3.6	0.8	1.5
C2,C3-benzene	1.0	4.1	1.1	3.6
C4-benzene	1.8	14.8	0.8	4.7
decalin	0.0	0.0	490.1	459.4
1-methylindane*	3.4	36.8	0.0	0.0
tetralin*	464.3	332.3	7.0	11.9
naphthalene*	26.6	92.5	1.3	4.8
Alkyl-tetralin*	0.7	2.3	0.3	0.4
Alkyl-naphthalene*	0.6	3.0	0.4	0.9
diphenylmethane	0.2	0.7	0.3	0.5
anthracene	0.2	0.5	0.2	0.3
tetralin dimmer*	2.5	5.0	0.0	0.2
naphthalene dimmer*	0.3	1.6	0.1	0.2
total	508.9	506.2	509.8	497.4

*: products from solvent mainly

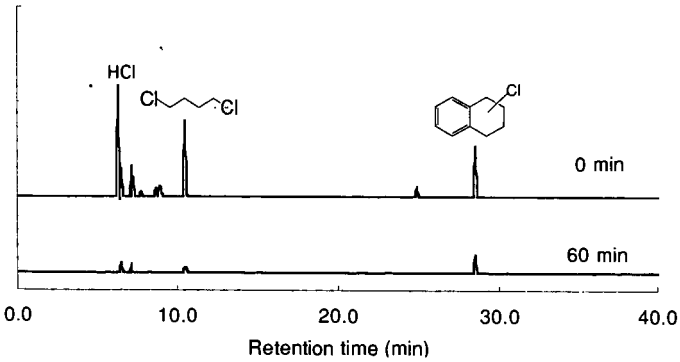

Fig. 2 Chlorine compounds in oil produced from PVC in tetralin at 440 °C

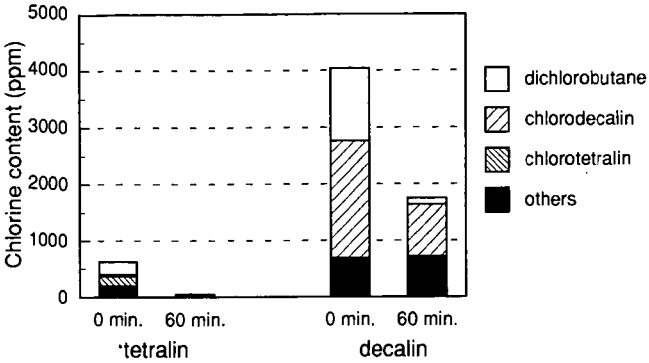

Fig. 3 Chlorine content of oil from PVC at 440 °C

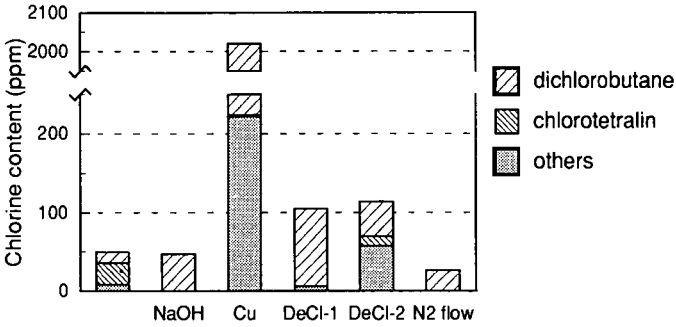

Fig. 4 Effect of additives and reaction procedures on chlorine content in oil from PVC at 440 °C

HYDROGEN DONOR EFFECT ON POLYMER DEGRADATION IN SOLUTION

Giridhar Madras and Ben J. McCoy
Department of Chemical Engineering and Materials Science
University of California, Davis, CA 95616
Phone: (916) 752-1435 Fax: (916) 752-1031
bjmccoy@ucdavis.edu.

ABSTRACT

An important effect in the degradation of solubilized polymers is the influence of the solvent on the degradation rate. Depending on the particular polymer, hydrogen (H-)donors can increase, decrease, or have no effect on degradation rate. We experimentally investigated the effect of H-donor 6-hydroxy tetralin on polystyrene degradation. In this case the rate decreases with increasing H-donor concentration. Mathematical expressions for the degradation rate parameters were obtained by applying continuous-distribution kinetics to the MWD of the reacting polymer. A model was developed for radical mechanisms based on the Rice-Herzfeld chain-reaction concept with the elementary steps of initiation, depropagation, H-abstraction and termination. The model accounted for the varied effects of the H-donor on polymer degradation.

INTRODUCTION

Thermochemical recycling of polymers as either fuel or feedstock has been receiving growing attention in recent years. The degradation of polystyrene has been extensively investigated by pyrolysis (Cameron and MacCallum, 1967) though the mechanism and kinetics of polystyrene degradation remain subjects of discussion (McNeill et al., 1990). Degradation of polymers in solution was proposed to counter the problems of low heat transfer rates and high viscosity of the melting polymer commonly encountered in polymer recycling by pyrolysis (Sato et al., 1990). The degradation of polystyrene (Murakata et al., 1993a; Madras et al., 1996), poly(styrene-allyl alcohol) (Wang et al., 1995), poly(methyl methacrylate) (Madras et al., 1996a), poly (p-methyl styrene) (Murakata et al., 1993b) and poly (α-methyl styrene) (Madras et al., 1996b) in solution have been investigated. By pyrolysis, we mean the thermal decomposition of a solid material at high temperatures to yield gas and liquid products of low MW. Thermolysis of polymers in solution produces a mixture of solubilized products. In either case, the decomposition yields a product mixture that can often be described as a continuous function of MW. The time evolution of the molecular weight distribution (MWD) can be examined by continuous-distribution kinetics to determine the rate parameters and provide insights into the decomposition mechanisms.

The solvent effect for polystyrene thermal degradation was investigated by Sato et al. (1990). The conversion of polystyrene to low molecular weight products decreased with the increase of the H-donating ability of the solvents. The study, however, did not determine degradation rate coefficients. Madras et al. (1995) found that tetralin enhanced the rate of degradation of poly(styrene-allyl alcohol). Rate coefficients were determined as a function of tetralin concentration and temperature. Madras et al. (1996a) found that tetralin had no effect on the degradation of poly(α-methyl styrene). These studies indicate the varied effect of the H-donor on polymer decomposition. Though there have been several experimental studies on H-donor solvents, an overall theory for the mechanism is not available.

EXPERIMENTS

The HPLC (Hewlett-Packard 1050) system consists of a 100 mL sample loop, a gradient pump, and an on-line variable wavelength ultraviolet (UV) detector. Three PLgel columns (Polymer Lab Inc.) (300 mm x 7.5 mm) packed with cross-linked poly(styrene-divinyl benzene) with pore sizes of 100, 500, and 10^4 Å are used in series. Tetrahydrofuran (HPLC grade, Fisher Chemicals) was pumped at a constant flow rate of 1.00 mL/min. Narrow MW polystyrene

standards of MW 162 to 0.93 million (Polymer Lab and Aldrich Chemicals) were used to obtain the calibration curve of retention time versus MW.

The thermal decomposition of polystyrene in mineral oil was conducted in a 100 mL flask equipped with a reflux condenser to ensure the condensation and retention of volatiles. A 60 mL volume of mineral oil (Fisher Chemicals) was heated to 275 °C, and various amounts (0 - 0.60 g) of the H-donor, 6-hydroxy tetralin (Aldrich Chemicals), and 0.12 g of monodisperse polystyrene (MW = 110,000) (Aldrich Chemicals) were added. The temperature of the solution was measured with a Type K thermocouple (Fisher Chemicals) and controlled within ± 3 °C using a Thermolyne 45500 power controller. Samples of 1.0 mL were taken at 15 minute intervals and dissolved in 1.0 mL of tetrahydrofuran (HPLC grade, Fisher Chemicals). An aliquot (100 μL) of this solution was injected into the HPLC-GPC system to obtain the chromatograph, which was converted to MWD with the calibration curve. Because the mineral oil is UV invisible, its MWD was determined by a refractive index (RI) detector. No change in the MWD of mineral oil was observed when the oil was heated for 3 hours at 275 °C without polystyrene.

THEORETICAL MODEL

According to the Rice-Herzfeld mechanism, polymers can react by transforming their structure without change in MW, e.g., by H-abstraction or isomerization. They can also undergo chain scission to form lower MW products, or undergo addition reactions yielding higher MW products. Chain scission can occur either at the chain-end yielding a specific product, or at a random position along the chain yielding a range of lower MW products. The radicals formed by H-abstraction or chain scission are usually influenced by the presence of the H-donor.

We propose continuous-distribution mass (population) balances for the various steps involved in the radical mechanism. The rate coefficients are assumed to be independent of MW, a reasonable assumption at low conversions (Madras et al., 1997). The integrodifferential equations obtained from the mass balances were solved for MW moments. In general, the moments are governed by coupled ordinary differential equations that can be solved numerically. In the present treatment, two common assumptions are made that allow the equations to be solved analytically. The long-chain approximation (LCA) (Nigam et al., 1994; Gavalas, 1966) is valid when initiation and termination events are infrequent compared to the hydrogen-abstraction and propagation-depropagation events. Thus the initiation-termination rates are assumed to be negligible. The quasi-stationary state approximation (QSSA) applies when radical concentrations are extremely small and their rates of change are negligible.

Polymer degradation in some circumstances can occur solely by random chain scission. We represent the chemical species of the reacting polymer, and the radicals as $P(x)$ and $R^{\bullet}(x)$ and their MWDs as $p(x,t)$ and $r(x,t)$, respectively, where x represents the continuous variable, MW. Since the polymer reactants and random scission products are not distinguished in the continuous distribution model, a single MWD, $p(x,t)$, represents the polymer mixture at any time, t. The initiation-termination reactions are ignored, according to the LCA. The reversible H-abstraction process is simplified to

$$P(x) \underset{k_H}{\overset{k_h}{\Leftrightarrow}} R^{\bullet}(x) \qquad (1)$$

The random-scission chain reaction is

$$R^{\bullet}(x) \xrightarrow{k_b} P(x') + R^{\bullet}(x-x') \qquad (2)$$

The reversible H-donor reactions are

$$P(x) + D^{\bullet} \underset{k_D}{\overset{k_d}{\Leftrightarrow}} R^{\bullet}(x) + D \qquad (3)$$

where D and $D^{\bullet}$ represent the H-donor and its dehydrogenated form, respectively. Because the MW of P(x) and $R^{\bullet}(x)$ differ only by the atomic weight of hydrogen, we consider their MWs are the same.

The population balance equations for the polymer MWD, p(x,t), and for the radical MWD, r(x,t), are formulated and solved by the moment method (McCoy and Madras, 1997). Both the LCA and the QSSA are applied to obtain the zeroth moment expression in terms of the initial condition, $p^{(0)}(t=0) = p_0^{(0)}$,

$$p^{(0)}(t) = p_0^{(0)} \exp(k_r t) \qquad (4)$$

and a plot of $\ln (p^{(0)}/ p_0^{(0)})$ should be linear in time with slope k_r,

$$k_r = k_b (k_h + k_d C)/(k_H + k_D C) \qquad (5)$$

This equation, showing how the degradation rate coefficient depends on H-donor concentration, C, is plotted in Figure 1 for several special cases.

Polymers like poly(α-methyl styrene) undergo degradation by chain-end scission yielding monomers and other low-MW specific products, $Q_s(x_s)$. The chain-end scission reaction is

$$P(x) \xrightarrow{k_{fs}} R_e^{\bullet}(x) + R_e^{\bullet}(x - x') \qquad (6)$$

H-abstraction by the chain-end radical is considered reversible,

$$P(x) \underset{k_{He}}{\overset{k_{he}}{\Leftrightarrow}} R_e^{\bullet}(x) \qquad (7)$$

The chain-end radical, $R_e^{\bullet}(x)$, can also undergo radical isomerization to form a specific radical, $R_s^{\bullet}(x)$, via a cyclic transition state,

$$R_e^{\bullet}(x) \underset{k_{iH}}{\overset{k_{ih}}{\Leftrightarrow}} R_s^{\bullet}(x) \qquad (8)$$

The reversible, propagation-depropagation reactions whereby a specific radical yields a specific product and a chain-end radical is

$$R_s^{\bullet}(x) \underset{k_{as}}{\overset{k_{bs}}{\Leftrightarrow}} Q_s(x_s) + R_e^{\bullet}(x-x_s) \qquad (9)$$

The reactions of the H-donor expressed in terms of D, the hydrogenated and $D^{\bullet}$, the dehydrogenated forms of the donor, are

$$P(x) + D^{\bullet} \underset{k_{De}}{\overset{k_{de}}{\Leftrightarrow}} R_e^{\bullet}(x) + D \qquad (10)$$

Applying the LCA and QSSA to the population balance equations yields for the specific product,

$$q_s^{(0)}(t) = k_s\, p_0^{(0)}\, t \qquad (11)$$

where

$$k_s = (k_{he} + k_{de}C)\, k_{bs}\, k_{ih} / ((k_{bs} + k_{iH})\,(k_{He} + k_{De}C)) \qquad (12)$$

This is a key result for chain-end scission influenced by H-donor concentration, C, and is similar to eq. 5 for random chain scission. A plot of $q_s^{(0)}(t)/p_0^{(0)}$ versus time would be linear with a slope k_s, which depends on C.

DISCUSSION

The random-scission degradation rate coefficient, k_r, was determined from the experimental data by analyzing the time dependence of the polystyrene MWDs. The graphs of

$p_{tot}^{(0)}/p_{tot0}^{(0)}$ versus time for various H-donor concentrations were linear after 45 minutes. For times less than 45 minutes, scission of weak links causes a rapid increase in the molar concentration (Stivala et al., 1983; Madras et al., 1997; Chiantore et al., 1981). The initial molar concentration of the strong links in polystyrene, $p_0^{(0)}$, is determined from the intercept of the regressed line of the $p_{tot}^{(0)}/p_{tot0}^{(0)}$ data for $t \geq 45$ minutes. The slopes, corresponding to the rate coefficient for random scission, k_r, are determined from the plot of ln $(p^{(0)}/p_0^{(0)})$ versus time. The rate coefficient decreases with increasing H-donor (6-hydroxy tetralin) concentration (Figure 2). This behavior is consistent with eq. 5 when $k_dC << k_h$ (Figure 1). This behavior is also observed for the polystyrene degradation in the presence of tetralin (Sato et al., 1990).

When $k_h << k_d$ C, the rate coefficient has a first-order dependence at low H-donor concentrations and a zero-order dependence at high H-donor concentrations. This has been experimentally observed for poly(styrene-allyl alcohol) degradation in the presence of tetralin at 150 °C (Madras et al., 1995). When $k_dC << k_h$ and $k_DC << k_H$, the rate coefficient is independent of the H-donor concentration. This is consistent with poly(α-methyl styrene) degradation in the presence of H-donor solvents.

For chain-end scission, the effect of H-donor concentration is qualitatively similar to that in Figure 1. For the chain-end scission rates for the degradation of poly(styrene allyl-alcohol) in the presence of tetralin at 150 °C (Madras et al., 1995), the specific product molar concentrations are linear in time, as predicted by eq. 11. The rate coefficient for chain-end scission, k_s, can be obtained from the slope of the molar concentration of the specific product versus time. The dependence is consistent with eq. 12 when $k_{he} << k_{de}$ C, which relates the chain-end scission rate coefficient to the H-donor concentration. The prediction of the continuous-kinetics model are thus consistent with the different observations of the H-donor effect on polymer decomposition.

ACKNOWLEDGEMENT

The financial support of Pittsburgh Energy Technology Center Grant No. DOE DE-FG22-94PC94204 and EPA Grant No. CR 822990-01-0 is gratefully acknowledged.

REFERENCES

Cameron, G.G., J.R. MacCallum, "The Thermal Degradation of Polystyrene," *J. Macromol. Sci., Rev. Macromol. Chem.*, **C1(2)**, 327 (1967).

Chiantore, O.; Camino, G.; Costa, L.; Grassie, N., "Weak Links in Polystyrene," *Poly. Deg. and Stab.*, **3**, 209 (1981).

Madras, G., J.M. Smith, B.J. McCoy, "Effect of Tetralin on the Degradation of Polymer in Solution," *I&EC Research*, **34**, 4222 (1995).

Madras, G., J.M. Smith, B.J. McCoy, "Thermal Degradation of Poly(a-Methylstyrene) in Solution," *Poly. Deg. and Stab.*, **52**, 349 (1996a).

Madras, G., J.M. Smith, B.J. McCoy, "Degradation of Poly(Methyl Methacrylate) in Solution," *I&EC Research*, **35**, 1795 (1996b).

Madras, G., J.M. Smith, B.J. McCoy, "Thermal Degradation Kinetics of Polystyrene in Solution," *Poly. Deg. and Stab.*, (1997); In press.

Madras, G., B.J. McCoy, "Oxidative Degradation Kinetics of Polystyrene in Solution," *Chem. Eng. Sci.*, (1996); In review.

McCaffrey, W.C., Brues, M.J.; Cooper, D.G.; Kamal, M.R., "Thermolysis of Polyethylene Polystyrene Mixtures," *J. App. Poly. Sci.*, **60**, 2133 (1996).

McCoy, B.J., G. Madras, "Degradation Kinetics of Polymers in Solution: Dynamics of Molecular Weight Distributions," *AIChE J.* **43**, 802 (1997).

McNeill, I.C.; Zulfiqar, M.; Kousar, T. "A Detailed Investigation of the Products of the Thermal Degradation of Polystyrene," *Poly. Degr. and Stab.*, **28**, 131 (1990).

Murakata, T.; Saito, Y.; Yosikawa, T.; Suzuki, T.; Sato, S. "Solvent Effect on Thermal Degradation of Polystrene and Poly-α -methylstyrene," *Polymer*, **34**, 1436 (1993a).

Murakata, T.; Wagatsuma, S..; Saito, Y.; Suzuki, T.; Sato, S. "Effect of Solvent on Thermal Degradation of Poly (para-methylstyrene)," *Polymer*, **34**, 1431 (1993b).

Nigam, A; Fake, D. M; Klein M.T. "Simple Approximate Rate Law for Both Short-Chain and Long Chain Rice Herzfeld Kinetics," *AIChE J.*, **40**, 908 (1994).

Sato, S.; Murakata, T.; Baba, S.; Saito, Y.; Watanabe, S. "Solvent Effect on Thermal Degradation of Polystyrene," *J. Appl. Poly. Sci.*, **40**, 2065 (1990).

Stivala, S.S.; Kimura, J.; Reich, L. "The Kinetics of Degradation Reactions," In *Degradation and Stabilization of Polymers*, H.H.G. Jellinek, ed., Elsevier, p. 1-66. (1983).

Wang, M., J.M. Smith, B.J. McCoy, "Continuous Kinetics for Thermal Degradation of Polymer in Solution," *AIChE J.*, **41**, 1521 (1995).

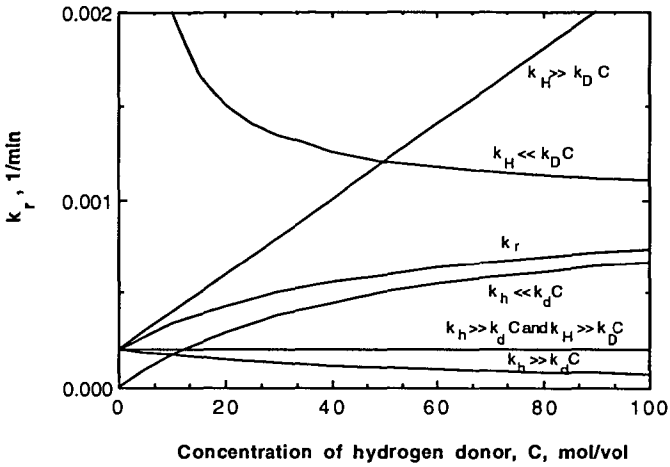

Figure 1. Plot of the rate coefficient of random chain scission, k_r, versus H-donor concentration, C, to show the different effects of the H-donor concentration and rate parameters (eq. 5).

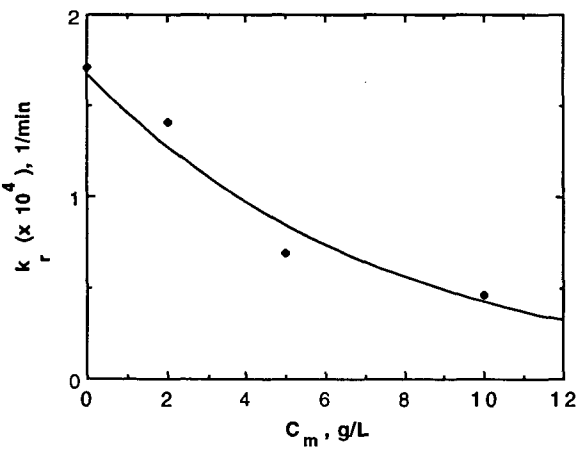

Figure 2. Effect of hydrogen donor (6-hydroxy tetralin) mass concentration, C_m, on the rate coefficient of random chain scission, k_r, of polystyrene at 275 C.

RECOVERY OF PHENOLIC MONOMERS FROMINDUSTRIAL NOVOLAC PLASTICS

Stephen S. Kelley, Carolyn C. Elam, Robert J. Evans, and Michael J. Looker
Center for Renewable Chemical Technologies and Materials
National Renewable Energy Laboratory
1617 Cole Blvd., Golden, CO 80401

Keywords: Plastic recycling; pyrolysis; phenol formaldehyde resins.

Introduction

High performance thermoset composites used by the automotive, electronics and other industries are produced in large volumes using high value monomers. Resins used in thermoset composites include novolacs, crosslinked polyesters, epoxies, and polyarylates, and blends and alloys containing these components. These resins frequently contain aromatic monomers that provide the superior mechanical and thermal properties that are required for composite applications. Aromatic monomers are generally more expensive and have a higher embodied energy than most other classes of monomers (1).

Resins used in thermoset composites are generally viewed as non-recyclable. This perception exists for a variety of reasons including the presence of chemical crosslinks, inclusion of mineral fillers, and blend formulations that include a variety of different resins. These features prevent the use of traditional recycling techniques such as physical separation and melt extrusion, or simple chemical hydrolysis. Burning these composites for energy recovery or grinding into a flour for use as a filler does not provide any significant economic value. Landfilling is the most common route for disposal, illustrating the need for novel processes for the recovery and reuse of the monomers used in thermoset composites.

Selective pyrolysis has been demonstrated to be an effective method for the recovery of monomers or high-value chemicals from complex mixtures of waste plastics. Selective pyrolysis takes advantage of differences in the strengths of chemical bonds, and the potential for using catalysts and reactive atmospheres to selectively break specific bonds in the backbone of high molecular weight plastics.

Selective pyrolysis has been applied to novolac composites for the recovery of phenol and substituted phenolics. Novolac composites typically contain 30-50 percent organic resin. Inorganic fillers are added to improve mechanical properties and reduce the overall cost of the composite. Previous work on pure novolac resins has shown that the major pyrolysis products are phenol, ortho- and para-cresol, 2,4- and 2,6-xylenols, and some 2,4,6-trimethylphenol (2-5). To the best of our knowledge there is no work in the open literature on how inorganic fillers may effect the pyrolysis of novolac resins or the behavior of complex commercial thermosets. The goal of this work is to address these questions.

Experimental

Samples were supplied by member companies of the Phenolics Division of the Society of Plastics Industries. These samples represent the expected variability of fillers and formulations found for commercial novolac resins. The composition of the samples is shown in Table 1.

Novolacs were characterized using Molecular Beam Mass Spectrometry (MBMS) and Thermal Gravimetric Analysis (TGA). The MBMS is a versatile tool that can be used for real-time sampling of complex gas streams produced by high-temperature processes, and has been used to characterize a wide variety of plastics and biomass samples (6-8). Free-jet expansion of the high-temperature gases and vapors allows for the effective quenching of species in their sampled state (9) making MBMS a valuable tool for identifying complex mixture of products produced in pyrolysis.

The MBMS analysis were performed in triplicate using a quartz tube reactor. Helium was used as the carrier gas. Samples were in the range of 20-50 milligrams and the pyrolysis temperature for most of these experiments was 600°C, although selected samples were also pyrolyzed at 450°C. The complexity of the product suite makes interpretation of the results difficult, so multivariate statistical techniques are used to identify and characterize trends and variable interactions, resulting in greatly enhanced data interpretation.

A TA Instruments TGA 2950 was used to characterize weight losses using nitrogen as a purge gas. Samples sizes were between 10-12 mg and the heating rate was 20°C/min. Activation energies were determine with variable heating rates (10,11).

Results and Discussion

TGA Analysis - The results from the TGA studies were very complex due to the wide variety of fillers and commercial resin formulations. However several general trends in the weight loss data could be identified. The first derivative of the TGA weight curves of several of the samples are shown in Figure 1. Sample 1 contains resin and high amount of alumina filler, and shows a relatively sharp weight loss peak at about 284°C, which is assigned to bound water in the alumina, and a broad weight loss peak centered around 533°C, which is assigned to decomposition of the novolac resin. Sample 4 contains resin and wood filler, and shows a large weight loss peak at 380°C, which is assigned to decomposition of the carbohydrate component of the wood filler, and a broad weight loss peak between 482°C and 560°C which is assigned to both the lignin component of the wood and the novolac resin.

Sample 3 is a more typical resin formulation and shows more complex behavior. The weight loss curve for sample 3 shows at least four separate peaks, and several shoulders. The low temperature peak at about 269°C is assigned to loss of bound water from the inorganic filler, while the peak at 379°C is assigned to decomposition of the carbohydrate in the wood filler. The large broad peak centered around 517°C is assigned to decomposition of the novolac and lignin in the wood filler, while the high temperature peak at 678°C is assigned to decomposition of the calcium carbonate filler. All of the TGA curves showed a broad weight loss in the 500-600°C range, consistent with decomposition of the novolac resin (4,5). Thus, MBMS analysis of all the resins was conducted at 600°C.

MBMS Analysis - Multivariate analysis techniques allow for extensive data manipulation and interpretation. The average MBMS spectra, taken over all of the samples, is shown in Figure 2. The spectra shows that the major products seen at mass numbers of 94, 108, 122, and 136 are phenol, cresols (positional isomers were not distinguishable with the technique used), xylenols, and trimethyl phenol, respectively. A series of dimeric species are also seen in the mass region 180 to 230.

More detailed analysis of the MBMS spectra showed distinct differences due to the chemical nature of the novolac and the presence of specific fillers. The factor spectra relate to the chemical nature of the novolac resin is shown in Figure 3. This factor indicates the variability in the concentration of substituted phenols. Samples positively correlated with this factor have higher concentrations of phenol and cresol relative to xylenol and trimethyl phenol than do the rest of the samples. These variations are consistent with more methylene bridges connecting the phenolic rings or differences in the degree of crosslinking. Resins with more connecting methylene bridges have a higher degree of crosslinking.

An additional factor was related to the chemical structure of the novolac resins. This factor (not shown) is related to high concentrations of phenol relative to the other reaction products. This factor appears to be associated with the evolution of free phenol, phenol which is not fully incorporated into the polymer, but is physically trapped within the cured resin. Time-resolved results that show phenol is released from some samples at temperatures well below pyrolysis temperature.

The relationship between the degree of crosslinking and the amount of free phenol is shown in Figure 4. (This figure shows each of the individual data points, demonstrating the reproducibility of the MBMS experiment.) There are significant differences in the degree of crosslinking, as determined from the ratio of non-substituted and mono-substituted phenolics compared to di- and tri-substituted phenolics, across the samples. Samples with the highest degree of crosslinking and least amount of unreacted phenol are found in the upper, left-hand quadrant, such as samples #1 and #3. Surprisingly, the degree of crosslinking in the fully cured resin is not correlated with the amount of hexamethylene tetraamine (hexa) 'crosslinker' added to the resin. Hexa is a source of formaldehyde that can react with free sites on the phenolic rings and complete the conversion of the low molecular weight, melt processible resin into a fully cured product. Higher novolac/hexa ratios should result in a lower degree of crosslinking and produce fewer of the di- and tri- methylated phenols. In this case the extent of crosslinking appears to be related to the chemical structure of the original resins produced by different manufacturers rather than the novolac/hexa ratio. Samples 1-5, all produced by one manufacturer, show a higher degree of crosslinking than do samples 16-20, which were all produced by a second manufacturer. It is also worth noting that the sample with the highest amount of free phenol was formulated with a large amount of hexa. Thus, it appears that hexa is not capable of capturing all of the free phenol that is contained in the resin.

The ability to detect the presence of organic fillers is shown in Figure 5. In this figure the degree of crosslinking and the presence of wood filler are compared. Examination of the average spectra shows that the 'wood filler' response is due to

guaiacols that are generated by the decomposition of the lignin present in the wood. All of the samples with negative loadings for this factor did not contain any wood filler, while all of the samples with positive loadings contain varying amounts of wood filler.

The effect of a second filler, alumina, on the chemical composition of the pyrolysis products was also examined. Under some conditions alumina can act as a catalyst and could influence the chemical composition of the reaction products. However, for this set of novolacs, the chemical composition of the reaction products did not appear to be affected by the presence of alumina. Activation energies for the high temperature peak seen in samples 1 and 4 were also calculated. The activation energies were 215 kJ/mol and 230 kJ/mol for samples 1 and 4, respectively. These activation energies are essentially the same, indicating that the alumina filler present in sample 1 does not influence the decomposition of the novolac resin. These activation energies are similar to those measured for phenol-formaldehyde resins. (3).

Conclusion

The results of this study show that valuable, monomeric phenols can be recovered from the pyrolysis of cured commercial novolac resins. The major phenolic products are phenol, cresols, xylenols and trimethyl phenol, along with a small amount of dimeric species. The novolac/hexa ratio does not appear to have a significant an affect on the relative ratio of the various substituted phenols while the source of the original resin does influence the product composition. The presence of organic fillers can be easily detected and the pyrolysis degradation products from these fillers may complicate isolation of the desired phenols. The presence of inorganic fillers such as alumina did not influence the chemical composition of the pyrolysis product.

Acknowledgements

The support of the U.S. Department of Energy Office of Industrial Technology and Mr. Charlie Russomanno is gratefully acknowledged.

The assistance of member companies of the Phenolics Division of the Society of the Plastics Industry is also gratefully acknowledged.

References

1. Lipinsky, E. S., Ingham, J. D., Brief Characterization of the Top 50 Commodity Chemicals, DOE report ILA 207376-A-H1, Batelle Memorial Institute, (1994)
2. Blazso, M., Toth, T., J. Anal. and Appl. Pyrolysis, 10, 41, (1986)
3. Cohen, Y., Aizenshtat, J. Anal. and Appl. Pyrolysis, 22, 153, (1992)
4. Shulman, G. P., Lochte, H. W., J. Appl. Polym. Sci., 10, 619, (1966)
5. Chang, C., Tackett, J. R., Thermochimica Acta, 192, 181, (1991)
6. Chum, H. L., Evans, R. J., WO 92/2169, (1992)
7. Evans, R. J.; Tatsumoto, K.; Czernik, S.; and Chum, H. L., Proceedings of the RecyclingPlas VII Conference: Plastics Recycling as a Business Opportunity, 175 (1992)
8. Evans, R. J. and Milne, T. A., Energy & Fuels, 1(2), 123 (1987); 1(4), 311 (1987)
9. Atomic and Molecular Beams, Vol. 1, G. Scoles, ed., Oxford University Press, New York, 14-53, (1988)
10. Flynn, J.H., Wall, L. A., Polym. Lett., 4, 323, (1966)
11. Krizanovsky, L. J. Therm. Anal., 13, 571, (1978).

Table 1. Composition of Formulated Novolac Resins

Resin Component	Sample Number									
	1	**2**	**3**	**4**	**5**	**16**	**17**	**18**	**19**	**20**
Novolac	35	36	45	54	35	34	49	35	40	35
Hexa	9	4	8	10	9	4	4	4	8	10
Wood	0	5	4	35	33	14	39	0	13	4
$CaCO_2$	0	0	5	0	0	0	0	14	10	0
Clay	15	15	25	0	10	39	0	0	10	0
Alumina	40	15	5	0	10	0	0	38	0	4
Talc	0	15	5	0	0	0	0	0	10	39
Glass	0	5	0	0	0	0	0	0	5	0
$Ca(OH)_2$	0	1	1	0	0	6	6	6	1	6
Brown Umber	0	2	0	0	2	2	0	2	2	0
Nigrosine	0	0	1	0	0	0	1	0	0	1
Steric Acid	1	1	1	1	1	1	1	1	1	1

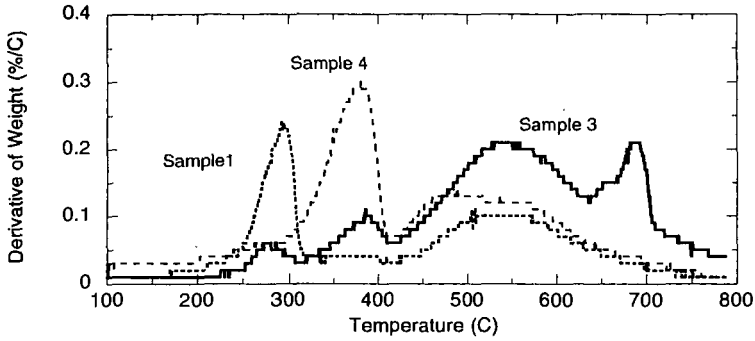

Figure 1 - DTGA Curves for Commercial Novolac Samples: a) Sample 1, b) Sample 4, and c) Sample 3.

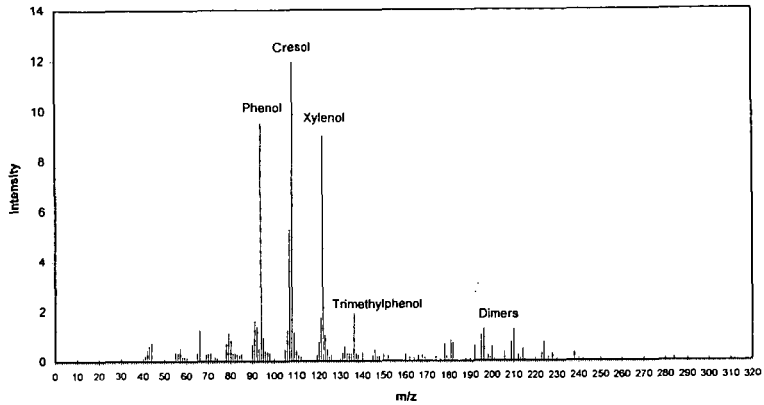

Figure 2 - Averaged MBMS spectra, taken over all of the samples, shows major phenolic products (phenol, cresol, xylenols, and trimethylphenol) and the characteristic dimer region.

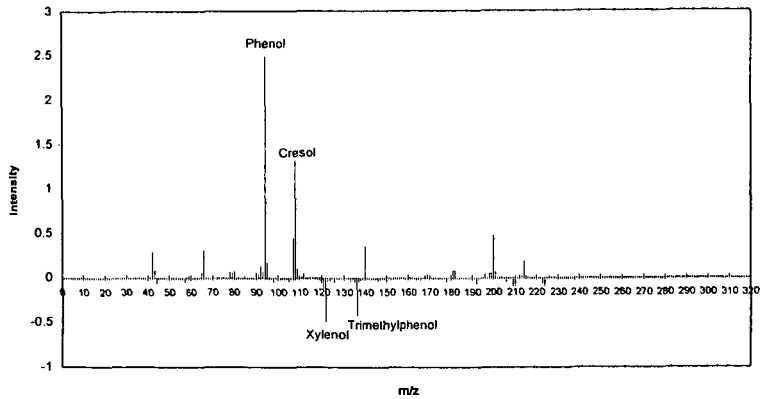

Figure 3 - Factor related to the degree of crosslinking. Those samples positively correlated with this factor have higher concentrations of less substituted phenolics and are considered to be "less" crosslinked than the other samples in the dataset.

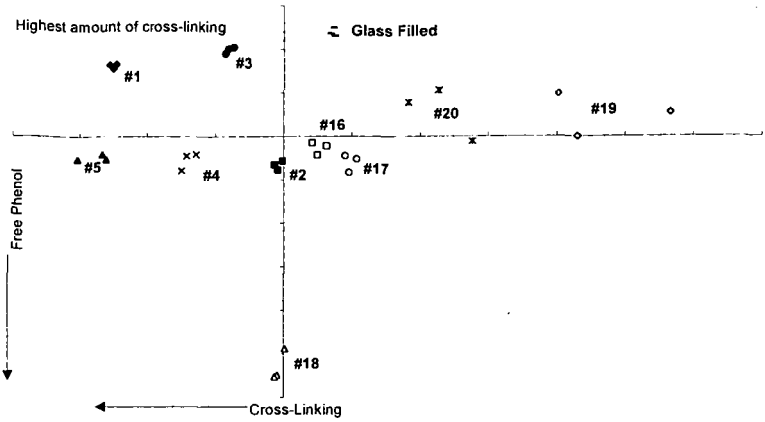

Figure 4 - *Plot showing the relationship between free phenol and the degree of crosslinking.* Those samples in the upper, left-hand quadrant are those with the highest degree of crosslinking and the least amount of unreacted phenol. Samples 1-5 were prepared by one manufacturer, while samples 15-20 were prepared by another. This shows that manufacturer has a greater influence on degree of crosslinking than does the amount of crosslinker or filler.

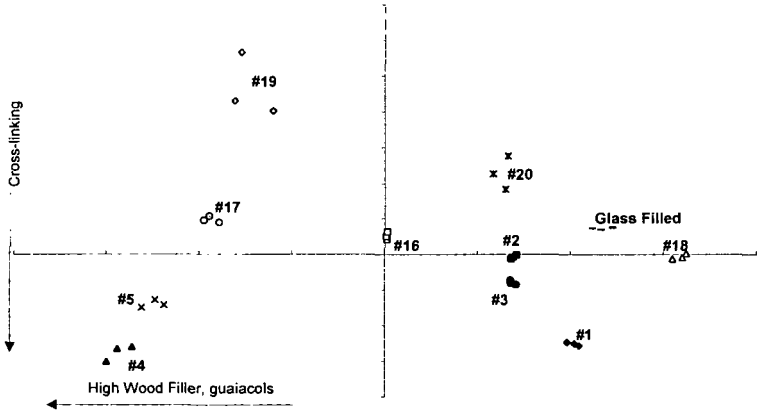

Figure 5 - Comparison of samples with and without wood filler. The presence of guaiacols in the pyrolysis spectra is indicative of the decomposition of the lignin from the wood filler.

IDENTIFICATION AND QUANTIFICATION OF POLYMERS IN WASTE PLASTICS USING DIFFERENTIAL SCANNING CALORIMETRY

A. Manivannan and M. S. Seehra
Physics Department, West Virginia University
Morgantown, WV 26506-6315, USA

KEYWORDS: Waste plastics, characterization, differential scanning calorimetry

ABSTRACT

Experimental results on the use of differential scanning calorimetry (DSC) for the identification and quantification of various polymers in post-consumer waste plastics are presented. Experimental studies are presented for the model polymers such as different grade of polyethylene (PE), polypropylene (PP), polyethylene terephthalate (PET), polystyrene (PS) and polyvinyl chloride (PVC). It is argued that the glass transition T_g and the melting temperature T_m of the polymers can be used for their identification whereas the enthalpy of fusion ΔH determined from the heat flux versus temperature curves of DSC is useful for quantification. For the standard mixtures of PE and PP, a linear curve of ΔH versus concentration is obtained showing the applicability of this technique. This methodology is then applied to analyze two samples of waste plastics. A sample of commingled plastics obtained from the American Plastics Council is found to contain high density PE (~82%), PP (~7%) and PET (~10%) whereas a German plastics sample is found to contain HDPE, MDPE, PP and PVC. Complementary information is obtained from thermogravimetric analysis for the PVC case.

INTRODUCTION

As an alternative to the serious environmental problem of the disposal of post-consumer waste plastics, some initial experiments into the liquefaction of waste plastics and their coliquefaction with coal have been reported recently [1-5]. The liquefaction approach is logical because the atomic hydrogen to carbon ratio in waste plastics vis-a-vis coal is closer to that in petroleum. The recently reported studies include the thermal and catalytic liquefaction of model polymers such as high density polyethylene (HDPE), polypropylene (PP), polystyrene (PS) polyethylene terephthalate (PET) and their mixtures [1-5]. Catalysts tested in these experiments included HZSM-5 zeolite, nanoscale FeOOH, SiO_2-Al_2O_3, M/SiO_2-Al_2O_3, M/TiO_2 (M = Pt, Ni, Pd, Fe), and NiMo/Al_2O_3. Also, two independent studies [6,7] have recently reported that elemental sulfur promotes depolymerization of PE and PP and improves the quality of liquefaction products.

A typical sample of post-consumer waste plastics may contain the above listed polymers, along with PVC (polyvinyl chloride) and other impurities. Determining the concentrations of each polymer in a sample thus becomes an important issue since each polymer may behave quite differently under the high temperature/high pressure conditions of liquefaction. In this paper, we report the results of our investigations on the detection and quantification of these polymers using DSC (Differential Scanning Calorimetry). After presenting the DSC results, we apply the technique to determine the polymer concentrations in two commercial samples. Both the success and limitations of the DSC technique for this purpose are outlined.

EXPERIMENTAL DETAILS

The samples of model polymers used in these experiments were obtained from commercial sources. The two samples of waste plastics investigated here include a sample from the American Plastic Council (APC), elemental analysis of which has been given in a recent paper [7]. X-ray diffraction analysis of this sample indicated it to contain primarily high density polyethylene (HDPE) with smaller amounts of PP and PET [7]. The second sample of waste plastics is of German origin (DSD waste plastics). The DSC measurements were carried out with the Mettler TA3000 system using the DSC 30 system.

As polymers are heated, they may undergo a number of phase changes such as the glass transition (T_g), crystallization transition (T_c) and melting (T_m). Locations of these transitions are used to identify the polymers whereas the heat of fusion ΔH determined from the heat flux versus temperature curves in DSC are used to quantify the polymers [8]. For HDPE and PP, we have used standard samples of known compositions to establish the linearity of ΔH with the concentration of a polymer.

RESULTS AND DISCUSSION

The typical heat flux versus temperature DSC curves for three grades of polyethylene (HDPE, MDPE and LDPE) are shown in Fig. 1. The sharp peaks are due to polymer melting to yield completely amorphous polymers above T_m whereas the smaller anomalies at the lower temperature are mostly likely due to the glass transition [9]. The areas under the peaks give the heats of fusion (ΔH). It is noted that in the above DSC curves, the melting point $T_m \simeq 131°C$ for HDPE is in complete agreement with the in-situ x-ray diffraction measurements where disappearance of the crystalline Bragg peaks was observed between 130°C and 135°C [10].

Normally, the melting transition are supposed to be first order; however, it is certainly not so in case of polymers since the transitions are spread over a large temperature range. For first order transition, the Gibbs free energy for the two phases equal at T_m, leading to the result [8]

$$T_m = \Delta H/\Delta S \qquad (1)$$

showing T_m depends on the enthalpy of fusion ΔH and entropy of fusion ΔS. In Fig. 2, we have plotted T_m against ΔH, both evaluated from Fig. 1. It should be kept in mind that differences in ΔH and ΔS between the melt and crystalline phase determine T_m, assuming first order transition.

In order to use ΔH for quantification, we prepared several standard mixtures of HDPE and PP and DSC plots of these mixtures are shown in Fig. 3. The higher $T_m \simeq 166°C$ of PP allows an easy identification of PP in the presence of PE in Fig. 3. The enthalpy of fusion for PE and PP were determined from the areas under the peak following the procedures shown in Fig. 1 and T_m is represented by the peak temperature. In Fig. 4 we show plots of ΔH versus % PE whereas similar plots for % PP are shown in Fig. 5. The fact that T_m does not change with % PE and % PP shows that there is no measurable interaction between PE and PP. On the other hand, ΔH varies linearly with % PE and % PP demonstrating that ΔH provides an excellent technique for quantifying the crystalline percentages of PE and PP in a mixture. This forms the basis for quantification of these polymers in a mixture.

Next we consider the DSC curves for other model polymers (viz. PET, PS and PVC) likely to be found in post-consumer plastics. In Fig. 6, we present a comparative view of the DSC curves for HDPE, PP, PET, PS and PVC. For PET, we show two figures. During the first heating, one observes T_g, an exothermic peak near $T_c \simeq 125°C$ due to crystallization [9] and polymer melting near $T_m = 260°C$. On subsequent cooling and then reheating, only the melting peak is observed. For PS, the glass transition $T_g \simeq 100°C$ is observed; however no melting peak is observed in this case. For isotactic polystyrene, a $T_m \simeq 240°C$ is known [8]. Our failure to observe a peak in the DSC curve is most likely to the nature of our sample. For PVC, a glass transition near $T_g \simeq 80°C$ is clearly observed and this agrees with the literature values. Also, syndiotactic PVC is known to have $T_m \simeq 280°C$ [8]. However our experiments (Fig. 6) show an exothermic peak around this temperature presumably because of the decomposition of our sample since the sample is severally charred. Further evidence for this comes from thermogravimetric experiments (Fig. 7) where large decreases in mass occur beginning around 280°C. This clearly is due to the decomposition of PVC.

Now we apply the above methodology to the identification and quantification of polymers in two post-consumer waste plastics. In Fig. 8, we show the DSC curve for the APC commingled plastic sample which has been the focus of studies in a number of recent papers [5,7,10]. The DSC curve clearly shows three peaks which are easily identified with HDPE, PP and PET from the known T_m values, with the largest peak being from HDPE. This is consistent with the earlier estimates from x-ray diffraction [7,10] although PET was difficult to detect in x-ray diffraction because of overlapping Bragg lines. In contrast, in DSC, the peaks from PE, PP and PET are well resolved (Fig. 8).

To determine the concentrations of PE, PP and PET in the APC sample, the calibrations of Fig. 4 and Fig. 5, along with assuming a similar linear curve for PET, are used. From this analysis, we find the following concentrations in the APC sample: HDPE $\simeq 82 \pm 3\%$, PP $\simeq 7 \pm 3\%$, PET $\simeq 10 \pm 3\%$. These concentrations are consistent with those determined from x-ray diffraction, although the actual numbers for HDPE and PET are somewhat different. As indicated earlier, PET is difficult to identify by x-ray diffraction because of interferences of its Bragg lines by those from PE.

For the German sample of DSD waste plastics, the DSC curve is shown in Fig. 9. The peaks due to MDPE, HDPE and PP are easily identified and their concentrations from linear calibrations are as follows: PE $\simeq 38\%$, PP $\simeq 7\%$. The other major feature of the data in Fig. 9 is the exothermic peak near 230°C. Thermogravimetric measurements in the German plastics sample (Fig. 10) show mass loss beginning near 300°C, with the massive loss occurring between 450 and 500°C. These observations are very similar to the thermogravimetric and DSC data for PVC. Thus it is likely that this sample contains a significant amount of PVC. Since x-ray diffraction of PVC does not contain any sharp Bragg lines, additional confirmatory evidence for PVC from x-ray diffraction could not be obtained.

CONCLUSIONS

Results presented here have shown that DSC is a promising technique for the identification and quantification of polymers in post-consumer plastics. However, supporting evidence from thermogravimetry and x-ray diffraction is occasionally required. Additional experience with other polymers likely to be found in post-consumer plastics is needed to provide additional confidence in the use of DSC for quantitative purposes. Further studies are in progress to establish the methodology for quantifying PVC by this technique.

ACKNOWLEDGEMENTS

This work was supported in part by the U.S. Department of Energy through the Consortium for Fossil Fuel Liquefaction Science, Contract No. DE-FC22-93PC93053. We thank Eric Hopkins for assistance with some of the experimental work.

REFERENCES

1. Taghiei, M. M.; Feng, Z.; Huggins, F. E.; Huffman, G. P., Energy Fuels 1994, 8, 1228-1232.
2. Feng, Z.; Zhao, J.; Rockwell, J.; Bailey, D.; Huffman, G., Fuel Process. Technol. 1996, 49, 17-30.
3. Liu, K.; Meuzelaar, H. L. C., Fuel Process. Technol. 1996, 49, 1-15.
4. Joo, H. K.; Curtis, C. W., Energy Fuels 1996, 10, 603-611.
5. Ding, W. B.; Tuntawiroon, W.; Liang, J. and Anderson, L. L., Fuel Process. Technol. 1996, 49, 49-63.
6. Sivakumar, P.; Jung, H.; Tierney, J. W.; Wender, I., Fuel Process. Technol. 1996, 49, 219-232.
7. Ibrahim, M. M.; Seehra, M. S., Energy Fuels 1997, July issue (in press).
8. See e.g. Polymer Chemistry, an Introducation by G. Challa (Ellis Horwood, 1993), page 147.
9. Introduction to Physical Polymer Science by L. H. Sperling (John Wiley & Sons, second edition 1992) page 322.
10. Ibrahim, M. M.; Hopkins, E.; Seehra, M. S., Fuel Process. Technol. 1996, 49, 65-73.

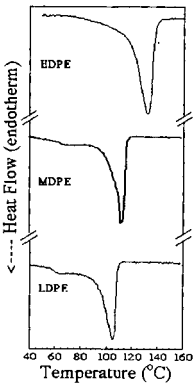

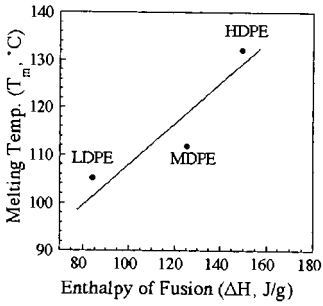

(left) Figure 1. DSC curves for high, medium and low density polyethylene. (right) Figure 2. Enthalpy of Fusion(Δ H) vs. melting point (T_m) for low, medium and high density polyethylene

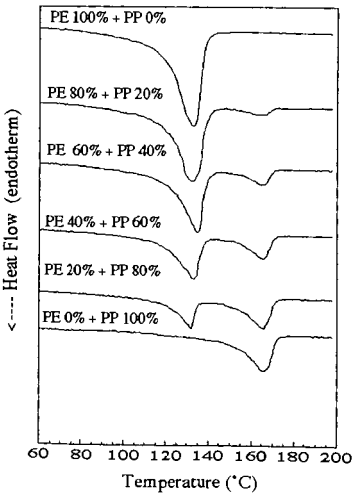

Figure. 3 DSC curves for PE/PP blends of various compositions.

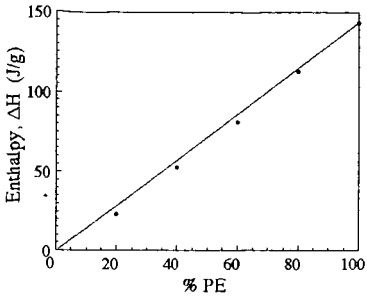

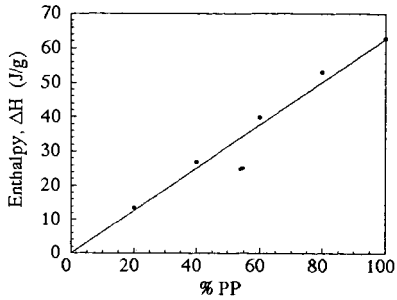

(left) Figure 4. Plot for Δ H vs.% PE and (right) Figure 5. Plot for Δ H vs. % PP measured from various compositions of PE+PP.

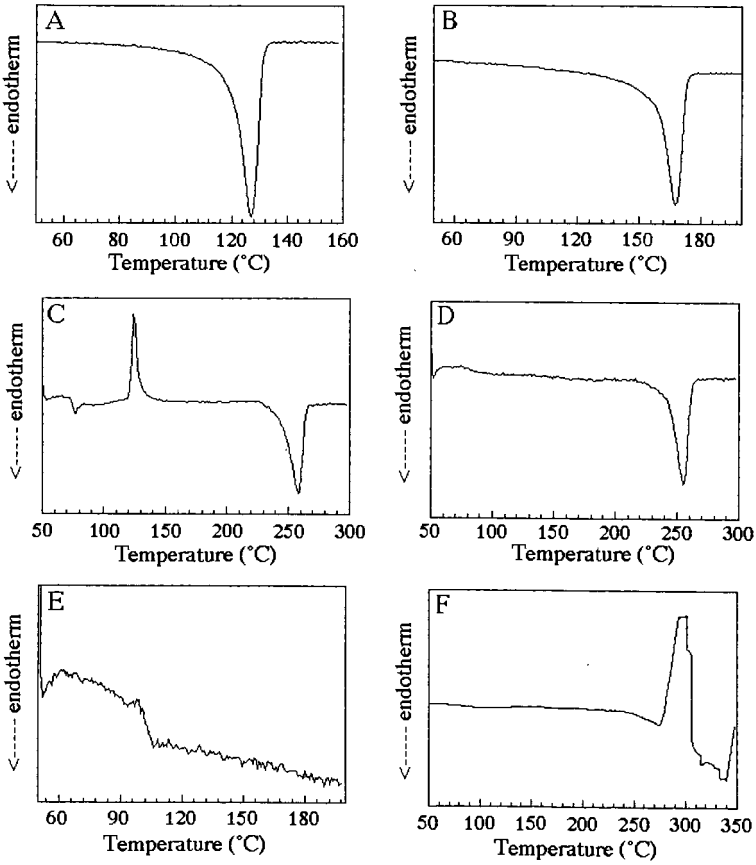

Figure. 6 DSC curves for A) PE, B) PP, C) PET (1st run), D) PET (2nd run), E) PS, and F) PVC.

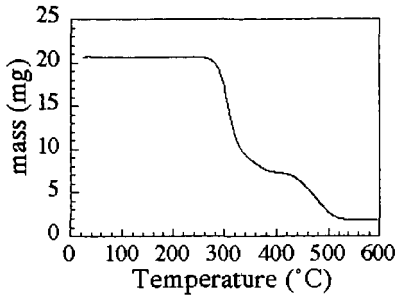

Figure 7. TGA of PVC indicating weight loss beginning around 280 °C.

Figure 8. DSC of APC commingled plastics. The endotherms for HDPE, PP, PET are identified.

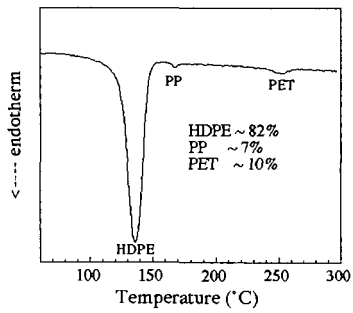

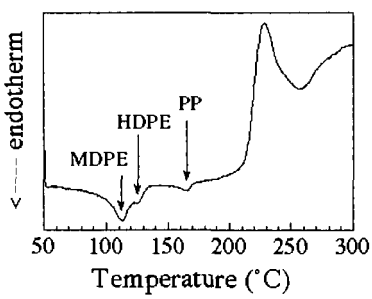

Figure 9. DSC of DSD waste plastics. Endotherms for HDPE, MDPE and PP are noted. Large exothermal peak around 230 °C is due to PVC.

Figure. 10 TGA of DSD waste plastics showing the weight loss occuring from 300 - 500 °C.

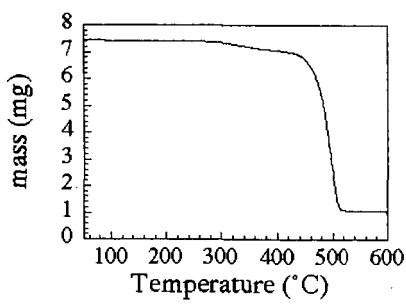

Feasibility Study for a Demonstration Plant for Liquefaction and Coprocessing of Waste Plastics and Tires

Gerald P. Huffman
CFFLS, 533 S. Limestone St., Rm. 111
University of Kentucky
Lexington, KY 40506
Keywords: Liquefaction, plastics, tires, demonstration plant, flowsheet, economics

Introduction

For the past several years, a research program on the conversion of waste polymers and coal into oil using direct liquefaction technology has been sponsored by the U.S. Department of Energy. The research has been carried out by a combination of academic, industrial and government scientists and engineers. Most of the laboratory research has been conducted by the Consortium for Fossil Fuel Liquefaction Science (CFFLS), a five university research consortium with participants from the University of Kentucky, Auburn University, the University of Pittsburgh, the University of Utah and West Virginia University. Industrial participation has been provided by Hydrocarbon Technologies, Inc. (HTI), where pilot scale and continuous tests have conducted, Consol, where specialized analytical techniques have been employed, and the Mitre Corporation, where economic analyses have been carried out. The in house research staff at the Federal Energy Technology Center (FETC), Pittsburgh, have conducted a variety of experiments to complement work in the academic and industrial sectors.

The current paper presents a brief summary of a feasibility study for a first demonstration plant for this technology. A complete report of this study [1] should be available by the time of the current meeting. The study was conducted by a committee (see acknowledgement for a list of members) that included participants from the CFFLS, FETC and Burns & Roe. The goals of the study were as follows:

1. To establish a conceptual design for the demonstration plant.
2. To carry out an economic analysis and environmental assessment.
3. To develop a group of stakeholders for the technology.

Potential Resource and Current Practice

Currently, over 44 billion lbs. of waste plastic [2] are disposed of in the U.S. each year. This is approximately 175 lbs. of waste plastics for every man, woman and child in the country. Plastic recycling in the U.S. is primarily mechanical recycling - melting and re-extruding used plastics into recycled plastic components. Uncolored high density polyethylene (HDPE), or milk jugs, is the preferred feedstock for mechanical recycling, although colored HDPE can be used for some types of products, such as plastic lumber, park benches, and marine pilings. Polyethylene terephthalate (PET), used primarily for soft drink bottles, can be recycled into synthetic fibers and carpet feedstock. According to the EPA, [3] approximately 50% of PET soft drink bottles and 30% of HDPE milk and water bottles are recycled but only about 5% of all waste plastics.

Over 280 million automotive tires [4] are disposed of annually in the U.S., or approximately one tire (~20 lbs.) for each person. Furthermore, it is estimated that there are 4 billion tires "on the ground" in this country. Tires are combusted, usually with coal, in utility boilers to produce electricity [5] and they are burned in cement kilns; although these methods of utilizing waste tires are productive, they are not recycling. As part of this study, visits were made to a tire shredding and recycling company. [6] Most of the tires are shredded to a nominal size of 2-4 inches and sold to utilities for combustion. The tipping fee of $0.75 - $1.00 per tire approximately pays the cost of shredding. The price paid by utilities for shredded tires is $20 –25 per ton. At a size of 2-4 inches, most of the steel wire is retained in the tires and it is incorporated into the slag or ash.

A smaller percentage of used tires is shredded to small particle sizes, either by means of recycling through the shredder with finer screen sizes or using such methods as cryogenic comminution, which produces a product known as crumb rubber. [6] Steel wire is separated in the process by magnetic and other methods and can be sold as scrap steel. Crumb rubber is used as an additive to asphalt [7] and for fabrication of rubber mats used for playgrounds, running tracks, stables, etc. A small percentage of crumb rubber (5-10%) from used tires can be added back into new tires; automobile manufacturers may require this in the near future. The cost of producing crumb rubber is approximately 10-20¢ per pound and it is normally sold for 40-50¢ per pound. [6] Currently, 15% of the tires disposed of in this country are recycled. [3]

Waste oils, greases and fuels are also considered in the current report. Although they are not polymers, they are petroleum-derived and coprocess with waste plastics and rubber extremely well. Currently, approximately 30 million barrels of waste lubricating oil, grease and fuel must be either reprocessed or disposed of in the U.S. each year. [8]

The quantities of oil and valuable by-products that could be recovered by liquefaction and upgrading the waste polymers generated annually in the U.S. are estimated in Table 1, assuming a yield of 5 barrels of oil per ton of hydrocarbon feedstock. Important byproducts include carbon black and steel wire from the tires, and aluminum foil derived from labels and lids on plastic containers.

Table 1. Quantities and value of potential products from waste polymers

Waste polymer	Tons/year	Oil (barrels/yr)	By-product (tons/yr)	Value ($/yr)
Plastics	22 million	110 million	Al foil (220,000)	44,000,000
Tires	2.8 million	8.4 million	Carbon black (840,000)	168,000,000
			Steel wire (280,000)	14,000,000
Waste oil		30 million		
Total Oil		148 million		2,960,000,000
Total Potential Revenue				**$3,186,000,000**

In arriving at the dollar values of the products in Table 1, rather conservative values have been assumed: oil - $20/barrel; activated carbon black - $200/ton; aluminum - $200/ton; and steel - $50/ton. It is assumed that the carbon black has been activated and cleaned. In addition to the loss of this potential revenue, approximately a billion dollars per year is currently being spent to put most of these waste materials into landfills. Furthermore, coprocessing these wastes with coal and petroleum resid could approximately double the potential oil resource.

German feedstock recycling industry

The country with the most aggressive recycling program in the world is undoubtedly Germany. The development of the German recycling industry has been in response to very restrictive legislation that requires 80% of all consumer packaging materials to be recovered and 80% of all materials recovered to be recycled. The response of German industry to this law has been the creation of the Duales System Deutschland or DSD. Member companies of the DSD place a small surcharge (roughly a penny) on every container they sell. The money collected (~4 billion DM) is used to subsidize companies that collect, separate, prepare and recycle waste packaging material. DSD supports processing plants that convert the waste plastic into oil, olefins, synthesis gas, and reducing gases for production of steel in blast furnaces. The processing plant closest to the technology discussed in the current report is the liquefaction plant of Koheöl-Anlage Bottrop, GmbH (KAB), which is currently liquefying 80,000 tons of DSD waste plastic feedstock per year. As part of the feasibility study, members of the committee had many valuable interactions with representatives of the DSD and their contractors and a complete description of their operations is given in the full feasibility study report. [1]

Research Summary

Recent research in the U.S. has been summarized in several conference proceedings volumes. [9-11] Much research and development has also taken place in Germany. [12-16] Some of the results that are most pertinent for demonstration plant development are given below.

Plastic liquefaction and coprocessing: The liquefaction of commingled waste plastic typically yields 80-90% oil, 5-10% gas, and 5-10% solid residue. Solid acid catalysts and metal-promoted solid acid catalysts improve oil yields and oil quality. At temperatures above 440 °C, thermal and catalytic oil yields are comparable but lighter oil products are produced catalytically. No solvent is required but good results have been with mixtures of waste oil and plastic. The reactions can be carried out at low hydrogen pressures (~100-200 psig) and with low hydrogen consumption (~1%).

Coprocessing of plastic with coal and resid has been investigated. Generally, the best results have been obtained when using catalysts with both hydrogenation and hydrocracking functions, such as metal-promoted SiO_2-Al_2O_3 or mixtures of metal hydrogenation catalysts with HZSM-5.

Oil yields of 60-70% and total conversions of 80-90% have been obtained. High hydrogen pressures and a solvent with some aromatic character such as petroleum resid are required.

Rubber liquefaction: Crumb rubber is readily liquefied at 400 °C under low hydrogen pressures (~100-200 psig), yielding 50-60% oil, 5-10% gas, and 30-40% carbon black. The oil product is improved by the presence of a metal hydrogenation catalyst such as nanoscale iron or molybdenum sulfide. Experiments on the coprocessing of tire rubber with coal indicate that rubber converts to oil in the same manner as it does when coal is not present. High hydrogen pressures and a hydrogenation catalysts are required for coprocessing of rubber and coal. Because of their relatively high content of carbon black (~30%) and wire (~10%), the feasibility committee concluded that the best approach for tires is to pyrolyse them and hydrotreat the pyrolysis oil, either alone or in mixtures with coal and/or plastic. The carbon black and wire can then be easily separated as byproducts of the process. Activation of the carbon black yields a carbon product with a surface area of several hundred m^2/g.

Plant Design

A modular design was chosen for the demonstration plant. The three principal modules for the base design, illustrated in Figure 1, are as follows:

(1) Tire module - tire pyrolysis, separation of steel wire, and activation/upgrading of carbon black.

(2) Waste plastic module - Melting/depolymerization (M/D) of plastics at a moderate temperature (~380 °C), condensation of light volatile oils with removal of volatile HCl, removal of Al foil and other inerts, and hydrocracking of the liquid product.

(3) Upgrading module - catalytic upgrading of the liquid products from modules 1 and 2 in a slurry phase reactor using a dispersed, nanoscale, iron-based catalyst and distillation of the upgraded product.

An alternative for the waste plastic module is to replace the M/D reactor with a pyrolysis reactor. Such reactors operate at temperatures of 500-750 °C, depending on the type of reactor and residence time, and typically produce about half as much liquid product and two to four times as much gas and solid residue. However, the capital investment is smaller.

A modular approach was adopted to allow potential developers to choose the modules that best suit their needs. For example, if tire recycling is the main objective, modules 1 and 3 would be needed. If converting plastics into high quality oil is the goal, modules 2 and 3 are required. However, module 2 alone would produce a good oil product that could meet the requirements of some developers.

Other feedstocks considered are pyrolysis oils and tars from coal, petroleum resid, and waste oil. It is assumed that these feedstocks require no preparation module, other than possibly heating to lower the viscosity to allow easy feeding to the upgrading module.

Economic analysis: Independent economic analyses for the plant were carried out by Harvey Schindler of Burns & Roe Services Corp. and by Mahmoud El-Halwagi and Mark Shelley of the CFFLS and Auburn University. The uncertainty in the results of the economic analysis is considered to be fairly large (± 30%) for the following reasons:

(1) The small size of the plant (200 tons/day of plastics and 100 tons/day of tires) necessitated scaling down the cost of much larger units.

(2) There were wide variations in equipment cost quotes from different manufacturers.

(3) The committee identified several unanswered research questions related to plant design.

Several modular combinations are considered in the economic analysis given in the complete feasibility report. [1] In the current paper, however, in the interest of space, only the base design shown in Figure 1 will be discussed. The results are summarized in Tables 2-4 and Figure 2. In Tables 2 and 3, Schindler's results are given in column 2 and El-Halwagi's and Shelley's appear in column 3. The costs are given in units of millions of dollars ($MM). It is seen that some of the capital and operating costs in columns 2 and 3 are in reasonable agreement, while others differ significantly. The differences reflect markedly different equipment cost quotations received from different vendors and differences of opinion on the operating requirements of different units in the plant. Currently, the committee is still working to resolve these differences. For the current paper, the author has assumed a set of capital and operating costs arrived at after discussions with Schindler, El-Halwagi and Shelley that appear to be a reasonable compromise. These costs appear in column 4 of Tables 2 and 3. Table 4 gives the product values, total revenues, profits and returns on investment (ROI) for the plant using the compromise costs. The results in Table 4 are arrived at assuming plant operation for 330 days per year with the product values and tipping fees indicated in column 1. Four different scenarios are considered for waste

tires. Case A is the most conservative; it assumes that the shredded tires are purchased from a tire recycling company at a cost of $20/ton. Cases B assumes that shredded tires are delivered to the plant free, while case C assumes that shredded tires are delivered to the plant and the supplier pays the plant a tipping fee of $20/ton. These cases are based on discussions with environmental officials from two states who indicate that they are now paying to have waste tires shredded and then paying to have the shredded tires placed in landfills. Finally, case D assumes that whole tires are delivered to the plant with a tipping fee of $0.75/tire and are shredded at the plant.

The results are quite promising. With a tipping fee of $30/ton for waste plastics, the ROI ranges from 8.6% to 13.5% for cases A to D at an oil price of $20/barrel and from 12.7% to 17.6% at an oil price of $25/barrel. For a 15 % ROI at $20/barrel, the required tipping fee per ton of waste plastic ranges from $41 to $78/ton. Anticipating that tipping fees will continue to rise in this country as they have in the rest of the world, the ROI has been calculated as a function of the tipping fee for waste plastics and the results are shown in Figure 2. Here, the four solid lines are the results for $20/barrel oil and the four dashed lines are the results for $25/barrel oil assuming the four scenarios discussed above for tire tipping fees. It is seen that ROIs of 15-25% are not unreasonable for this demonstration plant.

Conclusions

A brief summary has been given of some of the results of a feasibility study for a demonstration plant for the liquefaction of waste plastics and tires and the coprocessing of these solid wastes with coal, resid and waste oil. The current paper considers the economics only for liquefaction of plastics and tires. The results for a 300 ton/day (200 - plastics, 100 - tires) demonstration plant are quite promising. With oil priced at $20/barrel, the ROI on a capital investment of $49.7 million is estimated to range from 8.6 % to over 20 %, depending on the tipping fees received for waste plastics and tires. With oil priced at $25/barrel, the ROI ranges from 12.7 % to over 25 %. These results are considered particularly encouraging in view of the fact that significant economies of scale could be realized with larger plants. Thus, it seems quite possible that a successful demonstration plant of the size envisioned could lead to a new industry that converts waste polymers into oil and other valuable byproducts.

Acknowledgement: The author would like to acknowledge the U.S. Department of Energy for supporting this research under DOE contract No. DE-FC22-93-PC93053 as part of the research program of the Consortium for Fossil Fuel Liquefaction Science. I would also like to acknowledge all the members of the feasibility study committee who contributed to this work, particularly Mahmoud El-Halwagi, Mark Shelley, Naresh Shah, John Zondlo, Larry Anderson, Ray Tarrer, Irving Wender, and John Tierney of the CFFLS; Michael Eastman, Anthony Cugini, Michael Baird, Kurt Rothenberger, Svenam Lee, and Udaya Rao of the FETC; and Howard McIlvried, Harvey Schindler, John Wilbur and Ram Srivastava of Burns & Roe.

References

1. G.P. Huffman et al., **1997**, Feasibility Study for a Demonstration Plant for the Liquefaction and Coprocessing of Waste Polymers and Coal, report in preparation.
2. Franklin Associates, Ltd., Characterization of Plastic Products in Municipal Solid Waste, Feb., 1990; final report to the Council for Solid Waste Solutions.
3. U.S. Environmental Protection Agency, Characterization of Municipal Solid Waste in the United States: 1995 Update.
4. Hearing before the Subcommittee on Environment and Labor, House of Representatives, April 19, 1990. Scrap Tire Management and Recycling Opportunities, Serial No. 101-52.
5. M.R. Tesla, Power Eng., **1994**, 43-44.
6. John Zondlo, Report on Trip to Rochez Rubber, Appendix to reference 1.
7. Symposium on Modified Asphalt's, Chairpersons: G.M. Memon and B.H. Chollar, American Chemical Society, Division of Fuel Chemistry Preprints, **1996**, *41(4)*, 1192-1327.
8. Ray Tarrer, personal communication.
9. Symposium on Coprocessing of Waste Materials and Coal, Co-Chairs – L.L. Anderson and H.L.C. Meuzelaar, **1995**, *Amer. Chem. Soc., Div. Fuel Chem. Preprints*, **40(1)**.
10. *Fuel Processing Technology, Special Issue,* **Coal and Waste**, Eds. – G.P. Huffman and L.L. Anderson, **1996**, Vol. **49**.
11. Symposium on Liquefaction/Coprocessing, Co-Chairs – Christine Curtis and Francis Stohl, **1996**, *Amer. Chem. Soc., Div. Fuel Chem. Preprints*, **41(3)**.
12. R. Holighaus and Klaus Nieman, "Hydrocracking of Waste Plastics", **1996**; to be published.
13. W. Kaminsky, J. de Physique IV, Colloque C7, supplement III, **1993**, 1543-1552.
14. W. Kaminsky, B. Schlesselmann, and C. Simon, **1996**, *Poly. Degrad. and Stab.*, **53**, 189-197.
15. W. Kaminsky, B. Schlesselmann, and C. Simon, **1995**, *J. Anal.&Appl. Pyrolysis*, **32**, 19-27.
16. B.O. Strobel and K-D. Dohms, **1993**, Proc. Int. Conf. Coal Sci., II, 536-539.

Table 2. Capital costs - case 1: tire pyrolysis, plastics M/D, and upgrading modules.

Unit	Schindler, $MM	Auburn, $MM	Compromise, $MM
Tire pyrolysis	4.300	4.500	4.400
Plastics shredding	10.000	0.339	3.500
Plastics M/D	7.000	9.000	8.000
Plastics hydrocracker	2.910	11.41	7.16
Hydrogenation reactor	4.703	8.55	4.703
Carbon black activation	2.000	2.000	2.000
Hydrogen purification	1.698	0.085	0.085
Product fractionater	0.826	0.594	0.710
General offsites	11.032	11.006	11.019
Subtotal	44.469	47.484	41.417
Contingency(20%)	8.894	9.497	8.315
Total	53.363	56.981	49.732
Capital recovery (15%)	8.004	8.547	7.460

Table 3. Operating costs - case 1: tire pyrolysis, plastics M/D, and upgrading modules.

Cost Item	Schindler, $MM	Auburn, $MM	Compromise, $MM
Maintenance	1.512	2.432	1.678
Labor	3.160	1.920	2.54
Utilities	0.771	1.015	0.893
Purchased hydrogen	0.823	0.774	0.799
Catalysts	0.628	0.338	0.483
Lime	0.327	0.074	0.201
Other chemicals	0.077	0.088	0.083
Solid waste disposal	0.026	0.702	0.297
Wastewater treatment	0	0.009	0.009
Total	**7.984**	**8.012**	**7.643**

Table 4. Product values, profit and ROI for Compromise costs in Tables 2 and 3. Plant is assumed to operate 330 days per year.

Product	$MM[(A)]	$MM[(B)]	$MM[(C)]	$MM[(D)]
Oil at $20/bl	8.296	8.296	8.296	8.296
Act. carbon black - $200/ton	1.795	1.795	1.795	1.795
Steel - $50/ton	0.238	0.238	0.238	0.238
Aluminum - $200/ton	0.264	0.264	0.264	0.264
Plastic tipping fee - $30/ton	1.980	1.980	1.980	1.980
[(A)]Shredded tires cost $20/ton	-0.660			
[(B)]Shredded tires are free		0		
[(C)]Shredded tires bring tipping fee of $20/ton			0.660	
[(D)]Tires shredded at plant; tipping fee of $0.75/tire.*				2.475
Total Revenue with oil at $20/barrel	**11.913**	**12.573**	**13.233**	**15.048**
Profit	4.270	4.930	5.590	6.845
ROI with $30/ton tipping fee for plastics	8.59 %	9.91 %	11.24 %	13.50 %
Plastic tipping fee for 15% ROI	$78/ton	$68/ton	$58/ton	$41/ton
Total Revenue with oil at $25/barrel	**13.976**	**14.636**	**15.296**	**17.111**
Profit	6.333	6.933	7.653	8.808
ROI with $30/ton tipping fee for plastics	12.73 %	14.06 %	15.39 %	17.62 %

*For case D, in which the tires are shredded at the demonstration plant, there is an increase in total capital costs of $248,000 and an increase in annual operating costs of $660,000.

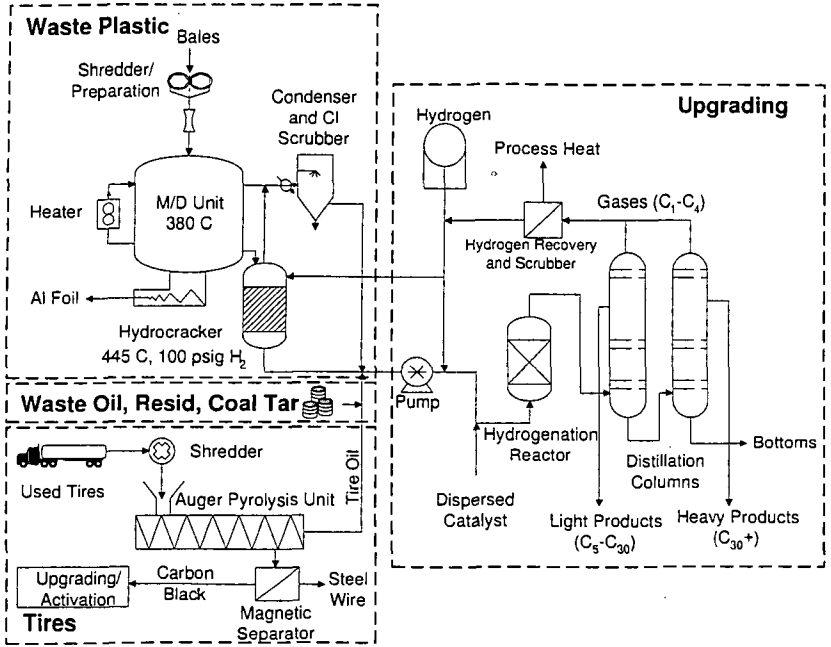

Figure 1. Conceptual design for a demonstration plant for liquefaction and co-processing of waste plastics and tires.

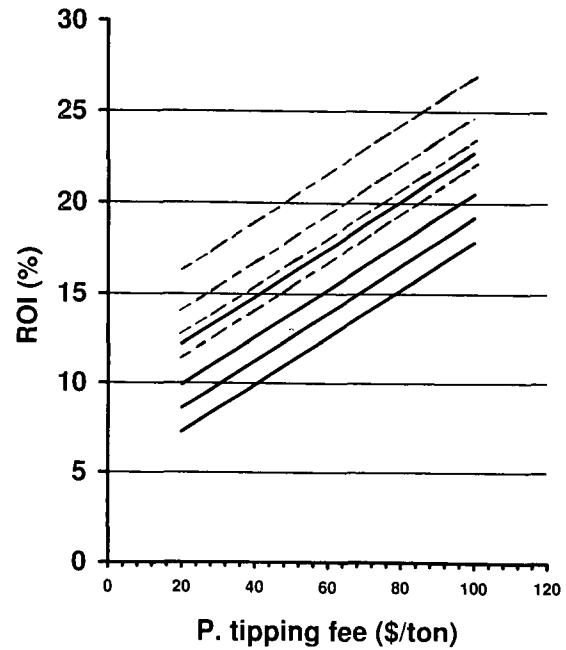

Figure 2. ROI vs. plastic tipping fee.

COPROCESSING COAL WITH HYDROGENATED VACUUM PYROLYZED TIRE OIL

Yanlong Shi, Lian Shao, William F. Olson and Edward M. Eyring
Department of Chemistry, University of Utah, Salt Lake City, Utah 84112

Keywords: coprocessing, vacuum pyrolyzed tire oil, hydrogenation, coal

Abstract

A two-step coprocessing of waste rubber tires with a high volatile bituminous coal is advantageous. The first step involves pyrolyzing the waste rubber tires under vacuum at 600 °C. The condensed volatile material, called vacuum pyrolyzed tire oil (VPTO), is then used as a coal solvent. This solvent increases coal conversion to liquids by 20% when compared to coal conversion with waste rubber tire crumb. GC/MS and NMR analyses of the VPTO show the presence of non-hydrogen donor molecules, such as naphthalene, anthracene, phenanthrene, pyrene, and their methylated derivatives. Partial hydrogenations of VPTO were carried out using different types of presulfided hydrogenation catalysts, including Ni/Al_2O_3, $CoMo/Al_2O_3$, $NiMo/Al_2O_3$, NiW/Al_2O_3, Ni/SiO_2-Al_2O_3, Pd/activated carbon, unsulfided Pt/Al_2O_3 and Pt/activated carbon. The hydrogenations of VPTO were also investigated under different temperatures and hydrogenation pressures when the catalyst was Ni/Al_2O_3. The hydrogenated products were characterized by NMR, GC, GC/MS and elemental analysis. The partially hydrogenated VPTO (HVPTO) products were then coprocessed with different coal ranks at different reaction temperatures and pressures with and without finely dispersed Mo naphthenate, $Mo(CO)_6$, $(NH_4)_2MoS_4$ and $Mo/Fe_2O_3/SO_4$ catalysts. Several model compounds were coprocessed with coal in order to make comparisons with the HVPTO.

Introduction

Solvent plays an important role in coal liquefaction processes. Two features are critical for a solvent to be effective. It must be a good physical solvent for coal products, and it must have H-donor or H-shuttling capacity in order to hydrogenate and stabilize free radicals derived from coal. For a commercial coal liquefaction plant a plentiful and economical supply of process solvent must be available. A possible answer is to utilize various waste oils as coal liquefaction solvents. Converting waste rubber tires back into vacuum pyrolyzed tire oil (VPTO) is one approach.[1-2] Williams and Taylor have shown depolymerization of tire polymer by pyrolysis produces butadiene and styrene products and fragments thereof.[3] The pyrolysis products then proceed through Diels-Alder type reactions to form cyclic compounds which dehydrogenate to yield aromatic molecules that are poor hydrogen donors.[4-5] These products facilitate coal dissolution during liquefaction, and increase coal conversion by 20 % when compared to coal conversion with rubber tire crumb.[2] McMillen and coworkers suggested that non-donor molecules aid in the cleavage of coal bonds.[6] Mochida *et al.*[7] and de Marco and coworkers[8] have shown that partial hydrogenation of non-donors to form H-donor molecules using a hydrogenation catalyst followed by processing the hydrogenated solvent with coal can be an effective method of coal liquefaction

In the present study, the objectives of hydrogenating VPTO were to (1) convert aromatic molecules (especially polyaromatic nondonors) in the oil to hydroaromatics with the capability of donating hydrogen; (2) crack some large polyaromatic molecules to lower molecular weight material that might serve as a better solvent; (3) reduce the coking effect generated by the large polyaromatic molecules; (4) eliminate the need for a disposable coal liquefaction catalyst, making the coprocessing more economical and (5) optimize coal conversion to liquids by coprocessing the partially hydrogenated VPTO (denoted HVPTO) with coals under a range of conditions.

Experimental

Materials. All coals (-60 mesh) were obtained from the Penn State Coal Bank and stored under nitrogen at 0 °C, including Blind Canyon (Utah) coal (DECS-6), Illinois #6 coal (DECS-2), Smith-Roland coal (DECS-8), Beulah coal (DECS-11), Pocahontas coal (DECS-19) and Wyodak-Anderson coal (DECS-26). The model compounds were obtained from Aldrich and used without further purification, including tetralin, naphthalene, pyrene, phenanthrene, anthracene and 9,10-dihydroanthracene. Oil obtained by vacuum pyrolysis of waste rubber tires was produced by Conrad Industries, Chehalis, WA. The VPTO was stored under ambient conditions. Properties of the VPTO

are listed in Table 1. Several hydrogenation catalysts were used on the VPTO, including Ni/Al_2O_3 (Harshaw), $NiMo/Al_2O_3$ (Katalco, 6.7% NiO% and 27.0% MoO_3), $CoMo/Al_2O_3$ (Nalco), $NiMo/Al_2O_3$ (Harshaw), $NiMo/Al_2O_3$ (5.4% NiO% and 20.0% MoO_3), Ni/SiO_2-Al_2O_3 (Harshaw), Pt/activated carbon (5%Pt, Alfa), Pt/Al_2O_3 (5%Pt, Alfa) and Pd/activated carbon (5% Pd, Alfa). Four finely dispersed catalytic systems were used for the coprocessing of HVPTO with coal: Mo naphthenate (ICN Biomedical Inc.), $(NH_4)_2MoS_4$ (Aldrich), $Mo(CO)_6$ (Aldrich) + S and $Mo/Fe_2O_3/SO_4$ + S (Prof. Wender's laboratory).

Hydrogenation of VPTO. All hydrogenation catalysts were presulfided at 350 °C for two hours except Pt catalysts. The presulfidation apparatus is shown in Figure 1. The hydrogenation experiments were completed using a well-stirred stainless-steel 150 cm^3 autoclave reactor (see Figure 2) under various reaction conditions for 1 h. Most reactions were carried out at 325 °C and 1000 psig of H_2(cold). During a typical hydrogenation run, the reactor was charged with 4 g freshly presulfided catalyst and 20 g of VPTO.The reactor was then sealed, purged with N_2 twice, and charged with 1000 psig (cold) of H_2. An electric furnace brought the reactants to the set point temperature at a rate of about 8 °C/min. At the end of the reaction time, measured from the time reaction temperature was reached, the reactor was cooled with a fan to room temperature. The gases were vented (H_2S was trapped by NaOH solution) and the hydrogenated liquids with solid catalyst were collected for further use or analyses. The separation of the liquid from the solid catalyst was completed by filtration with fritted glass filters (medium pore size).

Coal-VPTO or HVPTO Coprocessing. Coprocessing experiments were carried out in 27 cm^3 horizontal tubing reactors. Reactants were brought to the set-point temperature, usually within 10 min, by immersing the reactor in a preheated fluidized sand bath. The reactor was shaken horizontally (3 times/s) to ensure adequate mixing. At the end of a 1 h reaction time, the reactor was removed from the sand bath and allowed to cool at room temperature for 5 mins, and quenched in cold water. Reaction products and solids were removed and extracted with THF, and then the solvent was removed with a rotary evaporator. The THF soluble portion was dried under vacuum for two hours and weighed. The THF insoluble residue remaining in the Soxhlet extractor thimble was also dried for two hours under vacuum. The dried THF solubles were then extracted with cyclohexane. The cyclohexane was removed from the oil sample using a rotary evaporator. The cyclohexane insoluble residue is referred to as asphaltenes. The cyclohexane soluble portion is referred to as oil. $(NH_4)_2MoS_4$ was used as received to impregnate the coal from aqueous solution by the incipient wetness technique. Mo naphthenate was dissolved in HVPTO and then mixed with the coal to get a fine dispersion. $Mo(CO)_6$ (Aldrich) + S was ground to a fine powder and then mixed up with the coal. $Mo/Fe_2O_3/SO_4$ was calcined at 550 °C for approximately 2.5 hours before use. All four of the catalysts were used with 1% by weight presence of Mo or its equivalent (for $Mo/Fe_2O_3/SO_4$ system).

Reactant and Product Characterization Techniques. GC-MS analyses were completed on a Hewlett-Packard 5890 series II gas chromatograph coupled to a Hewlett-Packard 5971 mass spectrometer. A J & W 100 meter DB-1 column was used for the GC-MS analyses. Elemental analyses were completed by Atlantic Microlabs, Norcross, Georgia. ^1H NMR analyses were completed on a Varian XL-300 NMR spectrometer, and $CDCl_3$ with 1% TMS (tetramethylsilane) was used as solvent.

Total conversion of coal and conversions to product fractions were defined on an ash-free basis as follows :

coal conversion: $Y_T = 100(1-Y)$; $Y = (W_I - W_C - W_{ash})/W_{maf}$

conversion to asphaltenes: $Y_A = 100(W_A/W_{maf})$

conversion to oils and gases: $Y_{O+G} = 100(Y_T - Y_A)$

where W_I, W_c, W_{ash}, W_A and W_{maf} are masses of THF insoluble products, catalyst, ash, asphaltenes and moisture- and ash-free coal; Y_T, Y_A, and Y_{O+G} denote total, asphaltenes and gas + oil yields, respectively.

Results and Discussion

Hydrogenation of VPTO

An ideal hydrogenated VPTO would serve as both a good solvent and a good hydrogen donor during processing with coal. That means that one should seek a suitable hydrogenation catalyst under proper reaction conditions to convert the polyaromatic molecules to partially hydrogenated ones, e.g., converting naphthalene to tetralin instead of decalin. Our GC/MS (Fig. 3a) and ^1H NMR (Fig. 4a) analyses show a high percentage of non-donor aromatic molecules in VPTO, such as benzene, naphthalene, anthracene, phenanthrene, pyrene, and their methylated derivatives. Seeking to achieve mild hydrogenation, different types of presulfided hydrogenation catalysts were tested at 325 °C and 1000 psig of H_2 (cold) for 1 h, including Ni/Al_2O_3, $CoMo/Al_2O_3$, $NiMo/Al_2O_3$, NiW/Al_2O_3, Ni/SiO_2-

Al_2O_3, Pd/activated carbon, unsulfided Pt/Al_2O_3 and Pt/activated carbon. Hydrogenation of VPTO was also investigated at different temperatures and hydrogenation pressures when the catalyst was Ni/Al_2O_3. NMR, GC and GC/MS data indicate that the degree of hydrogenation depends not only on the catalysts used but also on the reaction temperature and H_2 pressure. We found that $NiMo/Al_2O_3$ (6.7% NiO and MoO_3) and Ni/Al_2O_3 are the best catalysts, and 325 °C and 1000 psig of H_2 (cold) are the optimum reaction conditions for the subsequent coprocessing of HVPTO with coal. Two typical ^1H NMR spectra of HVPTO are shown in Fig. 3b (Pt/Al_2O_3, 325 °C and 1000 psig of H_2) and 3c (Ni/Al_2O_3, 325 °C and 2000 psig of H_2). GC/MS data shown in Figs. 4a and 4b indicate that many polyaromatic molecules were changed to hydroaromatics, e.g. methylated derivatives of naphthalene were converted to those of tetralin.

Effect of Hydrogenation Catalysts

Figure 5 shows the effect of using nine different hydrogenation catalysts (A: Ni/Al_2O_3; B: $CoMo/Al_2O_3$; C: NiW/Al_2O_3; D: $NiMo/Al_2O_3$ (6.7% of NiO and 27%MoO_3); E: $NiMo/Al_2O_3$ (5.4% of NiO and 20%MoO_3); F: Pt/Al_2O_3; G: Pt/Carbon; H: Pd/Carbon and I: Ni/SiO_2-Al_2O_3) in preparing HVPTO (Hydrogenation conditions: 325 °C, 1 h and 1000 psig of H_2 (cold)) on the coal conversions of the the subsequent stage, when Blind Canyon coal was coprocessed with the hydrogenated oils without coal liquefaction catalysts at 430 °C and 1000 psig of H_2 (cold) for 1 h. For comparison purposes the coprocessing of Blind Canyon coal with unhydrogenated VPTO was also carried out under the same reaction conditions (represented by column J). Differences in the effects of hydrogenation catalysts on the coal conversion are not large from one catalyst to another and vary in the following order: $NiMo/Al_2O_3$ (D, 67.1%) > Ni/Al_2O_3 (A, 63.8%) > NiW/Al_2O_3 (C, 61.6%) ~ Pt/Carbon (G, 61.1%) ~$CoMo/Al_2O_3$ (B, 59.8%) > $NiMo/Al_2O_3$ (E, 57.2%) > Pt/Al_2O_3 (F, 55.7%) > Pd/Carbon (H, 50.3%) ~ Ni/SiO_2-Al_2O_3 (I, 50.2%) > No catalyst, VPTO (J, 34.1%). The coal conversion yield does indirectly reflect the hydrogenation behavior. The highest conversions for $NiMo/Al_2O_3$ (6.7% of NiO and 27% of MoO_3) and Ni/Al_2O_3 mean that they convert the polyaromatics to hydrogen donor-rich hydroaromatics to the optimum extent. It is not surprising that the conversion yield for the coprocessing of VPTO with Blind Canyon coal is the lowest (roughly half of the highest conversion) because no hydroaromatics are present in VPTO. The advantage of the hydrogenation pretreatment over unhydrogenated VPTO for the coprocessing is proven conclusively.

Comparison Between Model Compounds and the Hydrogenated VPTO

Figure 6 shows the comparison of HVPTO (hydrogenated by Ni/Al_2O_3) as solvent with six model compounds, when coprocessed with Blind Canyon coal without a coal liquefaction catalyst. It can be seen that naphthalene, anthracene, phenanthrene and pyrene, which are polyaromatic compounds, give relatively low coal conversions (<52%), due to their non-donor character. The low but still significant conversions obtained with these solvents must be attributed either to direct interaction of H_2 with coal or to H-shuttling reactions in which solvent transfers hydrogen to coal from the gas phase or from hydrogen-rich portions of coal. On the other hand, HVPTO like tetralin and 9,10-dihydroanthracene, which are hydroaromatic compounds, gives a relatively high liquefaction yield (HVPTO (63.8%) < 9,10-dihydroanthracene (66.0%) < tetralin (69.1%)). These results are consistent with the strong H-donor capacity of these model compounds.

Influence of the Hydrogenation Temperatures and Pressures

The effects of hydrogenation temperatures and pressures on the coprocessing of HVPTO with Blind Canyon coal (without a coal liquefaction catalyst) at 430 °C are shown in Fig. 7 and Fig. 8, respectively. Figure 7 indicates that when the hydrogenation temperature is 325 °C the highest coal conversion can be obtained (40.9% at 400 °C < 54.3% at 170 °C < 55.2% at 260 °C < 63.8% at 325 °C). Figure 8 shows that when H_2 pressure is 1000 psig (cold), coal conversion is better than when H_2 pressure is either 500 psig (cold) or 1500 psig (cold). Therefore, hydrogenation at 325 °C and 1000 psig of H_2 (cold) are the optimum reaction conditions. HVPTO obtained at these optimum hydrogenation conditions was used in the subsequent studies. These results are supported by Demirel's detailed hydrogenation studies of polyaromatics.[9]

Effect of the Rank of Coals

Coal conversion values as a function of coal ranks, when the coal was coprocessed with the HVPTO hydrogenated by Ni/Al_2O_3 without a coprocessing catalyst are reported in Fig. 9. The coals are listed according to rank with Pocahontas the highest ranking coal and Beulah the coal of lowest rank. The conversions vary as follows: Illinois #6 (81.9%) > Smith-Roland (68.0%) > Wyodak-

Anderson (65.1%) > Blind Canyon (63.8%) > Beulah (52.9%) > Pocahontas (49.5%). The data indicate that the coal conversion has no correlation with coal rank when the coals are coprocessed with HVPTO. Illinois #6 coal has the largest proportion of sulfur and iron oxide among all six coals. These two substances combine to form pyrite or pyrrhotite which can then act as a catalyst. Thus, Illinois #6 coal shows the highest conversion. Pocahontas has a high fixed carbon content and a low volatile matter content and thus is unreactive. We chose Blind Canyon coal for the coprocessing investigations because it has the lowest percentage of sulfur and iron.

Effects of Coal Liquefaction Catalysts and Coprocessing Temperatures

The comparison of the coprocessing of HVPTO (hydrogenated by Ni/Al_2O_3) and VPTO with or without coal liquefaction catalysts at 430 °C and 350 °C is reported in Fig. 10 and Fig. 11, respectively. In either Fig. 10 or Fig. 11, the catalytic effect is obvious, especially when $(NH_4)_2MoS_4$ or $Mo/Fe_2O_3/SO_4$ + S were used. These two catalysts increased the coal conversion to 94.2% and 91.3% from 63.8% without coal liquefaction catalyst at 430 °C. The incipient wetness technique for the $(NH_4)_2MoS_4$ impregnation provided a very fine catalyst dispersion, which is probably the reason why it yielded the highest conversion. The high conversion obtained from the $Mo/Fe_2O_3/SO_4$ + S system is possibly due to the superacid structure of the catalyst, which increased the cracking or hydrocracking of coal considerably compared to other catalysts, such as $Mo(CO)_6$ + S and Mo naphthenate. When the coprocessing temperature was increased from 350 °C to 430 °C, the conversion for HVPTO without catalyst increased from 53.9% to 63.8%, but conversions with $(NH_4)_2MoS_4$ and $M(CO)_6$ + S as catalysts increased from 59.1% and 73.8 % to 70.1% and 94.2%, respectively.

Conclusions

Hydrogenated VPTO (HVPTO) is a much better solvent than unhydrogenated VPTO for coprocessing with coal, but no effect of varying coal rank is observed. $NiMo/Al_2O_3$ (6.7% of NiO and 27% MoO_3) and Ni/Al_2O_3 are the best catalysts for converting polyaromatics to hydrogen donor-rich hydroarmatics among nine tested catalysts. 325 °C and 1000 psig of H_2 (cold) are the optimum hydrogenation conditions. While HVPTO is a better solvent for coprocessing compared to non-donor polyaromatic model compounds, it is not as good as strong H-donor model compounds such as tetralin and 9,10- dihydroanthracene. $(NH_4)_2MoS_4$ and $Mo/Fe_2O_3/SO_4$ are excellent coal liquefaction catalysts when HVPTO is coprocessed with coal.

Acknowlegements

We gratefully acknowledge Philip Bridges of Conrad Industries, Chehalis, WA for his generous donation of vacuum pyrolzed tire oil. We are also grateful to Professor Joseph S. Shabtai (Department of Chemical and Fuels Engineering, University of Utah) for allowing us to use his autoclave reactor and for very helpful discussions. Special thanks go to Dr. Xin Xiao (Department of Chemical and Fuels Engineering, University of Utah) for some technical assistance with the hydrogenation experiments. The donation of a coal liquefaction catalyst ($Mo/Fe_2O_3/SO_4$) by Prof. Irving Wender (Department of Chemical and Petroleum Engineering, University of Pittsburgh) is also greatly appreciated. Financial support by the U.S. Department of Energy, Fossil Energy Division, through the Consortium for Fossil Fuel Liquefaction Sciences, Contract No. UKRF-4-21033-86-24, is gratefully acknowledged.

References

1. Orr, E.C.; Shi, Y.; Ji, Q.; Shao, L.; Villanueva, M.; Eyring, E. M. *Energy & Fuels* **1996**, *10*, 573.
2. Orr, E.C.; Shi, Y.; Shao, L.; Liang, J.; Ding, W.; Anderson, L. L.; Eyring, E. M. *Fuel Process. Technol.*, **1996**, *47*, 233.
3. Williams, P.T.; Taylor, D. T. *Fuel* **1993**, *72*, 1469.
4. Zmierczak, Z.; Xiao, X.; Shabtai, J. *Fuel Process. Technol.* **1996**, *47*, 177.
5. Orr, E. C.; Burghard, J. A.; Tuntawiroon, W.; Anderson, L. L.; Eyring, E. M. *Fuel Process. Technol.*, **1996**, *47*, 245.
6. McMillen, D. F.; Malhotra, R.; Hum, G. P.; Chang, S-J. *Energy & Fuels* **1987**, *1*, 193.
7. Mochida, I.; Yufu, A.; Sakanishi, K.; Korai, Y. *Fuel* **1988**, *67*, 114.
8. de Marco, I.; Caballero, B.; Chomon, M. J.; Legarreta, J. A.; Uria, P. *Fuel Process. Technol.* **1993**, *36*, 169.
9. Demirel, B. *Ph. D. Dissertation*, University of Utah, **1996**.

Table 1. Properties of vacuum pyrolyzed tire oil (VPTO) provided by Conrad Industries, Chehalis, WA.

C, wt%	87.7
H, wt%	11.0
S, wt%	0.6
N, wt%	0.3
O, wt%	0.4
atomic H/C	1.51
Zn	40 ppm
cyclohexane insolubles	5.2%

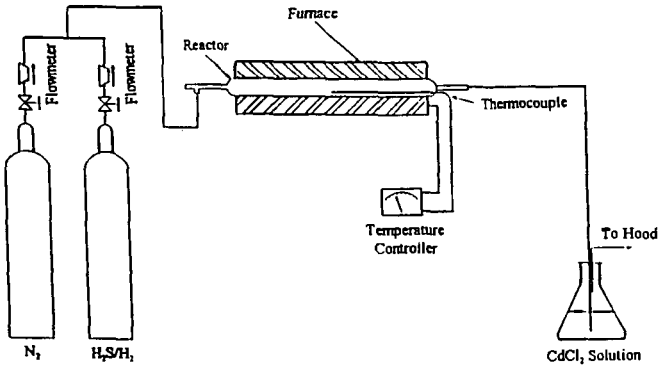

Figure 1. Hydrogenation catalyst presulfidation unit, cited from Ref. 9

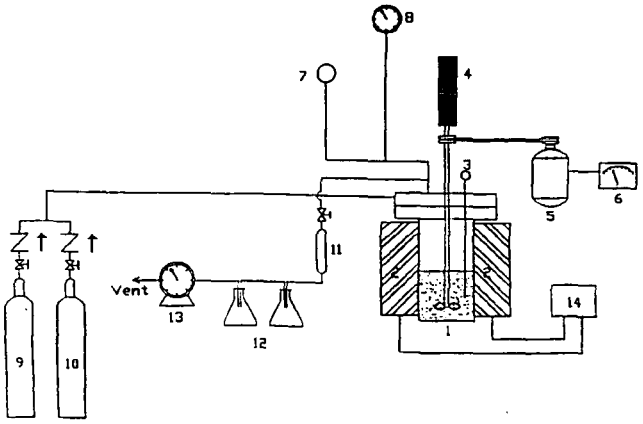

Figure 2. Autoclave reactor assembly for the hydrogenation experiments, cited from Ref. 9.
1: Reactor; 2: Heating jacket; 3: Thermocouple; 4: Magnetic drive assembly; 5: Motor; 6: Stirrer controller; 7: Emergency dump; 8: Pressure gauge; 9: Nitrogen cylinder; 10: Hydrogen cylinder; 11: Gas sample collector; 12: H_2S trap; 13: Wet flow meter and 14: Temperature controller

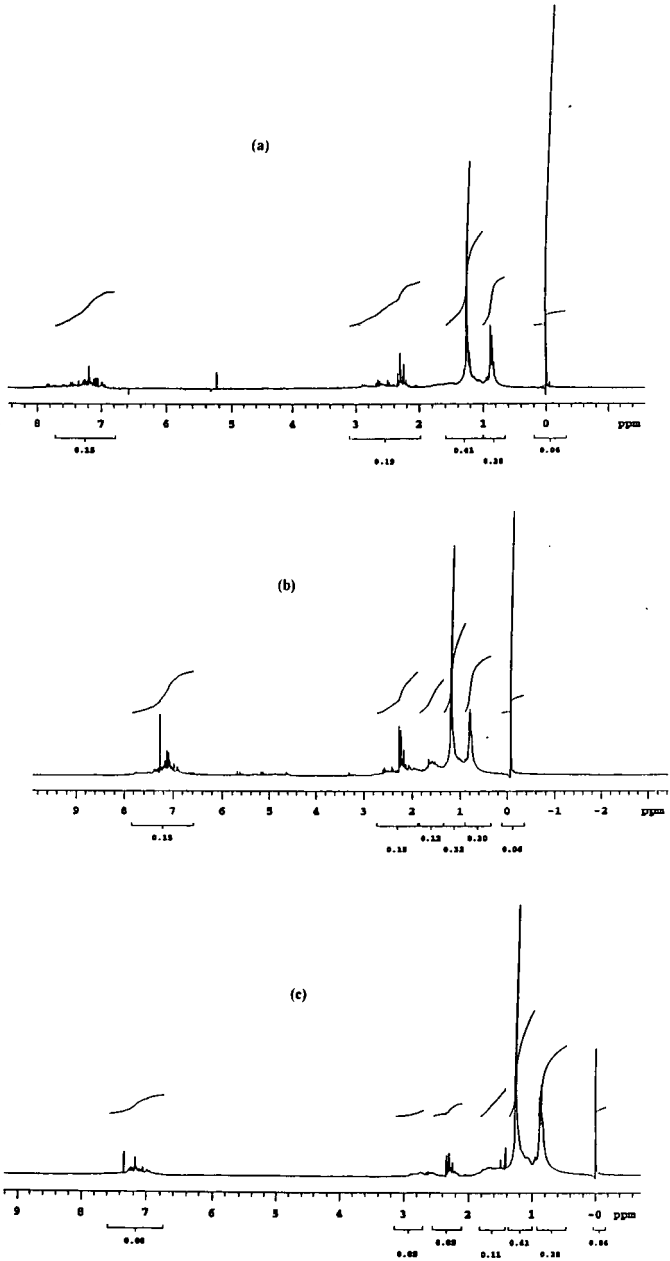

Figure 3. 300 MHz ^1H NMR spectra of VPTO and HVPTO ($CDCl_3$ with 1% TMS used as solvent). (a): VPTO; (b): HVPTO by Pt/Al_2O_3 at 325 °C, 1 h and 1000 psig of H_2 (cold) and (c): HVPTO by Ni/Al_2O_3 at 325 °C, 1 h and 2000 psig of H_2 (cold).

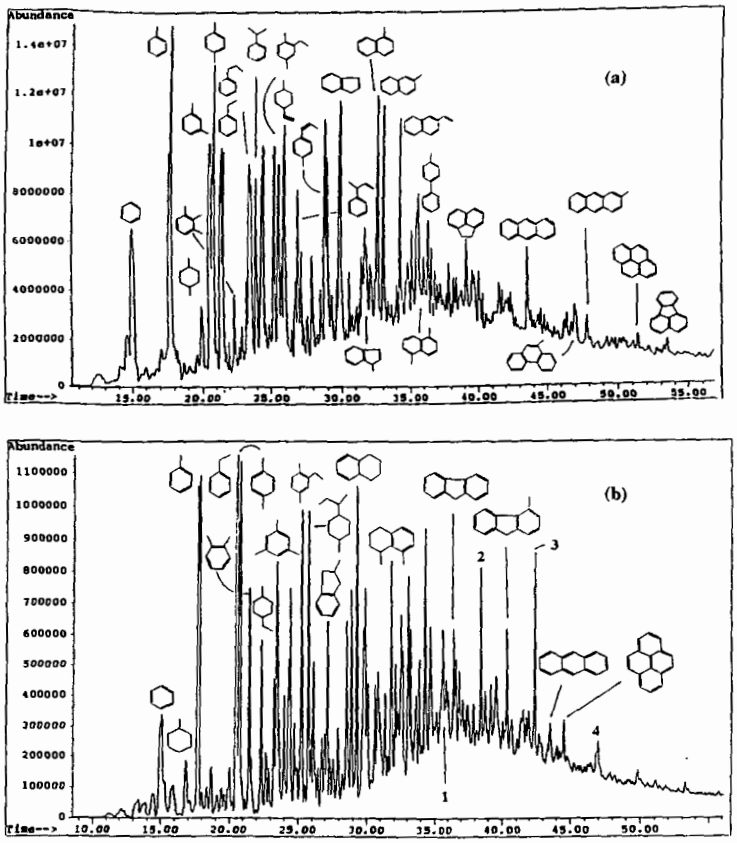

Figure 4. GC/MS analyses of VPTO and HVPTO. (a): VPTO and (b): HVPTO by Ni/Al_2O_3 at 325 °C, 1 h and 1000 psig of H_2 (cold). 1: Dodecane, 2-methyl-6-propyl; 2: Hexadecane; 3: Octadecane and 4: Heptadecane

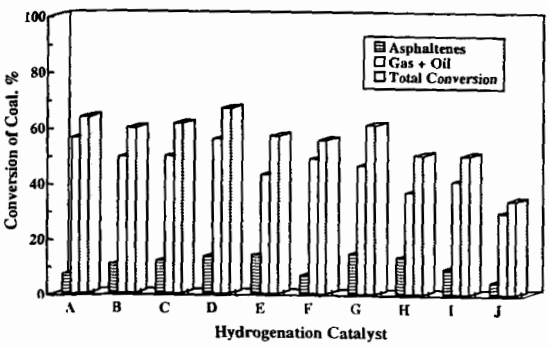

Catalysts used in preparing HVPTO:

A: Ni/Al_2O_3; B: $CoMo/Al_2O_3$;
C: NiW/Al_2O_3;
D: $NiMo/Al_2O_3$; (6.7% of NiO, 27% of MoO_3)
E: $NiMo/Al_2O_3$; (5.4% of NiO, 20% of MoO_3)
F: Pt/Al_2O_3; G: Pt/Carbon;
H: Pd/Carbon;
I: Ni/Al_2O_3-SiO_2;
J: No Catalyst

Figure 5. Effect of using nine different hydrogenation catalysts in preparing HVPTO. The catalysts indicated on the right (A, B, etc.) were used to prepare the HVPTO (Hydrogenation conditions: VPTO, 325 °C, 1 h and 1000 psig of H_2 (cold)). Then the resulting HVPTO was coprocessed with Blind Canyon coal with no catalyst present. (Coprocessing conditions: Blind Canyon coal with HVPTO or VPTO, 430 °C, 1 h, 1000 psig of H_2 (cold) and m_{HVPTO}/m_{coal} = 2g/2g). The last column (J) represents coprocessing of VPTO with Blind Canyon coal.

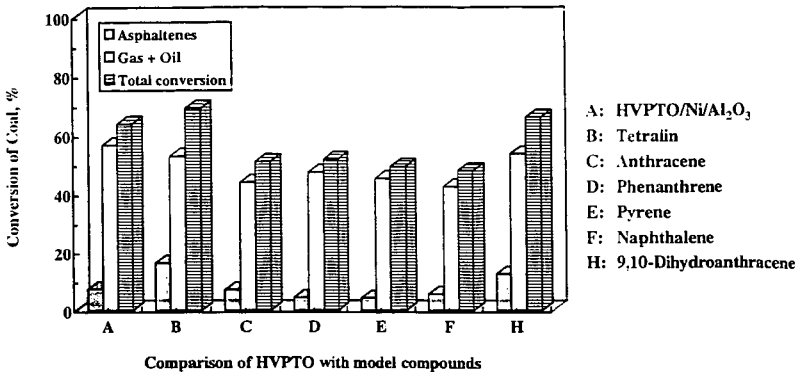

Figure 6. Comparison of HVPTO (hydrogenated by Ni/Al_2O_3 at 325 °C, 1 h and 1000 psig of H_2 (cold)) as solvent with several model compounds for the coprocessing with Blind Canyon coal. (Coprocessing conditions: 430 °C, 1 h, no catalyst, 1000 psig of H_2 and $m_{solvent}/m_{coal}$: 2g/2g)

Figure 7. Effect of hydrogenation temperatures on the second stage of coal liquefaction.
Hydrogenation conditions:
VPTO
Ni/Al_2O_3 as catalyst,
1 h
1000 psig of H_2 (cold)
Coprocessing conditions:
Blind Canyon coal
HVPTO
430 °C and 1 h
1000 psig of H_2 (coal)
m_{HVPTO}/m_{coal} = 2g/2g

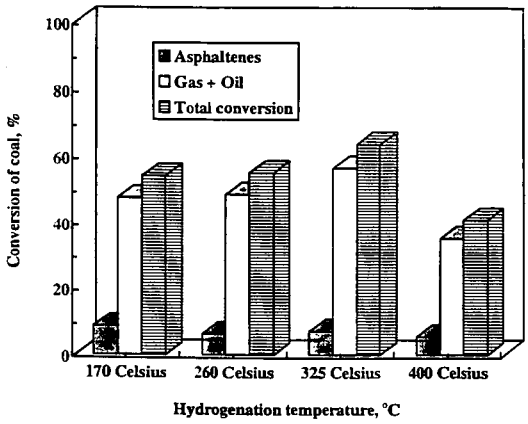

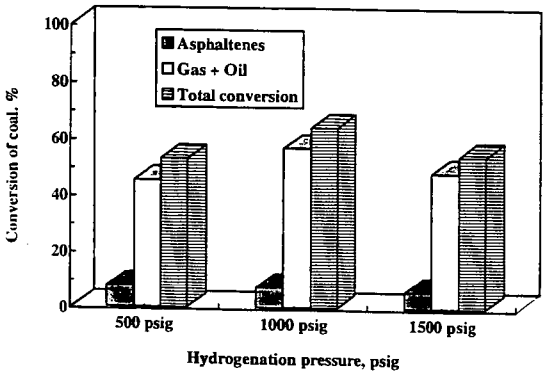

Figure 8. Effect of hydrogenation pressures on the second stage of coal liquefaction.
Hydrogenation conditions:
VPTO
Ni/Al_2O_3 as catalyst
1 h and 325 °C
Coprocessing conditions:
Blind Canyon coal
HVPTO
430 °C and 1 h
1000 psig of H_2 (cold)
m_{HVPTO}/m_{coal} = 2g/2g

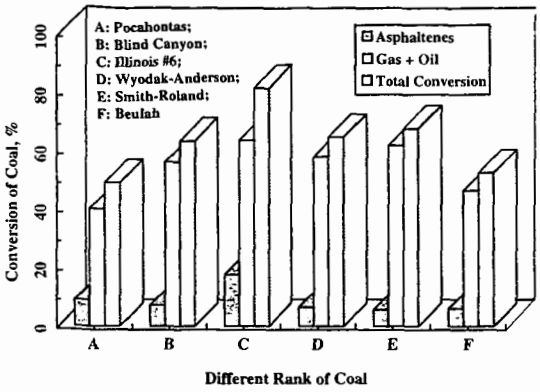

Figure 9. Effect of different ranks of coal on the second stage of coal liquefaction. Hydrogenation conditions: VPTO
Ni/Al_2O_3 as catalyst
1 h and 325 °C
1000 psig of H_2 (cold)
Coprocessing conditions:
Blind Canyon coal
HVPTO
1 h and 430 °C
1000 psig of H_2 (cold)
m_{HVPTO}/m_{coal} = 2g/2g

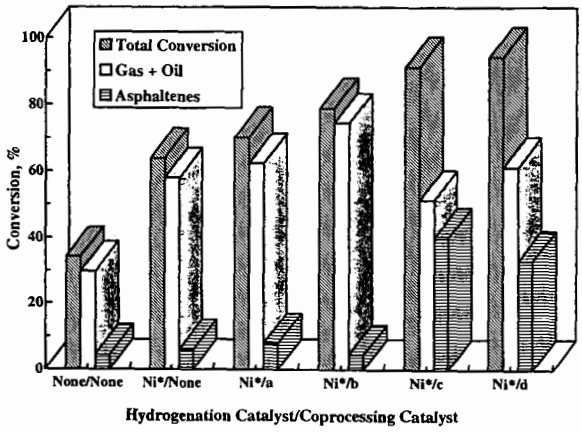

Figure 10. Effect of coal liquefaction catalysts on the coprocessing of HVPTO (hydrogenated by Ni/Al_2O_3 at 325 °C, 1 h and 1000 psig of H_2 (cold)) with Blind Canyon coal.
Coprocessing conditions: 430 °C, 1 h, 1000 psig of H_2 (cold) and m_{oil}/m_{coal}: 2g/2g
Ni* = Ni/Al_2O_3; a: $Mo(CO)_6$ + S; b: Mo naphthenate; c: $Mo/Fe_2O_3/SO_4$ + S; d: $(NH_4)_2MoS_4$

Figure 11. Effect of coal liquefaction catalysts on coprocessing of HVPTO with Blind Canyon coal at 350 °C.
Hydrogenation conditions:
Ni/Al_2O_3 as catalyst
325 °C and 1 h
1000 psig of H_2 (cold)
Coprocessing conditions:
350 °C and 1 h
1000 psig of H_2 (cold)
m_{oil}/m_{coal}: 2g/2g)

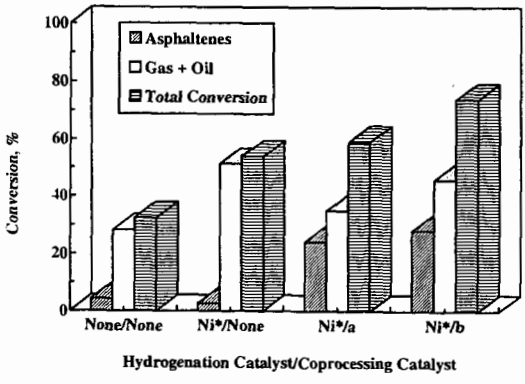

Ni* = Ni/Al_2O_3
a: $Mo(CO)_6$ + S; b: $(NH_4)_2MoS_4$

TWO STAGE CATALYTIC LIQUEFACTION OF COAL AND WASTE TIRE

Ramesh K. Sharma, Dacheng Tian, John W. Zondlo
and Dady B. Dadyburjor
Department of Chemical Engineering
West Virginia University
P.O. Box 6102, Morgantown, WV 26506-6102

INTRODUCTION

Disposal of waste tires is a major environmental problem. Liquefaction of such tires in conjunction with coal was suggested as an alternative for their disposal [1,2]. The addition of tire has a synergistic effect on coal conversion but the synergism decreases in the presence of catalyst at high tire/coal ratios. The synergistic effect is mainly due to the rubber portion of the tire and the effect of carbon black is small. The tire can be liquefied under fairly mild conditions whereas the liquefaction of coal requires relatively more severe conditions. This indicates that optimum conditions for liquefaction of coal and tire are not the same. Further, the simultaneous co-liquefaction of coal and tire has the disadvantage that the carbon black of the tire is essentially lost after the liquefaction since it is mixed with the unreacted coal residue. Hence, a multi-stage process for coal/tire liquefaction may be more appropriate. The first stage of this process is the liquefaction or pyrolysis of tire to obtain tire oil and tire residue (mostly carbon black), and the second stage is the liquefaction of coal with tire oil in the presence of a catalyst. Tang and Curtis [3] studied the two-stage liquefaction of coal and tire using $NiMo/Al_2O_3$ as catalyst and observed that the coal conversion was higher than in runs where the coal was co-liquefied with the whole tire.

In this work, two-stage catalytic liquefaction of coal and waste tire was studied using an impregnated ferric sulfide-based catalyst. This was shown to be a superior catalyst for coal liquefaction [4]. The tire was liquefied separately in first stage at 350° or 400°C under N_2 or H_2. In second stage, coal was liquefied with tire oil (obtained from first stage) at 350-450°C, 1000 psi (cold) H_2, using various tire oil/coal ratios. The effect of various tire oils, prepared under different conditions, on coal liquefaction was studied. The results are compared to those from single-stage co-liquefaction of coal and tire.

EXPERIMENTAL

The tire sample was obtained from the University of Utah Tire Bank and represents a mixture of waste, recycled tires ground to -30 mesh. The tire contains 29% fixed carbon which is essentially carbon black. Wyodak coal, which is a sub-bituminous B coal, was used. The coal was dried overnight at ~100°C. The dried coal has a moisture-content of <1% and 6.6% ash based on dry, ash-free (daf) coal.

Liquefaction of Tire in the First Stage. The liquefaction of tire was performed in first stage using an autoclave. The autoclave was loaded with about 500 g of tire, and was purged and pressurized with N_2 or H_2 to 1000 psi (cold). The autoclave was then heated to the desired temperature of 350° or 400°C and maintained at that temperature for 1h before being cooled. The gaseous products were vented into a hood. The solid and liquid products were washed and extracted with tetrahydrofuran (THF) for 24h. The THF-insoluble material was separated by filtration and represents tire residue. After the removal of THF by rotary evaporation, the THF-solubles were obtained as tire oil. The conversion of tire was ~70% at 400°C, which indicates that the entire organic portion of tire was converted to oil and gas. At 350°C, the conversion was ~53%. The conversions were not affected by the choice of N_2 or H_2. The various

tire oil samples were designated as Tire oil #1 (prepared at 400°C under H_2), Tire oil #2 (350°C, H_2) and Tire oil #3 (350°C, N_2).

Liquefaction of Coal and Tire Oil in the Second Stage. The coal was liquefied with various tire oils (obtained from first stage) at 350-450°C, 1000 psi H_2 (cold) using different tire-oil/coal ratios. The experimental equipment, run procedures and analytical techniques are essentially the same as those described earlier [2]. A stainless steel tubing bomb reactor with a volume of 27 ml was used for the liquefaction. The reactor was loaded with the feed and purged and pressurized with H_2 to 1000 psi (cold). The feed consisted of coal and tire-oil in different ratios. The catalyst was impregnated directly in the coal at a loading of 1.67% based on daf coal. The gaseous products were collected and analyzed by gas chromatography. The solid and liquid products in the reactor were analyzed in the same way as the products from the autoclave. The THF-insoluble material (TI) represents the unreacted coal. After the removal of THF by rotary evaporation, the THF-solubles were extracted with hexane for 2h. The extract was separated into hexane-insoluble (HI) and hexane-soluble fractions. The hexane-insoluble fraction (HI) represents asphaltenes. The conversion (X) and the yield of asphaltenes (A) were calculated as follows:

$$X = (F_m - TI)/F_{daf} \quad (1)$$

$$A = HI/F_{daf} \quad (2)$$

where F_m and F_{daf} represent the amount of coal on moisture-free and daf basis, respectively. The gas yield (G) was determined independently from the gas analysis. The oil yield (O) was obtained by difference:

$$O = X - A - G \quad (3)$$

In most cases, the combined oil+gas yield is reported since the gas yields were usually small (~4.5% at 400°C). The experimental error was ±2%, each, in conversion and asphaltenes yield and ±4% in oil+gas yield.

RESULTS AND DISCUSSION

Effect of Preparation Temperature in the First Stage. Figures 1-3 show the effect of equivalent tire/coal ratio, R_{ETC}, on conversion and oil+gas yield at 400°C for various tire oils. R_{ETC} represents tire/coal ratio for which the tire-oil/coal ratio is the same as in a given run. For example a tire-oil/coal ratio of 0.66 is equivalent to R_{ETC} of 1 since the yield of tire oil from tire at 400°C is ~66%.

As seen in Figure 1, the conversion of coal is low but increases dramatically in the presence of catalyst. The conversion also increases when the coal is liquefied with Tire oil #1. The increase is dependent on the value of R_{ETC} in both thermal and catalytic runs. The oil+gas yield in catalytic runs also increases slightly with increase in R_{ETC}. The results indicate that the tire oil has a synergistic effect on coal liquefaction. A similar synergism is observed in thermal runs using Tire oil #2 with coal (Figure 2). However, in the presence of catalyst, the synergistic effect of Tire oil #2 is negligible. Essentially similar observations are made with Tire oil #3 (Figure 3), except, in this case, the synergism is seen in both thermal and catalytic runs, as with Tire oil #1. Thus, the synergistic effect of tire oil is dependent on the preparation conditions for tire oil in the first stage. This indicates that the nature or composition of various tire oils may be different. Work is underway to characterize the three oils.

The major problem in first-stage-liquefaction of tire was the recovery of Tire oil #3 since the rate of filtration was extremely low. When a coarse filter was used, the tire oil contained significant concentration of carbon black particles and the

synergistic effect of tire oil on coal liquefaction was relatively small, as in the case of Tire oil #2. Both Tire oil #2 and Tire oil #3 were prepared at 350°C. In addition to the difficulties in the recovery of tire oil at 350°C, another disadvantage of using a low temperature in the first stage is that the conversion of tire at 350°C is low so that a significant fraction of the tire oil is lost to the carbon black-residue. This impedes the easy recycle of the carbon black.

Effect of Liquefaction Temperature in the Second Stage. The effect of addition of Tire oil #1 on the results of coal liquefaction at 450°C is presented in Figure 4. The synergism due to tire oil in the absence of catalyst is small. However, in the catalytic runs, both the conversion and yield increase in the presence of tire oil and are highest at R_{BTC}=1. At the higher R_{BTC} value, the conversion is essentially the same as at R_{BTC}=1 but the oil+gas yield is lower. This is in contrast to the results at 400°C where both the conversion and yield increased continuously with increase in R_{BTC}. The results of coal liquefaction at 350°C are not presented since the conversion of coal even in the presence of catalyst and tire oil was low.

Comparison of Two-Stage Results with Single-Stage Co-Liquefaction of Coal and Tire. Figures 5 and 6 compare the results of two-stage liquefaction to those from single-stage co-liquefaction of coal and tire. As seen in Figure 5, the conversion and oil+gas yields from two-stage liquefaction are higher than those from single-stage co-liquefaction at 400°C and the difference increases as the value of R_{BTC} is increased. Essentially similar observations are made at 450°C (Figure 6), except, in this case, the difference between the two-stage and single-stage results is maximum at R_{BTC}=1. Since the most appropriate value of R_{BTC}, from commercial point of view, is around 1, the two-stage catalytic liquefaction is particularly beneficial at high temperatures where the conversions are also high.

CONCLUSIONS

1. The addition of tire oil has a synergistic effect on coal conversion. In the absence of catalyst, the synergistic effects are similar with various tire oils prepared under different conditions. With catalyst, the synergism is greatest with tire oil prepared at 400°C under H_2.

2. The synergism due to tire oil increases continuously with R_{BTC} at 400°C. At 450°C, the maximum synergistic effect is observed at R_{BTC}~1.

3. The synergistic effect of tire oil is greater than that of the whole tire, especially at high tire-oil/coal ratios. This indicates that the two-stage liquefaction may be preferable to the single-stage co-liquefaction of coal and tire.

ACKNOWLEDGMENT. This work was conducted under U.S. Department of Energy Contract No. DE-FC22-90PC90029 under the cooperative Agreement to the Consortium for Fossil Fuel Liquefaction Science.

REFERENCES

1. Farcasiu, M. and Smith, C.M. *Prepr. Pap.- Am. Chem. Soc., Div. Fuel Chem.* 1992, 37(1), 472.

2. Liu, Z., Zondlo, J.W. and Dadyburjor, D.B. *Energy & Fuels* 1995, 9(4), 673.

3. Tang, Y. and Curtis C. W. *Fuel Process. Technol.* 1996, 46, 195.

4. Stohl, F.V., Diegert, K.V. and Goodnow, D.C. *Proc. Coal Liquefaction and Gas Conversion Contractors Review Conference*, Pittsburgh, 1995, 679.

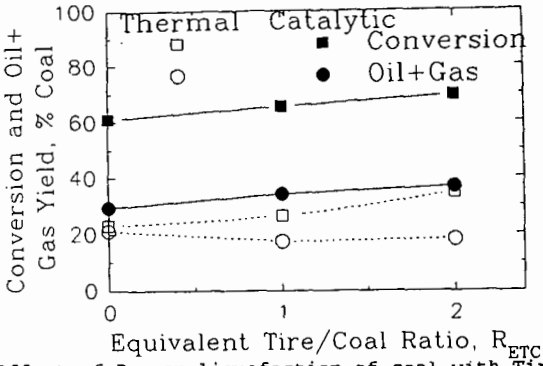

Figure 1. Effect of R_{ETC} on liquefaction of coal with Tire oil #1. Tire oil preparation conditions: 400°C, 1000 psi (cold) H_2. Liquefaction conditions: 400°C, 1000 psi H_2 (cold), 30 min, 1.67% catalyst loading.

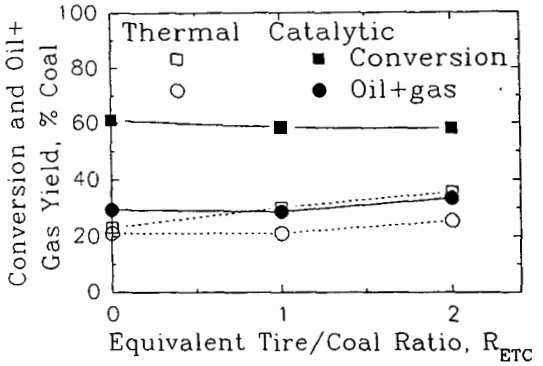

Figure 2. Effect of R_{ETC} on liquefaction of coal with Tire oil #2. Tire oil preparation conditions: 350°C, 1000 psi (cold) H_2. Liquefaction conditions are the same as in Figure 1.

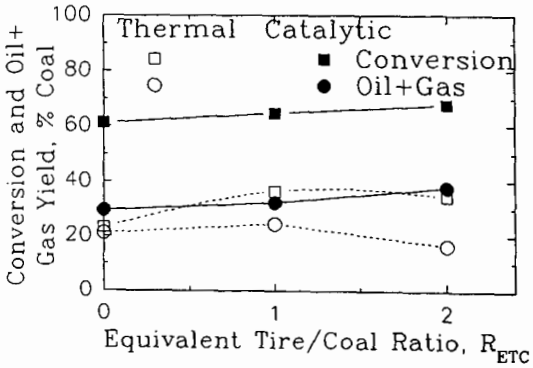

Figure 3. Effect of R_{ETC} on liquefaction of coal with Tire oil #3. Tire oil preparation conditions: 350°C, 1000 psi (cold) N_2. Liquefaction conditions are the same as in Figure 1

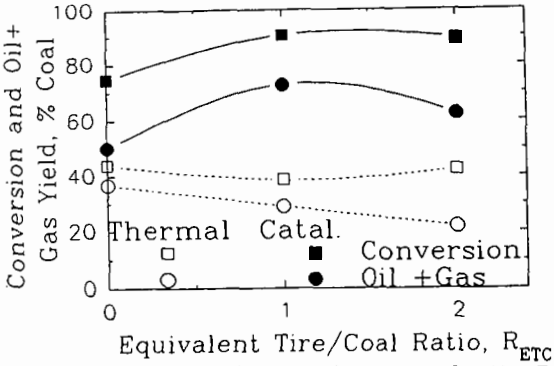

Figure 4. Effect of R_{ETC} on liquefaction of coal with Tire oil #1. Conditions are the same as in Figure 1, except the liquefaction temperature is 450°C.

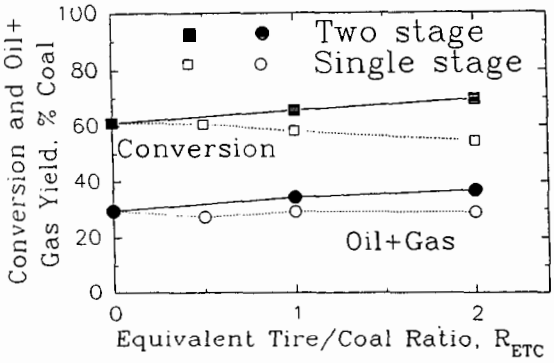

Figure 5. Comparison of two-stage results with single-stage co-liquefaction of coal and tire. Conditions are the same as in Figure 1. Tire oil #1 was used in two-stage and whole tire in single-stage process.

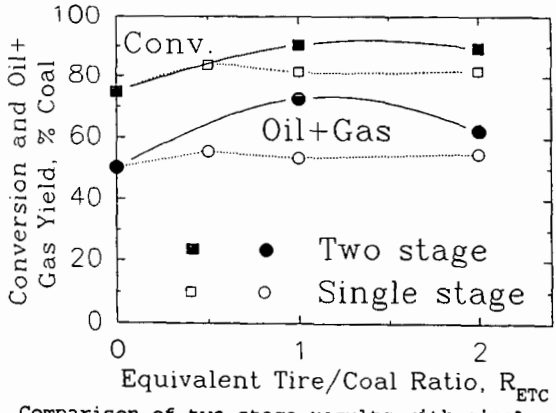

Figure 6. Comparison of two-stage results with single-stage co-liquefaction of coal and tire. Conditions are the same as in Figure 1, except the liquefaction temperature is 450°C. Tire oil #1 was used in two-stage and whole tire in single-stage process.

CO-PROCESSING OF SCRAP TIRES AND WASTE OILS

A.G. Comolli, R. Stalzer
Hydrocarbon Technologies Inc., 1501 New York Avenue, Lawrenceville, NJ 08648

ABSTRACT

In industrialized countries, new scrap tires are generated at approximately one tire per capita per year. In the past, land filling and stockpiling of tires were the most significant means of disposal. Today, both of these methods of disposal are environmentally unacceptable and pose a significant health and fire hazard. The disposal of waste oils represents another environmental problem. Hydrocarbon Technologies Inc. is developing a new process that offers an economically viable solution for converting both these waste materials into marketable products, namely oils and carbonous solids. The oils are easily hydrogenated to yield gasoline and diesel fuel components, while the solids have a potential market as modifiers for paving grade asphalt, filler/coloring agents for rubber goods, and a carbon black replacement. Asphalt testing has shown that the carbonous material is effective in addressing three major sources of roadway failure: rutting, moisture damage and embrittlement. This paper discusses the pilot plant results and preliminary economic assessment.

INTRODUCTION

In an industrialized country new scrap tires are generated at approximately one passenger car tire per capita per year. For the USA this amounts to 250 million tires per year and for the European Community it amounts to 300 million tires per year. In addition, the USA alone contains over one billion tires stored in scrap tire stockpiles. This is a problem that is continuing to grow with the increase in population and the increase in the number of cars per capita. Until a long term solution is found to the large number of scrap tires collected each year, this problem will continue to grow worse.

Less than half of the new scrap tires being generated are used as a fuel supplement in power plants, cement kilns, industrial boilers, etc. Land filling, a significant source of tire disposal in the past, is becoming both less viable and more expensive. More and more landfills are refusing to accept waste tires and many of those that still do also require the tires to be reduced in size by shredding. The only other significant source of tire disposal is stockpiling. Land filling and stockpiling are not environmentally acceptable and pose a significant health and fire hazard. Using tires as a fuel source recovers less than a quarter of the energy used to produce the rubber in the tire.

Waste oils from industrial sources and from automobiles represent another environmental disposal problem, with very little incentive to reprocess the waste oil. These oils are unpopular for reprocessing/upgrading as they have a high solids and metals content. They are typically burned for fuel with the requisite environmental treatment of the exit streams from the burning facility. One of the significant difficulties in using a catalytic process to upgrade waste oil to higher value products such as gasoline, diesel and home heating oil is the metals content of the waste oil. The high metals content normally seen in these streams has a major detrimental effect on the catalyst being used for upgrading. HTI has a long history of testing coal/oil co-processing using oil streams with very high metals content. In a co-processing environment the unconverted coal and the coal ash act as superb scavengers of the metals and the final light product oil is very low in metals content. It is expected that the much higher surface area of the carbon black will act as an even better medium for removing the metals in the waste oil, providing an easy method for improving the quality of the waste oil so that it would make a better feedstock to an upgrading facility.

HTI's new process offers an economically viable solution in converting both of these waste materials into marketable products, namely oils and carbonous solids. The process involves two-stage pyrolysis at moderate temperature. The process was originally developed at the University of Wyoming and thoroughly tested with a wide variety of scrap tires and waste oils allowing for a tailoring of the product slate to meet market demands. The product oils

are easily hydrogenated to yield gasoline and diesel fuel components, while the solids have a potential market as a modifier for paving grade asphalt, a filler/coloring agent for rubber goods and as a carbon black replacement.

MATERIAL AND METHODS

This work was performed in a 0.3 ton/day unit. A simplified overview of the process is shown in Figure 1. Waste tires are cut into pieces less than six inches long, preheated and then mixed with lime and preheated filtered waste oil before entering the first of two steam heated screw conveyor reactors in series. The primary screw conveyor reactor dissolves the rubber shreds in the waste oil and allows the steel and fibers to separate out at temperatures under 400°C. The upper zone of the first screw conveyor reactor is maintained at 425°C to 450°C and permits the ready removal of gases and light oils. The first reactor also permits the use of additives to modify the final product or to assist in the dissolution of the tires and to control the gas yields. One such additive that has been used is CaO. The heavy oils, carbonous material, steel and fibers move to the second reactor which is maintained at nearly 480°C. This second reactor is fine tuned to drive off most of the remaining oil, leaving behind just the residue and producing a solid carbonous residue material. The typical oil content of the carbonous product is less than 1 W%.

RESULTS AND DISCUSSION

The product oil was evaluated to determine its initial quality as a feedstock to a refinery or for hydrotreating. Table 1 summarizes the results indicating that the material would be acceptable for either use.

Modified asphalt was evaluated with the addition of 10 W% carbonous residue to the AC-10 asphalt. The four main criteria of asphalt quality that were investigated were rutting, oxidative ageing, embrittlement and moisture sensitivity. The improvement in rutting performance is measured by the improvement in the complex viscosity between a control sample and the modified sample. This showed a 50% improvement indicating that the modified sample should be less susceptible to rutting. The ageing effect was determined by looking at the change in the complex viscosity after the sample had been aged in an oxidative environment (163°C for 1.4 hr). The age index for the control sample was 2.65 while it was only 2.33 for the control sample. Embrittlement was determined by observing the change in the complex viscosity after 2 hours and after 4500 hours. The control sample showed an increase of 39% while the modified sample showed an increase of only 2%. Moisture sensitivity was determined by measuring the number of freeze-thaw cycles required for failure. This test was performed with five different aggregates. In all cases the modified samples shows a significant increase in the number of cycles required for failure.

Another potential commercial avenue for the carbonous product is as a carbon black replacement. An analysis of the carbonous product is shown in Table 3. As indicated by the composition analysis, the material is nearly entirely carbon black or ash, only a small amount of extender and polymer is still present. The ash content is significantly higher than that found in commercial carbon blacks which are normally less than 1%. This does not severely impact on the quality of the carbon black as measured by the surface area and DBP No. (dibutyl phthalate absorption number in cc dibutyl phthalate / 100 gms carbon black). The carbonous product has properties very similar to N660 which is a general purpose furnace black with a DBP No. of 90 and a surface area of 35 m^2 / gm.

ECONOMICS

The commercial size plant being evaluated is 30 tons/day of waste tires or roughly 1 million tires annually. Using current government statistics, this would be about 10% of the annual number of tires discarded in the three-state Delaware Valley region or in the New England region. The plant would also be sized to process 7 tons/day of waste oil. This is less than 5% of the market for the annual waste oil from 5 million cars, assuming four oil changes per car per year, and assuming each oil change produced four quarts of useable oil. Output

would be 12 tons/day of solids and 114 bbl/day of oil and 5 tons/day of steel and fiber byproducts. The cost of erecting a 30 ton/day plant was estimated to be $5.0 MM. The waste oil is considered to be available at no cost. The base case for the scrap tires is that they are also available at no cost and also at no tipping fee.

There are four significant product streams to be considered, two minor and two major. Of the two minor streams, the recovered steel fibers have a ready market in the recycle industry. The other very minor product stream is the reinforcing fiber present in tires. A market has not yet been identified for this stream and at present no value is placed on it. Even with a value it would have a very minor impact on the total process economics as it is such a small process stream. In order for this process to be economical a market needs to be found for the two main product streams, the oil product and carbonous residue material. The oil products can be readily upgraded and should have at least an equivalent value to crude oil. For this evaluation this was taken as $20/bbl. The carbonous material is the main product variable effecting the economics of this process.

In order to determine the required selling price of the carbonous product a sensitivity on the carbonous product price vs the main feed component in the carbonous product (ie. the scrap tires) was performed. The sensitivity was performed for two different rates of return, 10% and 15% (Figure 2). As the curves show, a selling price for the carbonous product of only $0.12/lb to $0.13/lb is required to make this process economically feasible.

CONCLUSIONS

The co-processing of waste oils and scrap tires is a viable method for dealing with the continuing disposal problem for both waste oil and scrap tires. The product oil is suitable as either a feedstock to a refinery or for subsequent hydrotreating for upgrading. The carbonous product has been demonstrated to have a positive impact on asphalt improving moisture resistance, embrittlement, rutting and ageing. It is expected that these improvements would substantially lengthen the useful life of a surface paved with an asphalt modified with this carbonous product. The carbonous product is also a potential replacement for a general purpose furnace black. The economics of this process are favorable even without a tipping fee for the scrap tires at a carbonous product price of $250 / ton or higher. Further work is being planned to improve process economics.

ACKNOWLEDGMENTS

Dr. Chang Y. Cha, University of Wyoming
Henry Plancher, University of Wyoming
Robert Lumpkin, Amoco

TABLE 1: PRODUCT OIL ANALYSIS			
Elemental Analysis, W%		Distillation, W%	
Carbon	85.91	IBP-177 °C	15.8
Hydrogen	11.60	177-343 °C	32.8
Nitrogen	0.36	343-538 °C	50.6
Sulfur	0.60	538 °C+	0.3
Oxygen	0.83		
Physical Properties			
API Gravity	26		
Aromatics Carbon, W%	27.8		

TABLE 2: ASPHALT TESTING RESULTS	Control	Modified
Complex Viscosity ($\eta^* 10^5$), poise	20.3	30.4
Oxidative Aged Complex Viscosity ($\eta^* 10^5$), poise	53.8	70.7
Age Index	2.65	2.33
Embrittlement as Measured by Complex Viscosity ($\eta^* 10^5$), poise		
After 2 hours cure	0.78	1.21
After 4500 hours cure	1.09	1.23
% increase	39.2	2.0
Moisture Sensitivity as Measured by Freeze-Thaw Cycles to Failure		
Brokaw Aggregate	3	13
Hardigan Aggregate	4	10
9th Street Aggregate	6	>50
Simon Pit Aggregate	4	>50
Southbend Aggregate	>50	>50

TABLE 3: CARBONOUS PRODUCT ANALYSIS			
Composition Analysis, W%		Elemental Analysis, W%	
Extender	0.24	Carbon	79.72
Polymer	3.36	Hydrogen	1.30
Carbon Black	80.40	Nitrogen	0.24
Ash	16.00	Sulfur	2.74
Quality Assessment			
BET Surface Area, m^2/gram		53	
Dibutyl Phthalate Absorption Number		84	
Oil Content, W%		<0.1	

FIGURE 1: SIMPLIFIED PROCESS DIAGRAM

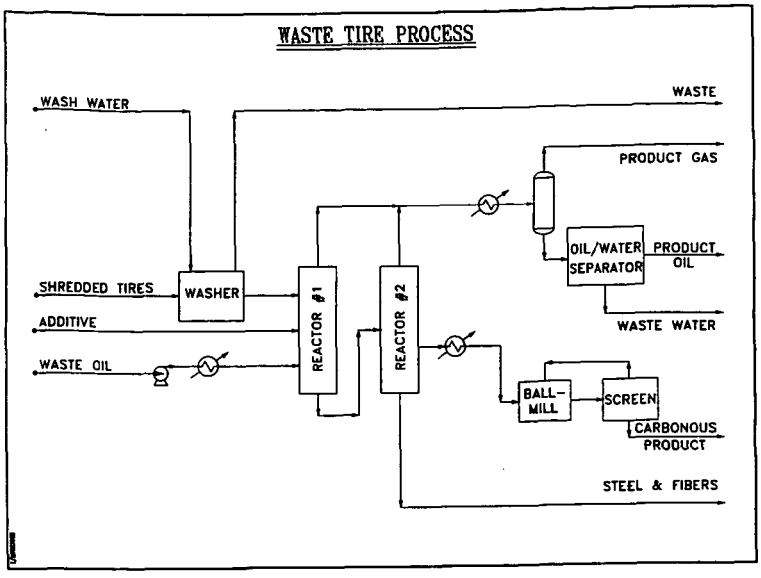

FIGURE 2: SENSITIVITY OF CARBONOUS PRODUCT PRICE AND TIRE COST

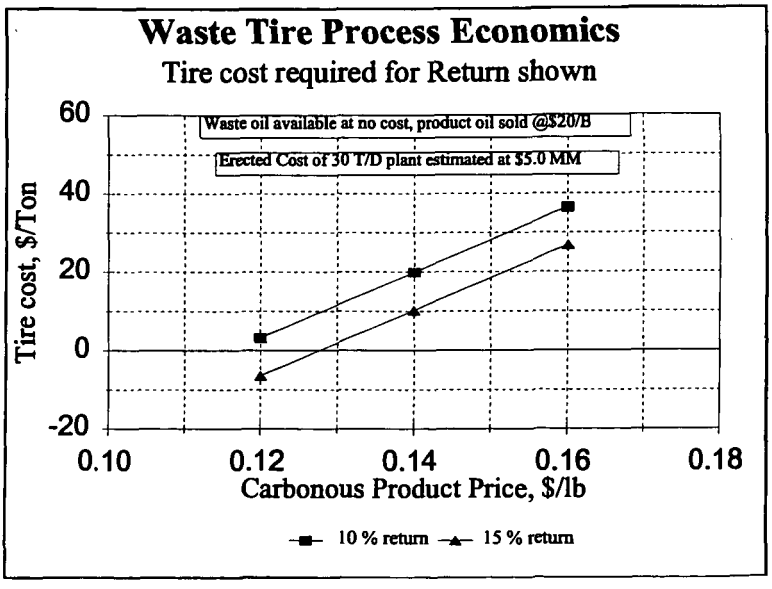

CATALYTIC LIQUEFACTION OF SURFACTANT-TREATED COALS

S. Mayes, K.B. Bota, G.M.K Abotsi, G. Saha
Department of Chemistry
Clark Atlanta University
Atlanta, Georgia 30314

Keywords: surfactant-treated coals, catalyst, zeta potential.

INTRODUCTION

The purpose of this study is to critically study the efficiency of the adsorption of catalysts onto coals that have been treated with surfactants. The diminishing supplies of petroleum requires that research be conducted to produce coal-derived liquids as supplements for transportation fuels. Catalyst dispersion on coal is dependent upon the nature of the catalyst and the coal surface. Pre-treatment of coal surface with an appropriate surfactant can enhance catalyst dispersion.[1] The aim of this work is to achieve improved catalyst dispersion on coal by preadsorption of various cationic, anionic, and neutral surfactants such as dodecyl dimethyl ethyl ammonium bromide (DDAB), sodium dodecyl sulfate (SDS) and Triton X-100 onto coal.

Potentially, this ongoing research can result in the development of a low cost technique for efficient dispersion of iron and molybdenum catalysts in coal by preadsorption of surfactants onto coal. This should make the coal surface hydrophobic and enhance the adsorption and dispersion of iron/molybdenum-containing organic compounds and carbonyls, and thus provide information about the roles of coal hydrophilic and hydrophobic sites on the chemistry of adsorption of coal conversion catalysts. Appropriate selection of the surfactants used for coal-water slurry preparation should allow successful integration of this catalyst loading technique into the coal-water slurry mode of transport which will allow sufficient time for catalyst penetration and dispersion in the coal.

EXPERIMENTAL

An Illinois No. 6 coal (DECS-24), obtained from the Penn State Coal Sample Bank, was used in this work. Its moisture, ash, volatile matter, and fixed carbon contents were 13.2, 11.6, 35.4, and 39.7 %wt, respectively, on as-received basis. Elemental analysis gave 11.6% ash, 57.3% carbon, 4.0% hydrogen, 1.0% nitrogen, 4.8% sulfur, and 8.1% wt oxygen (by difference). The surfactants were supplied by Aldrich Chemical Co. Ammonium molybdate(VI) tetrahydrate (AMT) was used as the molybdenum catalyst precursor.

The zeta potentials of the raw coal and its samples that were treated with the surfactants were measured at room temperature using a Pen Kem 501 zeta meter as described previously.[2] Zeta potential measurements allowed the determination of the surface charge properties of the coals. The effect of surfactants and pH on molybdenum adsorption was determined by elemental analysis for molybdenum after the adsorption studies using atomic absorption spectrophotometery. Pretreatment of the coal-water slurry with surfactants and subsequent catalyst loading was done by ion-exchange technique using a Burrel Wrist Action Mechanical Shaker, Model 75, manufactured by Burrell Corporation, Pittsburgh, PA.

Following the surfactant and catalyst loadings, the surfaces of the coal samples were examined using Atomic Force Microscopy (AFM) at the Savannah River Ecology Laboratory (SREL), Aiken, SC. The instrument used was a Burleigh ARIS-3300 AFM with two sample scanning modes. AFM is a variation of the Scanning Tunneling Microscope and it measures the interatomic forces and surface features.[3,4] The samples were mounted on epoxy and imaged by tapping with the probe tip of the AFM imaging instrument. Tapping mode imaging overcomes the limitation of conventional scanning modes

(contact and non-contact mode), by alternately placing the tip of the scanning probe in contact with the surface to provide high resolution and then lifting the probe tip off the surface to avoid dragging the tip across the surface. The technique allows high resolution topographic imaging of sample surfaces that are easily damaged, loosely held to their substrate, or otherwise difficult to image by other AFM techniques.

The effectiveness of the catalyst loading technique was measured by liquefaction activities of the raw coal and the catalyst-loaded samples. Liquefaction studies were conducted in a stainless steel batch microautoclave reactor. The internal volume of the reactor including all tubing and connections was 60 mL. For continuous monitoring of pressure and temperature during the experiment, an internal thermocouple and pressure transducer were used. The samples were tested using 6.6g of solvent, 3.3 g of coal and 6.9 MPa (1000 psi) ambient hydrogen pressure. The reactor was then attached to the rocker arm of a motor that vibrated at 180 cycles/min, and plunged into a pre-heated sandbath that was heated to 425°C in 40 minutes. This temperature was maintained for 30 minutes, after which the reactor was removed and cooled with water. The liquid and solid products were removed from the reactor using tetrahydrofuran(THF). Coal conversions were calculated based on THF and heptane solubility.

RESULTS AND DISCUSSION

Measurements of the surface charge densities of the coal samples gave the results expected for the surfactants. The raw sample produced negative zeta potentials over the pH range investigated. As discussed elsewhere,[2] the coal particles showed positive zeta potentials as a result of the adsorption of DDAB. Since DDAB is cationic, the positive charge density on the coal can be explained by the coulombic attraction of the surfactant to the negatively charged sites on the coal. The opposite effect was observed for the anionic surfactant, SDS.

As shown in Figure 1, the maximum zeta potential of the raw coal was about -80 mV. However, adsorption of 0.25 and 0.1 M Triton reduced the negative charge density appreciably. This is surprising since Triton is a neutral surfactant. Reasons for this behavior will be sought through further studies. The effects of surfactant concentration in the adsorption of molybdenum is shown in Figure 2. As shown this figure, a higher molybdenum adsorption occured when DDAB was used. The minimum amount of this surfactant required to saturate the surface is about 0.1 mol/L. However, the opposite effect (low catalyst loading) was observed when the anionic surfactant (SDS) was used. There is very little adsorption of molybdenum, which is ascribed to the fact that SDS and the molybdenum oxyanions in solution are negatively charged and create repulsive forces.

The results for the Atomic Force Microscopy studies are apparently consistent with the results observed from zeta potential and catalyst loading experiments. Figure 3 is a scan of the surface of the untreated coal, which shows that the surface has rough, uneven appearance with several crevices. The surface of the coal treated with SDS is depicted in Figure 4. In this micrograph rod-like structures are distributed in layered patterns on top of the rough surface of the coal. These rods are attributed to adsorbed surfactants and/or surfactant-molybdenum complexes onto the coal surface. Figure 5 shows the coal surface which has been treated with DDAB followed by molybdenum loading. This image shows a smoother, more defined coal surface, with pellets randomly distributed on the surface. However, the composition of the pellets is unknown at this time. The surfaces of the samples were imaged in the dimension range from 5μm to 100 nm. The imaging of the samples posed some difficulties in the area of uneven topology. Imaging even small areas of the particle surface was difficult since the topology was typically greater than the length of the AFM probe tip. In order to obtain better images so that definitive comparisons between samples can be made, furthur AFM studies will be conducted with thin polished sections of the samples. Another alternative would be to fractionate the samples and image very small (< 500 nm) size particles.

The liquefaction data are presented in Table 1. As can be seen from the results, the conversions for the raw coal and its sample that was treated with the surfactant (Triton X-100) were 72 and 78 wt%, respectively. However, a higher level of conversion (96 wt. %) was observed for the surfactant-assisted molybdenum impregnated coal. This result is also higher than that obtained for the nonsurfactant assisted molybdenum loading (89 wt %) and suggest that the surfactant may have enhanced the dispersion of the molybdenum catalyst. Further testing is in progress to evaluate the effects of other surfactants on the activities of the catalysts.

This work has shown that molybdenum loading can be enhanced by treatment of an Illinios No. 6 coal with cationic surfactants, such as DDAB prior to catalyst addition from solution. Compared to the untreated coal, higher liquefaction activity was obtained when the coal was pretreated with Triton X-100.

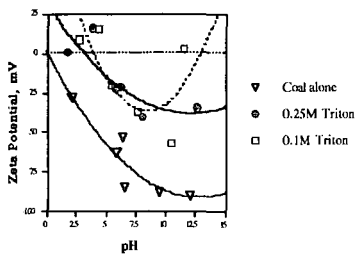

FIGURE 1. Zeta Potential of the Raw and the Triton-treated coals.

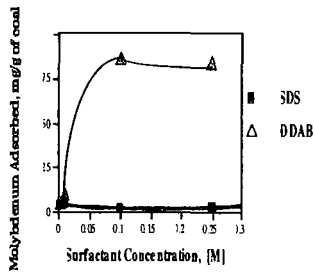

FIGURE 2. Dependence of molybdenum loading on DDAB and SDS concentration.

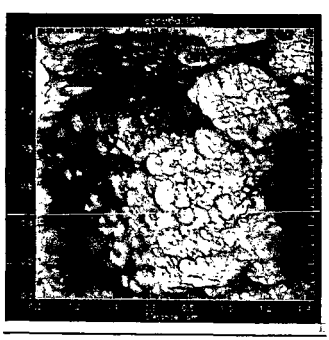

FIGURE 3. Atomic Force Micrograph of the raw coal.

FIGURE 4. Atomic Force Micrograph of the coal surface after treatment with SDS

FIGURE 5. Atomic Force Micrograph of the DDAB-treated coal.

Sample	THF Solubles (Total Coal Conversion to Liquids)	Hexane Solubles (Oils)
Coal + Mo + Triton	96.2%	46.7%
Coal (Original)	72.4%	33.8%
Coal + Triton	77.9%	33.2%
Coal + Mo	90.0%	50.0%

TABLE 1. THF and Hexane conversions of the various coal samples

REFERENCES

1. Abotsi, G. M. K.; Bota, K. B.; Saha, G., Mayes, S., "Effects of Surface Active Agents on Molybdenum Adsorption onto Coal for Liquefaction," Prep. Pap.-American Chemical Society, Division of Fuel Chemistry, ***41 (3), 984-987, 1996.***

2. Abotsi, G. M. K.; Bota, K. B.; Saha, G., "Enhanced Catalyst Loading on Surfactant-Treated Coals," 4th Annual Historically Black Colleges and Universities/Private Sector-Energy Research and Development Technology Transfer Symposium Proceedings, ***33-36, 1996.***

3. Zhong, Q.; Innis, D.; Kjoller, K.; Elings, V. B., "Fractured Polymer/Silica Fiber Surface Studied by TappingMode Force Microscopy" Surf. Sci. Lett. **290**, *L688-L692, 1993.*

4. Vatel O., et.al., "Atomic Force Microscopy and infrared spectroscopy studies of hydrogen baked Si surfaces," Japanese Journal of Applied Physics, **32**, *L1289-91, 1993.*

ACKNOWLEDGEMENTS

Financial support for this work, provided by the United States Department of Energy, under contract number DE-FG22-95PC95229 is gratefully acknowledged. We thank Dr. Anthony Cugini, FETC, Pittsburgh, PA, for his assistance with the coal liquefaction studies and Dr. Paul Bertsch, SREL, Aiken, SC, for the Atomic Force Microscopy work.

TWO STAGE PROCESSING OF POST CONSUMER PLASTICS WITH COAL

Mingsheng Luo and Christine W. Curtis
Chemical Engineering Department
Auburn University
Auburn, Alabama 35849-5127

KEYWORDS: waste plastics, coal, two stage coprocessing

ABSTRACT

Coprocessing of coal with plastics oil from Conrad Industries and post-consumer plastics from Germany was performed to evaluate the effect of first stage waste plastics processing on the final products obtained from the two stage processing of waste plastics with coal. The plastics oil was obtained from the pyrolysis of waste plastics, and yielded an oil with a considerable amount of light materials that were removed by distillation prior to use. The heavier fraction from the plastics oil was coprocessed with the coal. The post consumer plastics which were introduced as solids were processed at 440 °C for 60 min, with 2.75 MPa of H_2, introduced at ambient temperature, and a first stage catalyst which was either HZSM-5 or Low Alumina. For both sources of plastics, the second stage reaction, in which the liquid plastics from the first stage were combined with coal, was performed at 400 °C using either Fe or Mo naphthenate slurry phase catalyst precursors. The effect of the waste plastics sources and processing on the product distribution and the boiling point distribution from coprocessing with coal was evaluated and compared.

INTRODUCTION

Post consumer plastics are waste materials that are usually disposed of in land-fills. The feasibility of taking waste plastics from actual waste streams and converting them to usable materials, such as fuels and chemical feedstocks, is important for minimizing waste and fully utilizing our natural resources. These post-consumer plastics contain not only the polymers composing the plastics, but also the compounds that have been added to serve as antioxidants and fillers. Hence, these plastics, both because of the composition of the plastic itself and because of the variety in the mixture composition, may have different liquefaction properties and characteristics to those of the pure polymer. The available supply of post-consumer plastics is relatively small and, if converted to a liquid fuel, would only produce an annual amount that was sufficient to provide a one month's supply of fuel for the United States. (Techline, 1996)

Previous research has been performed investigating the coprocessing of waste plastics with coal. The results showed that single stage reactions of these disparate materials were difficult, as neither the reaction conditions nor the catalysts could be tailored simultaneously for both materials. (Luo and Curtis, 1996a,b) Subsequent research involved the two stage processing of coal and waste plastics such that the waste plastics were reacted in the first stage at conditions that promoted their conversion to liquids. (Ding et al, 1996; Luo and Curtis, 1996c) The liquid products obtained were then used as a solvent and reacted with coal in a less severe second stage reaction that used hydrotreatment catalysts designed to promote the liquefaction of coal. The second stage reaction temperature affected the breakdown of the waste plastics solvent and, if too high, would result in substantial gas production. (Luo, 1997)

This study investigated the effect of the type of first stage processing and the source of waste plastics on waste plastics coprocessing with coal. Two different types of first stage processing were investigated. The first type of processing consisted of pyrolyzing waste plastics in the Conrad Industries process. (Meszaros, 1994) The pyrolyzed oil produced was the source of the plastics oil used in this research. The second type of first stage processing was the liquefaction of post consumer plastics, which came from households and businesses in Germany. The oil from both of these processes was used as the solvent for the coal in the second stage coprocessing reactions.

EXPERIMENTAL

Two batches of post consumer waste were obtained. The first, from Conrad Industries, was a pyrolysis liquid produced from post-consumer plastics. The second was obtained from Germany, and was composed of post-consumer plastics that had been collected and extruded to increase their

density. The European plastics mixture was supplied by Dr. Gerald P. Huffman of the University of Kentucky, and contained small amounts of other materials such as Al granules, Al foil and paper which were removed prior to reaction. Illinois No. 6 coal, obtained from the Argonne Premium Coal Sample Bank, was used as received.

In this study, slurry phase hydrotreating catalyst precursors, Mo naphthenate (MoNaph) and Fe naphthenate (FeNaph), were used for the reaction of distilled Conrad plastics oil and coal, and for the second stage reaction of the European plastics with coal. A fluid cracking catalyst, Low Alumina, and a zeolite, HZSM-5, were used individually in the first stage processing of the waste plastics. Both HZSM-5 and Low Alumina catalysts were pretreated prior to be being used in the reaction by heating for 2 hr at 477 K followed by 2 hr at 811 K.

Reactions. Before the Conrad plastics oil was used as a coprocessing solvent for coal, it was distilled at 90 °C under 30 mm of Hg to remove the light fractions. The residual fraction was used as a coprocessing solvent. The coprocessing reaction was performed with 2 g of coal and 2 g of distilled Conrad oil in 20 cm^3 stainless steel microtubular reactors at 713 K for 30 min. The reactors were charged with 5.6 MPa of H_2, introduced at ambient temperature, and were agitated horizontally at 435 rpm during the reactions. Slurry phase catalyst precursors, MoNaph and FeNaph, were introduced at 1000 ppm of active metal with 6000 ppm of elemental sulfur on a total reactant basis.

The European plastics mixture was reacted in the first stage in 50 cm^3 stainless steel microtubular reactors at 713 K for 60 min under an initial H_2 pressure of 2.8 MPa, introduced at ambient temperature. The reactors were agitated vertically at 450 rpm. Ten grams of plastics mixture were charged to the reactor with 10% Low Alumina or HZSM-5 on a total plastics charge basis. The hexane soluble fraction produced from the first stage was used as the solvent for the second stage. The second stage reaction was performed using the same procedures and conditions as those used for the distilled Conrad oil and coal.

Product Analysis. The liquid products from the coprocessing reactions were analyzed by solvent fractionation using hexane as the initial solvent followed by tetrahydrofuran (THF). The amount of gas, hexane, and THF soluble and insoluble materials produced, was determined. The total boiling point distribution of the reaction products after coprocessing was also determined by combining analyses of the product distribution with that of simulated distillation of the hexane soluble fraction.

RESULTS AND DISCUSSION

Conrad Waste Plastics Oil. The research performed evaluated the effect of the type of first stage processing and of the source of waste plastics used in the first stage. The first set of experiments that were performed involved using the pyrolysis product from the Conrad Industries waste plastics pyrolysis process as the coprocessing solvent. The plastics oil produced contained a substantial amount of light materials that were distilled prior to the coprocessing reactions. Hence, in these experiments the Conrad process was effectively the first stage process. The distilled Conrad oil was then used as the second stage coprocessing solvent.

Three types of reactions were performed: thermal, catalytic with FeNaph and excess sulfur, and catalytic with MoNaph and excess sulfur. The presence of a catalyst had a pronounced effect on the amount of each fraction, hexane solubles, THF solubles and insoluble organic material (IOM) produced. Thermal coprocessing reactions yielded the lowest conversions and catalytic coprocessing reactions with MoNaph yielded the highest conversions. The two catalysts had different effects on the reaction product obtained. The slurry phase FeNaph and excess sulfur produced a larger amount of hexane solubles, while MoNaph produced a larger amount of THF solubles. The coprocessing reaction with MoNaph converted 90.4% of the solid coal to THF solubles, while the high total recovery of 91.5% indicated that few volatiles were produced. By contrast, the coprocessing reactions with FeNaph did not convert as much coal, yielding an 82.8% conversion, and also had a somewhat lower total recovery of 86.8%, which indicated that FeNaph had a greater propensity for producing volatiles from the plastics oil solvent than did MoNaph.

The total boiling point distributions from these reactions compared well with the results from the product distributions (Table 2). The amount of volatiles that are shown in the <100 °C fraction

are the highest for the reactions with FeNaph and the lowest for the thermal reactions. The amount of material boiling between 100 and 500 °C was greatest for the coprocessing reactions containing MoNaph and excess sulfur. When the results are viewed in terms of the overall heaviness of the reaction product, the thermal reactions contained the most material 87.0% in the >500 °C range and the IOM while the reactions with FeNaph and MoNaph produced similar amounts of 69.7 and 70.4%, respectively. The reaction with FeNaph resulted in less material being converted to THF soluble material than did the reactions with MoNaph.

European Waste Plastics. The second material used in this study was post-consumer waste plastics that had been collected and concentrated for transportation to processing plants. The first stage reaction was performed using hydrocracking catalysts, either HZSM-5 or Low Alumina, to shorten the polymeric chains and produce a liquefied product. The reaction was performed at a temperature of 440 °C with a low H_2 pressure, to promote hydrocracking. These conditions were chosen because the less severe conditions did not convert the solid European waste plastics into hexane soluble materials, and because more severe conditions would result in a substantial portion of the waste plastics being converted into gases or highly volatile liquids. After the European waste plastics were reacted in the first stage, the hexane soluble fraction was used as the solvent for the second stage processing with coal. The second stage reaction was performed with a slurry phase hydrotreating catalyst, either FeNaph or MoNaph and excess sulfur.

The product distributions from the second stage coprocessing reaction of the hexane soluble fraction of the European waste plastics reacted with coal showed little effect due to either the first stage or the hydrotreating catalyst (Table 3). The conversions from the second stage reactions using HZSM-5/FeNaph and Low Alumina/FeNaph yielded very similar conversions of 83.3 and 84.7%, respectively. The conversions from the second stage reactions with MoNaph were slightly higher, 87.1% for HZSM-5/MoNaph and 88.0% for Low Alumina/MoNaph. Some differences were observed in the product distribution. The hexane solubles for the second stage reactions with FeNaph averaged 19.5% and were lower than the average of 25.0% produced from the reactions with MoNaph. The second stage reactions with FeNaph were not as effective as those with MoNaph for converting the reactants to hexane soluble or THF soluble material.

The boiling point distributions from the two stage processing of European waste plastics and coal were calculated by combining the simulated distillation results from hexane solubles produced in the second stage with the product distributions from the combined first and second stages. The total boiling point distributions, given in Table 4, show a bimodal distribution of the reaction products. The products were either gases or light hydrocarbons boiling at <100 °C, or extremely heavy material with boiling points of >500 °C, or IOM. The HZSM-5 first stage products, when introduced as a solvent for the second stage coal reaction, resulted in less IOM from the two stages than in the two stage reactions using Low Alumina as the first stage catalyst.

SUMMARY

Two stage coprocessing of waste plastics with coal was found to be affected by the source of waste plastics and by the type of first stage processing. Pyrolysis as the first stage process cracked the polymeric molecules into much smaller molecules, forming gases, liquids and some residual solids. The oil fraction contained a considerable amount of light materials which were removed by distillation prior to its use as a second stage solvent for coal. Similarly, the removal of the heavy plastics material from the Conrad plastics oil by the pyrolysis process yielded a solvent that was inherently lighter and, hence, resulted in less heavy products in the second stage process than the liquefaction solvent. By contrast, the first stage liquefaction of the European plastics was a less severe first stage condition. Even though only the hexane fraction of the first stage products was used as the solvent in the second stage coprocessing reaction, that solvent contained a heavier product slate than did the Conrad plastics oil. Overall conversion from two stage coprocessing reactions with corresponding catalysts was reduced when a liquefaction first stage was used rather than a pyrolysis first stage.

The more active Mo naphthenate catalyst promoted higher second stage conversions that Fe naphthenate regardless of the first stage material. The second stage conversions from reactions in which Conrad plastics oil and liquefaction were used as the first stage process were quite similar when Mo naphthenate was used as the second stage catalyst. Fe naphthenate showed a lower activity than Mo naphthenate for promoting conversion, regardless of first stage processing. When

liquefaction was used as the first stage, the overall conversion from two stage processing was reduced due to the substantial amount of waste plastics that remained unconverted in the first stage. It is highly likely that this material would be converted if it were recycled.(Joo and Curtis, 1997) The catalyst present in the first stage also affected the overall conversion from two stage processing. HZSM-5 was a more effective catalyst for promoting first stage and overall conversion than was Low Alumina.

References

Ding, W., Liang, J., Anderson, L., *ACS Fuel Chem. Div. Prep., 41 (3)*, 1037, 1996.

Joo, H.K., Curtis, C.W., "Effect of Reaction Time on the Coprocessing of LDPE with Coal and Petroleum Resid" *Energy Fuels*, in press, 1997.

Luo, M., Curtis, C.W., *Fuel Process. Technol., 49*, 91, 1996a.

Luo, M., Curtis, C.W., *Fuel Process. Technol., 49*, 177, 1996b.

Luo, M., Curtis, C.W., *ACS Fuel Div Prep., 41 (3)*, 1032, 1996c.

Luo, M., Ph.D. Dissertation, Auburn University, Auburn, Alabama, June, 1997.

Meszaros, M.W., *Recycle '94*, Davos, Switzerland, March, 1994.

Techline, from Pittsburgh Energy Technology Center, 1996.

Acknowledgements

The support of the Department of Energy through Contract No. DE-FC22-93PC 93053 is sincerely appreciated.

Table 1. Product Distributions from Coprocessing Reactions of Distilled Conrad Plastics Oil and Illinois No. 6 Coal

Reaction System	Product Distribution, (wt %)				Conversion (%)	Recovery (%)
	Gas	Hexane Solubles	THF Solubles	IOM		
Thermal	5.5 ± 0.2	7.8 ± 1.0	60.1 ± 0.2	26.2 ± 1.0	73.8 ± 1.0	95.0 ± 1.1
FeNaph	5.8 ± 0.2	32.3 ± 1.9	44.7 ± 1.5	17.2 ± 0.6	82.8 ± 0.6	86.8 ± 1.6
MoNaph	5.3 ± 0.8	30.3 ± 2.6	54.8 ± 3.8	9.6 ± 0.4	90.4 ± 0.4	91.5 ± 2.2

Table 2. Boiling Point Distributions from Coprocessing Reactions of Distilled Conrad Oil and Illinois No. 6 Coal

Reaction System	Boiling Point Distribution (%)				
	Gas	<100 °C	100-500 °C	>500 °C	IOM
Thermal	5.8	5.0	3.1	60.8	26.2
FeNaph	5.8	13.3	11.2	52.5	17.2
MoNaph	5.3	8.6	15.7	60.8	9.6

Table 3. Product Distributions from Coprocessing Reactions of European Waste Plastics with Illinois No. 6 Coal

First Stage Catalyst	Second Stage Catalyst	Production Distribution (wt%)				Conversion (%)	Recovery (%)
		Gas	Hexane Solubles	THF Solubles	IOM		
HZSM-5	FeNaph	4.1 ± 0.0	18.9 ± 1.4	60.3 ± 2.0	16.7 ± 0.6	83.3 ± 0.7	83.1
L Alumina	FeNaph	4.1 ± 0.1	19.5 ± 0.7	61.1 ± 1.7	15.3 ±1.0	84.7 ± 1.0	88.3
HZSM-5	MoNaph	4.1 ± 0.1	24.7 ± 0.4	58.3 ± 0.4	12.9 ± 0.7	87.1 ± 0.7	90.3
L Alumina	MoNaph	3.7 ± 0.1	25.2 ± 0.2	59.1 ± 1.3	12.0 ±1.6	88.0 ± 1.6	87.7

Table 4. Boiling Point Distribution from Coprocessing Reactions of European Waste Plastics with Illinois No.6 Coal

Reaction System	Boiling Point Distribution (wt%)				
	Gas	<100 °C	100-500 °C	>500 °C	IOM
HZSM-5/Fe	9.1	15.1	0.0	52.4	23.6
Alumina/Fe	7.9	9.4	0.0	54.1	28.7
HZSM-5/Mo	9.1	16.6	0.0	53.0	21.2
Alumina/Mo	7.6	12.0	0.0	53.6	26.7

EVALUATION OF TWO STAGE PROCESSING OF WASTE PLASTICS WITH COAL AND PETROLEUM RESID

Hyun Ku Joo, Christine W. Curtis[a], and James M. Hool[b]
[a]Chemical Engineering Department
[b]Industrial Engineering Department
Auburn University
Auburn, Alabama 36849

KEYWORDS: coprocessing coal , resid, waste plastics , post consumer plastics, fractional factorial design

ABSTRACT

Two stage coprocessing of waste plastics with coal and petroleum resid was investigated using a one-third factorial design. In the two stage process, waste plastics were reacted in the first stage and the liquid products from the first stage were introduced into the second stage which consisted of coal and petroleum resid. Four factors were evaluated in the study including the type of catalyst, the weight percent of coal, and the compositions of plastic and resid. The catalysts investigated included $NiMo/Al_2O_3$, NiMo/zeolite, and HZSM-5; the weight percents of coal investigated were 0, 10, and 29%; the plastics investigated were low density polyethylene (LDPE), polystyrene, and mixed plastics; and the resids used were Manji, Maya, and Hondo. The results from these factorial experiments were evaluated by determining their distributions using solvent fractionation. The production of gas and hexane soluble materials as well as the conversion to THF soluble materials was determined. The significance of each factor for producing these products and converting the two stage materials was determined and compared.

INTRODUCTION

The direct coprocessing of waste plastics with coal in a single stage reaction presents problems in effectively converting each material for the reaction conditions, and the catalyst needed for each material are quite different. (Luo and Curtis, 1996 a, b) Two stage coprocessing in which the waste plastics were reacted and the resulting product then used as a solvent for coal, allowed for customizing the reaction conditions and catalysts for the needs of each material. (Luo and Curtis, 1996 c; Luo, 1997; Ding et al., 1996) Previous research has shown that incorporating a solvent such as petroleum resid, which has been used previously as a solvent for the coprocessing of coal (Speight and Moschopedis, 1986; Yan and Espencheid, 1983; Curtis and Hwang, 1992; Curtis et al., 1987a,b; Guin et al., 1986), into the reaction effectively provides a bridging solvent in which the two chemically incompatible coal and waste plastics can be coprocessed effectively. (Joo and Curtis, 1996a; 1996b; 1996c; 1997a)

Two stage coprocessing of coal, waste plastics, and resid has been explored to determine the most effective method of staging the reactions and the best sequencing of reaction conditions. (Joo and Curtis, 1997 b) The results indicated that converting the waste plastics in the first stage under fairly severe conditions, and then reacting the first stage product in the second stage with coal and resid under less severe conditions, converted the most material to liquid products. The previous study involved LDPE only as the waste plastic material. The current study extends that research and involves post consumer plastics obtained by crushing and grinding commercially available plastic products and by using post consumer plastics collected in Germany. This study uses a one-third fractional factorial design to determine the effect of four factors, the types of catalyst, waste plastic, and resid used, and the coal concentration, on the products from two stage coprocessing of waste plastics, coal and resid. Each of these four factors was tested at three levels. The efficacy of the two stage coprocessing was evaluated by quantitatively determining the relation between the chosen factors and response variables which were the product fractions produced.

EXPERIMENTAL

Materials. A mixture of waste plastics including polystyrene (PS), polypropylene (PP) and low density polyethylene (LDPE) was made by chopping and subsequently grinding trash baskets and disposable plates. Post consumer LDPE was also used as an individual reactant. A waste

plastics mixture obtained from a German recycling company was supplied to us by Dr. Gerald P. Huffman of the University of Kentucky. In addition, post consumer LDPE was also used. Blind Canyon DECS-17 bituminous coal, obtained from the Penn State Coal Sample Bank, was used in this study. The proximate analysis of the coal is 45% fixed carbon, 45% volatile matter, 6.3% ash and 3.7% moisture. The ultimate analysis of the coal is 82.1% C, 6.2% H, 0.4% S, 1.4% N and 0.12% Cl. The resids used in the coprocessing reactions were Manji, Maya, and Hondo which were obtained from Amoco. These resids had different amounts of their material boiling in the range of 650 to 1000 °F: Manji had 1.24%; Hondo, 6.58%; and Maya, 19.0%. The remaining material boiled above 1000 °F. The catalysts tested in the study were $NiMo/Al_2O_3$ (Shell 2.72 wt % Ni and 13.16 wt % Mo), NiMo/ zeolite (Akzo, <25 wt % MoO_2 and 1-10 wt% Ni_2O_3 with ultrastable zeolite), and HZSM-5 (United Catalysts). The $NiMo/Al_2O_3$ catalyst was presulfided and powdered prior to use. The catalysts were introduced into each stage at a level of 1 wt% on a total charge basis.

Reaction Procedures. This study involved a factorial design in which the effect, composition, and concentration of the reactants and type of catalyst were evaluated. The design parameters and their levels are presented in Table 1. Two stage reactions were performed in which the plastic was reacted in the first stage. The total first stage product without extraction was added to the second stage coprocessing reaction. The second stage reaction contained resid and either 0, 10, or 29 wt % coal. The reactions conditions in the first stage were 430 °C, 60 min and 500 psi (3.4 MPa) of H_2, introduced at ambient temperature. The second stage reaction conditions were 430 °C, 30 min and 1200 psi (8.3 Mpa) of H_2, introduced at ambient temperature.

Analysis. The solid and liquid reaction products were analyzed by solvent fractionation using a series of extraction solvents. The amount of gaseous products was determined by weighing the gaseous products before and after they were released from the reactor. The liquid products were fractionated by using a series of solvents, into hexane soluble (HXs), toluene soluble, hexane insoluble (TOLs), THF soluble, and toluene insoluble (THFs) materials, or IOM, defined as insoluble organic matter that is moisture and ash-free. Conversion was defined as:

$$\%Conversion\text{-}[1-\frac{gIOM_{maf}}{gTotalCharged_{maf}}]\times 100$$

EXPERIMENTAL DESIGN

Catalytic two stage coprocessing of post consumer plastics, resid, and coal was performed to evaluate the effect of different sources and compositions of plastics and resids on the final products obtained. In addition, the effect of having coal present at different concentrations in the coprocessing reaction was also an important aspect of this research. The four factors that were selected for analysis in this study were catalyst type, post consumer plastic type, resid type, and coal content. Three levels for each factor were chosen for the purpose of investigating the effect of different types of catalysts, plastics and resids as shown in Table 1. The effect of having coal present as nearly one-third of the reactants in the second stage reaction, as only a small (10%) portion of the total second stage reactants, or not at all, was evaluated in terms of product distributions and conversion.

The total number of factor-level combinations (FLCs) used was $3^4 = 81$. A one-third (1/3) fractional factorial design was used for this study, therefore, $3^{4-1} = 27$ FLCs were required. The effects that were selected to be sacrificed were $I = AB^2CD = (AB^2CD)^2$, each of which had two degrees of freedom (df). The effects that were investigated in this design were: (1) the main effects (8 df) A, B, C, D, each with 2 df; and (2) the two factor interactions AB, BC, $A \times C = AC$, AC^2, $A \times D = AD$, AD^2, $C \times D = CD$, CD^2, with a total of 18 df.

RESULTS AND DISCUSSION

The one-third fractional factorial design required that 27 two stage coprocessing reactions be performed. The factor levels that were chosen and the reactions that were performed are given in Table 2. The first column describes the type of post consumer plastic used in the first stage, the

type of resid used in the second stage, and the type of catalyst used in both stages. The second column describes the coal weight percentage, ranging from 0 to 29 wt %, that was used in the second stage. The next four columns describe the product distributions achieved in the reaction. The last two columns are the conversion to THF soluble products and the recovery, respectively.

The first stage of the two stage sequence was performed using one of the three types of plastics, with a sufficient amount of plastic (usually about 5 g) being introduced so that 2 g of the first stage reaction product was produced for use as a solvent in the second stage. The reactants in the second stage reaction were the first stage reaction product, the resid chosen from the factorial design, and coal, if present in the reaction. The conversion that is described is the conversion of the reactants entering the second stage to THF soluble products. The recovery was also based on the second stage only, therefore, the first stage conversion and recovery were not used in these calculations. The loss of converted material in terms of gases and volatiles from the first stage was not considered.

The effect of the different reaction parameters is evident in the product distributions obtained. The amount of gas produced was fairly stable for all of the combinations, and ranged from 8.5 to 13.6%. Much larger ranges were observed in the HXs soluble fraction where the lowest amount of HXs produced was 40.7% and the highest amount was 75.4%. The amount of HXs produced was directly influenced by the amount of coal that was present in the reaction. When coal was present at 29 wt % in the second stage, the HXs ranged from 40.7 to 57.9%; when coal was present at 10 wt %, the HXs ranged from 50.6 to 71.9%; and when no coal was present, the HXs ranged from 50.0 to 75.3%. The highest production of HXs was obtained when no coal or 10 wt % coal was present in the second stage reaction. The range of THF solubles and IOM yielded a greater variability than that observed in the gases, but less than that observed in the Hxs.

The conversion also was directly influenced by the type and amount of the reactants, and ranged from 64.6 to 99.0%. The conversions from the second stage reactions ranged from 64.6 to 88.0% when coal was present at 29 wt % in the second stage, and from 72.5 to 93.8% when coal was present at 10 wt % in the second stage reaction. When coal was not present, the conversions ranged from 70.7 to 99.0%. No coal or a low weight percentage (10%) of coal present in the second stage coprocessing reaction yielded higher conversions than those obtained when 29 wt % coal was present. Therefore, not only the presence of the coal but also the other factors, including the type of catalyst, type of waste plastic and type of resid, influenced the conversion of solid reactants.

Analysis of variance (ANOVA) calculations were performed on three product parameters: gas production, HXs production, and conversion. Only the catalyst type affected the gas production at the 0.01 significance level. However, HXs production was much more affected by all of the factors. The type of catalyst, resid, and waste plastic used as well as the weight percent coal all affected the production of HXs materials at the 0.01 significance level. Similarly, the factors of catalyst type, waste plastics composition, and weight percent coal affected conversion at the 0.01 significance level while the resid type affected conversion at the 0.025 significance level. All three parameters, gas production, HXs production, and conversions were affected by the interaction between catalyst type and was plastics type at the 0.01 significance level. The activity and selectivity of the catalyst used in the first stage reaction strongly affected the products and conversions achieved from two stage coprocessing of coal, waste plastics, and resid.

SUMMARY

The results from the one-third fractional factorial design coprocessing experiment clearly demonstrated that the products from two stage coprocessing reactions were strongly affected by the type of catalyst, waste plastic and resid used, and by the amount of coal present in the second stage reaction. Each of these factors affected the production of hexane solubles at the 0.01 significance level. All of the factors except for resid type affected the conversion at the same level. A strong interaction between the types of catalyst and waste plastic was observed, and affected gas production, hexane solubles production and conversion.

Several consistent trends were observed in the reactions performed. The absence of coal or the presence of coal at low concentrations (10%) resulted in a higher production of hexane solubles and higher conversion. Coal is a difficult material to convert to lighter liquids and requires extensive hydrotreating to produced light products. The two stage coprocessing reaction performed did not

have sufficient selectivity for hydrotreating to produce light products from coal. The conversion was similarly affected by the coal concentration, since again substantial hydrotreating was required to convert coal to THF soluble products. The conversion was also affected by the reactivity of the waste plastic material and by the propensity of waste plastics to be converted to liquid and gaseous products in the first stage. This factorial design demonstrated that through the selection of certain sets of factor combinations that two stage catalytic coprocessing of coal, waste plastics, and resid is a feasible processing method for utilizing waste plastics.

REFERENCES

Curtis, C.W., Hwang, J.S., *Fuel Process. Technol.*, *30*, 47, 1992.

Curtis, C.W., Guin, J.A., Tsai, K.J., *Ind. Eng. Chem. Res.*, *26*, 12, 1987a.

Curtis, C.W., Pass, M.C., Guin, J.A., Tsai, K.J., *Fuel Sci. Tech. Intl.*, *5*, 245, 1987b.

Ding, W., Liang, J., Anderson, L., *ACS Fuel Chem. Div. Prep.*, *41 (3)* 1037, 1996.

Guin, J.A., Curtis, C.W., Tsai, K.J., *Fuel Proc. Tech.*, *12 III*, 111, 1986.

Joo, H.K., Curtis, C.W., *Energy Fuels*, *10* ,603, 1996a.

Joo, H.K., Curtis, C.W., *ACS Fuel Chem. Div. Prepr.*, *41 (3)*, 1048, 1996b.

Joo, H.K., Curtis, C.W., submitted to *Fuel Process. Technol.*, 1996c.

Joo, H.K., Curtis, C.W., *Energy Fuels*, in press, 1997a.

Joo, H.K., Curtis, C.W., submitted to *Energy Fuels*, 1997b.

Luo, M., Ph.D. Dissertation, Auburn University, Auburn, Alabama, June, 1997.

Luo, M., Curtis, C.W., *Fuel Process. Technol.*, *49*, 91, 1996a.

Luo, M., Curtis, C.W., *Fuel Process. Technol.*, *49*, 177, 1996b.

Luo, M., Curtis, C.W., *ACS Fuel Div Prep.*, *41 (3)*, 1032, 1996c.

Speight, J.G., Mochopedis, S.E., *Fuel Process. Technol.*, *13*, 215, 1986.

Yan, T.Y., Espenchied, W.F., *Fuel Process. Technol.*, *7*, 121, 1983.

ACKNOWLEDGEMENTS

The support of the Department of Energy through Contract No. DE-FC22-93PC 93053 is gratefully acknowledged.

Table 1. Factors and Factor Levels

Factors	Levels
Catalysts (A)	$NiMo/Al_2O_3$ NiMo/zeolite HZSM-5
Resids (B)	Manji Maya Hondo
Plastics (C)	post- LDPE post - Mixture European mixture
Weight percent of Coal (D)	0 % 10 % 29 %

Table 2. Product Distributions from Post-Consumer Plastics Coprocessing Reactions

Plastic, Resid, Catalyst	Coal weight %	Product Distribution (%)				Conversion (%)	Recovery (%)
		gas	HXs	THFs	IOM		
R, J, NZ	10	9.4	71.9	11.7	7.0	93.0	87.8
D, J, NZ	29	9.5	40.7	14.4	35.4	64.6	99.1
E, J, NZ	0	11.4	71.1	7.4	10.1	89.9	86.1
R, J, NA	29	9.1	57.9	19.7	13.3	86.7	90.4
E, J, NA	10	9.5	60.5	11.6	18.5	81.5	94.1
D, J, NA	0	8.6	63.9	7.0	20.5	79.5	91.0
D, J, Z	10	12.5	69.4	11.3	6.8	93.2	73.7
R, J, Z	0	11.9	75.3	11.8	1.0	99.0	75.1
E, J, Z	29	10.1	46.3	14.4	29.2	70.8	96.4
D, Y, NA	10	7.9	50.6	14.0	27.5	72.5	96.2
R, Y, NA	0	10.3	68.3	16.5	4.9	95.1	82.5
E, Y, NA	29	9.6	42.9	17.2	30.3	69.7	90.5
D, Y, NZ	0	9.3	50.0	11.4	29.3	70.7	95.3
R, Y, NZ	29	10.3	50.0	21.1	18.6	81.4	91.6
E, Y, NZ	10	10.0	56.1	14.5	19.4	80.6	92.2
R, Y, Z	10	11.0	65.0	17.9	6.2	93.8	79.5
E, Y, Z	0	10.0	57.4	14.5	18.1	81.9	90.6
D, Y, Z	29	11.1	45.2	16.7	27.0	73.0	92.9
R, O, NA	10	9.5	61.8	16.4	12.3	87.7	90.0
E, O, NA	0	10.2	62.5	10.9	16.4	83.6	90.5
D, O, NA	29	8.5	42.6	13.5	35.4	64.6	91.1
D, O, NZ	10	10.8	48.9	15.1	25.2	74.8	93.4
R, O, NZ	0	9.1	71.6	11.7	7.6	92.4	82.6
E, O, NZ	29	10.4	48.0	20.2	21.4	78.6	93.1
D, O, Z	0	13.6	73.5	9.7	3.1	96.9	62.2
R, O, Z	29	12.1	54.6	21.3	12.0	88.0	82.9
E, O, Z	10	11.0	61.9	13.1	14.0	86.0	86.3

[a] : Fractional factorial design of $3 \times 3 \times 3 \times 3 = 81$ factor-level combinations into three fractions.

[b] : 430 °C, 60 min → 430 °C, 30 min, Plastic → Coal + Resid, 500 psi → 1200 psi H_2 introduced at ambient temperature. Reactant: C = Blind Canyon DECS-17. D = Post-consumed LDPE, E = European, R = Mixture of post- consumed LDPE, PP, PS. J = Manji, Y = Maya, O = Hondo. NA = presulfided $NiMo/Al_2O_3$, NZ = NiMo/zeolite, Z = HZSM-5.

[d] : gas = gaseous product, HXs = hexane solubles; TOLs = toluene soluble, hexane insolubles, THFs = THF solubles, toluene insolubles and IOM = insoluble organic matter.

VIABILITY OF CO-PROCESSING OF COAL, OIL AND WASTE PLASTICS

L.K.(Theo) Lee, J.Hu, G.Popper and A.G. Comolli
Hydrocarbon Technologies, Inc., Lawrenceville, New Jersey 08648

INTRODUCTION

The disposal of wastes represents not only a significant cost but also concerns such as loss of a valuable resource, a health hazard, and pollution resulting from conventional disposal methods, such as landfilling and incineration. Through the efforts of the U.S. Department of Energy and Hydrocarbon Technologies, Inc(HTI), a novel process, HTI CoPro Plus™, has been developed to produce alternative fuels and chemicals from combined liquefaction of waste plastics with coal and heavy petroleum residues. The new process concept that has been successfully tested in HTI strives to:

- Direct organic waste away from landfills.
- Produce valuable products, basic and intermediate chemicals and fuels.
- Solve existing environmental problems created by current disposal methods.
- Reduce refinery waste oil pond and land fill inventories.
- Enhance domestic resources by
  - -Supplanting oil and fuel supply imports.
  - -Seducing energy consumption through recycling.
  - -Improving the trade balance.
  - -Creating a new industry and U.S. jobs.

With the rapid decreasing in availability of landfills but nationwide increasing in waste plastics generation, co-processing is a viable option for addressing this environmental problem. Economical evaluation has shown that co-processing of plastics with oil, coal or their mixture reduced the equivalent crude oil price to a compatible level.

The new approaches involve continuous pilot plant operation utilizing finely dispersed catalyst (HTI Gel Cat™) to simultaneously liquefy the solid feed and upgrade residuum from either liquefied solid or petroleum oil to lower boiling (<524°C) premium products. The HTI GelCat™ has a high surface area exceeding 100 m^2/g in dried form and has particle size smaller than about 50 Angstrom units. Because the fine-sized catalyst are produced based on use of available relative inexpensive material and since the principal component is cheap and environmentally benign, they are usually disposable for large scale process and do not require recovery and regeneration.

This paper discusses the results from several successful pilot tests of DOE's POC program performed in HTI. Different waste materials, such as MSW plastics, auto-fluff, Hondo VTB resid, were co-processed with coal directly, or pretreated by pyrolysis prior to co-processing with coal. Apart from exploring HTI Gel Cat™ catalyst, integrated reactor configurations including interstage separator, in-line hydrotreating and combination of dispersed and supported catalyst system have been evaluated during these pilot tests. One significant characteristics of HTI's CoPro Plus™ is the increase in hydrogen efficiency as both hydrogen consumption and C_1-C_3 gas yield decrease. Promising process performance, in terms of high distillate yield and extensive removal of heteroatoms, has been demonstrated through HTI's new approaches.

PROCESS DESCRIPTION

The HTI CoPro Plus process entails co-liquefaction of organic wastes with coal and/or oil is a liquid phase hydrogenation process that takes place at temperatures of about 425°C and pressures of 15 MPa. Under these conditions, large molecules are cracked, hydrogen is added and sulfur, nitrogen, and chlorine, etc. are easily separated and recovered after conversion to their basic hydrogenated form. Also, because the process is contained under pressure, all gases and inert components can be captured and reused if desired. Co-liquefaction of random waste organic materials with coal provides for the efficient recovery and recycle of problem wastes back into the economy as premium transportation fuels and feedstocks for virgin plastics. Direct liquefaction is also applicable to the conversion and liquefaction of densified solids refuse derived fuels (RDF), formed from municipal and industrial wastes and automobile shredder residue (ASR). On a conversion to transportation fuel basis the recycle and conversion of waste plastics, waste oils, tires and organic wastes with only 50% of the waste being recovered shows that this process can supplement 10% of the United States' daily transportation fuel requirements:

Waste Type	Quantity Per Year	Oil Equivalent Million Barrels/Year
Plastics	3.5 Million Tons	200
Used Waste Oil	1.4 Billion Gallons	33
Rubber Tires	350 Million PTE*	8
Other Organic	34.4 Million Tons	212
Total Waste		453
Total Coal/Waste (1:1)		906
Total at 50% Waste		453+

*Passenger Tire Equivalents
+About 10% of daily U.S. Transportation Fuel Use

A techno-economic analysis for a site specific waste/coal direct liquefaction plant at 12,000 bbls/day adjacent to and integrated with an oil refinery with random waste delivered to the plant shows an average required selling price at zero acquisition cost and at 15% ROI of about $16.00 per barrel. If tipping fees are included and if high value plastic feedstocks are recovered, the price could be less than $14/bbl and is cost effective today. This selling price will be in the competitive range by the end of this century, even with a +$20/ton acquisition cost, particularly if the environmental cost benefits of recycling are included. The current national average tipping fee is $28/ton for landfilling and $54/ton for incineration.

EXPERIMENTAL

Pilot scale tests were carried out at HTI using a 25 Kg/h two-stage pilot plant. The coal, oil, waste materials and HTI Gel Cat™ catalyst were premixed in a mixing tank prior to charging to the Feed Tank. Joined by feed hydrogen, the gas/feed slurry stream passed through a short residence time coiled preheater. Reaction was conducted at 15MPa of hydrogen, 400-460°C and 1000-5000 ppm of Fe catalyst loading. An internal circulating pump returned a portion of the reactor slurry to the bottom of the reactor providing the backmixing action. The first stage light reaction product was cooled and separated from the main slurry. This light product, along with other second stage non-hydrotreated products, were fed to the direct-coupled hydrotreater. The intermediate slurry product was further liquefied in the second stage backmixed reactor.

The hot vapor products from the second stage liquefaction reactor were separated in the hot separator and fed directly into a fixed bed hydrotreater. The hydrotreater was connected directly with the hot separator without pressure reduction. Hydrogen, C_1-C_3 hydrocarbons, heteroatom gaseous products, water and volatile liquid products from the overhead of the separator passed through a mixing phase trickled bed hydrotreater. The main function of the hydrotreater was to stabilize the hydrocarbon products and to reduce heteroatom (N,S,and O) content.

The backend separation included pressure filtration and batch vacuum distillation. The major net product streams are product gases (1st and 2nd stages), dissolved gas (2nd stage only), 2nd stage separator overheads (hydrotreated product) and toluene extracted solids and excess pressure filter liquid (PFL) or vacuum still overhead (VSOH). Process performance is determined by feed composition, operating conditions, yield and quality of C_4-524°C distillate, and by hydrogen utilization efficiency.

RESULTS AND DISCUSSION

The process performance and economic evaluation obtained from recent pilot scale co-processing operations are summarized in this paper. The economic evaluation studies were based on construction of a fully-integrated grass-roots commercial coal/oil/waste (plastics) co-liquefaction complex to manufacture finished gasoline and diesel fuel liquid products. The co-liquefaction plant in the complex is a multi reactor-train facility and the total feed processing capacity has been selected assuming the construction of maximum-sized heavy-walled pressure vessels to carry out the co-liquefaction reactions. Coal and waste plastics required in the co-liquefaction plant are prepared on site and storage is provided for the oil received. Unconverted feed plus residual oil from the co-liquefaction are gasified to meet a part of the hydrogen requirements of the complex.

Part of the fuel requirement is met by the waste process gases. Natural gas is imported to meet the remaining fuel requirements and to satisfy the remainder of the hydrogen requirements. The costs and operating requirements of the other process facilities and the off-sites have been estimated from

the Bechtel Baseline Design Study, which was developed for the Department of Energy. The most significant criterion reported is the equivalent crude oil price. This concept was developed by Bechtel in their Baseline Design Study, and modified slightly for use in this study.

Table 1 presents the comparisons of the performance of five run conditions. Coprocessing of Black Thunder coal, Hondo oil and ASR resulted in 83.6 W% resid conversion and 66.8 W% distillate yield. A dramatic drop in both resid conversion and distillate yield was observed when Hondo oil was removed from the mixture of coal and ASR(PB-04-4). It seemed that vehicle solvent is essential in converting ASR and coal. In Run PB-04-5, 25 W% of plastics was added to the coal and ASR mixture, it is interesting to note that distillate yield was increased from 56.6 to 61.4 W% while 524°C+ resid conversion was increased proportionally, from 72.4 to 77.2 W%. Also, it is observed that addition of plastics has a significant impact on hydrogen consumption. Not only does the addition of plastics to coal/ASR improved the process performance it also decreased hydrogen consumption by about 2 W%. Economical analysis showed that by adding plastics to coal/ASR feedstock, equivalent crude oil price dropped by $6/barrel.

It was concluded that auto-fluff, that contains primarily polyurethanes and high impact polystyrene as its principal polymeric constitutes, was not as effective as the MSW plastics in improving the coal hydroconversion process performance, i.e. auto-fluff was not found to either increase the light distillate yields or decrease the light gas make and chemical hydrogen consumption in coal liquefaction, in the manner done by MSW plastics

In Run PB-06, waste plastics was pretreated by pyrolysis and only 343 °C+ pyrolysis oil was coprocessed with coal and Hondo oil. As shown in *Table 1*, Run PB-06-3, performance of coprocessing of coal/Pyrolysis oil, in terms of distillate yield and resid conversion, was similar to coprocessing of coal/ASR (PB-04-4), slightly decrease in hydrogen consumption was observed. Considering Mo catalyst was not used in Run PB-06-03, this result seemed to suggest that pyrolysis oil was more reactive in improving coal conversion than ASR. Run PB-06-4, using a mixed feed of coal, Hondo oil and pyrolysis oil, was performed at higher space velocity. Distillate yield and 524°C+ resid conversion was decreased by 3 and 7 W%, respectively. However, C_1-C_3 light gas yield and hydrogen consumption decreased significantly.
Result from Run PB-06-4 demonstrated the potential for commercialization because the equivalent crude price dropped to $ 19.6/barrel.

Table 2 illustrated the comparison of co-processing performance using different coals. In comparing the same feed mixture, Illinois #6 coal (Run PB-05-4) appeared to be more reactive than Black Thunder coal (Run PB-06-2), as both the distillate yield and resid conversion were higher. However, the use of Illinois #6 coal resulted in higher hydrogen consumption under the same conditions. Significant improvement were obtained in co-processing of Illinois #6 coal, Hondo oil and plastics (PB-05-3).

The liquid products from these co-processing operations were clean and good feedstocks for the refining operations, including hydrotreating, reforming, and hvdrocracking. For these distillates. heteroatoms could be easily reduced- if needed, also, better FCC gasoline yields require less hydrocracking capacity for coal liquids than petroleum. These distillates made acceptable blendstock for diesel and jet fuel, due to their high cetane number (42-46) and high naphthenes (over 50 v%) content. The superior quality of distillate products from HTI's coprocessing runs (attributable to HTI's in-line hydrotreating operation) was found to fetch a three-dollar premium over the neat petroleum liquids.

CONCLUSIONS

The new dispersed catalyst, developed by HTI, GelCat™, has been very effective for co-processing of coal, plastics and other organic waste material. Excellent process performance in terms of carbonaceous feed conversion to liquid and gaseous products, light distillate yields, and hydrogen consumption have been obtained during the co-processing of different types of feed materials including coal, heavy petroleum resid, municipal solid waste plastics, and auto-fluff. The addition of waste plastics, or pyrolysis oil, from plastics to the feed increase hydrogen efficiency as both hydrogen consumption and C_1-C_3 light gas yield decrease. The co-processing of coal, oil and plastics has achieved an extremely low equivalent crude oil price of $19.64/barrel, putting it nearly in the range of economically commercializing.

Table 1: Performance Comparison-Yields(Black Thunder Coal)					
Run ID	PB-04-3	PB-04-4	PB-04-5	PB-06-3	PB-06-4
Feed Comp.W%	Coal/Oil/ASR	Coal/ASR	Coal/ASR/PLS	Coal/Pyr. Oil	Coal/Oil/Pyr
Coal (Black Thunder)	50	75	50	67	45
Hondo Oil	30				28
Plastics			25		
ASR	20	25	25		
343°C+ Pyr. Oil				33	27
Catalyst					
Fe/P	1000	1000	1000	1000	1000
Mo	50	50	50	0	0
Space Velocity ($kg/h/m^3$)	602	632	621	655	1356
Performance (W% maf feed)					
Conversion	94.1	90.5	91.3	91	86
C_4-524°C Yield	66.8	56.6	61.4	57	54
524°C+ Conv.	83.6	72.4	77.2	73	66
C_1-C_3 Gas Yield	8.6	6.9	7.8	8.8	3.5
H_2 Consumption	5.7	6.0	4.0	5.4	2.2
Economic Comparison (12,000 Tons/Day Total Feed)					
Feed Rate, T/D					
Coal	6000	9000	6000	8040	5400
Hondo Oil	3600				3360
Plastics			3000		
ASR	2400	3000	3000		
343°C+ Pyr Oil				3960	3240
Liquid Prod, B/D					
Gasoline	13196	10141	12205	11527	10310
Diesel Fuel	32048	24629	29641	41238	35875
Total Investment ($MM)	2680	2654	2644	2734	2852
Operating Cost ($MM/Yr)	583.6	519.5	561.9	505.2	639.9
Eq. Crude Oil,$/b	30.34	36.25	28.99	23.41	19.64

ASR=Auto Shredder Residue
PLS=Plastics
Pyr Oil=Pyrolysis Oil

Table 2: Performance Comparison-Yields(Black Thunder vs Illinois#6 Coal)					
Run ID	PB-04-5	PB-06-2	PB-05-3	PB-05-4	PB-05-5
Feed Comp.W%	Coal/ASR/PLS	Coal/PLS	Coal/Oil/PLS	Coal/PLS	Coal/ASR/PLS
Coal (Black Thunder)	50	67			
Coal (Illinois # 6)			33	67	67
Hondo Oil			33		
Plastics	25	33	33	33	17
ASR	25				16
343°C+ Pyr. Oil					
Catalyst					
Fe/P	1000	1000	1000	1000	1000
Mo	50	0	50	50	50
Space Velocity (kg/h/m^3)	621	560	579	669	758
Performance (W% maf feed)					
Conversion	91.3	91	99.1	97.1	96.2
C_4-524°C Yield	61.4	59	78.8	74.6	72.4
524°C+ Conv.	77.2	75	89.6	84.3	81.6
C_1-C_3 Gas Yield	7.8	7.9	9.0	8.2	7.1
H_2 Consumption	4.0	3.9	3.9	5.4	5.8
Economic Comparison (12,000 Tons/Day Total Feed)					
Feed Rate, T/D					
Coal	6000	8040	4000	8040	8040
Hondo Oil			4000		
Plastics	3000	3960	4000	3960	2040
ASR	3000				1920
343°C+ Pyr Oil					
Liquid Prod, B/D					
Gasoline	12205	12305	16201	14354	13645
Diesel Fuel	29641	29885	39346	34860	33137
Total Investment ($MM)	2644	2469	2450	2449	2551
Operating Cost ($MM/Yr)	561.9	446	514.3	486.3	515.9
Eq. Crude Oil,$/b	28.99	26.19	22.43	24.20	25.20

CO-LIQUEFACTION OF COAL AND POLYVINYL CHLORIDE (PVC)

Dhaveji S. Ch., Dady B. Dadyburjor, and John W. Zondlo
Department of Chemical Engineering, P.O. Box 6101
West Virginia University,
Morgantown WV 26506-6101

Keywords: Coal liquefaction, PVC liquefaction, Catalyst, Chlorine distribution

INTRODUCTION

The use of waste plastics as co-liquefaction agents for direct coal liquefaction (DCL) is being explored. Co-liquefaction of waste plastics with coal serves the aim of producing alternative fuels and effectively utilizing waste plastics[1]. PVC is a plastic that is discarded heavily. However, there has been very limited study done on the liquefaction of PVC because it releases corrosive HCl into the gaseous phase, and various chlorinated organics into the liquid phase, at liquefaction temperatures (350-450°C).[2] A recent study showed that the vacuum pyrolysis of PVC at 500 °C resulted in an HCl-gas yield of 53%.[2] Benzene is one of the main minor products.[2]

Ferric sulfide (Fe_2S_3) has been observed to behave as a good "once-through" catalyst for DCL.[3] The addition of another metal, such as magnesium, to the Fe_2S_3 catalyst can enhance its activity. A mixed-metal ferric-sulfide-based Mg-Fe-S catalyst is used in this study for improving the yields as well as possibly capturing chlorine from the products of liquefaction into the residue.

In this paper, the effects of reaction parameters, i.e., temperature, time, hydrogen pressure, and the catalyst on PVC liquefaction, coal liquefaction, co-liquefaction of coal and PVC are presented. Distribution of chlorine among the liquefaction products for the non-catalytic/catalytic liquefaction runs is also presented. The effect of the catalyst on the chlorine distribution is assessed.

EXPERIMENTAL PROCEDURE

PVC is obtained from the Aldrich Chemical Company. The coal is DECS-6 from the Pennsylvania State Coal Bank (PSCB). The catalyst is made in an aerosol reactor and the atomic ratio of Mg to Fe-plus-Mg is 0.25, as prepared. A batch tubing-bomb reactor is used for the liquefaction experiment. The quantity of the feed, i.e., the mixture of coal, PVC, and the catalyst, is kept constant at three grams in all runs. Typical reaction conditions are 350-400°C temperature; at 15-60 min, and 0-2000 psig hydrogen pressure (hot). The reaction is carried out with vertical agitation in a heated, fluidized sand bath. After the reaction, the HCl gas is analyzed by dissolving the gas in water followed by titration. A gas chromatograph (GC) is employed in analyzing the HCl-free gas. The remaining solid product in the reactor is analyzed for the THF-soluble product (THF-S) and the THF-soluble and hexane-insoluble product (Hex-I). The amount of the THF-soluble and hexane-soluble product (Hex-S) is obtained by difference. The yields are calculated on a coal-alone basis by subtracting the contribution of PVC.

For the noncatalytic liquefaction of PVC-alone and coal-alone, an experimental design with 14 experimental conditions is used. The ratio of PVC-to-coal (P/C) is varied from 0.25 to 1.00 for the catalytic/noncatalytic co-liquefaction of coal and PVC. In the catalytic liquefaction runs that involve coal, the catalyst loading is kept at 8.4% on a weight-coal basis, daf (dry, ash-free). The catalytic runs for coal-alone and PVC-alone are conducted at the center point conditions of 400°C, 30 min, and 1000 psig hydrogen pressure (hot). For the catalytic run for PVC-alone, the catalyst loading is 8.4% on a dry basis.

RESULTS

Results of noncatalytic liquefaction of PVC-alone and coal-alone are modeled using second-order polynomials. The model equations are presented in Table 1. The yields are influenced most significantly by the temperature. The parameters of time and hydrogen pressure have modest effects. It is noteworthy that for liquefaction of PVC-alone, the *HCl gas yield* is not influenced by the process parameters and always remains constant at 52%.

As shown in Figure 1, for the co-liquefaction of coal plus PVC, addition of PVC increases the *THF-S+Gas yield*, the *Hex-I yield*, and the *HCl-Free Gas yield*. Negative values of *HCl Gas yields* are observed, which suggest an interaction between coal and PVC. The *Hex-S yield* goes through a minimum. These results suggest that addition of PVC to coal has synergistic effects on some yields. The higher hydrogen content of PVC might be the reason for this effect.

For the catalytic liquefaction of coal-alone, increases in all the yields are observed. The catalyst has a minimal effect on the liquefaction of PVC-alone. The effect of the catalyst on the co-liquefaction is shown in Figure 2. The catalyst is showing a slight effect on the *THF-S+Gas yield*, and a negative effect on the *Hex-I yield* and the *Hex-S yield*. These results indicate that the presence of PVC in the feed reduces the activity of the catalyst. One reason might be that the chlorine species liberated in the liquefaction of PVC are destroying the activity of the catalyst.

Figure 3 shows that in the liquefaction of PVC-alone, most of the chlorine in the raw PVC goes to the gas phase in the form of HCl. Some goes to the Hex-I and THF-I portions. A little goes to the Hex-S portion. However, the pattern of the chlorine distribution changes dramatically if coal is introduced into the feed. The effect of feed ratio on the chlorine distribution in the products is shown in Figure 4. Addition of coal to the feed decreases the chlorine present in the gas phase while increasing the chlorine in the THF-I and Hex-I portions. These results indicate that addition of coal to PVC is beneficial in that the chlorine in the gas phase is decreased. However, an increase of the chlorine in the Hex-I is observed.

Figure 5 shows the effect of the catalyst on the chlorine distribution in catalytic co-liquefaction runs. The addition of the catalyst carries mixed effects. The amount of chlorine in the gas phase and the Hex-S portion decreases at the expense of an increased amount in the THF-I and Hex-I portions. Finally, utilization of the catalyst is serving the purpose of sequestering chlorine, on a qualitative basis, as it is observed that the amount of chorine in the residue (THF-I portion) increases upon employing the catalyst.

CONCLUSIONS

The product from the liquefaction of PVC-alone is mostly the HCl gas. All the yields of PVC-alone liquefaction and coal-alone liquefaction are influenced mostly by temperature. Time and hydrogen pressure have modest effects. Addition of PVC to coal has a synergistic effect for some of the liquefaction product yields. Negative values of *HCl gas yield* indicate an interaction between coal and PVC during co-liquefaction. The mixed-metal catalyst is not influencing the co-liquefaction yields much. The addition of coal to PVC is beneficial in reducing the chlorine present in the gas phase. The residue (THF-I portion) is observed to capture chlorine during co-liquefaction experiments. However, more chlorine is going into the Hex-I portion during co-liquefaction than for the liquefaction of PVC-alone. Addition of the catalyst to the feed brings mixed effects to the chlorine distribution in the products. In the presence of the catalyst, more chlorine is observed in the THF-I portion.

ACKNOWLEDGMENTS

The work was conducted under U.S. Department of Energy Contract No. DE-FC22-93PC9053 under the Cooperative Agreement to the Consortium for Fossil Fuel Liquefaction Science. The authors gratefully acknowledge the support.

REFERENCES

1. Anderson, L. L. And Tuntawiroon, W., Coliquefaction of Waste Plastics with Coal, ACS Div. Fuel Chemistry, *Fuel*, **38**, 1993.

2. McNeill, C.I., Memetea, L., and Cole, J.W., A Study of the Products of PVC Thermal Degradation, *Polymer Degradation and Stability*, **49**, 1995.

3. Dadyburjor D.B., Stewart W.R., Stiller A.H., Stinespring C.D., Wann J.-P., and Zondlo J.W., Disproportionated Ferric Sulfide Catalysts for Coal Liquefaction, *Energy & Fuels*, **8**, 1994.

TABLE I

Model Equations for the Liquefaction Yields of PVC-Alone and Coal-Alone, as Functions of Normalized Values of Temperature, Time and Hydrogen Pressure*

PVC-Alone

THF-S+Gas Yield % $= 78.19 + 10.12*T + 7.80*t + 1.69*P + 1.12*T*P - 5.21*T^2 - 6.62*t^2 - 3.85*P^2$

Hex-I Yield %$= 18.60 + 1.87*T + 5.18*t - 5.81*T^2 - 9.32*t^2 - 5.19*P^2$

HCl-free Gas Yield $= 3.12 + 2.09*T + 0.99*t + 0.51*P + 0.62*P*t + 0.70*T^2 + 0.51*P^2$

Hex-S Yield $= 4.91 + 6.1*T + 2.32*t + 0.79*P + 2.07*T*t - 2.30*t^2 + 1.20*P^2$

Coal-Alone

THF-S+Gas Yield % $= 29.80 + 7.74*T + 3.91*t + 4.30*P + 2.13*T*P - 6.12*T^2 - 3.12*t^2 + 1.07*P^2$

Hex-I Yield %$= 13.37 - 3.06*T - 1.53*t + 1.86*P - 1.63*T*t - 1.97*P*t - 6.65*T^2 + 0.90*P^2$

HCl-free Gas Yield $= 3.37 + 5.06*T + 1.35*t + 0.55*P + 1.16*T*t + 0.89*T*P + 2.6327*T^2$

Hex-S Yield $= 12.95 + 5.96*T + 6.55*t + 1.65*P + 1.82*T*P - 4.47*t^2$

* T = (Temperature - 400)/50; t = (time - 30)/30; P = (Hydrogen Pressure - 1000)/1000

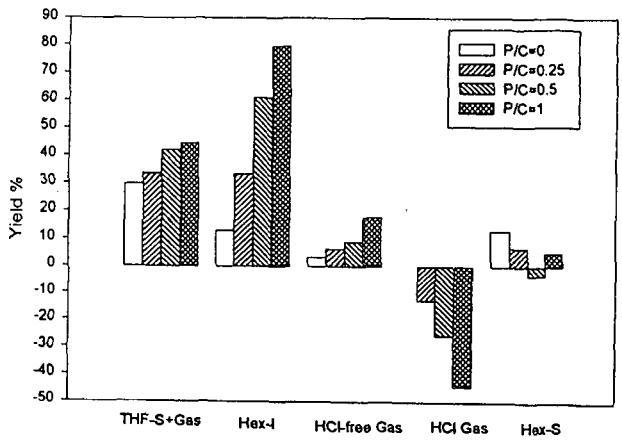

Figure 1. Effect of Feed Ratio on Co-Liquefaction of PVC and Coal at 400°C, 30 min and 1000 psig H_2(hot)

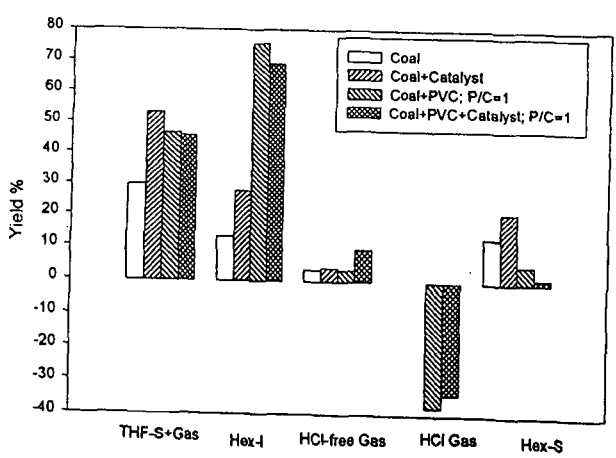

Figure 2. Effect of the Catalyst on Co-Liquefaction of PVC and Coal at 400°C, 30 min and 1000 psig H_2(hot)

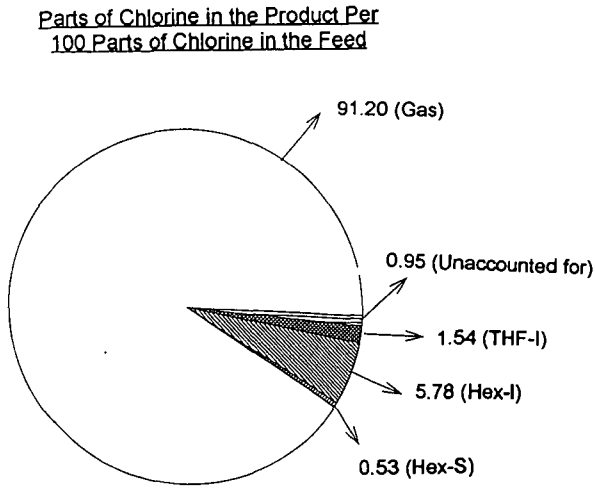

Figure 3. Distribution of Chlorine among the Products for Liquefaction of PVC-alone.
Reaction Conditions -- 400°C, 30 min and 1000 psig H_2 (hot)

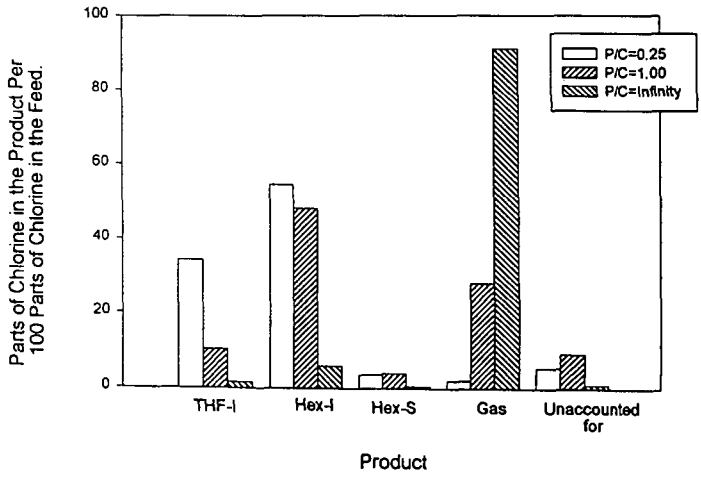

Figure 4. Effect of the Feed Ratio on the Chlorine Distribution in Noncatalytic Co-Liquefaction
Reaction Conditions -- 400°C, 30 min and 1000 psig H_2(hot)

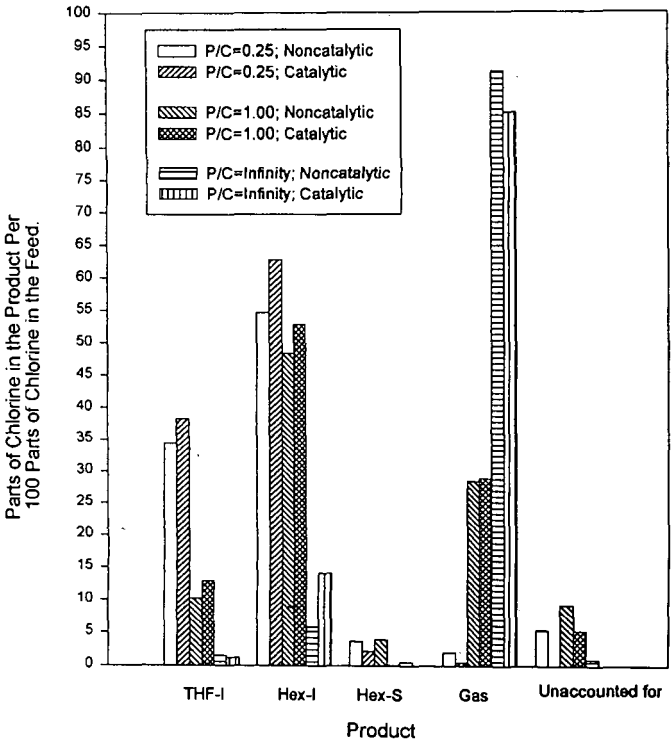

Figure 4. Effect of the Feed Ratio on the Chlorine Distribution in Catalytic Co-Liquefaction Reaction Conditions -- 400°C, 30 min and 1000 psig H_2(hot)

Feed Flow Studies of Waste Coprocessing Feed Slurries

A.V. Cugini, M.V. Ciocco[+], and R.V. Hirsh[+]
U.S. Department of Energy, Federal Energy Technology Center
P.O. Box 10940, Pittsburgh, PA 15236-0940
[+]Parsons Power Group Inc., P.O. Box 618, Library, PA 15129

Introduction

Advanced methods of recycling waste materials are being developed[1]. These methods attempt to use existing technologies, such as direct liquefaction, to convert waste materials into higher value fuels and chemicals. These technologies require a feed system capable of handling a diverse suite of feed materials. Most likely, the resulting slurry would be a heterogeneous mixture of components differing in state, viscosity and density. This heterogeneity creates a difficult problem with respeet to potential feed systems. Recently, a feed flow loop unit was designed and constructed at FETC capable of studying the flow properties of these mixtures. This paper discusses the feed flow loop design and some of the initial results that have been obtained with the unit.

Experimental

A feed flow loop was designed and constructed to investigate the flow properties of slurries containing heterogeneous mixtures of coal, oil, waste plastics, rubber, or biomass. The loop essentially allows for controlled straight flow through a channel. The pressure drop across the channel is measured using a differential pressure transducer. The pressure drop, flowrate, cross-sectional area of the pipe, and pipe length can then be used to calculate the effective viscosity.

The flow loop was designed to measure the effective viscosities of coprocessing slurries. A simplified schematic of the loop is detailed in Figure 1. The lines following the pump are 0.0127 m (0.5") ss tubing, 0.00089 m (0.035") wall. The loop has two straight sections each 5.03 m in length. A pressure transmitter, with a remote seal and range of $0\text{-}5.17\times10^6$ Pa, is near the end of the return straight length. A differential pressure transmitter, with remote seals and pressure differential range of $0\text{-}6.89\times10^5$ Pa, is also on the return length with the remote seals 3.05 m apart. A thermocouple is located in the middle of the 3.05 m section where the pressure drop is measured. All instrumentation readings are monitored and recorded on a computer.

The loop is designed to be used with slurries and mixtures having effective viscosities in the range of 100 - 10,000 cP at temperatures up to 200°C and flow rates of 0.38 - 3.8 l/min. This allows for testing of mixtures at shear stresses and shear rates ranging from 10 - 500 Pa and 50 - 500 s^{-1}, respectively.

In the operation of the flow loop, the feed slurries are prepared and heated to the desired temperature in the mix tank. The slurry is then circulated in a short loop until it is well-mixed. Once the slurry is well-mixed and the desired temperature reached, the slurry is routed through the flow loop. Samples are collected in the product receiver at specific time intervals and used to provide mass flow rates and densities. Samples and measurements are taken at different flow rates and temperatures and the conditions are repeated to insure that the slurry rheology is not time dependent.

Effective Viscosity Calculation

The general viscosity equation for laminar, fully developed, incompressible, and steady flow in a pipe is:

$$\mu_e = \tau_w / (8*v/d)$$

where:
τ_w = shear stress at the wall = $d*\Delta P/(4*L)$
v = average velocity (m/s)
d = diameter (m)
L = length (m)
ΔP = pressure drop (Pa)

$\mu_e = d*\Delta P/ (4*L) / (8*v/d) = d*\Delta P/ (4*L) * (d/8*v) = d^2*\Delta P/ (32*L*v)$

$\mu_e = d^2*\Delta P/ (32*L*v)$

The Reynolds Number (N_{Re}) for flow in a pipe is:

$N_{Re} = \rho*d*v / (\mu_e)$

where: ρ = density (kg/m^3)

For the fluids reported in this paper the N_{Re} is in the range of 3-24, in the laminar flow region.

The entrance length (L_E) for fully developed flow is defined by Langhaar[2] as:

$L_E = 0.0575*d*N_{Re}$

For the fluids reported in this paper the L_E is in the range of 0.002 - 0.03 m. The distance of the pressure transmitter from the bend is 1.14 m (greater than L_E).

A plot of the effective viscosity versus shear rate, $8*v/d$ (s^{-1}), can be used to determine Newtonian or Non-Newtonian behavior.

Results:

Several feed mixtures containing coal, plastics, and heavy oil have been tested in continuous operations at FETC. The conversions and yields observed during these tests have been reported[3]. A typical composition was: 70 wt% heavy oil, 15 wt% coal, 7.5 wt% high density polyethylene, 5.5 wt% polystyrene and 2 wt% polyethylene terephthalate (or polypropylene), essentially a 70:15:15 mixture of oil:coal:plastics. At the feed conditions for the test (temperatures of 50-200°C), the feed slurry contained a solid component (coal) and a viscosity that ranged from 250 to 2000 cP measured by a Brookfield Rotating Spindle Model MV8000 Viscometer.

The importance of controlling viscosity of the feed mixture was evident early in the waste coprocessing effort. For example, a typical feed, consisting of a 70:15:15 mixture was investigated using the Brookfield Viscometer prior to construction of the flow loop. At temperatures of 150°C, the viscosity of such a slurry was approximately 1800 cP. High pressure drop was observed in the feed lines of the continuous unit at this temperature, resulting in operating difficulties that eventually caused the unit to be shut down. At the same temperature, a different feed mixture (70:22.5:7.5) possessed a viscosity of 250 cP. Under these conditions, the coal solids were not adequately suspended in the slurry and settled out, causing plugging in the lines of the continuous unit.

Smoothest operation of the continuous unit occurred when feed viscosities were maintained in the range of 800 to 1000 cP. For a feed mixture of 70:15:15, the viscosity was 1000 cP at 180°C; for a feed mixture of 70:22.5:7.5, the viscosity was 800 cP at 110°C. (Further details of the feed viscosities and flow properties have been reported elsewhere[4].) Therefore, during continuous operations, the optimum conditions for feeding varied widely with feed composition.

The feed flow loop was designed and constructed to test the flow properties of feed slurries. This will enable a more detailed evaluation of the flow properties and the requirements to effectively feed these slurries. This will eliminate the necessity of operating the continuous unit to evaluate the ease of operation. Essentially, the feed flow loop will permit "on-line" measurement and prediction of the rheological and flow properties of prepared feed slurries prior to continuous testing. To date, the feed flow loop has been shaken down and tested with an FCC decant oil. The unit was operated at two temperatures; 50°C and 60°C. A plot of the effective viscosity versus shear rate for the two temperatures is shown in Figure 2. Also included in Figure 2 are separate viscosity measurements for the materials at the same temperature using the Brookfield viscometer. Deviation from a

horizontal line would indicate that the fluid is behaving in a non-Newtonian manner. The slope of the lines at the two temperatures indicates a slight shear-thinning behavior for the decant oil over the shear rate tested. Also, it is encouraging that the calculated effective viscosities from the flow loop are similar to the viscosities measured by the Brookfield Viscometer.

Summary

Waste/Coal feed mixtures can be successfully fed and converted in units designed for hydrogenation and coal liquefaction. An envelope of 250-1800 cP exists outside of which continuous operations can not be maintained. The optimal envelope for feeding these slurries appeared to be in the range of 800-1000 cP. The design and construction of the feed flow loop described here will permit more detailed evaluations of the flow properties of heterogeneous mixtures. The flow loop was successfully tested using decant oil.

Disclaimer

Reference in this paper to any specific commercial product or service is to facilitate understanding and does not imply its endorsement or favoring by the United States Department of Energy.

References

1. Winslow, J.C., Eastman, M.L., Lee, S.R., McBride, C.W., Madden, D.R., Rothenberger, K.S., Munford, W., Rao, U.S., and Cugini, A.V., "Promising Potential for Fossil Fuel/Waste Coprocessing," presented at the 1997 Historically Black Colleges and Universities Conference.

2. Langhaar, H.L., "Steady Flow in the Transition Length of a Straight Tube," **Trans. ASME**, **64**, A-55 (1942).

3. Rothenberger, K.S., Cugini, A.V., Ciocco, M.V., and Thompson, R.L., "Investigation of First Stage Liquefaction of Coal with Model Plastic Waste Mixtures," accepted for publication in **Energy Fuels**.

4. Ciocco, M.V., Cugini, A.V., Wildman, D.J., Erinc, J.B., and Staymates, W.J., "Rheology of Coal/Waste Coprocessing Mixtures," accepted for publication in **Powder Technology**.

Figure 1. Simplified Flow Diagram of the Flow Loop

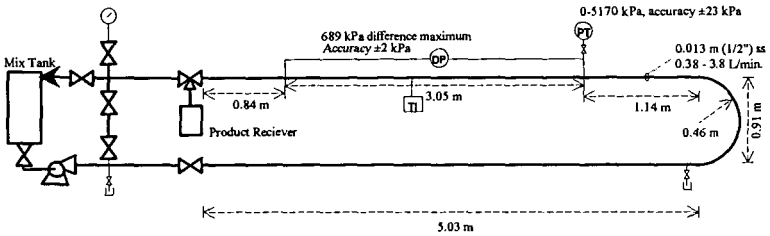

Figure 2. FCC Decant Oil Flow Curve

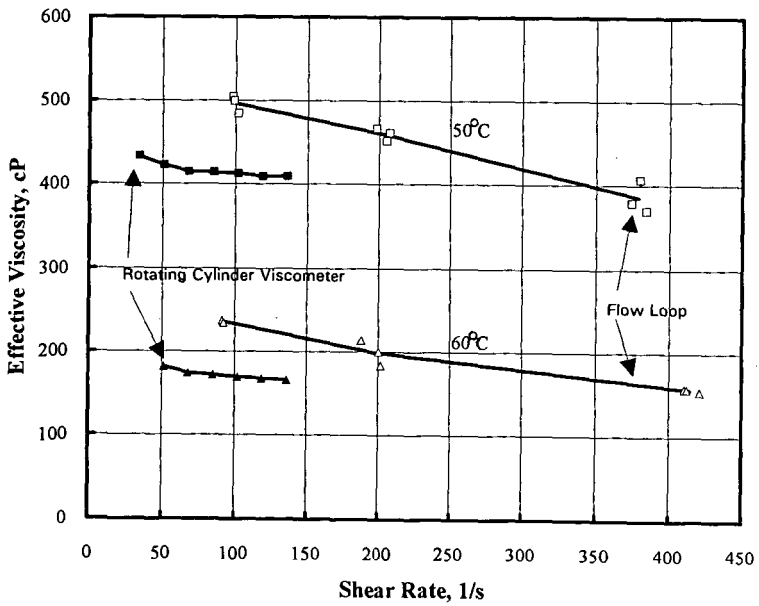

CHARACTERIZATION OF PROCESS STREAM SAMPLES FROM BENCH-SCALE CO-LIQUEFACTION RUNS THAT UTILIZED WASTE POLYMERS AS FEEDSTOCKS

Gary A. Robbins and Richard A. Winschel
CONSOL Inc., Research and Development
4000 Brownsville Road
Library, PA 15129

INTRODUCTION

Since 1994, CONSOL has characterized feed, recycle, and product samples from DOE-sponsored co-liquefaction experiments with polymers and coal.[1-5] The objective is to understand the process chemistry and the fate of the polymer components during continuous operations. CONSOL used conventional liquefaction process stream characterization methods, supplemented by methods specifically developed for polymer components. In the earliest Hydrocarbon Technologies, Inc. (HTI) runs, virgin polymers were used to simulate municipal waste polymers (Proof-of-Concept scale in Run POC-2, bench scale in Runs CMSL-8 and CMSL-9). More recently, HTI began using authentic municipal solid waste polymers (Run CMSL-11[6]) and auto shredder residue (Run PB-04[7]) as co-liquefaction feedstocks in various combinations with coal, petroleum resid, and virgin polymers. Process stream samples were characterized from HTI runs in which authentic municipal or industrial waste polymers were liquefied with coal and petroleum resid. The conversion of relatively unreactive polyolefins was determined by an extraction procedure. The fate of polystyrene was determined by gas chromatography-mass spectrometry of net liquid products.

BRIEF DESCRIPTION OF PLANT AND CO-LIQUEFACTION RUNS

The co-liquefaction runs were performed in HTI's bench unit 227. Fresh feed materials (catalyst precursors, coal, waste feedstocks, petroleum resid, and/or virgin polymers) were mixed batchwise with process recycle materials in a tank and transferred to a feed slurry tank that continuously fed the slurry to the liquefaction process. The feed slurry was fed to a preheater that also conditioned the dispersed catalyst. Next, the slurry was fed to two successive stages of liquefaction. No supported catalysts were used in the liquefaction reactors; only disposable dispersed catalysts were used. A high-pressure separator after the first reactor allows light products to be taken off, and the hydrogen concentration to be increased in the second reactor. The first-stage oil, called the first-stage separator overhead oil, or SOH1, is sent with second-stage light oils and light distillate to an in-line fixed-bed hydrotreater. The in-line hydrotreater upgrades the product using the liquefaction reactor system offgases. The second stage of liquefaction is followed by high- and low-pressure separators. The separator overheads are fed to the in-line product hydrotreater, and the separator bottoms to distillation. The distillate (ca. IBP-371 °C) is sent to the product hydrotreater, and the resid is filtered to provide a liquid for recycle and solids to reject ash.

Major streams analyzed typically included the feed slurry, individual fresh feeds, the unhydrotreated first-stage separator overhead (SOH1) oil, the separator bottoms (flashed liquefaction product), the filter liquid (recycle), filter cake (solids), and the hydrotreated net product oil. On occasion, an unhydrotreated net product oil is available through bypass of the hydrotreater.

Operating conditions for relevant portions of Runs CMSL-11[6] and PB-04[7] are shown in Table 1. In both runs, co-liquefaction operation was successfully demonstrated using the municipal or industrial waste feedstocks (municipal solid waste (MSW) plastics in Run CMSL-11, and automobile shredder residue (ASR) in Run PB-04). When MSW was fed with coal, Condition 3B of Run CMSL-11, H consumption and gas yield were reduced and distillate yield increased. In general, ASR was not as beneficial as MSW to liquefaction process performance. Operating difficulties were encountered throughout the ASR run. HTI observed that: 1) ASR caused repeated feed pump problems; 2) the resid conversion was lower when ASR was fed (relative to feeding coal only); and 3) ASR lowered the H consumption, distillate yield, and light gas yield. HTI speculated that polyurethane and (cross-linked) high impact polystyrene in the ASR were less reactive than polymers previously processed (including the MSW). It is important to determine the relative reactivity of the polymers that could be identified in the ASR.

DESCRIPTION OF CHARACTERIZATION METHODS

Three analytical techniques supplemented the normal liquefaction work-up procedures (which usually include distillation, tetrahydrofuran (THF) extraction, ashing, and determinations of phenolic -OH concentration and proton distribution). When polymers are present in co-liquefaction samples, hot decalin extraction, FTIR spectroscopy, and GC-MS characterization are the supplementary techniques. The decalin extraction and FTIR are used typically for resid- and solids-containing samples, and GC-MS is used typically for light net product oils. The hot decalin extraction method was described previously;[5] it generates a solubles fraction, a "plastic" fraction, and an insolubles fraction from a liquefaction sample. The "plastic" fraction consists of polyolefins (primarily high-density polyethylene (HDPE) and polypropylene (PP)) that are soluble in hot decalin, but insoluble in THF or room-temperature decalin. The polymers are subsequently

characterized by FTIR spectroscopy. The GC-MS total ion chromatograms and individual mass spectra are usually examined for information on n-paraffins from polyethylene and other feedstocks, and for marker compounds from PS liquefaction. Various sample preparation techniques have been used at CONSOL for qualitative FTIR examination of polymeric materials. Unsupported and supported thin films and thin slices have been used for transmission IR measurements. Powder, or fine cuttings or filings have been mixed with KBr (1-10% polymer) for diffuse reflectance measurements.

CHARACTERISTICS OF PROCESS STREAMS SAMPLES

Table 2 is a summary of the overall characterization results of the various process streams analyzed, components found or expected, and methods used. Ash, polyethylene, polypropylene, and polystyrene were components of the MSW and ASR feedstocks that were directly or indirectly identified. PS was identified via marker PS-derived compounds found in product oils using GC-MS. Ash was determined directly on the MSW and indirectly on the ASR, using the ash content of the feed slurry. A polyolefin component was extracted from the feed slurry samples, and identified as HDPE and PP using FTIR spectroscopy. Spectroscopic features suggest the presence of low-density polyethylene (LDPE), or some unidentified polyethylene, in some samples. Based on combined results from several of these methods, overall composition of the MSW feed is approximately 96% HDPE+PP, 2% PS, and 1.6% ash. Using the same procedure, the estimated composition of the ASR feed was 68% HDPE+PP, 11% PS, 20% ash (as reported by HTI[7]), and 1% unaccounted.

FATE OF HDPE AND PP

Previous work demonstrated that polyolefins, primarily HDPE and PP, could be extracted from co-liquefaction stream samples. The amount of this material rejected from the process represents the amount that is not converted to liquid products. FTIR spectroscopy (Figure 1) was used to identify PP and HDPE in polyolefin material extracted from feed slurries from Run PB-04. These results indicate that PP was a significant component of the feed ASR. The material extracted from the pressure-filter cake stream that is used to reject solids from the process consists entirely of polyethylene (Figure 1, apparently HDPE). This indicates that the PP is more reactive than the HDPE at reaction conditions.

Table 3 presents the ash-balanced, overall conversions of the total MAF feed, the total MAF waste/polymer feed, and the decalin-extracted polyolefins. The overall conversion is calculated from the compositions and flow rates of the net product and fresh feeds. However, decalin-extracted polyolefins were determined on the (Run PB-04) feed slurry samples, since no ASR sample was available. The recycled ash and polyolefins contributions were backed out to determine the relative concentrations of fresh polyolefins and ash. In turn, this allowed the percentage polyolefins in the ASR to be estimated at 79-90% MAF, or 62-73% (average of 68%) MF.

The CONSOL MAF fresh feed conversion is compared with HTI results in Table 3 to demonstrate that the ash balance technique typically gives conversions very similar to those of HTI. The exception in these data are the results for Conditions 4 and 5, for which the CONSOL conversions were ~3-5% lower than those obtained by HTI, possibly due to the difference between the solvents used. CONSOL used THF to define conversion (THF does not dissolve the unconverted polyolefins). HTI used hot quinoline to define conversion (hot quinoline does dissolve the unconverted polyolefins). The same ash balance method was used to calculate conversions of the total wastes and the decalin-extracted polyolefins. The results indicate high conversion of the total waste/polymer stream and of the polyolefins, ~95-99%. The conversions of these components were typically about 5% higher than HTI's conversions of the total fresh feed. The lower conversions observed by CONSOL for the total waste/polymer component and for the decalin-extracted polyolefins corresponded to Conditions 4 and 5 of Run PB-04, in which HTI also observed the lowest fresh feed conversions. Recycle of unconverted polyolefins (apparently chiefly HDPE) is required to achieve these high conversions. Evidently, conditions used in Conditions 4 and 5 of Run PB-04 were not optimal to convert all of the ASR or polyolefin component of the ASR. In Run CMSL-11, HTI used higher reactor temperatures, higher Mo and Fe catalyst concentrations (and different catalyst precursors) to achieve high conversion of the MSW polymers.

FATE OF PS

Earlier work with samples from Runs POC-2, CMSL-8, and CMSL-9, in which virgin polystyrene (PS) was a feedstock, indicated that ~70% of the PS fed could be identified as components (toluene, ethylbenzene, and cumene) in the unhydrotreated product oil and ~50% in the hydrotreated product oil.[1-4] Cumene alone accounted for ~16% of the PS fed in the unhydrotreated product oil, and ~10% in the hydrotreated product oil. Cumene is a good marker for PS-derived products, because it is found in product oil samples from co-liquefaction with PS as a feed component. In the unhydrotreated first-stage product oils from Run PB-04, 1,3-dimethyl propane was also identified as a unique PS marker. However, this compound seems to be clearly identifiable and quantifiable primarily when the product oil is unhydrotreated. The components used for identification and quantification by CONSOL contain aromatic rings, because these components are readily identified by their mass spectra using automated searches of spectral databases.

Concentrations of four PS-derived compounds identified by GC-MS in the SOH1 samples from Run PB-04 and in the Run CMSL-11 product oil from Condition 3B are shown in Table 4. The presence of cumene in products from liquefaction of MSW in Run CMSL-11 and ASR in Run PB-04 demonstrates the presence of PS as a feed component. The ASR and MSW feed materials are very heterogeneous and are difficult to characterize directly to quantify individual polymer components. Based on earlier work with virgin plastics, the amount of PS in the waste feedstocks can be estimated for Runs CMSL-11 and PB-04. If the same degree of conversion takes place, and the yield of the product oils are known or estimated, it is estimated that PS constitutes about 2 wt % of the MF feed MSW in Condition 3B of Run CMSL-11. Similarly, it is estimated that PS constitutes about 11 wt % of the MF feed ASR in Conditions 3 and 4 of Run PB-04.

The four marker compounds (Table 4, Figure 2) constituted about 11-42% of the SOH1 samples in Conditions 3-5 of Run PB-04. In contrast, the Condition 1 (coal-only) SOH1 contained only 2% of three of these markers (1,3 diphenyl propane was not present). In general, these marker compounds seem to represent the lowest-boiling primary fragments of PS liquefaction, as shown in Figure 1. Benzene, methane, and ethane could also be primary products, but they also are produced from coal. Hydrotreating these components may cause cracking or ring hydrogenation. Any products that elute before toluene, or do not contain an aromatic ring, are less-readily identified or quantified because they are not unique to PS liquefaction.

The observed distribution of these four components on a relative weight percent basis is: toluene - 12.5 ±2.5%, ethylbenzene - 64.7 ±3.9%, cumene - 20.6 ±2.6%, and 1,3-diphenylpropane - 2.2 ±0.3%. On a mol percent basis, the distribution becomes: toluene - 14.6%, ethylbenzene - 65.7%, cumene - 18.5%, and 1,3-diphenylpropane - 1.2%. An uneven distribution of alkyl vs. phenyl groups in the products (ethylbenzene has the proper distribution) would imply that these products are accompanied by the production of some (unobserved) combination of methane, ethane, benzene, and cyclohexane (in the simplest possible molecules). The observed distribution indicates that 2.6 mol % benzene + 2.6 mol % methane would account for the imbalance (i.e., there is more cumene than toluene plus 1,3-diphenylpropane). Although the data may not support a rigorous analysis like this, qualitatively the results suggest that the production of light gases such as methane and ethane from liquefaction of polystyrene is minor. These estimates leave about 20% of the PS as unaccounted. In addition to benzene, the unaccounted portion could be cyclic alkyls that are hydrogenation products and not readily identified.

CONCLUSIONS

These results show that several components of authentic waste polymers can be identified and sometimes quantified in co-liquefaction process stream samples. Different characterization strategies are needed to accommodate different polymers. PS and PP appear to be reactive, and there is no hint that the ASR contains an unreactive PS component, as was speculated based on Run PB-04. HDPE is less reactive and requires a substantial recycle rate to convert it. Ultimately, nearly all of the HDPE is converted. Marker compounds that appear to be primary PS products were observed in the light product range. The distribution of these light PS products suggests that little gas production is associated with PS liquefaction.

FUTURE NEEDS

It is desirable to develop methods for speciation of more polymers (e.g., polyurethane). Quantitative FTIR methods would allow the determination of relative or absolute amounts of PP and HDPE present. Other information, such as molecular weight distributions, would be informative; however, their expense usually cannot be justified for a large number of process samples.

ACKNOWLEDGMENTS

This work was supported by the U.S. Dept. of Energy under Contract No. DE-AC22-94PC93054. Samples and background information were supplied by Dr. V. Pradhan of HTI.

REFERENCES

1. Robbins, G. A.; Brandes, S. D.; Winschel, R. A.; Burke, F. P., DOE/PC 93054-10, May 1995.
2. Robbins, G. A.; Brandes, S. D.; Winschel, R. A.; Burke, F. P., DOE/PC 93054-18, September 1995.
3. Robbins, G. A.; Brandes, S. D.; Winschel, R. A.; Burke, F. P., DOE/PC 93054-25, May 1996.
4. Robbins, G. A.; Brandes, S. D.; Winschel, R. A., DOE/PC 93054-34, March 1997.
5. Robbins, G. A.; Winschel, R. A.; Burke, F. P. Prepr. ACS Div. Fuel Chem. 1996, 41 (3), 1069.
6. Draft internal HTI report on Run CMSL-11.
7. Draft internal HTI report on Run PB-04.

Table 1. Conditions and Yields for HTI Runs PB-04 (227-95) and CMSL-11 (227-89)

Run	PB-04					CMSL-11	
Condition	1	2	3	4	5	2	3B
Feed, wt % MF							
Blk. Thunder Coal	100	-	50	75	50	100	75
Hondo resid	-	70	30	-	-	-	-
ASR or MSW	-	30	20	25	25	-	25
HDPE/PS (60:40)	-	-	-	-	25	-	-
Temp. Stg 1/Stg 2, °C	440/450					450/460	
Disp. Cat. Loading, mg/kg	Fe :1000, Mo:50, P:100					Fe:5000, Mo:100	
Yields, wt % MAF Fresh Feed							
C_1-C_3 Gases	9.9	7.0	8.6	6.9	7.8	18.2	7.4
C_4-343 °C	46.0	44.4	48.3	31.2	40.3	49.4	39.5
343-524 °C	21.6	24.7	18.5	25.4	21.2	13.5	28.1
524 °C+	3.7	16.0	10.5	18.0	14.0	6.0	11.2
Unconverted Feed	6.8	3.6	6.0	9.6	8.8	4.9	5.3
H_2O+COx	18.6	5.0	11.6	15.2	12.1	14.5	13.6
NH_3+H_2S	0.6	4.2	2.3	-0.3	-0.8	0.4	-0.2
H_2 Consumption	7.2	4.8	5.7	6.0	4.0	6.9	4.9
MAF Feed Conv., wt % (SO_3-Free)	93.2	96.4	94.1	90.5	91.3	95.1	94.7

Table 2. Components Found in Process Stream Samples From Co-Liquefaction of Waste Polymers With Coal

	Component						
Stream Sample from Process	HDPE	PP	LDPE or Other PE	PS	Ash	Other Polymers	Methods
Feed MSW	X	X		I	X	E	DE,FTIR
Feed ASR	I	I		I	X	E	
MSW Feed Slurry	X	X		I	X	E	DE,FTIR
ASR Feed Slurry	X	X	S	I	X	E	DE,FTIR
Separator Bottoms	X	C*			X		DE,FTIR
Filter Liquid	X	C*	S*				DE,FTIR
Filter Solids	X	C*	S*		X		DE,FTIR
1st Stage Oil*	P	E		P			GC-MS
Product Oil	P	E		P			GC-MS

Legend: X = Direct evidence; I = Indirect evidence; P = Evidence for a product; E = Expected, but not identified; S = Suspected, i.d. uncertain; C = Contrary evidence (i.e., that it is not present); DE = Hot decalin extraction

* Applies to Run PB-04 samples only.

Table 3. Overall conversion of Feed and Polymer Feed Components in HTI Runs PB-04 and CMSL-11

	Overall Conversion, %					
Source	PB-04 Cond. 1	PB-04 Cond. 2	PB-04 Cond. 3	PB-04 Cond. 4	PB-04 Cond. 5	CMSL-11 Cond. 3B
Basis: MAF Fresh Feed, Ash-Balanced						
CONSOL	93.7	95.0	95.7	87.1	85.5	94.3
HTI(a)	93.2	96.4	94.1	90.5	91.3	94.7
Basis: MAF Fresh Waste/Polymer, Ash-Balanced						
CONSOL	NA	99.9(b)	99.4(b)	95.8(b)	96.8(b)	99.1(c)
Basis: Fresh Decalin-Extractable Polyolefins in Feed, Ash-Balanced						
CONSOL	NA	NA	99.3(c,d)	95.4(c,d)	NA	NA

(a) SO_3-free ash basis
(b) % MAF ASR in feed (+virgin polymers in feed in Cond. 5)
(c) % Decalin-extracted polyolefin in feed
(d) Back-calculation from Condition 3 results indicates that the feed ASR contains 79% MAF decalin-extracted polyolefin (63% on MF basis). From Condition 4 results, the feed ASR contains 90% MAF decalin-extracted polyolefin (72% on MF basis).

Table 4. PS Liquefaction Products Found in Run PB-04 First-Stage Oils

Component	Toluene	Ethylbenzene	Cumene	1,3-Diphenyl propane	Sum
Conc. in SOH1, wt %					
Cond. 1	0.3	1.5	0.2	0.0	2.0
Cond. 3	1.3	7.5	1.9	0.2	10.8
Cond. 4	4.3	17.7	5.7	0.6	28.3
Cond. 5	4.4	26.8	9.4	1.0	41.6
Conc. in SOH1 as wt % of ASR fed, adjusted to eliminate coal contribution					
Cond. 3	1.0	6.0	1.6	0.2	8.8
Cond. 4	1.4	5.4	1.9	0.2	8.9
Cond. 5	3.1	18.7	6.6	0.7	29.1
Avg. Relative Distribution					
Wt %	12.5	64.7 ±3.9	20.6	2.2 ±0.3	100.0
mol%	±2.5	65.7	±2.6	1.2	100.0
	14.6		18.5		
C Balance	$+1CH_2$	0	$-1CH_2$	$+1CH_2$	
Net C Balance	-2.6 mol% CH_2, or +2.6 mol% (benzene $+CH_2$)				

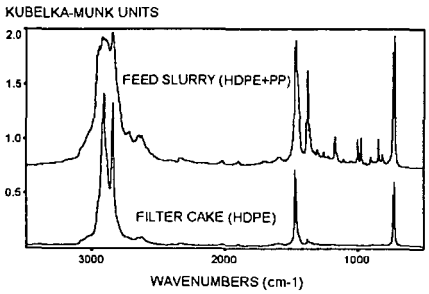

Figure 1. FTIR Spectra of Decalin-Extracts From Feed Slurry and Filter Cake Produced in Condition 5 of HTI Run PB-04.

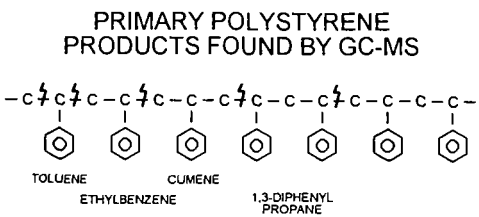

Figure 2. PS Liquefaction Products Found in Net Product Oils.

THE EFFECTS OF FUEL-BOUND CHLORINE AND ALKALI ON CORROSION INITIATION

Larry L. Baxter, Hanne P. Nielsen[1]
Sandia National Laboratories
Combustion Research Facility
Livermore, CA 94550

ABSTRACT

This investigation explores the effects of fuel-bound chlorine and alkali metals on the initial phases of metal corrosion under conditions typical of superheaters and reheaters in electric power generating boilers. Experiments were conducted with a variety of fuels in an entrained-flow, pilot-scale combustor that simulates conditions found in commercial-scale, pulverized-coal-fired boilers. Temperature-regulated probes simulated superheater tubes and were sized to reproduce similar mechanisms of deposition as are found in commercial systems. Fuels examined include coals with a wide range of chlorine concentrations, biomass fuels, and coals blended with chlorine-containing biomass fuels. Scanning electron micrographs reveal regions of the interfaces of some such probes that show evidence of chloride condensation and subsequent conversion to sulfates. This chemical conversion releases chlorine-containing gases that can facilitate the corrosion of the surface without being consumed. Hypothesized mechanisms for this corrosion have been presented in the literature and are reviewed. The extent to which chlorine-containing materials accumulate on surfaces and subsequently sulfate is shown to depend strongly on the mechanisms of ash deposition and on surface temperature. Interactions between alkali and other ash constituents are shown to effect the extent of alkali deposition and the amount of sulfation. Implications for combustion of chlorinated fuels are discussed.

INTRODUCTION

One of the primary economic drivers of this investigation is the determination of the level of chlorine in coal that can be allowed before corrosion of heat transfer surfaces becomes intolerable and how this level may vary among coals of similar properties but from different seams. In particular, authors have cited anecdotal evidence that coals from the Illinois region do not cause corrosion problems in boilers to the extent that UK coals with similar chlorine levels do. The UK has a great many chlorinated coals whereas the most commercially significant chlorinated coal in the US derive from the Herron Basin, largely within Illinois, and represent a fairly small fraction of the overall US coal market. Operational practices relative to chlorine-induced corrosion rely heavily on UK recommendations, where the greatest experience lies. Generally, these practices suggest not firing coals with greater than 0.3% chlorine unless materials and operations are specifically altered to deal with potential corrosion problems associated with high-chlorine coals.

There have been no direct comparisons of the corrosion behaviors of UK and US coals in the same utility-scale boiler under the same operating conditions. Since such comparisons are both unlikely to occur and are subject to large uncertainty due to the nature of commercial-scale operation, this investigation was commissioned. The objective of this work is to establish fundamental relationships among operating conditions, fuel properties, and corrosion mechanisms that could be used to establish the corrosion potential of fuels.

Sandia National Laboratories is engaged in a series of investigations regarding the role of chlorine in corrosion in power plants. These investigation focus on deposit formation and initiation of corrosion processes. Chlorine-based corrosion is often associated with alkali metals, and corrosion in general is often aggravated by alkali metals with or without chlorine present. The purpose of this investigation is to establish which corrosion-related species are most likely to form in the gas-phase and on surfaces under typical combustion conditions and to demonstrate how fuel properties influence their formation. This information leads to a postulated mechanism for chlorine-related corrosion and distinguishing characteristics among fuels that may indicate their corrosion potential.

THERMODYNAMIC STABILITY

Early work on this subject indicated that there may be differences in the rates of release of chlorine depending on the origin of the coal. Specifically, coals from the UK were observed to release chlorine slightly earlier in their combustion histories than were US coals of otherwise similar properties. There was some speculation that this could lead to differing corrosion rates or mechanisms. However, in all cases essentially all of the chlorine was released well before the coals completed

[1] Work completed while visiting Sandia National Laboratories, Livermore, CA, from the Technical University of Denmark, Copenhagen.

combustion. Therefore, all of the chlorine would be in the gas phase long before entering the convection passes of commercial boilers, where corrosion is typically of greatest concern. We view it as unlikely that differences in these early release mechanisms could significantly alter the corrosion rates that occur far downstream from where the differences are observed. However, there may be differences in the coals that lead to differing amounts of alkali being released. These may be more closely related to modes of alkali occurrence than to release rates and mechanisms of chlorine. Alkali metals are clearly implicated in high-temperature corrosion and their most stable gas-phase form is as chlorides at furnace exit gas temperatures.

Table 1 Elemental composition on which equilibrium calculations are based representing an oxidizing, moist environment typical of lower-furnace regions in many coal-fired boilers. There is excess oxygen, carbon and hydrogen for formation of alkali carbonates and hydroxides, but insufficient sulfur or chlorine to react with all of the alkali to form sulfates or chlorides.

Element	Molar Ratio Element / Total Alkali
C	202
H	850
O	1593
N	5848
S	0.125
CL	0.375
Alkali (Na or K)	1

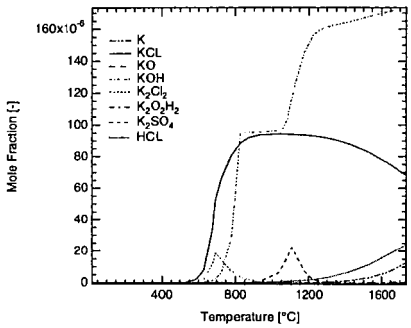

Figure 1 Equilibrium species concentrations for the major potassium-containing, gas-phase species present under typical coal combustion conditions. Compare with condensed-phase behavior illustrated in Figure 2.

Figure 1 through Figure 4 illustrate equilibrium predictions for the major alkali-containing gas- and condensed-phase species as a function of temperature. As illustrated, chlorine and alkali behavior are coupled and this coupling explains some aspects of how ash deposit structure develops. All of the calculations are performed under conditions representative of furnace regions where chlorine is released and char oxidation begins. The molar ratios of each of the atoms relative to the alkali-containing species are indicated in Table 1. In general, the oxygen and water mole concentrations in the equilibrium products are about 10%. The molar ratios allow for complete conversion of alkali to carbonates or hydroxides, but are insufficient to allow complete conversion to either sulfates or chlorides.

Chlorides represent among the most stable alkali-bearing species in the gas phase. Chlorine is shown to have a strong affinity for alkali metal in the temperature ranges of interest to convection pass entrances. In many cases, the amount of alkali vaporized during combustion is determined more by the amount of chlorine available to form stable vapors than by the amount of alkali in the fuel [1]. Figure 1 illustrates predicted equilibrium concentrations of gas-phase, potassium-containing species under typical coal-combustion conditions. Condensed-phase results are illustrated in Figure 2. Gas-phase sulfate is seen to play a relatively minor role in potassium equilibrium chemistry. Peak sulfate concentrations represent about 10% of the total gas-phase potassium and occur over a narrow temperature range at about 1100 °C. At lower temperatures, potassium sulfate vapor condenses to form liquid or solid sulfate. At higher temperatures, it decomposes. Thermodynamic predictions of sodium-bearing species are very similar to those of potassium and are illustrated separately in Figure 3 and Figure 4.

The dominant gas-phase, alkali-bearing species at flame temperatures (>1400 °C) is alkali hydroxide, followed by the chloride. In the absence of significant chlorine for reaction, only the hydroxide is present. As temperatures cool to convection-pass values (<1000 °C), hydroxides convert to chlorides, the only alklai-bearing species in significant quantities at lower temperatures. Sulfates are notable by their absence in the gas phase.

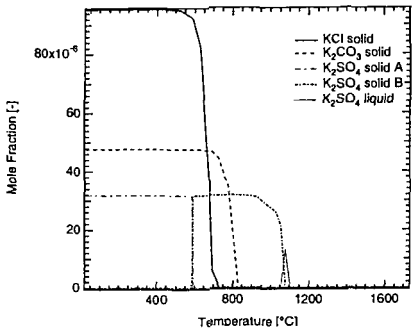

Figure 2 Condensed-phase equilibrium behavior of potassium-containing species. Compare with gas-phase behavior illustrated in Figure 1.

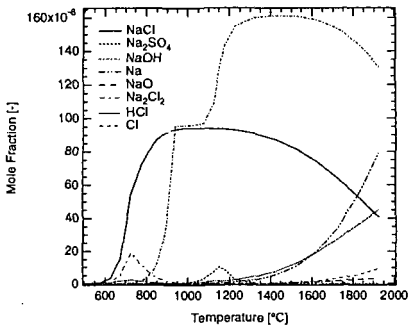

Figure 3 Equilibrium species concentrations for the major sodium-containing, gas-phase species present under typical coal-combustion conditions.

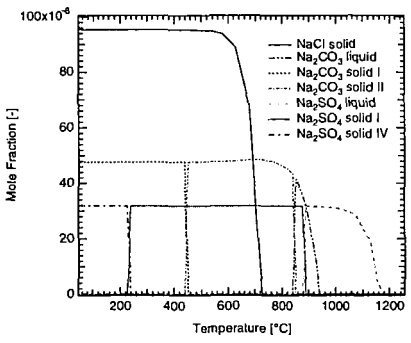

Figure 4 Equilibrium species concentrations for the major sodium-containing, condensed-phase species present under typical coal-combustion conditions.

The condensed-phase behavior of alkali-containing compounds is illustrated in Figure 2 and Figure 4 as a function of temperature. Many coals have more sulfur than the stoichiometric amount required for reaction with all of the available alkali. In addition, an ash deposit on a surface interacts with a continuous gas stream, providing a continuous source of sulfur. Often, the rate of accumulation of alkali in the deposit is slow compared to the rate of diffusion of sulfur from the bulk gas stream to the deposit surface. Under these conditions, the deposit has opportunity to react with a much larger amount of sulfur than the elemental composition of the fuel may suggest. However, these calculations include less sulfur than is required to react with available alkali to illustrate the relative stability of chlorides and sulfates in the condensed phase. Sulfates are the most stable of the condensed-phase alkali species at temperatures indicative of heat transfer surfaces and deposits (1200 °C and less

Equilibrium predictions show that the dominant condensed-phase species at the highest temperatures are sulfates, followed by carbonates and chlorides as temperature decreases. Historical Multifuel Combustor data and field data have shown that sulfates, carbonates, and chlorides are commonly found on heat transfer surfaces when combusting fuels that contain none of these compounds; i.e. these species are formed in the furnace and not simply transported with the ash to the surface. Sulfates are invariably found in highest concentrations and can be seen to form with time on the surface [2]. Carbonates and chlorides are less commonly found but have been observed in deposits from highly chlorinated coals and under reducing conditions.

MODE OF OCCURRENCE

Essentially all of the chlorine in fuels is available for reaction in the gas phase. The same is not true of the alkali. A large fraction of the alkali material occurs in a mode that is either thermodynamically stable or physically constrained such that is not available for interaction with other compounds. An extraction technique known as chemical fractionation is used to distinguish between these modes of occurrence of different inorganic species in coal, including the alkalis. Specifically, the technique is used to determine the relative availabilities of inorganic material for vaporization or other release processes during combustion. The technique involves extracting material from a sample of coal using increasingly aggressive reagents and monitoring the fraction of inorganics extracted at each step. We typically separate inorganics into four groups: (1) water soluble materials such as halides, some salts, and some chemisorbed or otherwise lightly

bound inorganics; (2) ion exchangeable materials such as ions of salts formed from carboxyl and hydroxyl groups in the coal; (3) acid soluble materials such as carbonates and sulfates; and (4) residual materials such as clays and most oxides (silica, titania, etc.).

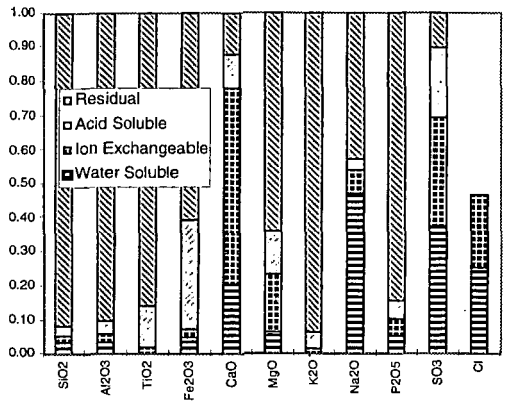

Figure 5 Chemical fractionation results for the UK coal indicating the major modes of occurrence for the inorganic components. Compare with Figure 6.

Results of this procedure are available for representative UK and a US coals with similar chlorine contents. The results indicate that there is approximately 50% more sodium available from the UK coal for participation in the corrosion-inducing reactions indicated above than there is for the US coal. However, the difference arises from the total sodium content and not from a large difference in the mode of occurrence of the sodium in the fuels. Figure 5 illustrates the results for the UK coal. The fraction of total mass is illustrated for each of the major elements in coal. Sodium is of primary interest for corrosion for these fuels. Sodium occurring in mobile forms is more likely to vaporize during combustion than sodium in the form of clay or other stable compounds. The mobile forms of sodium include the water soluble and ion exchangeable components. The sum of these two forms represents 54% of the sodium in the UK coal and 66% in the Rend Lake coal. This difference is larger than the inherent error in making these measurements (± 3%), but is probably not significantly larger than the fluctuations in coal properties as delivered from the mine. We find no indication that the modes of occurrence of sodium or chlorine in these t.) samples of fuels would produce significantly different corrosion results. There are large variations in the mode of occurrence of sodium in coal, and other fuels may show different tendencies. We do anticipate the UK coal would be more corrosive that the US coal in this case, but only because it has a higher overall sodium content. The modes of occurrence of sodium in the two fuels are similar.

Table 2 Chemical fractionation results for the UK coal indicating the major modes of occurrence for the inorganic components on a % dry fuel basis. Compare with Table 3.

	SiO_2	Al_2O_3	TiO_2	Fe_2O_3	CaO	MgO	K_2O	Na_2O	P_2O_5	SO_3	Cl
Water Soluble	0.251	0.135	0.000	0.046	0.053	0.014	0.000	0.133	0.001	0.086	0.017
Ion Exchangeable	0.179	0.085	0.002	0.025	0.152	0.040	0.008	0.020	0.001	0.073	0.014
Acid Soluble	0.213	0.159	0.016	0.299	0.026	0.031	0.025	0.009	0.001	0.048	
Residual	7.457	3.553	0.108	0.577	0.032	0.152	0.506	0.121	0.022	0.024	

Table 3 Chemical fractionation results for the Illinois coal indicating the major modes of occurrence for the inorganic components on a % dry fuel basis. Compare with Table 2.

	SiO_2	Al_2O_3	TiO_2	Fe_2O_3	CaO	MgO	K_2O	Na_2O	P_2O_5	SO_3	Cl
Water Soluble	0.042	0.014	0.000	0.087	0.098	0.018	0.005	0.090	0.001	0.056	0.008
Ion Exchangeable	0.220	0.107	0.006	0.030	0.153	0.049	0.011	0.001	0.002	0.093	0.007
Acid Soluble	0.067	0.063	0.006	0.208	0.008	0.008	0.007	0.004	0.001	0.024	
Residual	3.497	1.614	0.080	0.814	0.038	0.064	0.166	0.042	0.015	0.027	

THE ROLES OF CHLORINE AND ALKALI IN CORROSION

On the basis of these data we postulate the following relationships among operating conditions, boiler design, and fuel properties that impact corrosion. The three fuel properties that most significantly impact rates of corrosion are sulfur, available alkali, and chlorine contents. Corrosion is

strongly influenced by the presence of alkali on the surface of the deposit. This alkali is generally sulfated on the surface, but it appears that the sulfate represents a reaction product from the gas phase and is not, in general, directly deposited. Chlorine enhances corrosion by at least two mechanisms. First, increased chlorine concentrations lead to increased alkali-containing vapors in combustion gases as chlorides are among the most stable alkali-laden species under most combustion conditions. Increased gas-phase alkali concentrations lead to increased rates of alkali deposition on surfaces. Secondly, if the alkali chlorides from the gas phase convert to alkali sulfates on or near heat transfer surfaces, the chlorinated product of the reaction will be concentrated near the heat transfer surface. Chlorine is known to enhance metal corrosion rates significantly under typical superheater conditions. The rate of alkali vaporization and subsequent sulfation can be limited by chlorine, alkali, or sulfur contents. If it is limited by sulfur content, we would expect to see chlorides on the surfaces of heat transfer equipment. If it is limited by chlorine content or alkali content, chloride content on the surface would be very low even though chlorine plays an important role in both transport of alkali to the surface and corrosion of the metal.

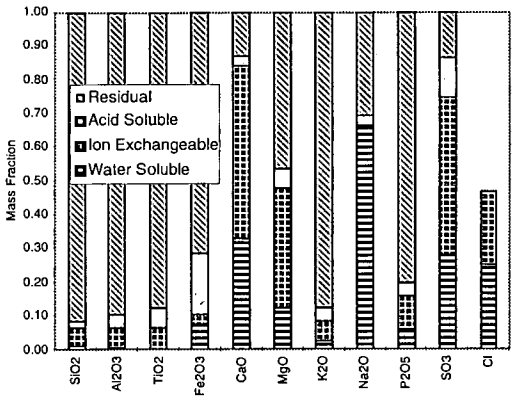

Figure 6 Chemical fractionation results for the Illinois coal indicating the major modes of occurrence for the inorganic components. Compare with Figure 5.

In a series of investigations we have tested essentially all of the aspects of this conceptual model of chlorine-enhanced corrosion. Alkali vaporization rates increase with increased fuel chlorine content. Alkali sulfates are commonly found concentrated at the metal-deposit interface of probes in the form of sulfates. Chlorides are found on the surface when chlorine levels are increased and sulfur contents are decreased. Figure 7 illustrates a layer of sodium and sulfur found on the surface of a simulated superheater tube during one such investigation. The duration of our tests is insufficient to determine whether these observations can be directly related to long-term corrosion rates, but they are consistent with investigations available in the literature regarding long-term corrosion.

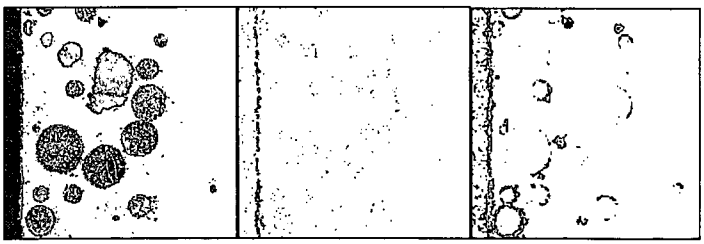

Figure 7 SEM image of cross-section of deposits formed on a probe in the Multifuel Combustor. The probe surface is on the left of each image. The images represent the probe surface with deposited particles (left), a sodium map (center), and a sulfur map (right).

REFERENCES

1. Baxter, L.L., *et al. The Behavior or Inorganic Material in Biomass-Fired Power Boilers -- Field and Laboratory Experiences: Volume II of Alkali Deposits Found in Biomass Power Plants* Sandia National Laboratories; National Renewable Energy Laboratory, 1996; pp.

2. Baxter, L.L. *In Situ, Real-Time Emission FTIR Spectroscopy as a Diagnostic for Ash Deposition During Coal Combustion* ; Engineering Foundation Conference on The Impact of Ash Deposition on Coal-Fired Plants, Solihull, England, 1993; pp.

ANALYSIS OF COMBUSTION PRODUCTS FROM THE COFIRING OF COAL WITH BIOMASS FUELS

Deirdre A. Belle-Oudry and David C. Dayton
National Renewable Energy Laboratory
1617 Cole Boulevard
Golden, CO 80401-3393

INTRODUCTION

The threat of increased global warming has subjected fossil fuels to increasing scrutiny in terms of greenhouse gas and pollutant emissions. As a result, using renewable and sustainable energy resources, such as biomass, for electricity production has become increasingly attractive. The use of dedicated biomass feedstocks for electricity generation could help reduce the accumulation of greenhouse gases because carbon dioxide is consumed during plant growth. The agricultural and wood products industries generate large quantities of biomass residues that could also provide fuel for electricity production. Increasing the use of these waste biomass fuels could alleviate the burdens of waste disposal in the agricultural and wood products industries.

Coal-fired power plants produce the most electricity in the United States. If biomass were cofired at low percentages in a small number of coal-fired power plants, the use of biomass for power production could dramatically increase. Cofiring biomass and coal increases the use of sustainable fuels without large capital investments, and takes advantage of the high efficiencies obtainable in coal-fired power plants. Fuel diversity is another advantage of biomass/coal cofiring. Cofiring reduces the need for a constant supply of biomass required as in a biomass power plant, and is a viable way to decrease the emissions of greenhouse gases and other pollutants from power-generating facilities.

Biomass and coal have fundamentally different fuel properties. Biomass is more volatile than coal and has a higher oxygen content. Coal, on the other hand, has more fixed carbon than biomass. In general, biomass contains less sulfur than coal, which translates into lower sulfur emissions in higher blending ratios of biomass. Wood fuels generally contain very little ash (~1% or less), so increasing the ratio of wood in biomass/coal blends can reduce the amount of ash that must be disposed. A negative aspect of biomass is that it can contain more potassium and chlorine than coal. This is particularly true for some grasses and straws.

Several utilities have tested biomass/coal cofiring in utility boilers.[1,2] Several issues still remain regarding how blending biomass and coal will affect combustion performance, emissions, fouling and slagging propensities, corrosion, and ash saleability.[3] In an effort to further address some issues that biomass/coal cofiring faces, representatives from the National Renewable Energy Laboratory, Sandia National Laboratories Combustion Research Facility, and the Federal Energy Technology Center have embarked on a collaborative effort to study many of the fireside issues pertaining to biomass/coal cocombustion such as ash behavior, particle capture efficiency, carbon burnout, NO_x and SO_x emissions, and reactivity. This paper describes bench-scale biomass/coal cofiring experiments that support this effort.

EXPERIMENTAL APPROACH

The combustion behavior, gaseous emissions, and alkali metals released during the combustion of several biomass/coal blends were investigated with a direct sampling, molecular beam mass spectrometer (MBMS) system[4] in conjunction with a high temperature quartz-tube reactor that has been described in detail in the literature.[5,6]

The biomass and coal samples, including the blends, were provided by L. Baxter of the Sandia Combustion Research Facility. In this study, results are presented for blends of Pittsburgh #8 coal with red oak wood chips, Danish wheat straw, and Imperial wheat straw (from California). Blends are reported as a percentage on an energy input basis, based on the higher heating value of the feedstock. The blends investigated during this study consisted of 15% biomass, on an energy input basis, with Pittsburgh #8 coal.

Twenty to thirty milligrams of the blended samples were loaded into hemi-capsular quartz boats that were placed in a platinum mesh basket attached to the end of a ¼- inch diameter quartz rod. This quartz rod can be translated into a heated quartz-tube reactor enclosed in a two-zone variable temperature furnace. Furnace temperatures were maintained at 1100°C, and a mixture of 20% O_2 in He was flowed through the reactor at a total flow rate of 3.0 standard liters per minute. Gas temperatures near the quartz boat were measured with a type-K thermocouple inserted through the quartz rod. The actual boat temperature and the flame temperature were not measured.

Triplicate samples were studied to establish experimental reproducibility. The MBMS results for the pure fuels and the blends were similar to previous results for biomass and coal combustion.[5,6] All of the samples exhibited multiple phases of combustion, including the devolatilization and char combustion phases. The char combustion phase for coal was generally longer than for biomass. The blends showed a similarly longer char combustion phase compared to the pure biomass.

RESULTS AND DISCUSSION

Pittsburgh #8/Biomass Blends

MBMS results were obtained for combustion of Pittsburgh #8 coal, the pure biomass fuels, and blends of 15% of the biomass with Pittsburgh #8, in 20% O_2 in He at 1100°C. The relative amounts of individual combustion products were determined by integrating the individual time versus intensity profiles for the given ions measured during the combustion event. Only results for four of the detected combustion products, NO, HCl, SO_2, and KCl, are presented. For example, Figure 1 presents the relative intensities of the ions with m/z = 30 (NO^+), m/z = 36 (HCl^+), m/z = 64 (SO_2^+), and m/z = 74 (KCl^+) as measured during the combustion of Pittsburgh #8 coal, Imperial wheat straw, Danish wheat straw, red oak, and the biomass/coal blends. The results represent the averages of the triplicate samples studied and the intensities were normalized to the background $^{34}O_2^+$ signal intensity and the sample weight. The error bars represent one standard deviation.

The Pittsburgh #8 sample contains 1.53% nitrogen. The most NO was observed during combustion of this coal sample. The wheat straws contain 1% nitrogen and the red oak contains only 0.09% nitrogen; hence, less NO was detected during combustion of the biomass samples. The amount of NO detected during combustion of the blends was less than that observed during combustion of the pure coal which suggests that the NO_x released during combustion of the blends (compared to the pure fuels) was diluted. The Imperial wheat straw contains the most chlorine (2.46%) of the four samples; as a result, the most HCl was observed during combustion of this sample. Less HCl was detected during the combustion of the coal/wheat straw blends compared to combustion of the pure wheat straws.

Pittsburgh #8 coal contains almost 4% sulfur, 10 times more than found in any of the biomass fuels. Not surprisingly, the largest amount of SO_2 was released during combustion of Pittsburgh #8 coal. The amount of SO_2 released during combustion of the biomass fuels was significantly less compared to the Pittsburgh #8 coal combustion. During combustion of the blends, the amount of SO_2 released was less than the pure coal but substantially more than detected during combustion of the biomass fuels.

As stated, the Imperial wheat straw sample has the highest chlorine content of the four pure fuels and has the highest potassium content (2.5%). Consequently, the most KCl^+ was detected during combustion of this biomass sample. The alkali metal released during the coal combustion was quite low, and blending the high alkali metal-containing biomass with the coal reduced the amount of alkali metal vapors detected during combustion compared to the pure biomass.

The remaining figures display the relative amounts of products detected during combustion of a Pittsburgh #8/biomass blend compared to what would be expected based on the combustion results for the pure fuels. For example, Figure 2 shows the relative amounts of SO_2 released during combustion of the three blends compared to a calculated amount of SO_2 expected for each blend. The calculated values were determined by taking the appropriate ratios of the amount of SO_2 detected during the combustion of the pure coal and pure biomass fuel that comprised the blend of interest. Within experimental error, the amount of SO_2 detected during combustion of the Pittsburgh #8/biomass blends was expected based on the combustion results for the pure fuels and any reduction in the amount of SO_2 observed during combustion of the blends was a result of dilution. The same conclusion can be drawn from Figure 3 for the amount of NO released during combustion of the blends.

The relative amounts of HCl^+ detected during combustion of the Pittsburgh #8/biomass blends are shown in Figure 4. The measured amount of HCl^+ detected during the combustion of the Pittsburgh #8/red oak blend appears to be close to that expected based on the combustion results for the pure fuels. In fact, both fuels have very low levels of chlorine, and not much HCl^+ was expected. Conversely, the wheat straws have much higher chlorine contents than either the red oak or the coal, and higher levels of HCl^+ were detected during combustion of the pure wheat straws and the blends of the coal with wheat straw. During combustion of the Imperial wheat straw blend, more HCl^+ was detected than expected based on the combustion results for the pure fuels. This difference is not statistically significant for the Danish wheat straw blend. Blending the coal with the high chlorine-containing wheat straws seems to affect the amount of HCl

produced during combustion. This may be a function of the chlorine content of the biomass fuel. The Imperial wheat straw was 2.46% chlorine; the Danish wheat straw was 0.61% chlorine. The error bars on these measurements are quite large; however, if this conclusion proves to be valid this could have important implications concerning high temperature corrosion in coal-fired boilers that cofire high chlorine-containing fuels such as herbaceous biomass, plastics, and municipal solid waste.

Figure 5 shows the relative amounts of KCl^+ detected during combustion of the Pittsburgh #8/biomass blends compared to the levels of KCl^+ expected based on the combustion results for the pure fuels. The amount of KCl^+ detected during combustion of the Pittsburgh #8/red oak blend was as expected. The amount of KCl^+ observed during combustion of the coal/wheat straw blends was less than expected based on the combustion results for the pure fuels. Based on the results in Figures 4 and 5, the partitioning of chlorine in the gas phase seems to have been affected by blending the high alkali metal- and chlorine-containing wheat straws with coal.

Thermochemical Equilibrium Calculations

An equilibrium analysis of the biomass/coal blend combustion was undertaken in an attempt to explain some of the observations made during the batch combustion experiments. The calculations were performed with a modified version of STANJAN,[7] a thermodynamic equilibrium computer code that minimizes the Gibbs free energy of the system via the method of element potentials with atom population constraints. Information about the mechanics and mathematics of the program is available in the literature.[8] The main program has been modified to accept as many as 600 species and 50 phases.[9] A comprehensive database of species and related thermodynamic data was used to predict the equilibrium gas- and condensed-phase compositions given an initial temperature and pressure as well as the populations of Al, Ba, C, Ca, Cl, Fe, H, He, K, Mg, Mn, N, Na, O, P, S, and Si. Gas-phase species were treated as ideal gases and the condensed-phases were assumed to be ideal solid solutions. This simplified treatment of the condensed phases may not be an accurate representation of reality, and caution should be exercised in overinterpreting the calculated condensed-phase species mole fractions.

Table 1 shows a small subset of the many gas- and condensed-phase species predicted by calculating the equilibrium concentrations of available products with the input elemental compositions of the various fuels and blends studied experimentally. Equilibrium product compositions were calculated for the Pittsburgh #8 coal, the three biomass fuels, and the three coal/biomass blends that were studied experimentally. The calculated values for the blends represent the equilibrium concentrations that would be expected based on the appropriate ratios of those species as predicted from the calculations for the pure fuels. The equilibrium mole fractions of NO and SO_2 are consistent with the expected mole fractions based on the calculations for the pure fuels. This signifies that any difference in the amounts of SO_2 and NO measured during combustion of Pittsburgh #8/biomass blends is caused by dilution. This is consistent with the experimental results.

The equilibrium amounts of HCl and KCl vapors show similar trends observed experimentally. There is more HCl in the gas phase based on the equilibrium calculations on the compositions of the blends compared to the amount of HCl calculated from the compositions of mixtures of the pure fuels. Conversely, less gas-phase KCl is predicted from the compositions of the blends versus the amount of KCl calculated from the ratios of the equilibrium results for the pure fuels.

Within the limitations of how realistically the equilibrium calculations treat the condensed phase, the effect of blending coal and biomass on the composition of the ash as determined from the equilibrium calculations can be interpolated. For instance, the amounts of condensed-phase KCl calculated for the blends are lower than expected based on the amounts of KCl determined for the pure fuels. The results of the calculations suggest that the concentrations of the alkali aluminosilicates are enhanced when the coal and biomass fuels are blended compared to a simple ratio based on the equilibrium results for the pure fuels.

CONCLUSIONS

The MBMS results for the relative amounts of NO and SO_2 detected during the combustion of the coal/biomass blends suggested that any decrease in the amount of NO or SO_2 observed because of blending coal and biomass was the result of diluting the nitrogen and sulfur present in the fuel blend. The chlorine released during the combustion of the coal/biomass blends, however, may have been affected by blending the two fuels beyond a dilution effect. Improving the experimental reproducibility in future studies would confirm this hypothesis. Particularly that the amount of HCl detected during the combustion of the coal/wheat straw blends was higher than expected based on the combustion results for the pure fuels and that the amount of KCl detected during the combustion of the coal/wheat straw blends was lower than expected.

Blending coal and high chlorine and alkali containing fuels seems to affect the chlorine equilibrium in such a way that cannot be explained based on just mixing of the pure fuels. Other chemical interactions between the two blended fuels affect the partitioning of chlorine in the gas phase between alkali and hydrogen chlorides.

The results of the equilibrium calculations qualitatively help to explain the repartitioning of the gas phase chlorine inferred from the MBMS results. The amount of HCl in the gas phase is enhanced compared to the amount expected from a simple blending of the pure fuels at the expense of gas phase KCl. The potassium, however, is sequestered in the ash in the form of potassium aluminosilicates. The high concentrations of aluminum and silica in the coal tend to interact with the large amount of potassium in the wheat straws.

ACKNOWLEDGMENTS
The authors acknowledge support from the Solar Thermal and Biomass Power Division of the Department of Energy, Office of Energy Efficiency and Renewable Energy. Special thanks go to Richard L. Bain and Thomas A. Milne for both programmatic and technical support and guidance, and to A. Michael Taylor for help with data acquisition and analysis. Dr. Larry Baxter, Sandia National Laboratories, supplied the biomass and coal samples.

REFERENCES
1. Boylan, D.M. (1993). "Southern Company Tests of Wood/Coal Cofiring in Pulverized Coal Units." Proceedings from the conference on Strategic Benefits of Biomass and Waste Fuels, March 30-April 1, 1993 in Washington, DC. EPRI Technical Report (TR-103146), pp. 4-33 - 4-45.
2. Gold, B.A. and Tillman, D.A. (1993). "Wood Cofiring Evaluation at TVA Power Plants EPRI Project RP 3704-1." Proceedings from the Conference on Strategic Benefits of Biomass and Waste Fuels, March 30-April 1, 1993 in Washington, DC. EPRI Technical Report (TR-103146), pp. 4-47 - 4-60.
3. Tillman, D.A. and Prinzing, D.E. (1995). "Fundamental Biofuel Characteristics Impacting Coal-Biomass Cofiring." Proceedings from the Fourth International Conference on the Effects of Coal Quality on Power Plants, August 17-19, 1994 in Charleston, SC. EPRI Technical Report (TR-104982), pp. 2-19.
4. Evans, R.J. and T.A. Milne, *Energy and Fuels* 1, 311-319 (1987).
5. Dayton, D.C.; French, R.J.; Milne, T.A., *Energy and Fuels*, 9(5), 855-865 (1995).
6. Dayton, D.C. and T.A. Milne, (1995). "Laboratory Measurements of Alkali Metal Containing Vapors Released during Biomass Combustion," in Application of Advanced Technologies to Ash-Related Problems in Boilers, edited by L. Baxter and R. DeSollar, Plenum Press, New York, pp. 161-185.
7. Reynolds, W.C., (1986). "The Element Potential Method for Chemical Equilibrium Analysis: Implementation in the Interactive Program STANJAN," Department of Mechanical Engineering, Stanford University. January 1986.
8. Van Zeggemon, F.; Storey, S.H. The Computation of Chemical Equilibria, Cambridge, England, 1970, Chapter 2.
9. Hildenbrand, D.L.; Lau, K.H., (1993). "Thermodynamic Predictions of Speciation of Alkalis in Biomass Gasification and Combustion." SRI International, Inc. Final Report for NREL Subcontract XD-2-11223-1, Menlo Park, CA, February 1993.

Table 1. Diluted and equilibrium mole fractions calculated for biomass/coal blends at 1100°C, multiplied by a factor of 10^4.

Species (phase: g = gas, c = condensed)	Pittsburgh #8/Imperial wheat straw blend		Pittsburgh #8/Danish wheat straw blend		Pittsburgh #8/Red oak blend	
	Diluted mole fraction	Equilibrium mole fraction	Diluted mole fraction	Equilibrium mole fraction	Diluted mole fraction	Equilibrium mole fraction
NO (g)	3.17	3.14	2.54	3.20	3.18	3.20
SO_2 (g)	15.6	17.9	16.0	18.2	16.1	17.8
HCl (g)	1.05	1.63	0.497	0.879	0.364	0.412
KCl (g)	3.27	1.01	1.12	0.212	0.0179	4.63×10^{-3}
KCl (c)	71.1	22.7	23.6	4.63	0.389	0.101
$NaAlSiO_4$ (c)	260	1320	250	400	320	310
$KalSiO_4$ (c)	25.5	250	25.7	230	110	19.7
$KAlSi_3O_8$ (c)	160	690	160	810	280	150

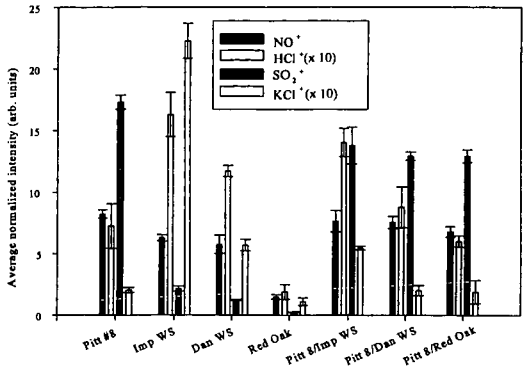

FIGURE 1. Measured amounts of NO, HCl, SO_2, and KCl released during the combustion of pure and blended fuels.

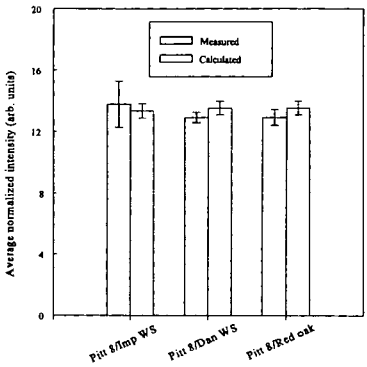

FIGURE 2. Measured and predicted amounts of SO_2 released from Pittsburgh #8/biomass blends.

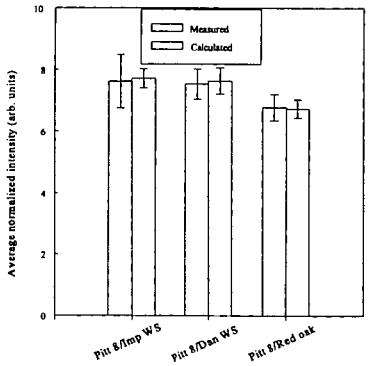

FIGURE 3. Measured and predicted amounts of NO released from Pittsburgh #8/biomass blends.

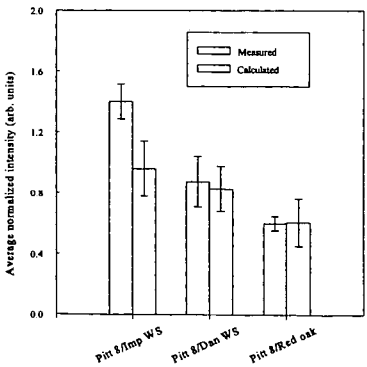

FIGURE 4. Measured and predicted amounts of HCl released from Pittsburgh #8/biomass blends.

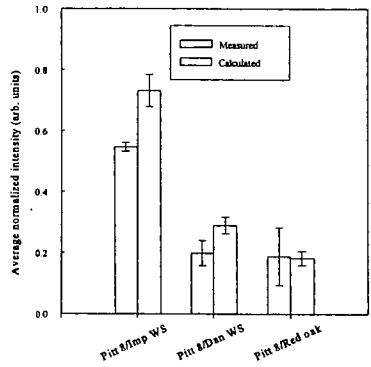

FIGURE 5. Measured and predicted amounts of KCl released from Pittsburgh #8/biomass blends.

ATMOSPHERIC EMISSIONS OF TRACE ELEMENTS AT THREE TYPES OF COAL-FIRED POWER PLANTS

I. Demir[1], R. E. Hughes[1], J. M. Lytle[1], and K. K. Ho[2]
[1]Illinois State Geological Survey, Champaign, IL 61820
[2]Illinois Clean Coal Institute, Carterville, IL 62918

INTRODUCTION AND BACKGROUND

A number of elements that occur in coal are of environmental concern because of their potential toxicity and atmospheric mobility during coal combustion. Sixteen of these elements (As, Be, Cd, Cl, Co, Cr, F, Hg, Mn, Ni, P, Pb, Sb, Se, Th, U) are among the 189 hazardous pollutants (HAPs) mentioned in the 1990 Clean Air Act Amendments (CAA) [U.S. Public Law 101-549, 1990]. The HAPs provisions of the 1990 CAA presently focuses on municipal incinerators and petrochemical and metal industries; a decision on whether to regulate HAPs emissions from electrical utilities will not be made until the U.S. Environmental Protection Agency (EPA) completes its risk analysis.

Numerous studies on environmental aspects of trace elements in coal were reviewed by Swaine [1990], Clarke and Sloss [1992], Wesnor [1993], and Davidson and Clarke [1996]. These reviews indicated a high variability of data on trace element partitioning among various phases of coal combustion residues (fly ash, bottom ash, flue gas). Such high variability results from the variations of types and operational conditions of combustion units, the characteristics of coal, and the modes of occurrence of trace elements in the coal. Difficulties in obtaining representative samples and analytical errors also add to the variability of data on trace element emissions from power plants.

In this study, the atmospheric emissions of 12 elements (As, Co, Cr, F, Hg, Mn, Ni, P, Sb, Se, Th, and U) of environmental concern from three types of power plants burning Illinois coals were inferred from the analytical data on the feed and combustion residues from the plants.

EXPERIMENTAL

Samples and Sample Preparation

Samples of feed coals and coal combustion residues were collected from a fluidized bed combustion (FBC) plant, a cyclone (CYC) plant, and a pulverized coal (PC) plant burning Illinois coals (Table 1). A sample of limestone used in the FBC plant was also collected. To prepare for chemical and mineralogical analysis, representative splits of the coal and coarse-grained coal combustion residues were ground to -60 mesh; representative splits of the fine-grained coal combustion residues were prepared by riffling and splitting.

Chemical and Mineralogical Analysis

The samples of coal and coal combustion residues were analyzed for major, minor, and trace elements following the procedures of Demir et al. [1994]. The samples were also analyzed for mineralogical composition using x-ray diffraction (XRD) methods. The XRD analysis procedures were described in Demir et al. [1997].

RESULTS AND DISCUSSION

Mass balances, emissions, and relative enrichments in the combustion residues were calculated for the 12 elements using the chemical analysis data (Table 2).

Mass balances and emissions. The mass balance value of an element was calculated by comparing the amount of the element in the feed (coal or, in the case of the FBC unit, coal (75%) + limestone (25%)) with the amount of the same element recovered in the combustion residues. The mass balance calculations took into consideration the mass ratios of fly ash to bottom ash, as well as the measured concentrations of ash and elements in the samples. The fly ash to bottom ash ratios were 80/20 for the FBC plant, 25/75 for the CYC plant, and 75/25 for the PC plant.

The mass balances of the 12 elements were normalized to that of Al to eliminate analytical errors. The reason is that Al is a refractory element with relatively high concentration in coal and expected to be retained almost completely in the combustion ashes; less than 5% of Al is expected to escape the particulate collection systems with ultra fine, air-borne fly ash particles. Mass balances of about 100% for Al for the CYC and PC units (Table 2) indicated that the mass balance calculations performed in this study were reliable. The Al mass balance for the FBC unit (76%) was not as good as the Al mass balance for the CYC and PC units; this can perhaps be attributed to the variability in the characteristics of the feeds used in the FBC plant. Both the limestone and the coal used in the FBC unit are blends of products from many different quarries

and mines in Illinois. Therefore, future studies should collect at least several sets of samples over a period of several months of operation from the FBC plant, and the average mass balance data on these samples should be used to smooth out the variance.

If the amount of an element recovered from the combustion residues accounted for 100% of the amount in the feed, then the emission of the element was assumed to be zero. If the mass balance of an element was less than 100%, then the difference was considered to indicate the percentage of the element emitted into the atmosphere through the gas phase or condensation on the ultra fine, air-borne fly ash particles.

For convenience, the emission values were divided into three categories:

Low:	<25%
Moderate:	25-50%
High:	>50%

Negative emission values resulting from the excess mass balance (101-135%) in some cases (Table 2) probably resulted partly from analytical error and partly from contamination of the combustion residues due to the erosion of hardware in the combustion process. Therefore, the negative emission values were assumed to be in the low emission category.

For the FBC plant, the emission of all elements, except F (85%) and Mn (58%), was low (Table 2). The low emission of normally volatile elements Hg (18%) and Se (13%) was somewhat surprising. Apparently, low combustion temperature required in the FBC process or the chemical environment created by the addition of limestone at the FBC unit generally reduced the emission of the elements investigated in this study. The FBC fly and bottom ashes naturally contain large amounts of Ca-bearing mineral phases, namely anhydrite and lime (Table 3). Several authors [Clarke and Sloss, 1992; Meij, 1993, 1994a; Gullet and Ragnunathan, 1994; Querol et al., 1995; Bool and Helble, 1995] reported that lime, limestone, or Ca has the ability to capture substantial amounts of As, Hg, Sb, and Se during combustion. Suarez-Fernandez et al. [1996], on the other hand, did not find any major difference between the combustion behavior of trace elements in a laboratory-scale FBC unit with and without the addition of limestone.

For the CYC plant, the emission of highly volatile elements F (89%), Hg (75%), and Se (53%) was high, as expected (Table 2). Arsenic, Co, Mn, Sb, and U were emitted in moderate amounts (29-46%) from the CYC plant; emissions of other elements from the CYC plant were low.

For the PC plant, high emissions were observed for the highly volatile elements F (92%), Hg (90%), and Se (79%), and moderate emissions were observed for Co (40%), Mn (38%), Ni (27%), and U (31%). The emission of other elements from the PC plant was low (0-13%).

Querol et al. [1995] reported that Mn has an affinity for Fe-oxide in the combustion residues. The feed (coal) from the CYC and PC plants contains less Mn than the feed (coal + limestone) from the FBC plant (Table 2). Furthermore, combustion residues from the CYC and PC plants contain more magnetite than the combustion residue from the FBC plant (Table 3). This may be the reason why the Mn emission from the CYC and PC plants was lower than that from the FBC plant.

According to the literature review [Clarke and Sloss, 1992; Davidson and Clarke, 1996], among the 12 elements investigated here, substantial portions of only F, Hg, and Se, are emitted in the gas phase during coal combustion. The emission of other elements generally takes place through their enrichment in the submicron size fly ash particles that pass through the particulate control systems.

<u>Enrichment in combustion residues.</u> The enrichment of trace elements in various coal combustion residues affects the emissions of the elements during coal combustion. A relative enrichment factor (RE) was calculated for each element using the formula of Meij [1992]:

$$RE = (C_{el\text{-}combustion\ ash}/C_{el\text{-}feed}) \times (\%Ash_{feed}/100)$$

where $C_{el\text{-}combustion\ ash}$ and $C_{el\text{-}feed}$ are the concentrations of an element in the combustion residue (fly ash or bottom ash) and feed, respectively, and $\%Ash_{feed}$ is the percent ash in the feed. The feed refers to coal or, in the case of the FBC unit, mixture of coal (75%) and limestone (25%).

The RE values of all elements, except Mn and F, were higher for the fly ash than for the bottom

ash samples from all three plants (Table 2). The RE value of Mn for the fly ash samples were smaller than or about equal to the value for the bottom ash samples. Fluorine had the same RE value for both the fly ash and bottom ash samples from the FBC unit. The comparison of the RE data of the elements investigated here indicated that a portion of most of these elements were volatilized during combustion and then upon cooling condensed on the fly ash particles or stayed in the gas phase, or partitioned between the fly ash particles and the gas phase.

Elements that are neither enriched nor depleted in the combustion residue should ideally have RE values of 1. Elements with RE values of greater or less than 1 are enriched or depleted, respectively, in the combustion residue. Based on the literature [Meij, 1992] and for convenience, the RE values in this study were divided into three categories as follows:

No enrichment or depletion:	RE = 0.7-1.3
Enrichment:	RE > 1.3
Depletion:	RE < 0.7

The RE values in the combustion products were used in the past to assign the inorganic elements in coal to differing volatility classes [Clarke and Sloss, 1992; Meij, 1992; Davidson and Clarke, 1996]. However, such a task is often complicated because of substantial variations in the combustion behavior of elements depending on the characteristics of coal, type and operation conditions of power plants, and the degree of sampling and analytical errors.

Only a few trends common to all three types of plants were apparent from the results of this study (Table 2):

(1) no elements were enriched in the bottom ashes,
(2) As, F, Hg, Sb, and Se were depleted in the bottom ashes, and
(3) Co, F and Mn were depleted in the fly ashes.

The RE values of other elements varied depending on the ash and plant types investigated. The reason why Al, a conservative element, was depleted in the bottom ash of the FBC unit is not clear although analytical error is a suspect. This study has not examined the enrichment of the trace elements in particle size fractions of the fly ash samples. Previous studies [Meij, 1994b; Tumati and DeVito, 1991, 1993; Dale et al., 1992; DeVito and Jackson, 1994; Helble, 1994; Querol et al., 1995; Cereda et al., 1995; Suarez-Fernandez et al., 1996] indicated that there is generally a positive correlation between ash particle size and the concentration of As, Co, Cr, Hg, Mn, Ni, Sb, and Se.

SUMMARY AND CONCLUSIONS

Mass balances, emissions, and relative enrichment factors (RE) were calculated to determine the combustion behavior of 12 elements (As, Co, Cr, F, Hg, Mn, Ni, P, Sb, Se, Th, U) of environmental concern at three types of power plants burning Illinois coals.

For convenience, the percentage of an element emitted from the power plants was classified as either low (<25%), moderate (25-50%), or high (>50%). Based on this classification, the emission results for the 12 elements were as follows:

	low emission	moderate emission	high emission
FBC plant	As, Co, Cr, Hg, Ni, P, Sb, Se, Th, U	none	F, Mn
CYC plant	Cr, Ni, P, Th	As, Co, Mn, Sb, U	F, Hg, Se
PC plant	As, Cr, P, Sb, Th	Co, Mn, Ni, U	F, Hg, Se

Overall low emissions at the FBC plant relative to the other plants likely resulted from either the lower operating temperature compared with other combustion methods or from the creation of a favorable chemical environment as a result of the addition of limestone.

The atmospheric emissions of trace elements are controlled by their volatility and affinity for various coal combustion phases. The elements investigated in this study had higher concentrations in the fly ash than in the bottom ash with a few exceptions. This results from the partial volatilization of the elements from the bottom ash and their subsequent condensation on the fly ash particles upon cooling.

Relative enrichment (RE) values calculated from the composition of feed, fly ash, and bottom ash showed only few trends common to all three plants: (1) no element was enriched in the bottom ashes, (2) As, F, Hg, Sb, and Se were depleted in the bottom ashes, and (3) Co, F and Mn were

depleted in the fly ashes. The RE of other elements varied depending on the ash and plant types.

ACKNOWLEDGEMENTS

We thank R. A. Cahill, P. J. DeMaris, Y. Zhang, and J. D. Steele, for analyzing the samples. This study was supported, in part, by grants made possible by the Illinois Department of Commerce and Community Affairs (IDCCA) through the Illinois Coal Development Board (ICDB) and the Illinois Clean Coal Institute (ICCI). Neither the authors, the IDCCA, ICDB, ICCI, nor any person acting on behalf of either: (a) makes any warranty of representation, express or implied, with respect to the accuracy, completeness, or usefulness of the information contained in this paper, or that the use of any information, apparatus, method, or process disclosed in this paper may not infringe privately owned rights; or (b) assumes any liabilities with respect to the use of, or for damages resulting from the use of, any information, apparatus, method, or process disclosed in this paper. Reference herein to any specific commercial product, process or service by trade name, trademark, manufacturer, or otherwise, does not necessarily constitute or imply its endorsement, recommendation, or favoring; nor do the views and opinions of the authors expressed herein necessarily state or reflect those of the IDCCA, ICDB, or ICCI.

REFERENCES

Bool, L. E. and Helble, J. J., 1995. A laboratory study of the partitioning of trace elements during pulverized coal combustion. Energy and Fuels, v. 9, p. 880-887.

Cereda, E., Braga, M. G. M., Pedretti, M., Grime, G. W., and Baldacci, A., 1995. Nuclear microscopy for the study of coal combustion related phenomena. Nuclear Instruments and Methods in Physics Research, B; B99 (1/4), p. 414-418.

Clarke L. B. and Sloss L. L., 1992. Trace Elements - Emission from Coal Combustion and Gasification. IEA Coal Research, IEACR/49, London.

Dale, L. S., Lawrensic, S. A., and Chapman, J. F., 1992. Mineralogical residence of trace elements in coal - environmental implications of combustion in power plants. CSIRO investigation report CET/IRO58, 79 p.

Davidson, R. M. and Clarke, L. B., 1996. Trace Elements in Coal. IEA Coal Research, IEAPER/21, London.

Demir, I., Harvey R. D., Ruch, R. R., Damberger, H. H., Chaven, C., Steele, J. D., and Frankie, W. T., 1994. Characterization of Available (Marketed) Coals From Illinois Mines. Illinois State Geological Survey, Open File Series 1994-2.

Demir, I., Hughes, R. E., Lytle, J. M., Ruch, R. R., Chou, C.-L., and DeMaris, P. J., 1997. Mineralogical and Chemical Composition of Inorganic Matter from Illinois Coals. Quarterly Technical Report for the period 12/1/1996-2/28/1997 submitted to the Illinois Clean Coal Institute.

DeVito, M. S. and Jackson, B. L., 1994. Trace element partitioning and emissions in coal-fired utility systems. Paper presented at the 87th Annual Mtg. and Exhib. of Air and Waste Management Assoc., Cincinnati, OH, June 19-24, 1994. 94-WP73.03, 16 p.

Gullet, B. K. and Ragnunathan, K., 1994. Reduction of coal-based metal emissions by furnace sorbent injection. Energy and Fuels, v. 8, p. 1068-1076.

Helble, J. J., 1994. Trace element behavior during coal combustion: results of a laboratory study. Fuel Processing Technology, v. 39, p. 159-172.

Meij, R., 1992. A mass balance study of trace elements in a coal-fired power plant with a wet FGD facility. In: Elemental Analysis of Coal and its By-products (ed. G. Vourvopolis). World Scientific Publishing Co., p. 299-318.

Meij, R., 1993. The fate of trace elements at coal-fired power plants. Proceedings of 2nd Intern. Conf. on Managing Hazardous Air Pollutants (eds. W. Chow and L. Lewin). EPRI TR-104295, p. V83-V105, Palo Alto, CA.

Meij, R., 1994a. Distribution of trace species in power plant streams: a European perspective. Proceedings of 56th Annual Mtg. of Amer. Power Conf., April 25-27, 1994, Chicago, IL., v. 56-I, p. 458-463.

Meij, R., 1994b. Trace element behavior in coal-fired power plants. Fuel Processing Technology, v. 39, p. 199-217.

Querol, X., Fernandez-Turiel, J. L., and Lopez-Soler, A., 1995. Trace elements in coal and their behavior during combustion in a large power station. Fuel, v. 74, p. 331-343.

Suarez-Fernandez, G., Querol, X., Fernandez-Turiel, J. L., Benito-Fuertes, A. B., and Martinez-Tarazona, M. R., 1996. The behavior of elements in fluidized bed combustion. Amer. Chem. Soc. Fuel Chem. Preprints, v. 41. p. 796-800.

Swaine, D. J., 1990. Trace Elements in Coal. Butterworth and Co., London, UK. 276 pp.

Tumati, P. R. and DeVito, M. S., 1991. Retention of condensed/solid phase trace elements in an electrostatic precipitator. In: Managing Hazardous Air Pollutants: State of The Art. EPRI, Palo Alto, CA. 20 p.

Tumati, P. R. and DeVito, M. S., 1993. Trace element emissions from coal combustion - a comparison of baghouse and ESP collection efficiency. Proceedings of 3rd Intern. Conf. on

Effects of Coal Quality on Power Plants. April 25-27, 1993, San Diego, CA. EPRI TR-1-2280, Palo Alto, CA, p. 3-35 - 3-48.
U.S. Public Law 101-549, 1990. Clean Air Act Amendments, Title 3, 104 Stat 2531-2535.
Wesnor J. D., 1993. EPRI/EPA SO_2 Conf., collection of papers, Boston, MA.

Table 1. Amounts and description of coal and coal combustion residues from three types (FBC, CYC, PC) of power plants.

Plant type	Sample type	Amount (lb)	Sample Description*
FBC	coal	25	<3/8" size coal
	fly ash	18	Very fine particle size, light gray color
	bottom ash	24	<1/4" particle size, mostly yellowish and grayish particles, and small number of black particles.
	limestone	25	Crushed and off-white color
CYC	coal	9	Crushed coal
	fly ash	8	Fine particle size, dark gray color
	bottom ash	12	<3/8" particle size, black color, and high moisture content because of quenching in water
PC	coal	12	Crushed coal
	fly ash	8	Fine particle size, light gray color
	bottom ash	15	<3/8" particle size, dark gray to black color, and high moisture content because of quenching in water

* The size ranges are semiquantitative values based on visual examination.

Table 2. Chemical analysis of coal, coal combustion residues, and limestone samples from three types of power plants, and emission and relative enrichment (RE) values of Al and the 12 elements of environmental concern. The concentration values are in mg/kg unless indicated otherwise. All the values are on a dry basis.

Plant type	Sample type	1000°C ash,%	Al,%	As	Co	Cr	F	Hg	Mn	Ni	P	Sb	Se	Th	U
FBC	coal	10.73	1.00	1.8	4.6	25	137	0.10	77	18	131	0.4	5.5	1.8	1.9
	fly ash	97.40	3.39	6.1	12.3	75	53	0.25	620	66	567	1.3	14.4	5.6	7.1
	bottom ash	97.49	1.09	4.0	4.3	35	48	0.01	310	14	480	0.8	<1	1.9	4.0
	limestone	59.18	0.63	3.3	3.5	11	5	<0.01	1394	9.4	262	0.2	<0.5	1.0	2.8
	%Mass balance		76	81	76	96	15	82	42	108	104	106	87	94	94
	%Emission*		24	19	24	4	85	18	58	0	0	0	13	4	6
	RE for fly ash		0.9	0.6	0.6	0.8	0.1	0.7	0.3	1.0	0.8	0.8	0.8	0.8	0.8
	RE for bottom ash		0.3	0.4	0.2	0.4	0.1	0.0	0.2	0.2	0.7	0.5	0.0	0.3	0.4
CYC	coal	10.48	0.80	2.6	4.0	17	63	0.08	77	8	44	0.7	2.7	1.2	2.0
	fly ash	87.52	7.02	50.6	24.2	227	230	0.73	310	173	742	13.6	43.3	14.6	21.7
	bottom ash	100.4	8.01	1.2	20.2	112	15	0.02	542	70	524	1.1	2.1	11.3	11.1
	%Mass balance		102	54	54	85	11	25	65	123	135	62	47	104	71
	%Emission*		0	46	46	15	89	75	35	0	0	38	53	0	29
	RE for fly ash		0.9	2.0	0.6	1.4	0.4	1.0	0.4	2.3	1.8	2.0	1.7	1.3	1.1
	RE for bottom ash		1.0	0.0	0.5	0.7	0.0	0.0	0.7	0.9	1.2	0.2	0.1	1.0	0.6
PC	coal	10.66	0.82	2.2	3.5	17	63	0.08	77	11	44	0.6	2.9	1.4	2.3
	fly ash	97.48	8.47	34.0	20.2	175	67	0.10	468	77	524	7.9	7.4	12.6	16.8
	bottom ash	99.96	6.91	3.0	22.2	136	5	<0.01	468	85	262	2.2	2.2	10.4	12.5
	%Mass balance		105	121	60	99	8	10	62	73	106	110	21	87	69
	%Emission*		0	0	40	1	92	90	38	27	0	0	79	13	31
	RE for fly ash		1.1	1.6	0.6	1.1	0.1	0.1	0.6	0.7	1.3	1.4	0.3	1.0	0.8
	RE for bottom ash		0.9	0.1	0.7	0.9	0.0	0.0	0.6	0.8	0.6	0.4	0.1	0.8	0.6

* %Emission = 100-mass balance. Negative trace element emission values resulting from greater than 100% mass balance were assumed to indicate no emissions (see text).

Table 3. Mineralogical composition of coal combustion residues and limestone from the three power plants.

Plant type	Sample type	Mineral content (wt%)									
		mullite	quartz	calcite	hematite	magnetite	anhydrite	gypsum	lime	portlandite	amorphous
FBC	fly ash	0.0	8.4	0.0	3.0	4.1	31	0.0	2.3	11	40
	bottom ash	0.0	8.2	1.9	0.0	0.0	29	2.0	40	13	6.1
CYC	fly ash	1.9	7.6	0.8	3.0	14	0.0	5.0	0.0	0.0	68
	bottom ash	0.0	1.3	0.0	0.0	1.3	0.0	0.5	0.0	0.0	97
PC	fly ash	5.1	trace	0.0	2.1	15	1.3	0.0	0.0	0.0	77
	bottom ash	0.0	1.0	0.4	2.0	16	0.0	0.0	0.0	0.0	81
FBC	limestone	3.4 % illite, 1.5% kaolinite and chlorite, 5.0% quartz, 86% calcite, and 4.0% dolomite.									

A PREDICTION OF COAL ASH SLAGGING UNDER THE GASIFICATION CONDITION FOR PREPRINTS OF THE AMERICAN CHEMICAL SOCIETY DIVISION OF FUEL CHEMISTRY

Hyun-Taek Kim and Han-jin Bae
Energy Department, Ajou University
San 5, Wonchun-Dong, Padal-gu, Suwon, 442-749, Korea

Shi-Hyun Lee
Korea Institute of Energy Research
71-2, Jang-Dong, Yusong-gu, Daejon, 305-343, Korea

ABSTRACT

Several candidate samples for coal gasification are experimented with proximate, ultimate and ash composition analysis and the fusion temperatures of coal ashes are determined with data from analysis. The effect of flux addition is also evaluated to find the optimum quantity for slagging condition, while considering negative effect of CaO addition on gasification reaction. In order to further expand the variety of candidate coals and the performance in an entrained-bed, the effect of ash fusion temperature drop is evaluated when blending coals. The results of the experiment suggested that optimum compositions of CaO flux are 10%, 20% with Alaska and Datong coal, respectively. However, the optimum value of blending ratio is not known when Posco coal is blended with candidate coals.

INTRODUCTION

As the need for electric power increases in Korea, large amounts of imported coal will be utilized in the future. One of the candidate technologies for producing electricity from coal in an environmentally sound manner and high efficiency is IGCC (integrated gasification combined cycle). In a slagging-type IGCC processes, ashes in the coal are cohered and formed slag which is discarded through the bottom of the gasifier. Slagging behavior of coal ash can be enhanced by adding a reduction agent such as limestone and dolomite.

The objective of this study is to predict the slagging and fluid behavior of various coal ashes for the optimum slag removal condition slagging-type IGCC power plants from the physical and chemical characteristics of original coals. The effect of flux addition is studied with candidate coal ash samples to evaluate optimum quantity of flux addition considering negative effect of CaO addition in the coal gasification reaction. The change of ash fusion temperature is also studied to find the optimum blending ratio of Posco coal with Datong coal and Alaska coal. The experimental values of ash fusion temperatures are compared with calculated values so that predictional methodology of ash slagging behavior will be verified within our experimental range. Another objective of the study is to prevent clogging of slag at the bottom of the gasifier which occurs due to solidation of melted slag. The result of this study will be used to determine optimum operation conditions of a 3 T/D slagging-type gasifier which is located in Ajou University, Korea.

SLAGGING BEHAVIOR IN COAL GASIFIER

Slag in the coal gasifier means the melt of coal ash which has constant viscosity and flow along the wall of gasifier. In order to remove ash by the slagging operation, the temperature of the gasifier should be maintained above the fusion temperature of the coal ash. Formed slag should easily flow down to the exit of the gasifier. To maintain this condition, viscosity of the slag should be maintained under the 100 poise [1]. Many empirical equations based on experimental data are proposed in order to explain relationship of chemical composition of coal ash and slag viscosity [-5]. In the present investigation, Urbain and Watt & Fereday equations are utilized in calculating slag viscosity which give reliable values under 100 poise.

(a) Prediction of slag viscosity

Ash slag viscosity can be predicted by Urbain or Watt & Fereday relation. The Urbain equation, in which composition of each slag component is expressed in mole fraction, is derived from CaO-Al_2O_3-SiO_2 three components system. The Urbain equation, as in Eqn (1), is mainly used to determine slag viscosity of low rank coal ash.

$$\ln \eta = \ln A + \ln T + 10^3 B/T - \Delta \quad (1)$$

in equation(1), T is the absolute temperature, A and B are functions of the chemical composition of the ash, and η is the viscosity in poise. Parameter "Δ" has different value with the quantity of silica in slag. If the quantity of silica is minimal, slag viscosity can be expanded from Eqns (2)-(13).

$$\Delta = mT + b \quad (2)$$

$$b = -1.8244(10^3 m) + 0.9416 \quad (3)$$

$$10^3 m = -55.3649F + 37.9186 \quad (4)$$

$$F = \frac{CaO}{CaO + MgO + Na_2O + K_2O} \quad (5)$$

$$\ln A = -(0.2693B + 11.6725) \quad (6)$$

$$B = B_o + B_1(SiO_2) + B_2(SiO_2)^2 + B_3(SiO_2)^3 \quad (7)$$

$$B_o = 13.8 + 39.9355\alpha - 44.049\alpha^2 \quad (8)$$

$$B_1 = 30.481 - 117.1505\alpha + 129.9987\alpha^2 \quad (9)$$

$$B_2 = -40.9429 + 234.0486\alpha - 300.04\alpha^2 \quad (10)$$

$$B_3 = 60.7619 - 153.9276\alpha + 211.1616\alpha^2 \quad (11)$$

$$\alpha = \frac{M}{M + Al_2O_3} \quad (12)$$

$$M = CaO + MgO + Na_2O + K_2O + FeO + 2TiO_2 + 3SO_3 \quad (13)$$

Meanwhile, in the case of medium silica quantity, Eqn(14)-(16) are used instead of Eqns. (3)-(5).

$$b = -2.0356(10^3 m) + 1.1094 \quad (14)$$

$$10^3 m = -1.3101F + 9.9279 \quad (15)$$

$$F = B(Al_2O_3 + FeO) \quad (16)$$

When the silica quantity is high in slag, similarly Eqns.(17)-(19) are used instead of Eqns(3)-(5).

$$b = -1.7737(10^3 m) + 0.0509 \quad (17)$$

$$10^3 m = -1.7264F + 8.4404 \quad (18)$$

$$F = \frac{SiO_2}{CaO + MgO + Na_2O + K_2O} \quad (19)$$

Using the Urbain equations in calculating slag viscosity of low rank coal, silica content should be cautiously determined. Silica content mostly affect the B value . In the case of a B value located in the boundary, the larger value is chosen. The experimental result of Watt and Fereday is accepted to determined a reliable relationship between the viscosity of slag and temperature. They proposed Eqn (20), which is derived from regression analysis of experimental data by Hoy et al [6].

$$Log_{10}\eta = \frac{10^7 m}{(T-150)^2} + C_2 \quad (20)$$

In Eqn. (20), m represents (0.00835 SiO2 + 0.00601 Al_2O_3 -1.09) where total percent of (SiO_2 +Al_2O_3 +Fe_2O_3+CaO+MgO) equals 100% and C_2 is (0.0415SiO2+0.0192 Al_2O_3 +0.0276 Fe_2O_3+ 0.0160CaO-3.92). η is viscosity in poise and T is in °C. This empirical equation is the best fit when the coal ash component is throughly melted so that no crystal exists. Prediction of slag viscosity is correct in the ash component range of Table 1.

The Urbain Watt and Fereday Equation utilized chemical composition of the ash derived by ASTM methods to predict ash fluidity behavior but not the exact behavior of ash fusion/slagging. Calculated viscosity data are represented for Alaska and Datong coal in Table 2 and 3.

(b) Prediction of critical viscosity temperature

Liquid phase slag behaves as a Newtonian fluid and, when decreasing temperature, it passes through

the pseudo-plastic state before solidification. The separation from solid phase depends on the composition of slag. When the transition takes place from liquid state to the solid state, the temperature is call Critical Viscosity Temperature (Tcv). Watt [6] derived the equation which is related to chemical composition and Tcv in Eqn(21).

$$T_{cv} = 2990-1470(SiO_2/Al_2O_3) + 360(SiO_2/Al_2O_3)^2-14.7(Fe_2O_3+CaO+MgO)+ 0.15(Fe_2O_3+CaO+MgO)^2 \quad (21)$$

In Eqn (21), T_{cv} is in °C, and the total percent of ash component of SiO_2, Al_2O_3, Fe_2O_3, CaO and MgO equals 100. Because of the limitation in using this equation, Tcv can be assigned as a hemispherical temperature determined by the ash fusion temperature plus 93°C [7].

EXPERIMENT OF ASH SLAGGING CHARACTERISTICS

Three different coal samples are utilized for ash fusion temperature and ash fluidity behavior. Proximate and ultimate analysis of coal samples are illustrated in Table 4.

From the experimental data of ash fusion determination, relationship fouling and slagging can be made from the coal combustion and gasification reactions. Determination of not only which coal is the best candidate for gasifier or combustor but also whether the dry or wet ash treatment method is appropriate for coal benification. It is well-known that the difference of fusion temperature are related to the degree of fouling and slagging. The greater the temperature difference between IDT and FT, the slower the fouling rate so that the intensity of fouling is decrease because more pores are generated in the fouling process.

The fusion temperature of samples has been measured by using the ash fusion determinator (LECO-600). The cones were manufactured to pyramidal shape, height 19mm, base 6.5mm. The temperature of 390°C, starting temperature of 538°C, final temperature of 1600°C and heating condition and air in oxidizing condition. Table 5 illustrates the measurement results of ash temperature of candidate coal while adding CaO as fluxing agent. Ash fusion temperature is decreased with CaO addition until a certain limit but it is increased after that limit because excess addition of CaO results in higher fusion temperature. Table 6 shows the change of the ash fusion temperature with mixing ratio and Table 7 shows fusion temperature change with the composition of surrounding gas.

Because ash viscosity measurement is performed in a nitrogen atmosphere, fusion temperature changes with the composition of the surrounding gas are evaluated as in Figure 1. Tcv measured in nitrogen is lower than the T_{cv} in air because Fe acted as strong fluxing agent in the high temperature range. Fusion temperature in a reducing atmosphere is lower than that in the oxidation atmosphere. The reason is that iron, which plays a significant role in ash slagging, exists as Fe_2O_3 in an oxidizing environment but FeO or Fe in reducing one. Actually, the fusion temperature of pure Fe_2O_3 is 1560°C, FeO is 1420°C and Fe is 1275°C. From Table 7, fusion temperature with N_2 as a surrounding gas is located in the midpoint between those in reduction and oxidation conditions. This result implies that Fe acts as fluxing agent in the inert environment. ΔT in Table 5, which is difference between fluidization temperature and initial deformation temperature is the index which estimates the degree of slagging. If ΔT is small, fusion takes place suddenly and thin layer of fusion slag is generated. Therefore, to carry out the optimal slagging in the gasifier, a candidate coal should be chosen that has an ash composition resulting in a lower ΔT value.

From figure 2 and 3, fusion temperature of Alaska, Datong and Posco coal are minimum when 10%, 20% and 30% CaO is added respectively. Also, ΔT value of Alaska, Datong, Posco coals is minimum when 20%, 20%, and 40% CaO is added respectively. Figure 4 shows the results if fusion temperature measurement when mixing Posco coal with Datong and Alaska coals from 10% to 50%, fusion temperatures increased with mixing ratio.

SUMMARY

The objectives of this study are minimization of the negative effects of CaO addition to maintain a slagging state and expanding the various candidate coals by use of the blending method. We considered the effect of degree of fusion by means of CaO addition and coal blending related with standard coals (Alaska, Datong) and a comparison coal (Posco). First, from the result of fusion temperature measurements when Posco coal with Datong and Alaska coals, fusion temperature is minimum when 10% of CaO is added to Alaska coal, 20% to Datong coal and 50% to Posco coal.

For Posco coal, we could estimate that fusion temperature is minimized by an increase of CaO content, because we varied the content of CaO from 10 to 50%. Also, when standard coal is blended with 10-50% of comparison coal, fusion temperature is minimized with blending of 10% comparison coal and increases with increasing blending ratio.

From the above experiments, we decided the optimal addition value. Fusion temperatures of Alaska, Datong and Posco coals are minimum when 10%, 20% and 30% CaO is added respectively. In the case of blending, there isn't a value which can satisfy viscosity less than 100 poise, because Alaska and Datong coals have viscosities greater than 100 poise at 1400°C. Therefore, we should determine a more suitable coal in using blending method. Also, we should measure viscosity using reduction gas in order to explain exactly the viscous flow and fusion of coal ash in the gasifier.

REFERENCES

[1] C.L. Senior and S. Srinivasachar, "Viscosity of Ash Particles in Combustion System for Particle Sticking", Energy & Fuel, P277~283, 1995
[2] William T. Reid, "The Relation of Mineral Combustion to Slagging, Fouling and Erosion During and after Combustion", Prog. Energy Combustion. Sci, Vol. 10, 1984
[3] Frank E. Huggins and Gerald P. Huffman, " Correlation Between Ash Fusion Temperature and Ternary Equilibrium Phase Diagrams", Fuel, Vol. 60, 1981
[4] Steve A. Benson, Inorganic Transformation and Ash Deposition During Combustion, 1991
[5] H.H. Schobert & E.K.Diehl, "Flow Properties of Low-rank Ash Slags : Implications for Slagging Gasification", Fuel, Vol.64,1985
[6] Eric Raask, "Mineral Impurities in Coal Combustion", P. 121~135
[7] H.J. Pac, "A Prediction Study on the Slagging and Fluid Behavior of Coal Ash under the Gasifier Condition", 1997

Table 1. Range of ash component used in Watt and Fereday equation

Silica	SiO_2/Al_2O_3	Fe_2O_3	CaO	MgO
40~80 wt%	1.4~2.4 wt%	3~30 wt%	2~30 wt%	1~30wt%

Table 2: Calculated viscosity of Alaska ash

Temperature	Viscosity (poise)			
(°C)	Alaska	Alaska (10%)	Alaska (20%)	Alaska (30%)
1000	263634	35906	6877	1711
1100	14857	2826	714	224
1200	1829	443	137	51
1300	379	110	40	16
1400	113	38	15	7
1500	44	16	7	4
1600	20	8	4	2

Table 3: Calculated viscosity of Datong coal ash

Temperature	Viscosity (poise)			
(°C)	Datong	Datong (10%)	Datong (20%)	Datong (30%)
1000	8035920	785161	114268	22600
1100	248254	35913	7235	1881
1200	19737	3799	970	307
1300	2950	703	214	79
1400	683	192	67	28
1500	216	69	27	12
1600	86	31	13	7

Table 4 Proximate, ultimate analysis of sample coal

Coal	Proximate Analysis (wt%)				Ultimate Analysis (wt%)				
	M	V.M.	F.C.	Ash	C	H	O	N	S
Alaska	5.09	44.85	35.64	14.42	54.40	4.55	40.24	0.64	0.17
Datong	6.87	29.30	54.65	9.18	67.08	4.31	27.35	0.66	0.60
Posco	1.58	30.11	58.32	9.99	71.05	3.71	11.08	3.61	0.56

Table 5 Influence of CaO content on ash melting temperature

Coal	AFT(°C)	%CaO (reducing condition)					
		Raw	10%	20%	30%	40%	50%
Alaska	IDT	1165	1143	1187	1256	1406	1413
	ST	1176	1163	1200	1275	1471	1525
	HT	1212	1183	1211	1289	1527	1535
	FT	1287	1208	1218	1344	1529	1537
ΔT (FT-IDT)		123	65	31	88	123	124
Datong	IDT	1178	1139	1166	1256	1406	1413
	ST	1230	1182	1181	1275	1471	1525
	HT	1268	1222	1188	1289	1520	1535
	FT	1362	1282	1201	1344	1527	1537
ΔT (FT-IDT)		184	143	35	88	121	124
Posco	IDT	1369	1245	1193	1219	1257	1380
	ST	1420	1278	1215	1234	1268	1440
	HT	1460	1308	1243	1245	1275	1467
	FT	1519	1379	1317	1260	1286	1486
ΔT (FT-IDT)		150	134	124	41	29	106

Table 6 Influence of blending ratio on ash melting temperature

Coal	Datong			Alaska		
AFT(°C)	Reduction	N_2	Oxidation	Reduction	N_2	Oxidation
IDT	1176	1261	1279	1164	1191	1210
ST	1230	1279	1300	1176	1224	1231
HT	1268	1315	1327	1212	1269	1278
FT	1362	1376	1386	1287	1298	1307

Table 7 Influence of atmospheric condition on ash melting temperature

Coal	AFT (°C)	Reducing Condition				
		10:90	20:80	30:70	40:60	50:50
P:A	IDT	1167	1189	1193	1212	1224
	ST	1208	1215	1216	1249	1256
	HT	1234	1240	1253	1278	1287
	FT	1304	1327	1334	1343	1355
P:D	IDT	1197	1210	1220	1239	1285
	ST	1220	1250	1267	1279	1310
	HT	1290	1313	1320	1328	1388
	FT	1355	1379	1397	1414	1429

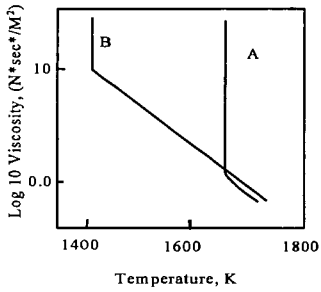

Fig. 1 Effect of atmospheric condition on slag viscosity (A: in air, B: in nitrogen).

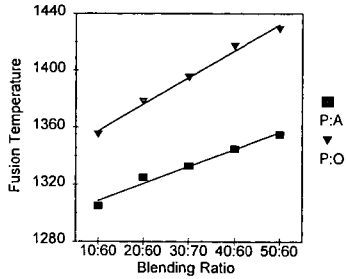

Fig. 2: Behavior of ash fusion drop due to blending coal.

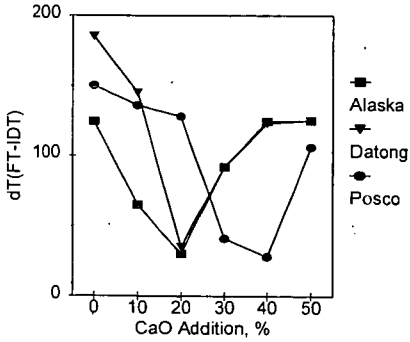

Fig. 3: Behavior of ash fusion temperature drop due to adding flux.

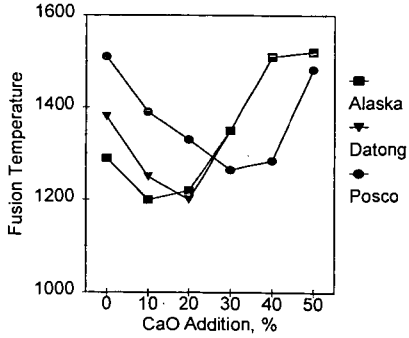

Fig. 4: Influence of CaO content on ash melting temperature.

THE FORMS OF TRACE METALS IN AN ILLINOIS BASIN COAL BY X-RAY ABSORPTION FINE STRUCTURE SPECTROSCOPY

M.-I.M. Chou, J.A. Bruinius, J.M. Lytle, and R.R. Ruch
Illinois State Geological Survey
Champaign, IL 61801

F.E. Huggins and G.P. Huffman
University of Kentucky
Lexington, KY 40506

K.K. Ho
Illinois Clean Coal Institute
Carterville, IL 62918

Abstract
Utilities burning Illinois coals currently do not consider trace elements in their flue gas emissions. After the US EPA completes an investigation on trace elements, however, this may change and flue gas emission standards may be established. The mode of occurrence of a trace element may determine its cleanability and flue gas emission potential. X-ray Absorption Fine Structure (XAFS) is a spectroscopic technique that can differentiate the mode of occurrence of an element, even at the low concentrations that trace elements are found in coal. This is principally accomplished by comparing the XAFS spectra of a coal to a database of reference sample spectra. This study evaluated the technique as a potential tool to examine six trace elements in an Illinois #6 coal. For the elements As and Zn, the present database provides a definitive interpretation on their mode of occurrence. For the elements Ti, V, Cr, and Mn the database of XAFS spectra of trace elements in coal was still too limited to allow a definitive interpretation. The data obtained on these elements, however, was sufficient to rule out several of the mineralogical possibilities that have been suggested previously. The results indicate that XAFS is a promising technique for the study of trace elements in coal.

Introduction
Currently, Illinois utilities are exempt from having to consider their trace element flue gas emission; however, this may eventually change after the U. S. EPA completes its risk analyses and establishes emission standards. The mode of occurrence of a trace element may determine its cleanability and flue gas emission potential. Trace elements associated with clays and minerals can be reduced by cleaning and those minerals highly dispersed in the coal may be further reduced by advanced cleaning techniques. Also, the volatility of trace elements associated with the organic matrix is different than the volatility of trace elements associated with the inorganic fraction of the coal.

From previous studies of specific gravity testing, many trace elements (such as As, Cd, Mn, Th, and Zn) were shown to have predominantly inorganic/mineral association[1]. Some elements (such as Be and B) exhibit an organic/maceral association while others (such as Co, Ni, Cu, Cr, and Se) indicate a mixed behavior resulting from different compounds or possibly being highly disseminated in the coal[1]. Recently, a database of trace element concentrations in a set of 34 commercially utilized coals from the Illinois Basin, which included the Illinois #6 coal used in this investigation, was established[2]. These data on cleaned and washed samples were compared with those on a set of 222 channel or equivalent samples in the Illinois State Geological Survey records, which represented coal in-place prior to mining and cleaning. A comparison of results indicated that with the exception of uranium (U) and vanadium (V), all other trace elements are reduced in the washed samples as a result of coal cleaning. This phenomenon could suggest that most trace elements may be associated with mineral matter and the U and V in coal may be associated with the organic portion of the coals.

The possibility of misleading results from previous investigations for organic/inorganic association of trace elements in coal was indicated by many investigators. For example, Finkelman stated that most studies so far offer "little beyond the very rudimentary, and possibly misleading, organic/inorganic affinity of an element" in coal[3]. Clarke and Sloss in their review stated that "Genuine organic affinity (organic bonding) has been overestimated in the past, and simple classifications based on rudimentary organic or inorganic affinities may be misleading[4]." It is important to verify previous results with a direct method of determination. This study was conducted to evaluate XAFS techniques as a direct, nondestructive method to determine the mode of occurrence (organic/inorganic affinity) of trace elements in coal.

Experimental

X-ray Absorption Fine Structures (XAFS) spectroscopy, a synchrotron-based technique, is direct and nondestructive. XAFS spectra for Ti and V were obtained at beam-line X19A of the National Synchrotron Light Source (NSLS), Brookhaven National Laboratory, and the XAFS spectra for Cr, Mn, Zn, and As were obtained at beam-line IV3 of the Stanford Synchrotron Radiation Laboratory. Essentially identical experimental procedure was carried out at the two synchrotron facilities. Samples of the coal were exposed to monochromatic X-rays and the fluorescent radiation emitted in response to the X-ray absorption process was detected in a 13 Ge-element solid-state detector. Normally, a scan was made from about 100 eV below the K absorption edge of the element of interest to as much as 1,000 eV above the K-edge. The individual signals recorded in each channel of the 13 Ge-element detector were combined into a single spectral scan. In addition, multiple scans were made for most elements and these scans were also combined to provide a single spectrum for each element. Hence, for most elements, the spectra shown in this paper represent 3 to 5 hours of spectral accumulation time. All spectra were collected and stored on a computer and were transferred electronically to a similar computer at the University of Kentucky for analysis.

The XAFS spectra obtained from different elements in the coal sample were divided into two separate regions: the X-ray Absorption Near-Edge Structure (XANES) region (from -20 to 100 eV of the absorption edge) and the Extended XAFS (EXAFS) region (from 30-50 eV above the edge to the high-energy limit). The XANES region was used directly as a fingerprint, whereas the EXAFS region was mathematically manipulated further to obtain a radial structure function (RSF) which provided information on the coordination environment of the element. For trace elements, the EXAFS structure is usually only useful if the element is somewhat concentrated (>50 ppm) or if the element is surrounded by heavy elements. Hence, as a consequence of this and other complications, the interpretation of the elemental mode of occurrence was based solely on the XANES region in many cases.

Results

Using the data previously obtained on average concentrations of trace elements in coal, a representative Illinois #6 coal sample was chosen for this study[2]. XAFS/XANES spectra were interpreted by comparing them to the spectra of standard compounds. Also, Ti and Mn XAFS spectra of an Argonne #3 coal sample (an Illinois #6 coal from the Argonne Premium Coal Sample) and the Zn XAFS spectra of coals previously studied[5] were compared with those in this study. The data obtained for the six trace elements in the coal are described as follows:

Arsenic: The Illinois #6 coal as well as its extensively oxidized sample was examined (Figure 1). In both spectra, two distinct peaks were observed, indicating two different forms of arsenic present in these samples. The peak to the negative side of 0 eV arose from arsenic in pyrite (FeAsS), while the higher energy peak arose from an arsenate (AsO_4^{3-}) phase, formed by oxidation of the arsenic in pyrite[6,7]. These assignments were confirmed by examining the RSF derived from the EXAFS region. Although the noise level was high for the arsenic XAFS spectrum of this sample, the RSFs for the two spectra did correctly locate the major peak for the dominant forms at about 2.05 Å for arsenic in pyrite and at about 1.30 Å for the arsenate anion (Figure 2).

Zinc: The spectrum for zinc in the Illinois #6 coal (Figure 3) was strong and was clearly derived largely from zinc sulfide (ZnS). The spectrum was consistent with that seen for other coals from the same seam[5]. The RSF derived from the EXAFS region for Zn was examined and found to be very similar to that from a ZnS standard (not shown).

Titanium: The titanium spectrum had a relatively weak pre-edge peak at about 3 eV and a broad main peak between 20 and 30 eV that consists of two components (Figure 4).The form of Ti cannot be identified. The spectrum was very similar to that from Ti in Argonne #3 that was examined previously[5]. Also, because no sharp minor features were discernable in the spectrum, and because the small pre-edge peak did not exhibit any apparent splitting, virtually all common minerals (rutile, anatase, sphene, Ti-illite, etc.) can be eliminated as being a major contributor to this spectrum.

Vanadium: The University of Kentucky has no database to draw upon to interpret V XAFS/XANES spectrum obtained; however, a V rich Kentucky #9 was extensively studied by Maylotte et al[8,99]. The spectrum of Illinois coal (Figure 5) had a sharp pre-edge feature at about 4 eV which was indicative of either a highly distorted V^{3+} environment or an unusual V^{4+} compound. This was followed by a two broad peaks from 10 to 30 eV. The spectra of the Illinois #6 coal was similar to the spectra of the float fraction of a Kentucky # 9 coal reported by Maylotte et al[8,9].

Chromium: A very weak pre-edge peak at about 2 eV above the K-edge calibration zero-point indicates that all (>95%) of the chromium was present as Cr^{3+}; there was no evidence for the more toxic Cr^{6+} oxidation state (Figure 6). The detection limit was about 5% for Cr^{6+} for this technique. The Cr spectrum for the Illinois #6 coal was similar to those for Cr in most bituminous coals[6,7]. Such a spectrum of the Illinois coal was tentatively identified as being derived from a chromium oxyhydroxide (CrOOH) phase.

Manganese: The spectrum from the Illinois #6 coal used in this study (Figure 7) was quite different from that from Argonne #3[5] and, except for a weak feature at about 17 eV, appeared to have a profile that was more similar to that of Mn in a lignite (Beulah lignite, ND)[5]. Additional study using a simulated sample which composited of calcite, illite, and carboxyl material was conducted. The results (Figure 7) suggested its mineral association of calcite and illite and its organic association of carboxyl material.

Summary and Conclusions

For the elements As and Zn, the present XAFS data provided a definitive interpretation of the predominant mode of occurrence in the specific sample of Illinois #6 coal investigated. The Zn in this coal was predominately ZnS. The As occurs as either pyritic arsenic or arsenate, and predominately in the arsenate form after extensive oxidation.

For the elements Ti, V, Cr, and Mn; the database of XAFS spectra of trace elements in coal was still too limited to allow definitive interpretations; however, the data obtained on some of these elements were sufficient to make preliminary interpretations. For Ti, the XANES spectrum was sufficient to rule out the minerals suggested previously[10]. The fact that the V XAFS spectra for the Illinois #6 coal was similar to the float fraction of the Kentucky #9 coal may indicate that V was associated with the organic fraction of coal. Most of the Cr in this coal was tentatively identified from coming from a CrOOH phase, but more importantly, the more toxic Cr^{6+} oxidation state was ruled out from being present in this coal (<5%). The Mn in coal appears to be associated with both mineral (calcite and illite) and organic (carboxyl) phases.

In general, XAFS is a promising technique to determine the mode of occurrence of trace elements in coals. However, more investigations on various coals and standard compounds to produce a larger database should be helpful in drawing solid conclusions for spectrum interpretation. Also, greater understanding of the modes of occurrence of trace elements may help control there flue gas emission.

Acknowledgment & disclaimer

This study was supported, in part, by grants made possible by U.S. department of Energy (DOE) Cooperative Agreement Number DEFC22-PC92521 and the Illinois Coal Development Board (ICDB) and the Illinois Clean Coal Institute (ICCI). Neither authors nor any of the subcontractors nor the U.S. DOE, ISGS, ICDB, ICCI, nor any person acting on behalf of either assumes any liabilities with respect to the use of, or for damages resulting from the use of, any information disclosed in this paper.

References

1. H.J. Gluskoter, R.R. Ruch, W.G. Miller, R.A. Cahill, G.B. Miller, and J.K. Kuhn, Trace Elements in Coal: Occurrence and Distribution, ISGS Circular 499, 1977.
2. I. Demir, R.D. Harvey, R.R. Ruch, H.H. Damberger, C. Chaven, J.D. Steele, and W.T. Frankie, Characterization of Available (Marketed) Coals form Illinois Mines, ISGS Open File Series 1994-2.
3. R.B. Finkelman, What We Don't Know About the Occurrence and Distribution of the Trace Elements in Coal, J. Coal Quality, v. 8, no. 3-4, pp. 63-66, 1992.
4. L.B. Clarke, and L.L. Sloss, Trace Elements-Emissions form Coal Combustion and Gasification, IEACR/49, IEA Coal Research, London, 1992.
5. University of Kentucky XAFS database, unpublished data.
6. F.E. Huggins, N. Shah, J. Zhao, and G.P. Huffman, Nondestructive Determination of Trace Elements Speciation in Coal and Coal Ash by XAFS Spectroscopy, Energy & Fuels, v. 7, no. 4, pp. 482-489, Jul-Aug 1993.
7. G.P. Huffman, F.E. Huggins, N. Shah, and J. Zhao, Speciation of Arsenic and Chromium in Coal and Combustion Ash by XAFS Spectroscopy, Fuel Processing Technology, v. 39, pp. 47-62, 1994.
8. D.H. Maylotte, J. Wong, R.L. St. Peters, F.W. Lytle, and R.B. Greegor, X-ray Absorption Spectroscopic Investigation of Trace Vanadium Sites in Coal, Science, v. 214, October 30, 1981.

9. D.H. Maylotte, J. Wong, R.L. St. Peters, F.W. Lytle, and R.B. Greegor, Trace Vanadium in Coal: An EXAFS Study, Proceeding of the International Conference on Coal Science, Düsseldorf, 1981.
10. D.J. Swaine, Trace Elements in Coal, Butterworths, London, 1990.

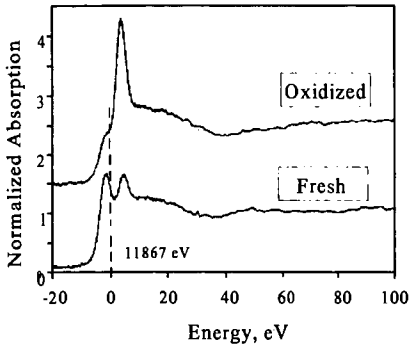

Figure 1: The As XANES spectrum of the fresh and oxidized Illinois #6 coal.

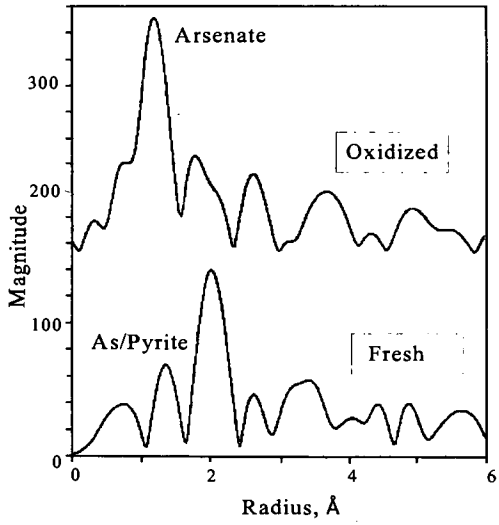

Figure 2: The radial structure functions for the fresh and oxidized coal from their As EXAFS spectrum.

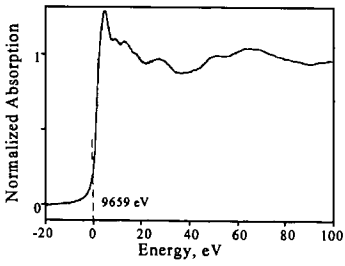

Figure 3: The Zn XANES spectrum.

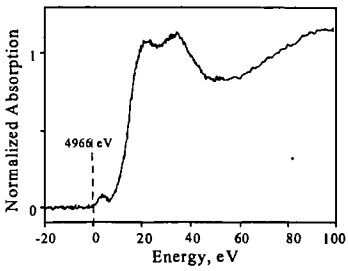

Figure 4: The Ti XANES spectrum.

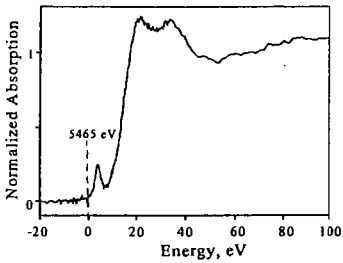

Figure 5: The V XANES spectrum

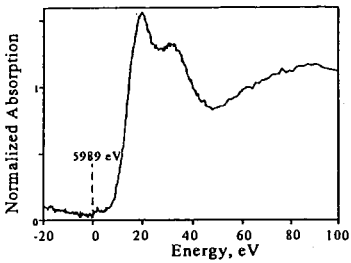

Figure 6: The Cr XANES spectrum.

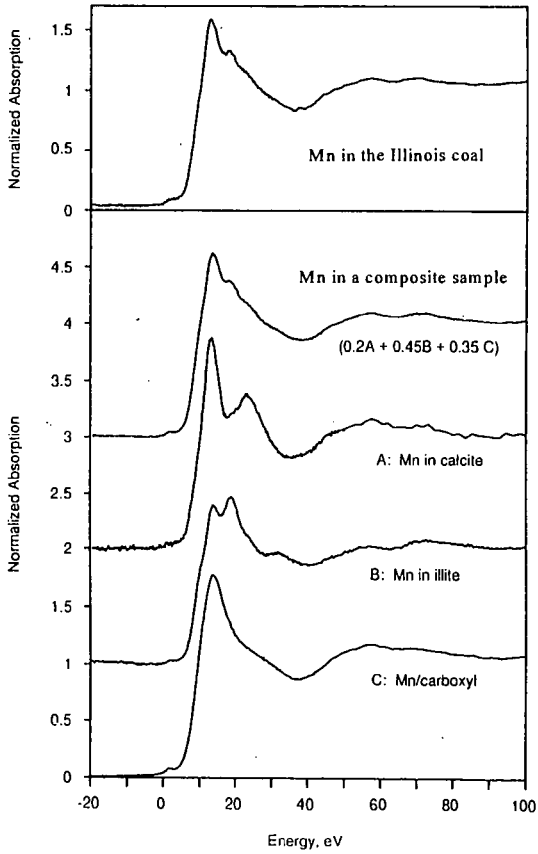

Figure 7: The Mn XANES spectra of the Illinois coal, a composite sample and samples of calcite, illite and carboxyl material.

XAFS EXAMINATION OF MERCURY CAPTURE ON THREE ACTIVATED CARBONS

Frank E. Huggins[1], Gerald P. Huffman[1], Grant E. Dunham[2], and Constance L. Senior[3]

[1]CME/CFFLS, University of Kentucky, Lexington, KY 40506-0043
[2]University of North Dakota - EERC, Grand Forks, ND 58202
[3]Physical Sciences, Inc., Andover, MA 01810

INTRODUCTION

Mercury is listed as one of the eleven so-called "air-toxics" elements in the Amendments to the 1990 Clean Air Act [1]. Furthermore, as a result of research stimulated by the passage of this legislation, mercury is now regarded as the single trace element of greatest concern to utilities generating electrical power from coal combustion, despite its extremely low average concentration in most U.S. coals, typically 0.05 - 0.2 ppm [2,3]. The reasons for this concern include the volatility of mercury and its compounds, the toxicity of its compounds, the ease with which mercury can enter the food chain, particularly by accumulation in fish [4], and the huge volumes of coal consumed by the power generation industry, which is now approaching one billion tons/year in the U.S. [5].

One promising approach to reducing the atmospheric emission of mercury from coal combustion is the development of sorbent materials that efficiently capture mercury from combustion flue gases at relatively low temperatures (below 150°C). Of the many types of materials considered for such applications, activated carbons have been shown to be among the best. In this work, X-ray absorption fine structure (XAFS) spectroscopy has been employed to examine the mechanism of mercury capture on three different activated carbon sorbents. The element-specific nature of the XAFS technique has also enabled complementary information to be obtained on the behavior of other important elements present either in the flue gases or in the original carbons.

EXPERIMENTAL

(i) Mercury Sorption Experiments

Three different activated carbons were prepared at the University of North Dakota Energy and Environmental Research Center (EERC): a lignite-derived activated carbon (LAC), an iodine-activated carbon (IAC), and a sulfur-activated carbon (SAC). Aliquots of each of these carbons were used in various experiments at EERC to absorb mercury from a simulated combustion flue gas in a bench-scale reactor. In a typical experiment, about 400 mg of sorbent was held in the simulated flue gas at a temperature between 225 F and 325 F for a period of up to 16 hours. The baseline flue gas consisted of a synthetic mixture of 6% O_2, 12% CO_2, 1600 ppm SO_2, 50 ppm HCl, 8% H_2O, and the balance N_2. Elemental mercury was added to the baseline flue gas at a concentration of 60 $\mu g/m^3$, although some experiments were run with addition of $HgCl_2$ at 12 $\mu g/m^3$. Three different sets of experiments were performed: the first set consisted of a comparison of the three sorbents before and after exposure to the simulated flue gas; the second set consisted of the three sorbents exposed to a simulated flue gas containing mercuric chloride ($HgCl_2$); and the third set consisted of the LAC sorbent exposed to different formulations of the flue gas under otherwise identical conditions. Details of specific experiments are summarized in Table 1.

(ii) XAFS Experiments

The form of mercury and other elements present in the activated carbons before and after the sorption experiments were investigated using XAFS spectroscopy performed at either the Stanford Synchrotron Radiation Laboratory (SSRL), Palo Alto, CA, or the National Synchrotron Light Source (NSLS), Brookhaven National Laboratory, NY. At both synchrotrons, a 13-element germanium detector [6,7], gated electronically to record the L-edge fluorescence from mercury, was used to record the mercury L_{III} XAFS spectra. A 6μ gallium filter was also employed to maximize the signal/noise ratio. The XAFS spectra of other elements (S, Cl, Ca, I) were recorded at NSLS using a conventional Lytle fluorescence detector [8]. Zero-points of energy for the XAFS spectra of the different elements are defined as follows: sulfur K-edge - white line peak in elemental sulfur at 2,472 eV; chlorine K-edge - major derivative peak in NaCl at 2,825 eV; calcium K-edge - major derivative peak in $CaCO_3$ at 4,038 eV; iodine L_{III} edge - major derivative peak in elemental iodine (I_2) at 4,557 eV; and mercury L_{III} edge - major derivative peak in elemental mercury at 12,284 eV. Data reduction followed well established procedures [9,10]: first, the XAFS spectrum was divided into X-ray absorption near-edge structure (XANES) and extended X-ray absorption fine structure (EXAFS) spectral regions and each of these regions

was then examined separately. Whereas the XANES spectrum was used without further modification to identify elemental occurrences, the EXAFS spectrum was used to develop a "radial structure function" (RSF). The step-height, determined from the XAFS spectrum as the difference in background absorption above and below the edge, was used as a semi-quantitative measure of the relative concentration of the elements in different sets of samples (Table 2).

TABLE 1

Experimental Details for Sorption Experiments

Sample	Filter Temp. deg. F	Hg Species	Sorbent Mass mg	Flue Gas Hg Conc. $\mu g/m^3$	Gas Flow Rate m^3/hr	Length Test hr	Comments
IAC-1	225	Hg	300	60	0.85	3.37	
IAC-2	---	--	---	--	--	--	Unreacted
LAC-1	275	Hg	400	60	0.85	NA	
LAC-2	325	Hg	500	60	0.85	NA	
LAC-3	---	--	---	--	--	--	Unreacted
SAC-1	225	Hg	300	60	0.85	12.42	
SAC-2	---	--	---	--	--	--	Unreacted
IAC -400	225	$HgCl_2$	400	12	0.85	12.17	
LAC -400	225	$HgCl_2$	400	12	0.85	16.15	
SAC -400	225	$HgCl_2$	400	12	0.85	7.2	
LAC-5	225	Hg	400	60	0.85	4.0	10%O_2, bal. N_2
LAC-6	225	Hg	400	60	0.85	4.0	8%H_2O, 10%O_2, N_2
LAC-7	225	Hg	400	60	0.85	4.0	Baseline minus SO_2
LAC-8	225	Hg	400	60	0.85	4.0	Baseline minus HCl

TABLE 2

Relative Step-Heights Determined from XAFS Spectra

Sample	S	Cl	Ca	I	Hg
IAC-I	20			0.1	1
IAC-2	1			1	0
LAC-1	15	60	6.5	0	2.1
LAC-2	18	42	6.0	0	1.5
LAC-3	7	1		0	0
SAC-1	60		0.9	0	2.8
SAC-2	65		1	0	0
IAC (-400)					1.5
LAC (-400)					1.7
SAC (-400)					1
LAC-5					1.6
LAC-6					1
LAC-7					2.0
LAC-8					6.7

" " (blank) field indicates no determination made.
"0" indicates no significant edge detected for that element.

RESULTS AND DISCUSSION

(a) Sulfur

Sulfur XAFS experiments were carried out on the first suite of seven activated carbons (Table 2). Except for sample IAC-2, the sulfur XAFS spectra were quite strong and different forms of sulfur were readily apparent in the XANES spectra of different samples (Figure 1). Whereas the two SAC samples contained predominantly elemental sulfur (indicated by the major peak at 0 eV), the other samples (IAC-1, LAC) were predominantly sulfate sulfur (indicated by the major peak at 10 eV). The LAC samples also contained a minor amount (<10%) of elemental sulfur. The increase in step-height noted between IAC-1 and IAC-2 and between LAC-1, LAC-2 and LAC-3 suggests that the IAC and LAC carbons may absorb or react with SO_2, forming a sulfate species, during exposure to the flue gas. For the two SAC samples, however, there is little

change in sulfur concentration and, moreover, the sulfur form is elemental, which is not consistent with the sulfur speciation in the flue gas as SO_2.

(b) Chlorine
Chlorine XAFS experiments have been performed only on the three LAC samples in set 1. For the two samples (LAC-1, LAC-2) exposed to the flue gas, a significant increase (approx. 50 times) in chlorine concentration was indicated by the step-height data (Table 2). These data indicate that the LAC carbon readily absorbs chlorine. The chlorine XANES spectra are shown in Figure 2 and are consistent with the capture of chlorine as HCl and not as Cl_2 [11].

(c) Iodine
Iodine XAFS experiments were performed on all seven samples in set 1, but as expected, only the two IAC samples gave positive indications of iodine. The iodine L_{III} spectra are shown in Figure 3 and appear closest to elemental iodine, although the match is not exact. Whether this reflects a highly dispersed state for elemental iodine in the activated carbons remains to be demonstrated. The step-height data (Table 2) suggest that the iodine content of the carbon after exposure to the flue gas is much less than that before, which may indicate that significant volatilization of iodine from the carbon has occurred during exposure to the flue gas.

(d) Calcium
Calcium XAFS experiments were performed only on the two SAC samples and on the two LAC samples exposed to the flue gas. The step-height data for calcium (Table 2) indicate little or no difference in concentration for calcium between the two samples in each pair, suggesting that there is no net loss or gain of calcium during the exposure to the flue gas. The spectra (Figure 4) are distinct for each pair of samples. For the LAC samples, the calcium XANES spectra are similar to that from calcium sulfate ($CaSO_4$) [12]; however, the Ca form that gives rise to the spectra for the SAC samples is not so readily identified.

(e) Mercury
The mercury XANES spectra for the four carbon samples in the first sample set that were exposed to the simulated flue gas are shown in Figure 5. As with all mercury XANES spectra, the fine structure is rather subtle and the first derivative spectrum has been used to accentuate differences among the spectra. As can be seen from the figure, the fine structure becomes more prominent in the order IAC-1 < LAC-1, LAC-2 < SAC-1 and is accompanied by an increasing separation of the two peaks in the first differential spectra. Based on work on other mercury standards [13], it would appear that the separation of the peaks is highest for ionic mercury compounds and least for covalent and metallic mercury compounds. The observed trend for the peak separation in the activated carbons would be consistent with Hg-S or Hg-Cl bonding in the LAC-1, LAC-2 and SAC-1 carbons and Hg-I bonding in the IAC-1 carbon. Further evidence for this trend can be seen from an analysis of the EXAFS regions of the XAFS spectra presented in Figure 6. The radial structure functions (RSFs) shown in Figure 6 indicate a significantly different local structure for Hg in the iodine-impregnated carbon. In particular, the Hg-X bond for IAC-1 is much longer than those indicated for Hg in SAC-1 and for LAC-1,2. The peak positions in the RSFs are consistent with Hg^{2+}-Cl, as in $HgCl_2$, and/or Hg^{2+}-S, as in HgS (cinnabar), for the LAC-1,2 and SAC-1 samples, and with Hg^{2+}-I, as in HgI_2, for the IAC-1 sample. The Hg-S bond distance in HgS (cinnabar) is about 2.36 Å, the Hg-Cl bond distance in $HgCl_2$ is about 2.25 Å, and the bond distance for Hg-I in HgI_2 is about 2.78 Å.

Very similar mercury XANES spectra to those shown in Figure 5 were obtained from the second set of three samples (IAC -400, SAC -400, LAC -400) that were exposed to the flue gas containing $HgCl_2$. The close similarity of these spectra to those obtained from the corresponding samples exposed to the flue gas containing Hg vapor implies either that the mercury species in the flue gas is the same regardless of whether mercury or mercuric chloride is added to the flue gas, or that the products of the chemisorption reaction on the carbons are not determined by the speciation of mercury in the gas phase, but, rather, are determined by the active species on the carbons. It is also interesting to note that the step-heights derived from the XAFS spectra appear to correlate reasonably well with the durations of the experiments.

Except for differences in the mercury step-height (Table 2) or, equivalently, in the concentration of the mercury captured on the carbons, the spectral data for the LAC samples exposed to different formulations of the flue gas were closely similar to those of other LAC samples investigated previously. Since the experimental conditions were identical, except for the composition of the flue gas, the differences in the mercury step-height must reflect the relative efficiency with which mercury is captured from the gas stream. It would appear that moisture retards the absorption of mercury, but that HCl and especially SO_2 enhance the adsorption of elemental mercury. Further experiments will be carried out to confirm these observations.

CONCLUSIONS

This work demonstrates that XAFS spectroscopy is a powerful technique for identifying elemental species on activated carbons and for examining reactions involved in the adsorption of mercury from flue gases on such carbons. Although more work is needed to complete this investigation, a number of interesting conclusions appear to have been reached: (1) the mechanism involved in adsorption of mercury appears to depend on the element or method used to activate the carbon; (2) the LAC carbons are very efficient in extracting HCl from the flue gas and both the IAC and LAC carbons appear to react with SO_2 to form sulfate species; and (3) the adsorption of these gases by the carbons may also aid the adsorption of mercury as the rate of adsorption of mercury appears to be significantly affected by the composition of the flue gas.

ACKNOWLEDGEMENTS

This work was supported by the U.S. Department of Energy through separate contracts to UND-EERC for preparation of the activated carbons and to PSI and UK for research on the "air-toxics" elements. Both contracts were also supplemented by the Electric Power Research Institute. We also wish to acknowledge Tom Brown, U.S. DOE-FETC, in bringing these efforts together. The U.S. DOE is also acknowledged for its support of the Synchrotron Radiation Laboratories, SSRL and NSLS, without which the XAFS experimentation could not have been carried out.

REFERENCES

1. U.S. Public Law 101-549, U.S. Government Printing Office, Nov. 15th, 1990, 314 pp.
2. Bragg, L.J., Oman, J.K, Tewalt, S., Oman, C.L., Rega, N.H., Washington, P.M. and Finkelman, R.B., *Coal quality (COALQUAL) database: version 1.3.* U.S. Geological Survey, Open-File Report 94-205, 35Mb CD-ROM, 1994.
3. Swaine, D.J., *Trace Elements in Coal*, Butterworths, 1990.
4. Porcella, D., EPRI Journal, pp. 46-49, Apr/May 1990.
5. Richardson, C.V., and Nielsen, G.F., (eds.), *1980 Keystone Coal Industry Manual*, McGraw-Hill, New York, NY, 1980.
6. Cramer, S.P., Tench, O., Yocum, N., and George, G.N., Nucl. Instrum. Methods A266, 586-591, 1988.
7. Huggins, F.E., and Huffman, G.P., Intern. J. Coal Geol. 32, 31-53, 1996.
8. Lytle, F.W., Greegor, R.B., Sandstrom, D.R., Marques, E.C., Wong, J., Spiro, C.L., Huffman, G.P., and Huggins, F.E., Nucl. Instrum. Methods 226, 542-548, 1984.
9. Lee, P.A., Citrin, P.H., Eisenberger, P.A., and Kincaid, B.M., Rev. Mod. Phys. 53, 769-808, 1981.
10. Brown, Jr., G.E., Calas, G., Waychunas, G.A., and Petiau, J., Chapter 11 in: *Reviews in Mineralogy*, Vol. 18, Mineral. Soc. America, Washington DC, pp. 431-512, 1988.
11. Huggins, F.E., and Huffman, G.P., Fuel 74, 556-569, 1995.
12. Huffman, G.P., Huggins, F.E., Levasseur, A.A., Durant, J.F., Lytle, F.W., Greegor, R.B., and Mehta, A., Fuel, 68, 238-242, 1989.
13. Huggins, F.E., et al., unpublished work.

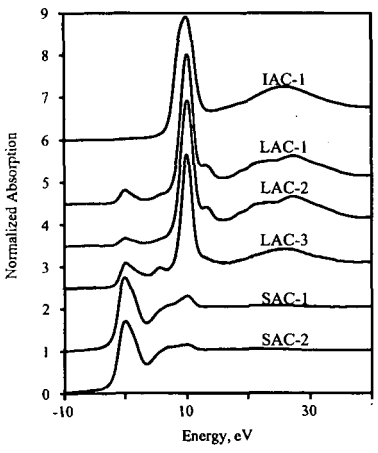

Figure 1: Sulfur XANES of activated carbons.

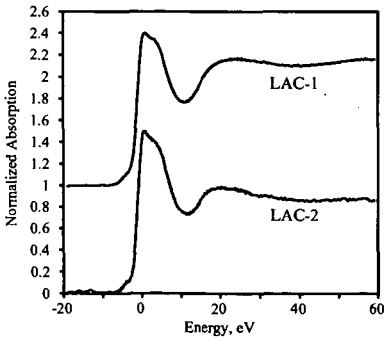

Figure 2: Chlorine XANES of LAC activated carbons.

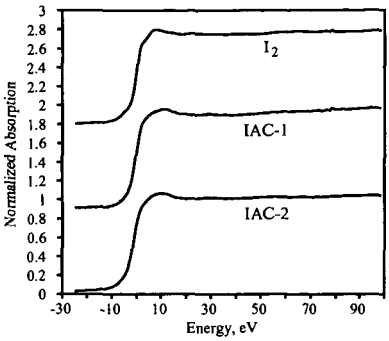

Figure 3: Iodine XANES of iodine activated carbons and elemental iodine (I_2).

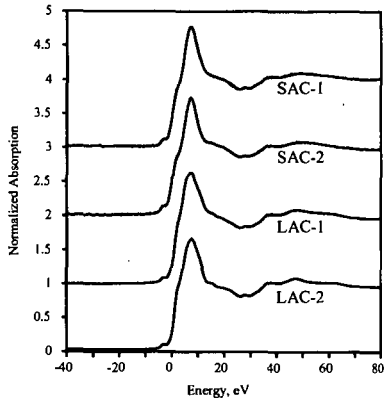

Figure 4: Calcium XANES of SAC and LAC carbons.

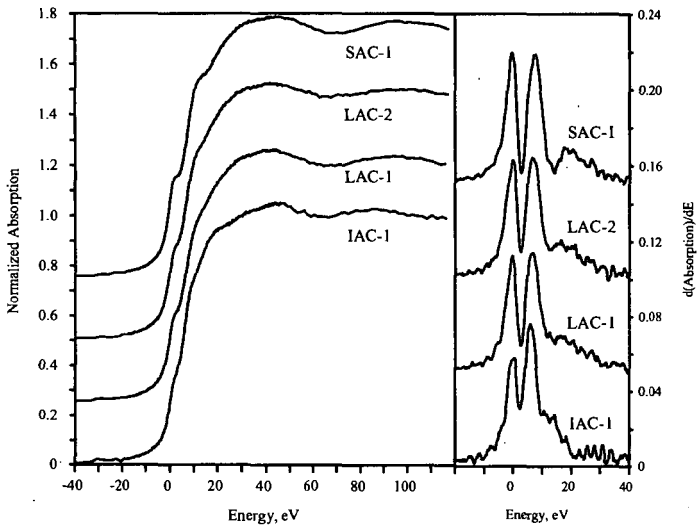

Figure 5: Mercury XANES and first derivative spectra of activated carbons exposed to simulated flue gas with mercury vapor.

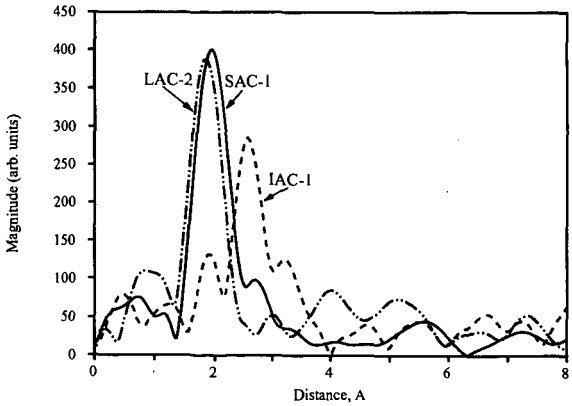

Figure 6: Radial structure functions for mercury in three activated carbons.

STRUCTURAL CHARACTERISTICS AND THERMAL STABILITY OF FGD SCRUBBER SLUDGE

P. S. Valimbe[a], V. M. Malhotra[a], and D. D. Banerjee[b]
a. Department of Physics, Southern Illinois University, Carbondale, IL 62901
b. Illinois Clean Coal Institute, Carterville, IL 62918.

ABSTRACT

We investigated the structural and thermal properties of flue gas desulfurization (FGD) scrubber sludge (CWLP, Springfield, Illinois) to explore this residue's suitability for conversion into structural materials. The structural characteristics of the sludge were obtained by undertaking transmission-Fourier transform infrared (FTIR), diffuse reflectance-FTIR (DRIFT), and scanning electron microscopy (SEM) measurements, while the thermal stability of the residue was gauged by conducting differential scanning calorimetry (DSC) and differential thermal analysis (DTA) experiments at 30°C < T < 1150°C. The SEM data and vibrational results suggest that this residue is largely gypsum and contains a few particles of fly ash. We did observe only very weak SO_3^{2-} bands in the sludge's FTIR spectrum. The sludge is primarily composed of two types of crystallites, i.e., rectangular-shaped needles and parallelogram-shaped crystals. The thermal results on the sludge indicate that the water is lost from the sample in a two step process at 150°C < T < 200°C. The observed dehydration enthalpy of 585 J/g was higher than that reported for gypsum. However, our results are consistent with the commercial gypsum samples we tested. After exothermic transformation at 380°C, the sludge sample and the commercial gypsum samples remained thermally inert at 400°C < T < 1150°C.

INTRODUCTION

Presently more than 90 million tons of coal combustion byproducts, i.e., fly ashes, bottom ashes, and scrubber sludges, are generated in the U.S. annually. These byproducts' yield is expected to grow in the near future as the Clean Air Act is stringently enforced [1-3]. The Midwestern USA coals are high in sulfur content, and the combustion of these coals results in emissions containing a high percentage of SO_x. Flue gas desulfurization (FGD) technology is commonly used in order to reduce the emission of these venomous gases. Some power plants use a scrubber unit to capture SO_x, and this produces about 20 million tons of scrubber sludge in the USA alone.

It is generally believed that the major components of scrubber sludge, depending upon whether it is a forced oxygen unit, are calcium sulfite ($CaSO_3$), calcium sulfate ($CaSO_4$), and gypsum ($CaSO_4.2H_2O$). In addition, small amounts of fly ash and excess scrubbing reagents have been reported in the sludges. When lime or limestone is used as a sorbent material in the FGD systems, the purity of calcium sulfate obtained as a byproduct ranges between 95% to 99%. Lime reacts with SO_2 in the scrubber unit, and different products are formed depending on the temperature of the system. It has been reported that only $CaSO_3$ was formed below 550°C, while a mixture of $CaSO_3$, $CaSO_4$ and CaS was produced at 600°C < T < 850°C [4]. Above 800°C, only $CaSO_4$ and CaS were formed. On the other hand, if $CaCO_3$ is used in a scrubber unit, different byproducts are formed depending on the temperature at which the flue gases react with it. The reactions of $CaCO_3$ with air (O_2) + SO_2 have been thoroughly investigated at different temperatures [5]. It was found that the amount of sulfite formed in such a system was always small compared to the other phases. Significant amounts of $CaSO_3$ were formed only at T > 600°C. Formation of $CaSO_4$ was extremely low but detectable at temperatures above 400°C. At T ≥ 600°C, the formation of $CaSO_4$ was significant and reached a maximum at 800°C. Other traces detected above 800°C were $CaCO_3$, CaO, CaS, $CaSO_3$, and $Ca(OH)_2$.

It has been reported that the hydrated calcium sulfate, particularly gypsum, produced as a byproduct of scrubbing flue gases, could be used in a variety of applications. Most of the scrubber sludge produced in the U.S. is currently used only in landfill applications [1-3]. Some other applications of this residue are road construction [6], wallboard manufacturing [7], and agricultural [8]. However, the quantity of these residues produced as well as the cost of disposal are very large and are increasing every year. Hence, it is necessary to develop more applications in which these residues can be utilized. If the gypsum is to be used in different market applications, the fly ash must be removed from the flue gas before the scrubbing process to avoid contamination. Also, it is necessary to ascertain whether scrubber sludges produced are environmentally safe.

We have initiated systematic microscopic, thermal, and spectroscopic measurements on various scrubber sludges produced by different power plants with a view to characterize these byproducts for their suitability in the construction industry. Here we report our results on a sludge which is rich in hydrated calcium sulfate

EXPERIMENTAL TECHNIQUES

The scrubber sludge we examined was from City Water and Light Power Plant (CWLP) in Springfield, Illinois. This power plant combusts Illinois No. 5 and Illinois No. 6 coals. The residue sample was obtained from the sample bank established at the Mining Engineering department of Southern Illinois University at Carbondale. For comparison purposes, we also characterized two gypsum samples, i.e., Satin Spar Gypsum (SSG), and Gypsum Var Alabaster (GVA), obtained from Sargent-Welch. The SEM study of the CWLP scrubber sludge sample was carried out using a Hitachi S570 scanning electron microscope. The thermal characterization of the scrubber sludge and the mineral gypsum samples was carried out using DSC and DTA techniques. In DSC experiments, the samples were subjected to heating in N_2 atmosphere at temperatures 40°C < T < 450°C using a well calibrated [9,10] Perkin-Elmer DSC 7 system. A heating rate of 10°C/min was used. Aluminum (Al) pans were used to encapsulate the sample with holes drilled in them so that any vapors or gases evolved from the sample could escape easily. The higher temperature (50°C < T < 1100°C) thermal behavior of our samples was probed by undertaking DTA measurements using a Perkin-Elmer DTA 7 system. A heating rate of 20°C/min was used under N_2 gas environment. We used KBr pellet technique to record FTIR spectra of CWLP sludge and gypsum samples at 4 cm^{-1} resolution. We also conducted *in-situ* diffuse reflectance-FTIR (DRIFT) measurements on CWLP scrubber sludge at 20°C < T < 275°C. While FTIR spectra were recorded on a IBM IR 44 FTIR spectrometer, the DRIFT spectra were collected on a Nicolet 740 FTIR spectrometer.

RESULTS AND DISCUSSION

A careful examination of SEM microphotographs of CWLP scrubber sludge indicates that the air dried scrubber sludge generally consisted of two distinct morphologies of crystals. In the first morphology, the crystals were parallelogram-shaped, and this shape is typical of gypsum ($CaSO_4.2H_2O$) [11]. The second type of morphology exhibited by sludge particles was rectangular-shaped crystals, ranging from 50 to 400 μm in length and about 50 μm in thickness. These rectangular-shaped crystals (see Fig. 1) showed a random pore structure within the crystallites and thus, will be difficult to dewater. It is worth pointing out that the CWLP scrubber sludge we examined did show a very few particles of fly ash. However, their concentration in the sludge was almost negligible.

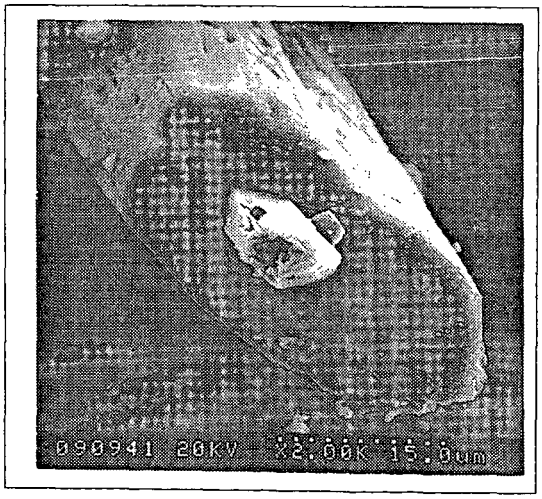

Fig. 1 SEM microphotograph of scrubber sludge crystallites.

Figure 2 depicts DSC thermographs for CWLP scrubber sludge, satin spar gypsum (SSG), and gypsum var alabaster (GVA) samples. The DSC thermograph of CWLP scrubber sludge showed two strong endothermic peaks located at 154°C and 189°C and a weak exothermic peak at 380°C. Similar thermal events were also observed for mineral gypsum samples except the peak temperatures were slightly different. Based on work reported in the literature [12,13], the endothermic peaks can be associated with the loss of water from the sludge. It appears

that the dehydration reaction in our CWLP scrubber sludge sample occurred in two steps, just as it has been reported for $CaSO_4.2H_2O$ [13]. The peak at 154°C may be due to the loss of 1.5 water molecules which resulted in the formation of hemihydrate, $CaSO_4.0.5H_2O$. The dehydration further continued when at 189°C, γ-anhydrite was formed by the loss of the remaining 0.5 water molecule. Even though there are some dissimilarities in the peak positions of the observed endothermic and exothermic reactions observed for CWLP scrubber sludge and mineral gypsum samples, we believe the CWLP scrubber sludge is largely composed of $CaSO_2.2H_2O$.

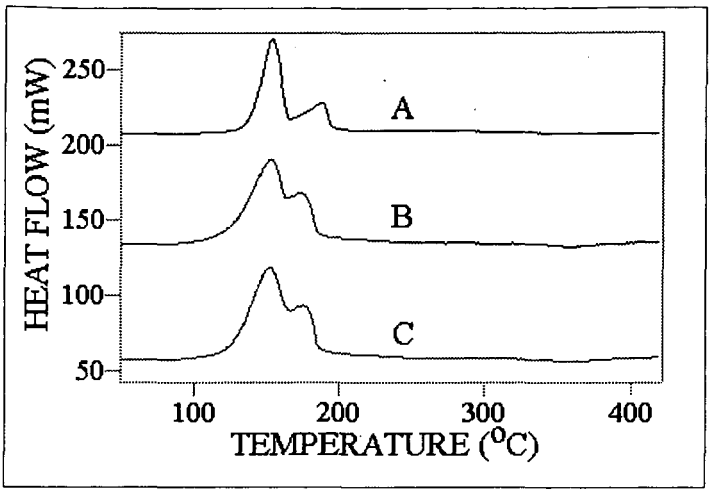

Fig. 2 DSC thermographs of (A) CWLP scrubber sludge, (B) Satin Spar Gypsum (SSG), and (c) Gypsum Var Alabaster (GVA) samples. The two endothermic peaks at 100°C < T < 200°C represent decomposition and desorption of water from the samples.

Our results indicate that the enthalpy of dehydration reaction for CWLP scrubber sludge was 592 J/g, which is much larger than that reported by Strydom et al. [14] for synthetic gypsum. Strydom et. al., using DSC technique, reported that the dehydration enthalpy of synthetic gypsum varied over a range of 377 J/g to 420 J/g. However, DSC experiments conducted on mineral gypsum samples in our laboratory revealed a value of 656 J/g and 704 J/g for GVA and SSG, respectively. Since the observed dehydration enthalpy will be strongly influenced by such factors as packing of the particles in the Al pans, the consistency and uniformity of the holes in the pans, and the ramping rates used, some variation in the enthalpy value is expected. However, to provide conclusive evidence, additional experiments will be needed and are in progress.

Table 1 summarizes our DTA results on scrubber as well as mineral gypsum samples at 50°C < T < 1100°C. Similar to DSC results, the DTA experiments on the sludge exhibited a two-step dehydration reaction. This was followed by a polymorphous transformation, i.e., γ-$CaSO_4$ transforms into β-$CaSO_4$ at 380°C. After the formation of β-anhydrite at 380°C, the DTA results did not show any other thermal event either for sludge or mineral gypsum samples at 380°C < T < 1100°C.

We attempted to ascertain the chemical structure and composition of CWLP scrubber sludge by conducting FTIR spectroscopic measurements. The infrared (IR) frequencies along with the observed peak heights are reproduced in Table 2. Also listed in Table 2 are the IR band frequencies for mineral gypsum samples. The IR spectrum of scrubber sludge showed two vibrational modes at 3615 cm^{-1} (ν_3 stretch of HO-H)) and 3557 cm^{-1} (ν_1 stretch of HO-H) in the water's stretching region, while a single oscillator at 1620 cm^{-1} was observed in the water's bending region. On the other hand, the mineral gypsum samples showed three vibrational bands in the water's stretching region and two IR bands in the water's bending region. Bensted and Prakash [15] have suggested that the different phases of calcium sulfate can be distinguished by the vibrational modes of water observed. For example, O-H stretching vibrations are observed at ~ 3555, ~ 3500, and ~ 3400 cm^{-1} in the water's stretching region for gypsum ($CaSO_4.2H_2O$) along with two oscillators at ~ 1680 and ~ 1620 cm^{-1} in the water's bending region. Hemihydrate ($CaSO_4.0.5H_2O$)

produces two vibrational bands in the O-H stretching region at around 3610 and 3560 cm^{-1} and a single oscillator in the H-O-H bending region. Since we observed only three vibrational modes of water at 1500 < frequency < 3800 cm^{-1} for our scrubber sludge sample, see Table 2, it is reasonable to argue that our sample is largely hemihydrate. This observation is not consistent with our DSC and DTA results which suggested that our CWLP scrubber sludge was mostly gypsum. It is possible that during the formation of KBr pellets and subsequent drying in a desiccator, the gypsum got converted into hemihydrate phase.

TABLE 1
Summary of DTA results on CWLP scrubber sludge and mineral gypsum samples at 50°C < T < 1100°C.

Sample	Peak Begins at (°C)	Peak End at (°C)	Peak Temperatures (°C)	Remark
CWLP Scrubber Sludge	93 335	273 480	165, 181 380	Endothermic Exothermic
Satin Spar Gypsum	64 330	316 480	203 378	Endothermic Exothermic
Gypsum Var Alabaster	97 338	300 432	183, 193 379	Endothermic Exothermic

TABLE 2
The observed infrared bands for CWLP scrubber sludge and mineral gypsum samples. The observed frequencies are in cm^{-1} (value in parentheses is peak height in arbitrary units).

CWLP Scrubber Sludge	Satin Spar Gypsum	Gypsum Var Alabaster	Assignment
3613(0.51)	3545 (0.45)	3548 (0.50)	O–H stretch (ν_3) (H_2O)
3560(0.36)	3494 (0.40)	3497 (0.39)	O–H stretch (ν_1) (H_2O)
	3405 (0.51)	3405 (0.59)	O–H stretch ν_1 (H_2O)
	3243 (0.18)	3243 (0.17)	2(ν_2) (H_2O)
2361 (0.10)	2240 (0.06)	2240 (0.06)	2(ν_3) in SO_4
2334 (0.09)	2116 (0.04)	2120 (0.04)	$\nu_1+\nu_3$ in SO_4
	1687 (0.15)	1686 (0.13)	H-O-H bend (ν_2)
1622 (0.32)	1622 (0.29)	1621 (0.30)	H–O–H bend (ν_2)
1154 (4.27)	1142 (0.95)	1144 (1.1)	ν_3 of SO_4
1126 (1.50)	1116 (0.96)	1117 (1.1)	ν_3 of SO_4
1105 (1.35)			ν_3 of SO_4
1007 (0.18)			ν_1 of SO_4
662 (0.52)	669 (0.31)	669 (0.32)	ν_4 of SO_4
602 (0.50)	602 (0.30)	602 (0.30)	ν_4 of SO_4
	463 (0.05)	461 (0.06)	

We performed in-situ DRIFT measurements at 20°C < T < 260°C on air-dried CWLP scrubber sludge to answer whether this sludge was in gypsum or hemihydrate phase. Figure 3 reproduces how temperature altered the DRIFT spectrum of the sludge. At 30°C the sludge's DRIFT spectrum showed four vibrational bands in the water's stretching region, i.e., at 3556, 3489, 3402, and 3249 cm^{-1} and two bands at 1687 and 1620 cm^{-1} in the water's bending region. As the temperature was raised above 30°C, the band at 3556 cm^{-1} lost intensity and shifted to 3570 cm^{-1} at 106°C. The band at 1687 cm^{-1} rapidly lost intensity at 106°C and disappeared at 135°C. At 135°C < T < 180°C, we observed two bands at 3630 and 3550 cm^{-1} in the O-H stretching region and a single band at around 1624 cm^{-1} in the water's bending region. Above T > 180°C, the H-O-H bands were very weak if they were observed at all. Based on our *in-situ* DRIFT results, we believe CWLP scrubber sludge mostly contains gypsum phase which readily loses water at 50°C < T <

135°C to form hemihydrate phase. It transforms into reversible anhydrite phase at 160°C < T < 260°C. The vibrational bands at 1154, 1126, and 1105 cm^{-1} could be assigned to ν_3 mode of SO_4^{2-} ions of gypsum, while the bands at 662 and 602 cm^{-1} are due to ν_4 mode of sulfate ions. It is known that SO_3^{2-} ions produce a characteristic band at around 975 cm^{-1}. We did observe a very weak band at 977 cm^{-1} in our DRIFT spectrum, suggesting that CWLP does contain a very small quantity of $CaSO_3$.

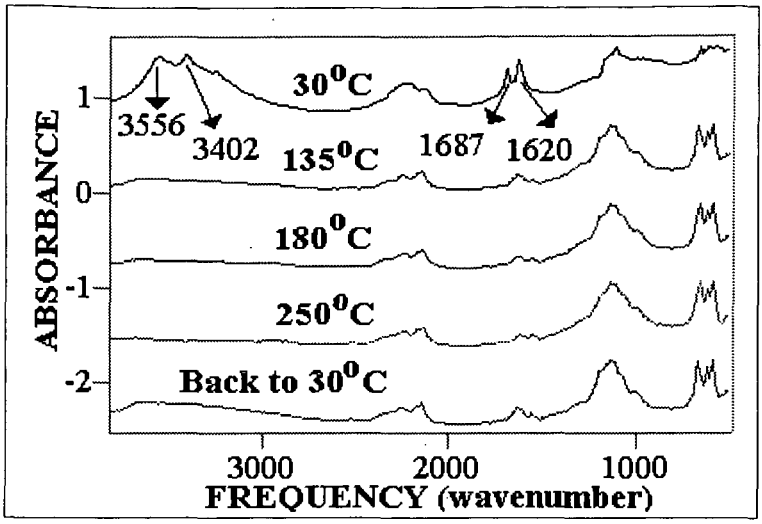

Fig. 3 This figure shows how temperature affected the diffuse reflectance-FTIR (DRIFT) spectrum of CWLP scrubber sludge.

ACKNOWLEDGMENTS

This work was supported in part by Illinois Clean Coal Institute (Department of Commerce and Community Affairs).

REFERENCES:

1. McCarthy, G. J.; Glasser, F. P.; Roy, D. M.; Hemmings, R. T. (eds.) *Mater. Res. Soc. Sympos. Proc.* Vol. **113**, 1988.
2. Lee, L. B., "Management of FGD Residues: An International Overview.", Proc. 10th Annual Int. Pittsburgh Coal Conf, pp. 561-566, 1993.
3. Valimbe, P. S.; Malhotra, V. M.; Banerjee, D. D.; *Am. Chem. Soc. Prep., Div. Fuel Chem.*, **40(4)**, 776, 1995.
4. Munoz-guillena, M. J., Linares-Solano, A; Salinas-Martinez de Lecea, C. *Appl. Surf. Sci.* **81**, 409, 1994.
5. Anderson, D. C.; Anderson, P.; Galway, A. K. *Fuel* **74**, 1018, 1995.
6. Goodrich-Mahoney, J. W. "Coal Combustion By-Products Field Research Program at EPRI: an overview" EPRI (Environmental division), 1994.
7. Henkels, P. J.; Gaynor, J. C. *Am. Chem. Soc. Prep., Div. Fuel Chem* **41(2)**, 569, 1996.
8. Chou, M.-I. M.; Bruinius, J. A.; Li, Y. C.; Rostam-Abadi, M.; Lytle, J. M. *Am. Chem. Soc. Prep., Div. Fuel Chem* **40(4)**, 896, 1995.
9. Jasty, S.; Robinson, P. D.; and Malhotra, V. M. *Phys. Rev. B* 43, 13215, 1991.
10. Mu, R.; Malhotra, V. M. *Phys. Rev. B* 44, 4296, 1991.
11. Mattigod, S. V.; Rai, D.; Zachara, J. M.; Amonette, J. E. *Mater. Res. Soc. Sympos. Proc.* Vol. **136**, 3, 1989.
12. Todor, D. N. 'Thermal Analysis of Minerals', Abacus Press, Kent (1976).
13. Dunn, J.; Oliver, K.; Nguyen, G.; Sills, I. *Thermochim. Acta* **121**, 181, 1987.
14. Strydom, C. A.; Hudson-Lamb, D. I.; Potgieter, J. M.; Dagg, E. *Thermochim. Acta* **269**, 631, 1995.
15. Bensted, J.; Prakash, S. *Nature* **219**, 60, 1968.

EFFECT OF PRE-TREATMENT ON METHANOL SYNTHESIS FROM CO_2/H_2 OVER $Cu/ZnO/Al_2O_3$

James T. Sun and Ian S. Metcalfe
Department of Chemical Engineering and Chemical Technology
Imperial College of Science, Technology and Medicine
London SW7 2BY, UK

INTRODUCTION

Methanol synthesis from CO_2 and H_2 has recently received much attention as one of the promising processes to convert CO_2 into raw materials for fuel and chemicals. Copper-based catalysts are highly effective for this reaction, and a number of studies have been done to understand the mechanisms of catalytic action. Chinchen et al.[1,2] have reported that methanol synthesis occurs exclusively on the surface of metallic copper and the activity is directly proportional to this copper surface area. They attributed no special role to the support other than to maintain the dispersion of copper on the catalyst surface. Evidence that Cu^+ is the pivotal catalytic species, however, has been presented by Sheffer and King[3,4] who found that the activity for methanol synthesis from CO over unsupported copper catalysts increases with the concentration of Cu^+ sites stabilised by alkali compounds. More recent studies by Fujitani et al.[5,6] have demonstrated the existence of an optimal level of oxygen coverage for methanol activity, although this was done for copper catalysts supported a very wide range of oxide materials. They found that the activity increased linearly with the oxygen coverage below $\Theta_o = 0.16$, and then decreased above $\Theta_o = 0.18$, suggesting that the active component is some combination of Cu^+ and Cu^0, where the ratio of Cu^+/Cu^0 controlled the specific activity.

The present paper reports the effect of CO_2/CO pre-treatment on methanol synthesis from CO_2/H_2 over $Cu/ZnO/Al_2O_3$ catalysts. Instead of using widely varying oxide materials, oxygen coverage is varied in the pre-treatment on a single well-studied catalyst via the gas phase, where the CO_2/CO ratio has been demonstrated to have a linear correlation with the oxygen coverage under reaction conditions[1]. Possible contributions from changes in surface state are explored by measuring the response of methanol rate to these conditions.

EXPERIMENTAL

The $Cu/ZnO/Al_2O_3$ catalyst were prepared by precipitation of the respective metal nitrates using Na_2CO_3 as the precipitating agent. The precipitate was washed with distilled water until analysis showed the presence of Na was no greater than 1-2 ppm. The dried precipitate was then calcined in air at 300 °C for 6 h. After the addition of 2% (w/w) graphite for binding purposes, pellets of 2 g cm^{-3} density were formed. These were crushed and sieved to a particle size range of 106-250 μm. Elemental analysis using x-ray fluorescence revealed the composition of the catalyst to be 61.0% CuO, 27.5% ZnO, and 11.5% Al_2O_3.

The reactor system used for the activity studies consisted of a continuous tubular flow fixed-bed microreactor which was operated at 4.5 MPa and 215 °C. The synthesis gas composition was a 1:4 CO_2/H_2 mixture fed through to the reactor via Brooks high pressure mass flow controllers. On-line gas analysis was accomplished using a GC-MS system. An isothermal sampling valve injects 0.5 ml samples from the heated effluent downstream of the reactor to a Perkin Elmer 8500 gas chromatograph. Separation and detection of products were performed by a Poropak Q column and a thermal conductivity detector, respectively. Downstream of the gas chromatograph sampling valve, the gas was analysed using a Leda-Mass quadrupole mass spectrometer with a Spectra Microvision analyser unit.

Prior to reaction, the catalysts were activated *in situ* by reduction of the CuO component to metallic copper. Under flowing 5% H_2 in He the temperature was increased by 2 °C min^{-1} to 215 °C and held for 12 h. After the initial reduction, the reactor is flushed with He and the pre-treatment gas mixture of CO_2 and CO introduced. These conditions are maintained for 1 h before the reactor is again flushed with He and pressurised to 4.5 MPa. At pressure, the synthesis gas mixture of 20% (v/v) CO_2 in H_2 is introduced, and the pressure maintained at 4.5 MPa. Rate

measurements were taken in a flow regime which obeys differential kinetics. Under these conditions, the rate is independent of the flow. This results in extremely low levels of conversion (generally less than 1%) such that the catalysts are essentially exposed only to reactants, and the rate reflects the intrinsic forward rate of reaction.

RESULTS AND DISCUSSION

In the absence of H_2, no methanol is produced. Reaction was carried out under a lower temperature of 215 °C which is the temperature under which the catalyst charge is reduced with a stream of 5% hydrogen in helium. Whereas methanol synthesis is normally carried out at 250 °C, these isothermal conditions were chosen to minimise the time required to switch between the CO_2/CO pre-treatment and reaction under CO_2/H_2.

At these temperatures, the initial rate of methanol synthesis from CO_2/H_2 (over the $Cu/ZnO/Al_2O_3$ catalyst reduced overnight with 5% hydrogen in helium but without further CO_2/CO pre-treatment) of about 0.045 mol h^{-1} g_{cat}^{-1} is substantially lower than those under industrial reactions conditions (about 0.20 mol h^{-1} g_{cat}^{-1} at 250 °C). Nevertheless, it is possible to observe the sensitivity of CO_2 hydrogenation to pre-treatment conditions of varying carbon dioxide concentrations as defined by R, where $R = CO_2/(CO_2 + CO)$, as described by Figure 1. Upon pre-treating with a stream of pure carbon monoxide (R = 0), hydrogenation of carbon dioxide yields methanol at a rate of about 0.045 mol h^{-1} g_{cat}^{-1}, which is identical to that found in the case without CO_2/CO pre-treatment. This confirms that pre-treatment under carbon monoxide maintains the catalyst surface in a completely reduced state. As small amounts of carbon dioxide is introduced into the pre-treatment, however, the specific methanol rate begins to increase. This behaviour continues as R is increased until a maximum rate is reached at an R value between 0.7 and 0.8. Further increases in pre-treatment carbon dioxide concentration beyond this point brings about a decrease in the rate of methanol synthesis. In the extreme case, pre-treatment under pure carbon dioxide for 1 hour leads to a methanol rate of 0.055 mol h^{-1} g_{cat}^{-1}.

The existence of an optimal CO_2/CO pre-treatment condition for methanol synthesis is significant as it supports the model where both Cu^0 and Cu^+ are important for the catalytic action. Interconversion between carbon dioxide and carbon monoxide takes place through a surface mediated process according to the equation

$$CO_{2(g)} = CO_{(g)} + O_{(s)}$$

where $O_{(s)}$ is a surface oxygen species. The formation of $O_{(s)}$ by the dissociative adsorption of carbon dioxide was observed on Cu(110) by Wachs and Madix[7], and on polycrystalline copper, Cu/Al_2O_3, and $Cu/ZnO/Al_2O_3$ by Chinchen and co-workers[2]. As one measure of the state of a catalyst is its oxygen coverage, this is largely determined by the balance of carbon dioxide and carbon monoxide present in the gas phase. Thus, pre-treating the catalyst with the full range of R values between 0 and 1 permits the study of methanol synthesis in response to a wide range of surface conditions.

In order to assess the significance of this behaviour, a more detailed study into the transient kinetics is also necessary. Figure 2 shows the evolution of methanol production upon switching to synthesis conditions (20% carbon dioxide in hydrogen, 4.5 MPa, 215 °C) after the reactor was pressurised under helium. It can be seen that the response of the methanol signal is relatively fast, achieving a steady-state value after about 10 minutes time-on-stream. During the course of this transient, conditions on the surface are responding to the introduction of the new synthesis condition in the gas phase. Because this process occurs so quickly, faster in fact than the time scale at which quantitative measurements can be taken with the gas chromatograph, the methanol rates observed actually occur over a surface which has already achieved a dynamic equilibrium with the gas phase. Although it would seem that such a fast response of the surface would effectively erase the previously established pre-treatment conditions, this clearly does not happen. Furthermore, rather than drifting toward a common level of convergence, the different rates achieved under synthesis conditions possess a high degree of stability, without much appreciable change over the course of 24 hours. Therefore, that the rate does in fact depend on pre-treatment and that this rate remains stable over a long period of time imply the possible existence of rate multiplicity in some form.

One of the possible mechanisms by which a memory effect can take hold is via the support material. Work by Kanai et al.[6] demonstrated the existence of a direct correlation between

increasing concentrations of ZnO_x species and increasing methanol activities. By reducing physical mixtures of Cu/SiO_2 and ZnO/SiO_2 at high temperatures, ZnO_x moieties migrate onto the surface of the copper particles creating a Cu^+-O-Zn site and giving rise to the observed promotional effect. The presence of surface oxygen species could facilitate this interaction along the metal-support interfacial region, so that once the partially oxidised copper species are formed, they can be more readily stabilised by the ZnO along the periphery.

Non-linear behaviour is also known to occur in heterogeneous catalysis, especially of reactions on transition metals involving oxygen. A well known system which exhibits rate multiplicity is that of CO oxidation[8]. The existence of two distinct steady states in these systems is attributed to disparate activation energies for CO adsorption depending on surface morphology and oxygen coverage. While the role of surface oxygen has yet to be unequivocally established in methanol synthesis systems, there is evidence to suggest that it is similarly important in influencing the overall kinetics. One example reported by Chinchen et al.[2] shows that the presence of surface oxygen enhances both the adsorption of CO_2 as well as H_2. It is possible, then, that this change to the adsorption activation energies of the reactant species brought about by surface oxygen can lead to multiple steady states.

CONCLUSIONS

The results show, therefore, that methanol synthesis from CO_2/H_2 is not most favoured over a highly reduced surface, but rather over one where both Cu^0 and Cu^+ are present. Despite the fast response of the surface to changes in the gas phase (i.e., in switching between the pre-treatment and synthesis conditions), there nevertheless seems to be a memory effect. The rate of methanol synthesis from CO_2/H_2 is dependent upon the pre-treatment with CO_2/CO mixtures, with an optimal pre-treatment corresponding to a CO_2 concentration of R = 0.7 to 0.8. The different rates achieved after pre-treatment remain relatively stable up to 24 hours. This suggests that catalytic methanol synthesis systems operate in a non-linear fashion, perhaps mediated by surface oxygen and/or the oxide support.

ACKNOWLEDGEMENTS

This work was supported by ICI Katalco and the Department of Chemical Engineering and Chemical Technology at Imperial College London.

REFERENCES

1. Chinchen, K.C. Waugh and D.A. Whan, *Appl Catal 25*, 101(1986)
2. Chinchen, M.S. Spencer, K.C. Waugh and D.A. Whan, *J Chem Soc, Faraday Trans 1 83*, 2193(1987)
3. G.R. Sheffer and T.S. King, *J Catal 115*, 376(1989)
4. G.R. Sheffer and T.S. King, *J Catal 116*, 488(1989)
5. T. Fujitani, M. Saito, Y. Kanai, T. Kakumoto, T. Watanabe, J. Nakamura and T. Uchijima, *Catal Lett 25*, 271(1994)
6. Y. Kanai, T. Watanabe, T. Fujitani, M. Saito, J. Nakamura and T. Uchijima, *Energy Convers Mgmt 36* (6-9), 649(1995)
7. I. Wachs and R. Madix, *J Catal 53*, 208(1978)
8. S. Scott, *Chemical Chaos*, Clarendon Press, Oxford, 1991, Ch. 10

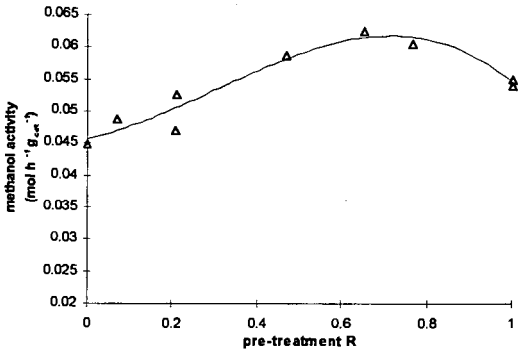

Figure 1. Methanol synthesis rate from CO_2/H_2 over $Cu/ZnO/Al_2O_3$at 215 C and 4.5 MPa following CO_2/CO pre-treatment. $R = CO_2/(CO_2 + CO)$.

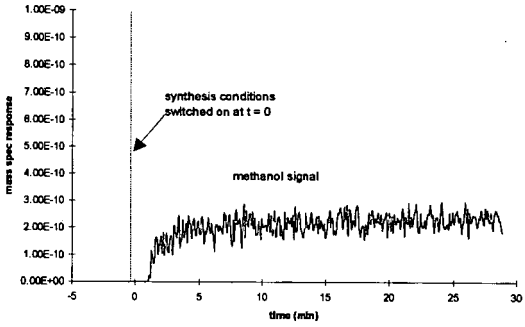

Figure 2. Transient response of methanol signal upon switching to synthesis conditions.